On the Reliable Generation of 3D City Models from Open Data

by

RENOY GIRINDRAN, MSc, M.Tech

Thesis submitted to the University of Nottingham for the Degree of Doctor of Philosophy

March 2021

ABSTRACT

The battle for sustainability will be won or lost in cities. Currently more than 50% of the World's population reside in urban areas and this figure is estimated to reach 68% by 2050. New and innovative approaches are needed for managing urban areas and this demands the generation of appropriate data for evidence-based decision making. Geospatial technologies play an important role in meeting this demand and it is evident that 3D geospatial data of cities provide richer intelligence than 2D geospatial data. However, presently, there is a dearth of free, high-resolution 3D city models available for use especially in developing and underdeveloped countries, which, it could be argued, is where these data are most required.

This thesis offers potential solutions to generating 3D data using open data and methods – it aims to provide globally replicable methodologies to generate low-cost Level of Detail 1(LOD) 3D city models from open data. Two geographically and morphologically different case study cities were used to develop and test this methodology: the Chinese city of Shanghai and the city of Nottingham in the UK. Two different methodologies for generating LOD1 3D city models are developed and tested, with their suitability for different applications discussed. The first method presented exploits that 2D building footprints are available as open data. However, this availability of 2D footprint data is not complete globally and so the second method presented seeks to generate 2D building footprint data with open data that has global coverage. It uses a method to spatial enhancement satellite remote sensing data (Sentinel-2) (from 10m to 1m resolution) for building footprint area generation, which is then used to generate a 3D city model.

As the idea of Digital Twin is gaining pace, this thesis represents a step in the journey towards Digital Twins of all cities – privileged with data or not. Digital twin is the virtual representation of the real world. Geographic Information System (GIS) creates Digital Twins of the natural and built environments and act as a unique base for integrating many subsequent data. It is concluded that the method presented goes some way to meeting the 3D data gap that currently exists for many cities. The successful use of these methods will depend on the application for which they are employed (e.g. disaster management, climate change and urban climate modelling), which in turn should point to what improvements in data models are required.

ACKNOWLEDGEMENT

I express my first and foremost gratitude and heartfelt thanks to my research supervisor Prof Doreen Boyd, who helped and guided me in the every walk of this Ph.D. The guidance provided both academically and psychologically to take the vigour of the PhD is beyond words and without her kind support, I wouldn't have been able to smoothly carryout the research. Similarly, heartfelt thanks is expressed herewith to my other supervisors Prof Giles Foody, Prof Darren Robinson and Dr Julian Rosser. I feel fortunate to do the PhD as part of the interdisciplinary team of academics, research fellows and PhD students at 'The Laboratory of Urban Complexity and Sustainability' (LUCAS). I wholeheartedly thank 'The Leverhulme Trust' for financing this project and for providing the academic freedom and finance to pursue my Ph.D.

I would like to deeply thank the School of Geography, University of Nottingham for my PhD registration and the constant support by the wonderful staff there. I wish to thank University of Nottingham for all the support provided for me as an international PhD student and also thank UK government for providing my VISA to pursue my PhD in UK. I thank Dr Gary Priestnall for the python classes and the internal reviews and comments. As a person constantly staying away from family, the friends at LUCAS was great in giving daily advice, guidance and emotional support. I thank all my colleagues of LUCAS with special mention to Dr Ben Purvis, Dr Phil Northall, Dr Hannah Keding, Dr Philipp Heyken, Ashley Lewis, Dr Amanda Winter and Dr Gavin Long.

I wish to thank Dr Andrew Sowter, Paul Singh Bhatia, Dr Ahmed Athab and David Gee of Terra Motion limited (spin-out company of University of Nottingham) for the wonderful time, while I was working part time at the esteemed organisation. I also sincerely thank Rights Lab colleagues, with special thanks to the director Prof Zoe Trodd for the ongoing part time Research Associate position.

I would like to thank Dr Dharmarajan Ramesh who taught me the basics and foundation for remote sensing and GIS during my studies in Master of Technology (M.Tech) in Remote Sensing. Also remembering my previous wonderful supervisors Dr Srikumar Chattopadhyay, Dr K.K Ramachandran, Dr Pradeep Srivastava and Dr Gejo Anna. I extend my sincere thanks to Dr Arun Babu for his initial advices about UK research and also to my friends Akhil Babu, Jandeep Janardhanan and Dr Praveen J Dev.

I would like to thank my parents Prof Girindran V.K and Sarada Girindran for all the advice and kind support throughout my life. I further thank my brother Dr Rojith Girindran and his wife Dr Dhanya Joseph for the constant advice and motivation and also to their wonderful daughter Dwani Rojith for her witty words and songs. Now I would like to thank my wife Dr Dhanya Vijayan for all the support and strength provided. There are so many beautiful hearts who helped me to do the PhD in one way or other, but I would like to dedicate this research to my daughter Rithanya Renoy. Last, not the least I thank almighty for all the experiences in life.

RECENT PUBLICATIONS

- Stephen Grebby, Andrew Sowter, Jon Gluyas, David Toll, David Gee, Ahmed Athab & **Renoy Girindran** (2021) Advanced analysis of satellite data reveals ground deformation precursors to the Brumadinho Tailings Dam collapse. Communication Earth and Environment **2,** 2. https://doi.org/10.1038/s43247-020-00079-2

- Dhanya Vijayan., Harald Kaechele, **Renoy Girindran,** Srikumar Chattopadhyay, Martin C. Lukas & Muhammad Arshad (2021) Tropical forest conversions and its impact on indigenous communities: Mapping forest loss and shrinking gathering grounds in the Western Ghats, India, Landuse Policy (102), 105133, https://doi.org/10.1016/j.landusepol.2020.105133

- **Renoy Girindran,** Doreen Boyd, Julian Rosser, Dhanya Vijayan, Gavin Long & Darren Robinson (2020), On the reliable generation of 3D city models, Urban Science, 4, 47, doi:10.3390/urbansci4040047

- Lingfei Shi, Giles M Foody, Doreen S Boyd, **Renoy Girindran,** Lihui Wang, Yun Du & Feng Ling (2020) Night-time lights are more strongly related to urban building volume than to urban area, Remote Sensing Letters, 11:1, 29-36, doi: 10.1080/2150704X.2019.1682709

RECENT PRESENTATION IN CONFERENCES

- Brick kilns as ‘objects of UN SGS intersectionality’. An insight from Space, A virtual weather and climate symposium, Hydromet India Virtual, 17th July 2020

- Approaches towards 3D city models using open source data: a global reality, at UK National Earth Observation Conference, Birmingham University, United Kingdom, 2018 (Poster presentation)

RELEVANT PART TIME WORK

- Working as Research Associate at Rights Lab, University of Nottingham from April 2020 onward

- Worked as technical officer at Terra Motion Limited (spin-out company of University of Nottingham) from May 2018 to March 2020

TABLE OF CONTENTS

LIST OF FIGURES

Chapter IV

Chapter V

LIST OF TABLES

ABBREVIATIONS

2D	Two Diamentional
3D	Three Diamentional
ALOS	Advanced Land Observing Satellite
ASTER	Advanced Spaceborne Thermal Emission And Reflection Radiometer
AW3D	ALOS World 3D
BHA	The Building Height Attribute
CDED	Canadian Digital Elevation Data
DEM	Digital Elevation Model
DN	Digital Number
DSM	Digital Surface Model
DTM	Digital Terrain Model
EIA	Environmental Impact Assessment
EO	Earth Observation
EROS	Earth Resources Observation Satellite
ERTS	Earth Resources Technology Satellite
ESA	European Space Agency
GDEM	Global Digital Elevation Model
GEDI	Global Ecosystems Dynamics Investigation Lidar
GIS	Geographic Information System
GMTED	Global Multi-Resolution Terrain Elevation Data
GTOPO30	Global 30 ArcSecond Elevation
ICESat-2	Ice, Cloud And Land Elevation Satellite
ICT	Information and Communication Technologies

JAXA	Japan Aerospace Exploration Agency
LANDSAT ETM+	Landsat The Enhanced Thematic Mapper Plus
LANDSAT OLI	Landsat Operational Land Imager
LANDSAT TM	Landsat Thematic Mapper
LHS	Left Hand Side
LiDAR	Light Detection and Ranging
LOD	Level of Details
MITI	Ministry of Economy, Trade and Industry
MSL	Mean Sea Level
nDSM	Normalised Digital Surface Model
NDVI	Normalized Difference Vegetation Index
NGA	National Geospatial Agency
NIR	Near Infra Red
NTL	Night Time Light
OS	Ordnance Survey
OSM	OpenStreetMap
RHS	Right Hand Side
RMSE	Root-Mean-Square Error
SDG	Sustainable Development Goals
SRTM	Shuttle Radar Topography Mission
TanDEM-X	Terrasar-X Add-on for Digital Elevation Measurements
TOA	Top-of-Atmosphere
UAS	Unoccupied Aerial System
UN	United Nations

USGS	United States Geological Survey
VGI	Volunteered Geographic Information
VHR	Very High Resolution
WV-3	World View-Three

CHAPTER I

INTRODUCTION

1.1 Introduction

Urbanisation refers to a broad based rural to urban transition involving population, land use, economic activity and culture, or indeed any one of these (Mcgranahan & Satterthwaite, 2014; Ritchie & Roser, 2018). Due to rapid urbanisation occurring the World over, achieving urban sustainability is now a global concern (Seto et al., 2017). With the agreement of the 2030 Agenda and the Sustainable Development Goals (SDGs) it is underlined that urban areas play a key role in achieving sustainability (United Nations, 2015). The SDG11, emphasizes the need to 'make cities and human settlements inclusive, safe, resilient and sustainable'.

According to the United Nations, Department of Economic and Social Affairs, Population Division (2019), at the census date of 2018, about 55% of the world population were living in urban areas, with a projected growth to 68% of the population to be urbanised by 2050 (United Nations, 2019). Urbanisation is commonly defined as the percentage of the population that lives in what each national statistics office calls as "urban areas'' (Chauvin et al., 2016) or it is the process by which a large number of people becomes permanently concentrated in relatively small areas, forming cities (Hofmann & Wan, 2013; Seto et al., 2013). The definitions for 'urban' and 'cities' varies among nations and in general cities are considered larger than towns in terms of area, population size, population density, and urban functions.

As cities will most likely continue to be home for a large population, it is of high importance to ensure that they are as liveable as possible, for present and future generations. The concept of sustainability is one approach to secure this significant goal and to be sustainable the cities must themselves, or in the resources, they command, become low carbon, resilient, and liveable (de Jong et al., 2015). A sustainable city is one that can generate the maximum socio economic benefits for its population without losing the environmental and equity parameters, as measured by appropriate indicators (Mori et al., 2015; Mori & Yamashita, 2015).

To achieve environmental sustainability, urban consumption must match or be below what the natural environment can provide, i.e., its carrying capacity (Yigitcanlar & Teriman, 2015). Henceforth, the sustainability of cities is constricted by the biophysical limits and finite resources that the surrounding environment, at multiple scales, can provide. However, cities today are generally not equipped to cope with the present rapid growth (Kammen & Sunter, 2016) and that warrants new ways of living towards sustainable cities. The sustainable approach implies that urban planning should be profound enough to tackle the multiple problems posed by the complexities around the present and future cities. Further, these approaches should be strategic in nature so as to contend with the changes, uncertainties, and multi-faceted challenges of modern cities (Bibri, 2019; Keivani, 2010; Kuddus et al., 2020). The solutions will vary with geography; nonetheless, all will require decision making at unprecedented levels. To assist such decision making data at the relevant scales, accuracy and temporal update are an absolute necessity.

1.2 Geospatial technologies and 3D city models for sustainable city planning

Geospatial data and geographic information systems (GIS) play a key role in urban planning, as well as for building cities (Akanbi et al., 2013; Jensen, 2005; Rai & Kumra, 2011; Sun & Du, 2017). In the digital city era, digital maps and geospatial databases have long been integrated into workflows in land management, urban planning and transportation by the governments (Tao, 2013). It can aid in public policy decisions for more effective allocation of resources, better managed planning and growth, as well as for the efficient delivery and use of public services (Nour, 2011; Un-Habitat, 2010). Geospatial technology has largely developed beyond its applications in urban land use change analysis, urban sprawl dynamics assessment (Ahmad & Goparaju, 2016; Kar et al., 2018), urban facility management (Manonmani et al., 2012), and sustainable transport planning (Ogryzek et al., 2020; Ruhé et al., 2013) to the modelling of urban systems to address the climate change challenges (Ahmed, 2018; Darabi et al., 2019; Hawchar et al., 2020), further to estimate the energy demand as well as to improve the energy efficiency (Dalla Longa et al., 2018; Schneider et al., 2017; Sztubecka et al., 2020).

The potential of geospatial technologies together with improved allied visual and 3D modelling technologies holds far greater promise for sustainable urban management than earlier waves of geospatial technologies (LeGates et al., 2009; Toschi et al., 2017; Yao et al., 2018). A 3D city model is a digital model that represents the urban environment with a three dimensional geometry of common urban objects and structures, with buildings as the most prominent feature (Biljecki et al., 2015; Zhu et al., 2009). The importance of 3D city models is significantly growing as a resource for planning, development and policy making in urban areas. Some of the present applications of 3D city models include environmental, training simulations, energy models, transport planning, navigation, and disaster management. All these applications have a common key goal to ensure sustainable cities in the context of the proportion of global residents present in cities.

1.3 Underpinning research

If poorly managed, urbanization itself can be detrimental to urban sustainability and many literatures already point out that urbanisation and cities will be either critical components or major threats in the transition to sustainability (Seto et al., 2017). Cities around the world are characterised by uneven urbanization. On one hand, cities are sites of economic growth, innovation and knowledge hubs with facilitation of access to employment, education and sanitation, as well as providing opportunities for higher resource efficiency in buildings, green urban planning, and low carbon urban mobility. However, on the other hand, cities can host high levels of pollution, environmental degradation as well as could be the key vulnerability hotspots of climatic change and natural hazards (Baker, 2013; Carter et al., 2015; Creutzig et al., 2015; Kharrazi et al., 2016). Sustainable urbanisation coupled with efficient management and planning will undoubtedly be the viable solution considering the milieu of growing global sustainability issues.

As mentioned in section 1.2, the wide range of applications makes it imperative that 3D city models can aid in sustainable urban management (for example, sustainable energy modelling, climate risk reduction etc). However globally, a huge gap exists among cities in the availability of 3D city models, especially between developing and developed countries which makes it vital to develop a globally replicable method for the generation of 3D city models, since unsustainable cities in one region have impacts elsewhere in the World.

This PhD research forms part of the wider project, 'Sustaining Urban Habitats: An interdisciplinary approach'. The overall aim of the project was to transform our understanding of how sustainable cities can be. The project intended to explore ways of combining environmental and economic modelling with social and cultural ethnographic work considering, one growing city in China (Shanghai) and one transition city in Europe (Nottingham, UK) as the empirical focus. Transition Cities aims cities to be more sustainable, self-sufficient, decarbonise and reduce the potential effects of pea oil and climate destruction (Alexander, 2012; https://www.climate-kic.org/projects/transition-cities/). During the project implementation, the unavailability of 3D city models as well as lack of open source high resolution 2D footprints became an issue for Shanghai, which in turn encouraged the search for solutions to develop a low cost, globally replicable method for 3D city model generation from open data and formed the underpinning research question for this research.

1.3.1 Measurement and data

Appropriate data is very important to gain insight on urban sustainability, as well as to transform our understanding on how sustainable cities can be. Within just the last few decades, the breadth and variety of datasets available for urban studies have expanded significantly. However, much of the research that involves new datasets and methods have focused on activity in Western and East Asian countries resulting in a growing inequality between our understanding of urban contexts in the developed and developing worlds (Manley & Dennett, 2019). The gap exists especially in the availability of different datasets between developed and developing/underdeveloped countries with the cost of data as a large reason. One approach to overcome is to use open data sources that include data from volunteered geographic information (VGI) or crowdsourced geographic information. However, there is a wide global disparity in the incompleteness of these datasets among and even within different countries (Barrington-Leigh & Millard-Ball, 2017). This is even more acute in the 3rd dimension of the data often required; the height of the buildings making up the urban area of focus. The question at this juncture is whether it is possible to generate a 3D city model from open source data, and if so, at what level of accuracy, temporal update, completeness and so on? Thus the major research questions this thesis aim to answer are:

1. Is there open data available to generate a 3D city model?
2. If so, what techniques are needed to generate the 3D city model from these open data?
3. What is the level of accuracy of the generated 3D city models and where these models can be applied in the real world?

The thesis uses the focal cities of Nottingham and Shanghai to explore these questions, with the following aim and objectives:

1.4 Thesis Aim

The principal aim of the study is to generate a 3D city model exclusively using open data with an intent to produce globally transferable methodologies and to discuss the applicability of these 3D city models in the real world.

1.5 Thesis Objectives

The objectives of this PhD are to:

1. Explore the availability of open data that can be used to generate 3D city models
2. Develop applicable workflows that affords the global generation of 3D city data models from these open data
3. Discuss the accuracy, execution and suitability of the different city data models (i.e., levels of detail) produced from open data for use in urban studies.

1.6 Overall methodology

In line with the already stated overarching aim of the research to generate 3D city models from open source data irrespective of the availability of 2D building footprints, the core chapters illustrate the methods to generate 3D city models regardless of the (un)availability of 2D buildings footprints. Figure 1.1 shows an overview of the core chapters.

The thesis is structured as Introduction (Chapter 1), followed by the presentation of literature (Chapter 2) and subsequent three research chapters prior to the final summary and conclusion chapter. The first research chapter (Chapter 3) deals with how to generate a 3D city model in the most ideal conditions where reliable 2D building footprints are available from open source. However, in many cases, reliable 2D building footprints may not be available or may not be complete. In such cases, the user has to depend on other sources including open source low resolution satellite datasets. Low resolution satellite datasets may hamper the proper interpretation of the open source satellite images.

The second core chapter (Chapter 4) demonstrates how to enhance low spatial resolution satellite images through sparse representation techniques. However, difficulties can arise even after the spatial resolution enhancement due to the misclassification of urban features. The third core chapter (Chapter 5) illustrates an innovative approach of combining digital surface models with spatially enhanced satellite images and classification of urban features from the imagery, so as to avoid misrepresentation or misclassification of urban features. The chapter demonstrates the generation of 3D city models through urban classification from spatially enhanced and elevation induced satellite images.

The methods adopted in each chapter are elaborated in detail in relevant chapters.

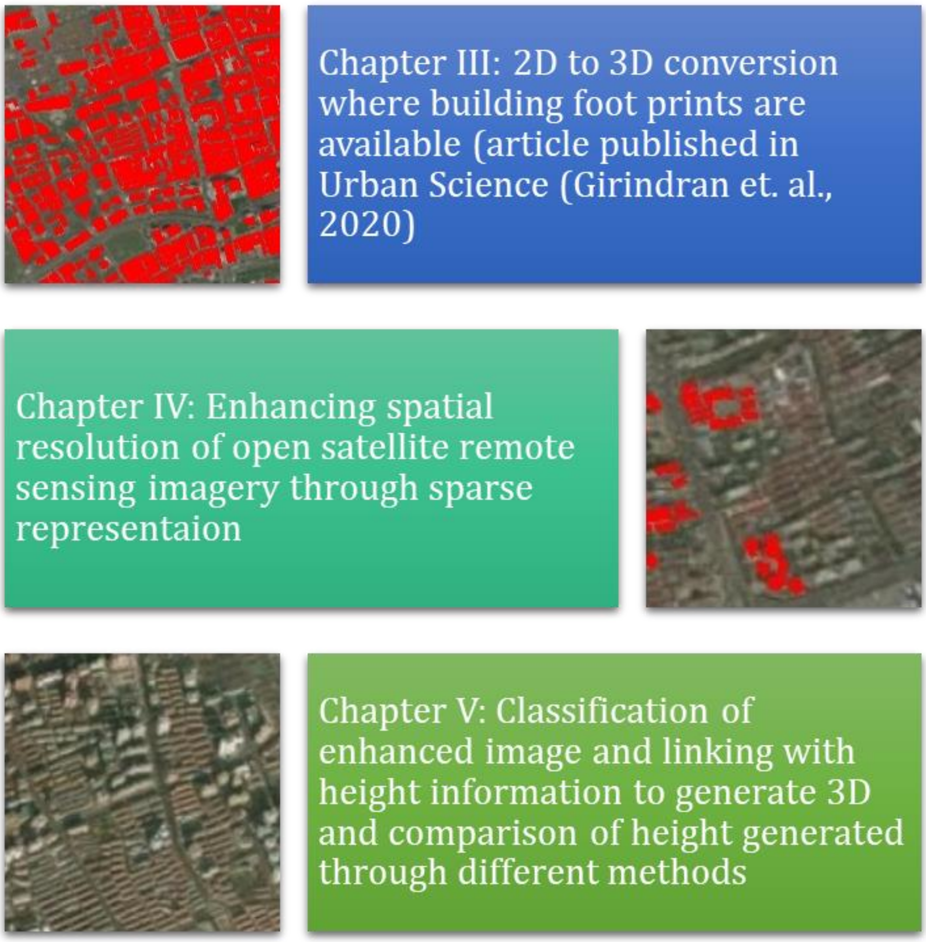

Figure 1.1 Overview of research chapters

1.7 Thesis structure

The thesis is organised into seven chapters as depicted below.

Chapter I covers the introduction, aims, objectives, research questions and overall methodology. The overall methodology provides an overview and rationale for adopting three different methods for the three analytical chapters.

Chapter II presents the literature review and includes information on urban sustainability, the role of geospatial technologies, urban management, the relevance of generating 3D city models from open data, open data sources, and existing challenges with using open data broadly. The chapter also presents a review of spatial enhancement techniques and different urban classification techniques.

Chapter III illustrates the generation of 3D city models from open data with two case study examples of Nottingham, U.K and Shanghai, China. The chapter presents a method to generate 3D city models for the areas that already possess valid open 2D building footprints (for example, OpenStreetMap), digital surface models (for example, AW3D DSM) and digital elevation models (for example, GMTED2010). Further, this chapter also illustrates accuracy enhancement techniques for the generated 3D city model using high resolution satellite data.

Chapter IV presents a spatial enhancement of open data based on sparse representation techniques in order to extract 3D buildings in areas where 2D footprints are not available. The chapter attempts the enhancement of Sentinel-2 satellite image with 10m spatial resolution with a high resolution WorldView III (1m spatial resolution) image for a sample area of Shanghai, China.

Chapter V demonstrates the extraction of 3D city models from enhanced Sentinel-2 image of 1m spatial resolution through the DSM fusion and unsupervised classification. It has three major sections. The first section presents the classification of fused ALOS-30m-DSM with enhanced Sentinel-2 (1m) images to eliminate non-building features based on elevation. Results provide the accuracy difference between 3D city models before and after combining DSM. The second section of the chapter provides a comparison between the accuracy differences of LOD1 3D city model generated using already existing 2D building footprints (mentioned in chapter III) and LOD0 3D city models generated from the satellite data i.e. without 2D building footprints (mentioned in chapter IV and the first section of chapter V). The third section of the chapter presents the LOD1 3D city model generated from fused enhanced satellite data with ALOS DSM and the associated challenges of this method.

Chapter VI provides a comprehensive discussion in relation to the major findings as well as potential areas of application for the present work. The chapter also discusses the potential to improve the research with new datasets.

Chapter VII concludes the thesis. This chapter delivers salient findings and scope of future research.

CHAPTER II

3D CITY MODELS FROM OPEN DATA: STATE OF THE ART AND NEED FOR NEWER APPROACHES

2.1 Introduction

Globally, urbanisation plays a key role in the transition towards sustainability, as urbanisation is also perceived as among the major threats to sustainability (Fuenfschilling et al., 2019; Seto et al., 2017; Soma et al., 2018). The phrase ‘urban sustainability’ fundamentally refers to the sustainability of the urban landscape as a whole (Huang et al., 2015; Wu, 2010). The 2030 Agenda for Sustainable Development, adopted by all United Nations Member States in 2015, recognise 17 Sustainable Development Goals (SDGs) also known as global goals that need urgent actions by all countries to end poverty, protect the planet and ensure that all people enjoy peace and prosperity by 2030 (UN Department of Economic and Social Affairs, n.d.). The SDG-11 particularly addresses sustainable cities and communities, i.e. to "make cities inclusive, safe, resilient and sustainable" and to address many challenges that exist to maintain cities in a way that continues to create jobs and prosperity without straining land and resources. Current urban development trails are often unsustainable and contrary to the UN SDGs as cities are perceived as hotspots for environmental change drivers at multiple scales (Valencia et al., 2019).

The question ‘How to achieve urban sustainability?’ is increasingly gaining attention and has been at the forefront of urban research for at least the last decade. Effective urban planning (Ahmadi & Toghyani, 2011; Diamantini & Zanon, 2000;

Rasoolimanesh et al., 2016), the inclusion of strategic actions in urban development (Rahman, 2016; Roy, 2009), urban facilities management through sustainable community assessment (Boyle & Michell, 2017), urban sustainability assessments (Cohen, 2017), consideration of sustainable transport in strategic planning (Pojani & Stead, 2015) and so on, are among the few of the proposed approaches to achieve urban sustainability. There are arguments that, in order to achieve urban sustainability, it is important to combine the quality of life, resilience and resource efficiency (Koch et al., 2017).

However, managing cities is often difficult as urban systems are highly complex, rapidly changing entities, shaped by a range of regional and global forces often beyond the control of local plans and planners. Many cities in developing countries display the relics of planned modernist urban cores, surrounded by vast areas of informal and 'slum' settlement together with elite, developer driven, commercial and residential enclaves (UN-HABITAT, 2009). Hence, in order to make cities sustainable, need exists for radical, large-scale and integrated changes, which go well beyond traditional policy approaches (Koch et al., 2017; Vanden Bergh et al., 2011). Developing methods and tools that, while sensitive to context, can address the social, ecological, and technical infrastructure complexity of cities are key to advance the goals of urban sustainability improvement, at the global scale (McPhearson et al., 2016).

There are also several misconceptions that city planning is a very costly and time consuming task. Even though many examples from developed country models may require advanced technology, high capacity analysis, wide-ranging modelling, and an extensive amount of resources, that is not the only form of planning. Instead, city plans should go beyond conventional forms of planning and should be able to make use of available resources in cost effective and optimal ways. Modern technologies including information and communication technologies (ICTs) can bring numerous benefits to the cities at a local level, and can support the goal of achieving sustainable cities (Chang et al., 2018). However, the implementation of ICTs as an end in itself is not enough to make a sustainable city (Ahvenniemi et al., 2017). In this context, geospatial data (data about objects, events, or phenomena that have a location on the surface of the Earth (Stock & Guesgen, 2016)) and geographic information systems (GIS) can play a key role in building sustainable cities (Jensen, 2005; LeGates et al., 2009; Rai & Kumra, 2011).

2.2 3D Geospatial data for city planning

As discussed in Chapter I, geospatial technologies together with 3D modelling hold great potential for sustainable city planning. Due to the unprecedented growth of cities, the rapid increase in the need for 3D geospatial information in 3D city planning and development is indisputable (Jones et al., 2009). A three-dimensional GIS simulation can more effectively communicate than two-dimensional forms (Rajpriya et al., 2014). A 3D city model is a digital model that represents the urban environment with a three-dimensional geometry of common urban objects and structures, with buildings as the most prominent feature (Zhu et al., 2009). According to Döllner et al., (2006), 3D city models usually consist of digital terrain models (DTMs), building models, street-space models, and green space models.

A 3D city model can be derived from different data resources, such as LiDAR point clouds (Kada & Mckinley, 2009), airborne captured images (Haala et al., 2015), satellite captured images (Krauß et al., 2009), UAS-captured (unoccupied aerial system) images or a combination of DSM (digital surface model) data with cadastral maps (Buyukdemircioglu et al., 2018). Acquisition techniques used to derive a 3D city model can also be different such as photogrammetry and laser scanning (Rajpriya et al., 2014; Tomljenovic et al., 2016), and volunteered geoinformation (Goetz & Zipf, 2012; Over et al., 2010). While there is no widely accepted taxonomy of (3D) urban models, there are a number of helpful classifications. For example, Meilland et al., (2015) distinguish between 3D parametric models and image based key frame models while Nebiker et al., (2010) distinguish between geometric 3D models, image based models, and a rich point cloud model. Nebiker et al., (2015) introduce the concept and implementation of geospatial 3D image spaces as new types of native urban models. Beyond the difference in data sources and techniques used for 3D model generation, the importance of 3D city models is growing significantly as a resource for planning, development and policy making in urban areas.

2.2.1 3D modelling applications

Several studies focus on the application of 3D modelling in urban studies (Chen, 2011; Czyńska & Rubinowicz, 2014; Rautenbach et al., 2015). Potential applications for 3D city models have moved from electromagnetic propagation for telecommunication to more demanding simulations for acoustic, urban planning, virtual or augmented reality applications (Flamanc et al., 2003; Mao et al., 2009). A conceptual study provided by Batty et al., (2012) segmented the use of 3D city models into 12 categories of endeavour: emergency services, urban planning, telecommunications, architecture, facilities and utility management, marketing and economic development, property analysis, tourism and entertainment, e-commerce, environment, education and learning, and city portals. Some of the significant areas of applications of 3D city models include:

a) Estimation of building geometry and shadow cast: Estimation of shadows cast by buildings is an important utility of 3D modelling as it can be used for assessment of the effectiveness of a planned building onto its neighbourhoods or to estimate the solar potential of buildings (Alam et al., 2012). Further, it can also be used to estimate how much a building is exposed to the Sun which can help to assess the suitability of solar panel installations on roofs (Wiginton et al., 2010).

Geometric information about buildings such as the tilt, orientation and area of the roof etc. can be acquired from 3D models which also enhance its utility for the solar empirical models (Biljecki et al., 2015). Further, 3D city models have a potential application to estimate the internal size of a building including net area, floor space and so on, which is important for energy usage estimation of buildings (Boeters et al., 2015).

b) Energy Demand Estimation: Energy Demand Estimation demonstrates the importance of semantic 3D city models in the estimation of the energy demand of individual level households (Biljecki et al., 2015). In recent years, studies explore the potential of 3D city models to combine the building information like volume and type of buildings, number of floors etc. to predict the energy demand for heating and cooling (Kaden & Kolbe, 2014; Robinson, 2006). Further, 3D city models in combination with other data can be used to determine thermal bridges and heat losses from the building envelope (Biljecki et al., 2015).

c) Climate Change Studies: The application of 3D modelling in climate change studies gains significant attention in recent years. Danahy et al., (2016) investigated the use of 3D city models as a visualization reference against which analytical models were visualized to identify micro scale mitigation scenarios of urban heat island effects in the Toronto region. Masson et al., (2014) noted the usage of the 3D city model in systemic modelling approaches to explore climate change adaptation.

2.2.2 Classification of buildings within models according to level of details (LOD)

CityGML is a common information model and XML based encoding for the representation, storage, and exchange of digital 3D city and landscape models. The CityGML standard defines five Levels of Details (LOD) varying from LOD0 to LOD4 to describe 3D building objects with respect to their geometry, topology, semantics and appearance (Groeger et al., 2008). It also considers generalization hierarchies between thematic classes, aggregations, relations between objects, and spatial properties (Groeger et al., 2008, 2012; Wate & Saran, 2015). As the LOD level of the model increases, it will have more detailed architectural information of the structures. Accordingly, different LODs can be used for different purposes (Buyukdemircioglu et al., 2018).

The coarsest level LOD0 represents the lowest level of geometry as a 2.5D DTM with building footprints or roof edge polygons. LOD0 is mainly used for regional and landscape applications, while LOD1 is well known as the blocks model. In LOD1 the building height would be extruded with flat roofs and is widely used for city and region coverage. Compared to LOD1 models, LOD2 buildings differentiate roof structures as well as boundary surfaces. LOD2 is mainly applicable to city districts. LOD3 has more architectural details including specific roof structures and wall structure details such as doors and windows. LOD3 models are widely used for landmarks. LoD4 has the highest level of detail and all interior details are represented with textures including rooms and furniture (Buyukdemircioglu et al., 2018; Groeger et al., 2012). Figure 2.1 shows LOD1 to LOD4. The data demand increases for each LOD class, and this demand needs consideration with the intended application for the models to be generated.

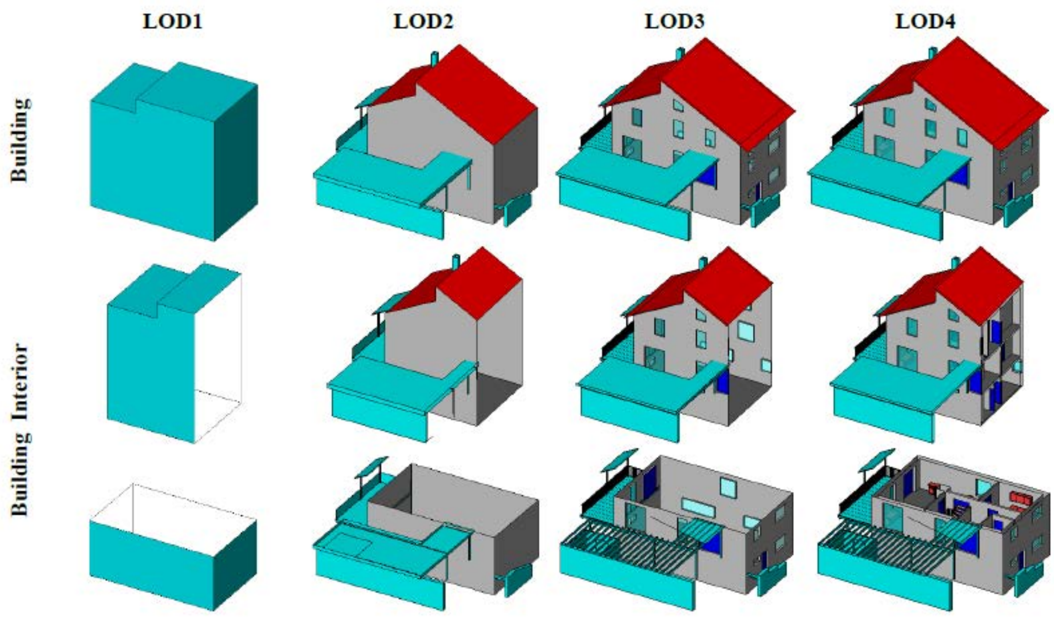

Figure 2.1 LOD Classification (Source: KIT)

2.3 Open data for 3D city model data generation

2.3.1 Need for the 3D city model generation from open data

As previously mentioned (section 2.2), standard techniques for the creation of city models at large scale automatically or semi-automatically commonly includes the use of stereo vision on aerial or satellite remote sensing imagery (Garouani et al., 2014). This can be an expensive and time/labour consuming process, particularly if high levels of accuracy in model outputs are required (Ohori et al., 2015). As a result, large scale

3D city models are mostly available in countries with developed economies and/or those with national mapping agencies. However countries, including many that are transitioning their economies (and where this information is perhaps of most value), do not have the resources available to produce high accuracy 3D city models. In such situations, use of low cost or open source online free satellite datasets as a source of input data for 3D city model generation can be a solution. Especially given that in developing countries, low cost/open source GIS software and free satellite images, which tend to be of lower resolutions than those acquired by commercial companies, are already being used to solve day to day urban planning management and development problems. Hence, open data can be used for possible spatial applications where higher LODs are not required. However, while using the open data, it is important to have an understanding of the types and availability of these datasets.

2.3.2 Existing scenario in open data 3D city model generation and GAP analysis

Digital Surface Models (DSM) and Digital Terrain Models (DTM) can provide elevation data to develop 3D city models. Shuttle Radar Topography Mission (SRTM), Advanced Spaceborne Thermal Emission and Reflection Radiometer Digital Elevation Model (ASTER DEM,) Advanced Land Observing Satellite DSM (ALOS DSM), Global Multi-resolution Terrain Elevation Data (GMTED 2010) are the prominent open source elevation datasets with global coverage and all these are generated from remote sensing as the means of data capture (Table 2.1). Studies show that these open elevation datasets are largely utilised in geomorphological studies, or hazard mapping, or inundation modelling etc. to cite a few (Misra et al., 2018; Yamazaki et al., 2017). However, so far it is apparent that developing 3D city models from open source data have not yet been explored sufficiently, particularly with respect to producing models of appropriate quality for use in aforementioned applications. There are only a few studies that have attempted to extract building heights from open DSMs. For example, Wang et al., (2018) derived 3D building structures by fusing Landsat and global elevation data, while Misra et al., (2018a) attempted a comparison of building heights extracted from open DSMs including ALOS World 3D (AW3D), TerraSAR-X add-on for digital elevation measurements (TanDEM-X), ASTER, and SRTM over Yangon City.

However, usage of open DSMs alone cannot provide exact building heights or shapes. Rather it can result in more generalized individual building heights and distorted shapes due to issues of mixed pixels and low spatial resolution (Misra et al., 2018). Usage of 2D data on building footprints along with high resolution DSMs can be a possible solution to the extraction of individual building heights without distorting building shapes. The recently available open source elevation datasets provide an excellent opportunity for data fusion by incorporating the elevation data with open licensed 2D building data for generating 3D city models. Conversely, so far, no studies have focussed on 3D city model generation using open licenced 2D building footprint data together with open source elevation datasets.

Table 2.1 Properties of open source terrain models

Terrain models	Spatial resolution	Ownership
SRTM	30m and 90m	NASA and NGA
ASTER	30m	METI and NASA
ALOS DSM	30m	JAXA
GMTED 2010	7.5 arc-second (250 m), 15 arc-second (500 m) and 30 arc-second (1 km)	USGS and NGA

2.3.3 Available open elevation data (ALOS DSM, GMTED 2010, ASTER, SRTM)

ALOS DSM: ALOS World 3D - 30m (AW3D-30), the global digital surface model (DSM) with a horizontal resolution of approximately 30-meter mesh (1 arcsec) is released free of charge by the Japan Aerospace Exploration Agency (JAXA). This dataset was generated from the DSM dataset (5-meter mesh version) of the precise global digital 3D map ALOS World 3D" (AW3D), which is the world's first and the most precise 3D map covering all global land scales with a 5-meter mesh (Santillan et al., 2016; Tadono et al., 2014, 2016). In March 2017, AW3D version 1.1 was released filling the void height values with existing DEMs and in April 2018 it has again been upgraded to version 2 (Takaku & Tadono, 2009). Continuous enhancements of AW3D-30 DSM are expected, which can improve its future utility. AW3D-30 DSM also has considerable future potential in sustainable urban development due to its global coverage and open licence.

GMTED2010: GMTED2010 is the digital elevation model produced by The United States Geological Survey (USGS) and The National Geospatial-Intelligence Agency (NGA). It has been available to the public since 2010 and replaces the existing model, Global 30 ArcSecond Elevation (GTOPO30) (Athmania & Achour, 2014; Grohmann, 2016). GMTED2010 is mainly available in three resolutions i.e. with a horizontal spacing of 7.5 arc-second (about 250 meters), 15 arc-second (about 500 meters) and 30 arc-second (about 1 kilometre). The main data source of GMTED2010 is SRTM version with a 01" resolution that is restricted to the NGA and not available to the general public (Khalid et al., 2016).

Other common data sources include the SPOT 5 Reference 3D, Canadian Digital Elevation Data (CDED), NED for the continental USA and Alaska, GEODATA 9 Second Digital Elevation Model for Australia, DEMs for Antarctica and Greenland from laser altimetry (ICESat and GLAS data) and satellite radar (ERS-1 data) (Grohmann, 2016; Khalid et al., 2016).

ASTER DEM**:** The first version of the Advanced Spaceborne Thermal Emission and Reflection Radiometer Global Digital Elevation Model (ASTER GDEM) was introduced to the global user community in July 2009. The DEM was later improved by compilation of over 1.5 million scenes acquired between 2000 and 2009 and was released in 2011 by NASA and Japan’s Ministry of Economy, Trade and Industry (METI) as an enhanced version (GDEM V2) (Tachikawa et al., 2011). GDEM V2 contained additional data with improved spatial resolution and coverage, water body mask as well as improved horizontal and vertical accuracy (Alganci et al., 2018). This data is freely available at a 1-arcsecond posting from NASA’s Earth Explorer. However, studies also report that the advanced version also contains disturbances in the values due to an increased frequency of noise on account of usage of a smaller correlation kernel to enhance the horizontal resolution (Misra et al., 2018). Further, the RMSE accuracy of the ASTER GDEM varies with the location as well as with land cover type (Santillan et al., 2016). For example, the RMSE value for forested mountainous areas is 15.1 while in the case of urban areas it is 23.3 (Jing et al., 2014; Tachikawa et al., 2011).

SRTM: The Shuttle Radar Topography Mission (SRTM) by NASA and NGA (US National Geospatial Agency) acquired a DEM of the Earth at a near global scale, covering about 80% of the Earth's total landmass. According to Rumpler et al., (2012) SRTM produced the most complete digital topographic database of the Earth. Until 2014, the global dataset was available at 1 arc-second resolution (SRTM-1, approximately 30 meters) for the United States and its territories and for the rest of the world at 3 arc-second resolution (SRTM-3, approximately 90 meters). In 2015, Land Processes Distributed Active Archive Center released the SRTM Version 3.0 Global 1-arcsecond dataset (SRTMGL1) (USGS 2015). The RMSE of SRTMGL1 varies from 5.9 m in urban areas to 10.4 m in bushland (Santillan et al., 2016).

2.3.4 Volunteered geographic information (VGI) and OpenStreetMap (OSM data)

The previous section provided an overview of existing open satellite datasets that could be used for the generation of 3D city models. However, apart from satellite data, there are several other sources of data, like governmental agencies or space and remote sensing centres data with varying degrees of availability for different scales and different administrative bodies. For example, most of the town planning offices possess cadastral level building information for their use which is however restricted for public use. Further, the conventional ways of mapping or collection, process and distribution of geographic information are being changed in recent years (Rumpler et al., 2012). In parallel with centralised managed and maintained geographic information there has been a growth in freely available, publicly maintained and voluntarily contributed geographic information (See et al., 2013; Senaratne et al., 2016). According to Elwood et al., (2012), when citizens collect geographic information and contribute it to crowd sourced data sets, to mark geographic locations, to annotate geographic features, or to add a geographic location to photographs by web based mapping interfaces, then these data are generally called volunteered geographic information. The power of the crowd can sometimes be used to derive information that was impossible or at least impractical to obtain by other means (Foody et al., 2013).

OpenStreetMap (OSM) is a prominent example of volunteered geographic information which is a collaborative project to create free editable geographic data (Knerr, 2013). The sites like OpenStreetMap and Wikimapia are empowering people to create a global patchwork of open source geographical information (Goodchild, 2007). OSM creates a set of free to use and editable maps which are licensed under new copyright schemes (Haklay, 2008). The OSM project has attracted more people from the developed world and acquired strikingly comprehensive data on large parts of the developed world. However, earlier studies have shown that other parts of the world are slightly under-represented (Elwood et al., 2012).

Studies report that there is a considerable increase in OSM building data in recent years. For example, there has been a 20 times increase in OSM building data in China from 2012 to 2017 alone (Tian et al., 2019). One of the major concerns in OSM data usage is its quality. Most of the OSM data are provided by non-professionals and hence not just the coverage, but the quality of the data is also questionable (Haklay, 2008; Nasiri et al., 2018; Senaratne et al., 2017). Despite this disadvantage, OSM is a good source of 2D building data, especially where free 2D building data are unavailable, as in China, where authorized building data are not freely available (Tian et al., 2019). Studies also reveal that the rate at which OSM receives contributions from users has been persistently increasing; complemented by OSM community's efforts of collaborative mapping to quality check and quality improvements of the contributions (Arsanjani et al., 2015).

2.4 2D to 3D city model data integration

Having secured open 2D building footprints and open elevation datasets, data integration is further required to generate 3D city models. It is recognized that acquiring data to represent a city area with a high LOD is expensive, complex and time consuming. At present, open data allows for the generation of low LOD city models (i.e. LOD0 or LOD1). In doing so, several queries are raised while generating 3D city models from open data: i) how the 2D data collected from many sources may be matched to generate 3D city models? And ii) how to integrate elevation attributes to 2D building footprints. There are also methods where buildings are directly extracted from DSMs and thereby evading the integration of elevation data with 2D building footprints. The following sections discuss this further.

2.4.1 Normalized digital surface model generation techniques (DSM – DTM)

A common approach for building detection exploits the difference between a digital surface model (DSM) and a digital terrain model (DTM). A DSM represents the three dimensional Earth surfaces that includes all of the terrain and non-terrain objects while a DTM characterizes only the 3D bare Earth topography (Sefercik et al., 2014). The difference between DSM and DTM, called normalized DSM (nDSM = DSM-DTM), is the local elevation which can be used as a threshold to detect building heights (Beumier & Idrissa, 2016). An nDSM contains all objects above the terrain (Geiß et al., 2015). The potential of nDSM with respect to building extraction was explored by few authors using airborne laser scanning data (Yu et al., 2010).

Brédif et al., (2013) proposed techniques to extract polygonal building outlines from raw DSMs as well as demonstrate a scalable and fully automatic process that converts robustly raw DSMs into 3D city models. In the study, they employed nDSM as a method to derive polygonal rectangular building footprints. Sefercik et al., (2014) explored the contribution of nDSM to the automatic building extraction from mono high resolution satellite imagery based on ortho rectified pan sharpened IKONOS and Quickbird high resolution imagery. Further the study revealed that with nDSM, the number of extracted buildings was increased while, the number of falsely extracted buildings that occurred by automatic extraction errors was sharply decreased. In another study, Zheng et al., (2017) use Light Detection and Ranging (LiDAR) nDSM, the 2D building footprint and the high resolution orthophoto to build a 3D city model for the City of Indianapolis, USA. By adopting a novel ridge detection method the study also overcomes the limitation that building reconstruction with coarse resolution LiDAR nDSM cannot be based on precise horizontal ridge locations.

2.4.2 Integration methods of 2D polygons with elevation information

As mentioned in section 2.2.1, 3D city models can be derived from different data sources, such as LiDAR point clouds, satellite images, UAV images or a combination of DSM data with cadastral maps and by different techniques such as photogrammetry and laser scanning. For example initially Haala & Anders (1996) discussed a method to reconstruct 3D city models by combining 2D outlines and aerial images. In the study, to develop the 3D city model, initially, the building ground plans were extracted from digital cadastral maps and subsequently heights of buildings based on their type and location. The following assumptions were included: Garage – 3m, residential buildings and office blocks 9m for the ridge, industrial buildings -15m, church – 12m, tower –

25m, kindergarten – 5m, and others – 7.5m. As the studies were mainly based on assumptions of building heights, the results were further verified with aerial images and matched against the lines of the object model for missing information. They concluded that image interpretation is far from being solved in complex areas like built-up regions. However, they also stated that due to increase in digital data availability 3d building reconstruction will gain more importance in future applications which proved to be true in later years.

In 1999, Stilla & Jurkiewicz demonstrated a different method for generating building models from large scale vector maps and laser altimeter data. They analysed the vector map to group the outlines of buildings and to obtain a hierarchical description of buildings or building complexes. Further, the base area has been used to mask the elevation data of single buildings and to derive a coarse 3D description by prismatic models. Later in 2009, Alexander et al., combined building footprints and LIDAR elevation data to visualise buildings and to classify roof structures. According to their results, high density LiDAR yielded the highest overall accuracy of building type detection and proved useful in identification of roof features; yet lower densities proved more useful to reveal the overall roof morphology.

Subsequently, Ledoux & Meijers, (2011) identified the extrusion of building footprints as one of the simplest methods to construct a 3D city model. Constrained triangulation was used, which is conceptually simple as well as offers great flexibility to create city models in different formats so as to develop a new extrusion procedure to construct topologically consistent 3D city models. Usage of existing 2D footprints and to extrude the footprints with a given height is a general procedure for 3D building construction.

The problem with this approach is that the detail of roofs cannot be modelled. However, this approach is very fast and sufficient for applications that do not need high LODs or many details (Stoter & Zlatanova, 2009).

Recently, a study from Bagheri et al., (2019) exploited the possibilities of fusing OSM data with DEMs. They derived the heights of building outlines from fused DEMs. Steps taken to derive building heights included classification of points' heights that are located inside and outside building outlines and exclusion of points located outside building outlines. For this purpose, they used heights derived from the TanDEM-X mission. Further they also implemented two DEM fusion experiments to improve the quality of TanDEM-X in urban areas. First is to fuse the TanDEM-X and Cartosat-1 DEMs and the second experiment was to fuse multiple TanDEM-X raw DEMs. Their results confirmed the quality improvement of TanDEM-X after DEM fusion.

2.4.3 Validation techniques for 3D city model data

The applications of 3D city models is growing rapidly and reliable data is crucial for the successful performance of modern applications. Hence, quality assessment of generated models becomes obligatory for the effective utilisation of these new models. According to Wagner et al., (2013), although quality standards for geospatial data have been published in the ISO 19100 series, there is no common understanding of quality for 3D city models.

Wagner et al., (2013) provide a validation process for the geometry of 3D city models. The modelling guidelines and recommendations based on the modelling handbook of SIG-3D Quality Working Group 2012 for the features in CityGML to define exact specifications for a new city model were followed. Subsequent to the creation of the model, validation of the model was undertaken with specifications defined in the handbook. Wagner et al., (2015) presented methods to validate common geometric requirements for building geometry. The different checks were developed based on several algorithms for the software tool CityDoctor. The checks mainly included polygon level checks to validate the correctness of each polygon in 3D city models. Ledoux, (2018) presented an open source software ‘val3dity’ to validate 3D primitives according to the international definitions of ISO19107. Val3dity also supports a few GIS input formats and the validation reports have been designed to help users easily identify errors (Ledoux, 2018).

However, different approaches and tools are in place for validating 3D city models. For example, in a study by Michelin et al., (2013) on quality evaluation of 3D city building models, with automatic error diagnosis validation of 3D features was done by using corresponding images. High radiometric discontinuities in images such as building edges, road marks, zinc roof battens etc. were considered. In another study, Buyukdemircioglu et al., (2018) did the validation of 3D city models based on reference data. Usage of software tools to validate 3D city models is also common. For example, Murshed et al., (2018), in a study on modelling, validation and quantification of climate and other sensitivities of building energy models on 3D city models, validated the model by simulation software TRNSYS. Janečka, (2019) used an open source geometric validation software val3dity for 3D model validation. Val3dity software is in accord with the international definitions of ISO 19107 (Ledoux, 2018).

2.5 VGI scenarios and possibilities for open data generation in VGI lacking areas

2.5.1 Accuracy of volunteered geographic information (VGI)

The main concern with VGI data used to be that it allows people with little knowledge in geographic information to contribute to the creation of maps that are made publicly available (Foody et al., 2013; Vandecasteele & Devillers, 2013). Hence as VGI was unlike in the past, where mapping was done by professional cartographers, it brought significant initial skepticism on the data quality.

Hence, despite the great potential of VGI, it has not been widely used due to the uncertainty over its data quality (Fonte et al., 2017; Haklay, 2008; Vandecasteele & Devillers, 2013). The highly variable quality of VGI data can create several challenges to potential end users who are particularly concerned about the validation and the quality assurance of the data which are collected (Eshghi & Alesheikh, 2015).

Furthermore, since the beginning VGI was perceived as datasets characterized by several lacking compared to earlier versions of professional maps. For example earlier studies showed that in VGI data some areas can be well mapped while others not (Goodchild, 2007), which is often the case with more data collection in urban areas than in rural areas (Neis & Zielstra, 2014). It can also be seen that popular and tourist areas get more attention. Studies on OSM from Europe have noted that dense areas appear to be better mapped (Neis et al., 2012). Studies also highlighted that VGI is characterized by lack of uniformity and included heterogeneous data (Fonte et al., 2017).

Further other issues pointed out included biases of contributors are influenced by several factors including access to, and knowledge of, digital resources, the language of the VGI application, cultural differences and how much time users have to participate (Zook & Graham, 2007; Zook & Breen, 2017). All these factors may ultimately feed to spatial biases and influence the data quality and accuracy of VGI. Further, there are no data specifications or standard way in which the data are collected, which vary between the places and contributors as well as also within initiatives (Fonte et al., 2017). For example Ballatore et al., (2013) and Mooney & Corcoran, (2013) also state how different names sometimes represent similar geographical categories (for example forest and wood) whilst sometimes the same names may represent different attributes. Therefore, the quality as well as attributes of VGI data can be unclear and can vary over space and time (Ballatore et al., 2013).

While the accuracy of VGI data remains something of consideration, the growing popularity of VGI projects such as OSM changes traditional geographic information (Vandecasteele & Devillers, 2013) and it can also be a valuable source of open data for 3D city model construction, provided the quality of the data can be assessed and enhanced. A study by Fan et al., (2016) demonstrated that the building footprints data on OSM has a high degree of completeness and semantic accuracy. Further it was stated that, with respect to shape, OSM building footprints have high similarity to those in authoritative data. Moreover, OSM also has information about building height and roof structures, which is required for the 3D city model reconstruction. This information could be further enriched and used for 3D city models while introducing related information from other VGI projects, such as Flickr, WikiMapia, Panoramio etc (Fan et al., 2016).

2.5.2 Existing coverage of VGI in developing and developed world

The sharp increases in VGI contributions have led to a number of diverse platforms that utilises the data in spatial decision making, participatory planning and citizen science (Neis & Zielstra, 2014). Among many VGI projects, OSM has grown into one of the most well-known, popular and largest VGI projects. OSM, provides good coverage in urban areas while considering particular completeness factors (Barron et al., 2014; Zielstra et al., 2013). However, when it comes to different regions of the world, results can potentially vary significantly. Studies point out that European cities provide quantitatively larger amounts of geodata and number of contributors in OSM, resulting in a better representation of the real world in the dataset (Barrington Leigh & Millard Ball, 2017; Zhuo et al., 2018, 2018). Reports of European countries have found that the network is virtually complete, and is comparable to or better than official or proprietary data sources (Graser et al., 2015; Neis et al., 2012). One way in which several countries achieved a large data collection in OSM was by importing commercial or governmental road network datasets that comply with the OSM license (for example Netherlands and Austria). While Spain and France have imported the cadastral building information to the OSM database.

Another reason for the higher level of completeness in Europe is a large number of contributors from Europe. It was reported in 2012 that among the total contributors, three-quarters of the contributors were located in Europe (Budhathoki & Haythornthwaite, 2012; Neis et al., 2012). The remaining quarter was distributed over North America and Asia. South America, Africa and Oceania proved to have only a small contributor number. Within Europe, the highest concentration of active contributors in OSM can be found in Germany (25% of all active OSM members) which also explains the higher quality of the German OSM dataset (Neis & Zielstra, 2014). Fan et al., (2016) observed that according to the statistics, the number of buildings in OSM are above 200 million, among which 18.4 million building footprints are in Germany.

However, when it comes to other parts of the world, such as China, Tehran and Brazil, the completeness of OSM is not as good as Europe (Camboim et al., 2015; Forghani & Delavar, 2014; Zheng & Zheng, 2014). Barrington Leigh & Millard Bal (2017), estimated that globally about 77 countries among 185 have more than 95% of completeness of OSM road map. They also observed that countries like Kiribati, Afghanistan, Egypt and China have less than one third completeness. Further the studies also revealed that not just developed countries have the maximum completeness but also areas with dense population and low income that faced humanitarian disasters. For example, Nepal and Haiti had intense mapping efforts following humanitarian disasters (Mooney & Corcoran, 2013). In case of developing countries, VGI contributions tend to be made in spurts, and also as previously mentioned, in response to a country that enters the global spotlight, as may be the case in the aftermath of a natural disaster (Verrucci et al., 2016), rather than as a regular, continuous process (Mahabir et al., 2017). The recent 'Mapathon VGI project' introduced by the Government of Kerala, India (https://mapmykerala.in/about) after the disastrous floods in 2018 and 2019 also serves as an example of the above mentioned argument.

However, studies also reveal that OSM data are increasing all over the world. For example, a very recent study by (Tian et al., 2019) proves an almost 20 times increase in the OSM building count in China from 2012 to 2017. Research by Arsanjani et al.,

(2015) projects many more contributions to OSM in the coming years. They also state that in the future more users will be involved in OSM mapping with contributions having more attributes that will be revised and edited by a greater number of users. However, due to several factors such as the lack of uniformity in attributes, diversity in spatial coverages (Barrington-Leigh & Millard-Ball, 2017), biases of contributors (Neis & Zielstra, 2014), unequal distribution of digital infrastructure (Haworth et al., 2018) etc. it is not possible to ensure the equal availability and quality of VGI data all over the world. Although it was shown that realistic estimates of land cover data and map accuracy can be derived easily and cost effectively (Foody & Boyd, 2013), as mentioned in the previous section, the quality and accuracy of VGI data can be varied in relation to the skills, knowledge and enthusiasm of the volunteers (Foody et al., 2013; See et al., 2013, 2016). The work also highlights the potential of satellite remote sensing to provide spatially and temporally detailed information on the Earth's surface as well as the requirements to generate building data from other reliable sources like open source satellite images.

2.5.3 Satellite images for urban studies

Satellite images can provide an important source of data for urban infrastructure and transportation system planning, monitoring and implementation, mapping individual settlements and internal roads, urban complexes, urban utilities and urban land use (Al-Bilbisi, 2019; Elfadaly & Lasaponara, 2019). Long before it was recognised that, in several countries, the lack of reliable mapping is a serious constraint to development in many sectors, particularly within the fields of urban development, planning and management (Maktav et al., 2006). Urban spaces are the areas developing most dynamically. No country can afford to update its maps at the same pace that development and land use changes occur. The largest cities of the industrial world share this same problem with the megacities of the developing world. Maps are often out of date before they are distributed. This is where the highest demands are made on geodata in terms of their actuality and spatial resolution. Very high resolution satellite imagery provides the wherewithal to keep the urban geodata inventories up to date and to document them.

Even before decades numerous studies have shown that satellite images are valuable tools for urban planning purposes. For example Maktav et al., (2006) illustrated map production and map updating in Turkey and also the importance of the use of satellite images for urban planning and detection of changes in ground features and further integration with existing maps into Geographic Information Systems. The study explained the relevance to utilise satellite images where traditional maps are old or non-existent. The scope of high resolution SPOT images in preparation of urban maps has been discussed as early as 1980's by Bertaud, (1989) based on a case study from Karachi, Pakistan. This study also highlighted how easily computerised information systems can be shared and updated among different planning agencies.

The scope of remote sensing have subsequently improved later with developments high resolution satellite images however low resolution of open data still remained a challenge. A study by Malarvizhi et al., (2016) explored and recommends the possibilities of extraction of information on urban changes from high resolution Google Earth data at instances where obtaining high resolution imagery are either comparatively costly or available open source free imageries are of low or medium resolution. In addition to these, studies also have shown satellite based indicators can be helpful to improve urban planning and management. Chrysoulakis et al., (2014) proposed satellite based indicators which have the potential to support assessments of urban environmental quality and the quality of life and further to provide useful information to urban planners and decision makers that can be exploited in sustainable urban planning. They suggested that although field data are important to climate change mitigation and adaptation activity, Earth Observation indicators can support urban planning, by saving time, reducing costs and providing higher flexibility, and have the potential to play an important role in managing land cover, designing the urban environment, transportation networks and sustainable development of economic, social and environmental initiatives.

2.5.4 Satellite data for land cover extraction

High resolution urban land cover maps have important applications in urban planning and management (Hu et al., 2016; Sztubecka et al., 2020; Zhuo et al., 2018). Information about land cover and land use concerns many groups of people like local governors, land managers, urban planners and decision makers, especially those in the urban areas that are undergoing dramatic land cover and land use changes (Tan & Wang, 2007). Numerous studies deal with the usage of satellite images in land use extraction in urban areas across the globe. To cite a few: Ahadnejad Reveshty, (2011) assessed and predicted the land use changes to urban areas based on LANDSAT datasets with a case study from Iran. Fonji & Taff, (2014) analysed LANDSAT data to detect the land use changes in North Eastern Latvia. Li et al., (2015) record annual urban dynamics of Beijing City, China based on LANDSAT images. Feltynowski, (2017) discusses the need for satellite images for land use planning and green area protection based on a case study from Poland.

Jacobson et al., (2015) used Google Earth grids to identify anthropogenic land use conversions in East Africa, while a similar study has been done by Malarvizhi et al., (2016) considering Chennai City, India. An earlier study conducted in Beijing by Tan & Wang, (2007) evaluated the feasibility of hyperspectral satellite imagery for urban land use/land cover mapping and compared the performance of multispectral and hyperspectral data in urban studies. The results showed that hyperspectral satellite imagery is suitable for urban land use/land cover mapping. They further argued that the hyperspectral satellite image provides more accurate classification results than those extracted from the multispectral satellite image in urban land use mapping. Hu et al., (2016) developed a protocol to identify urban land use functions over large areas by satellite images and open social data which was tested in Beijing, China. The results showed that the generated land use map had an overall accuracy of 81.04% and 69.89% for Level I and Level II classes, respectively. They also argued that the map revealed significantly more details of the spatial pattern of land uses in Beijing than the land use map released by the government. Thus the satellite data can be well used to differentiate various urban land cover classes including types of buildings.

2.6 Open source satellite data: the need for accuracy enhancement

Section 2.3 provides an overview of the availability of open source elevation data from satellite remote sensing. The main objective of acquiring these elevation datasets is to infuse elevation to the open source 2D building footprint datasets to generate 3D city models. However, as discussed before, the availability of open source 2D building footprints can be restrictive and open satellite data can be used as a source to generate 2D building footprint in data void areas. The next section provides an overview of available open source satellite datasets as well as the need to enhance their accuracy for effectively generating 2D building footprints.

2.6.1 Open source satellite data: spatial resolution

2.6.1.1 Landsat: The launch of the Earth Resource Technology Satellite (ERTS) 1, later called Landsat 1 in July 1972, has been widely recognised even many decades before in remote sensing applications such as land cover classification (see for example Goward et al., 2001; Haack, 1982). The main aim of the Landsat satellite program is to provide a tool for continuous monitoring of Earth's resources (Masek et al., 2006). The U.S. Landsat archive is held at the United States Geological Survey (USGS) Earth Resources Observation and Science (EROS) Center and contains > 5.6 million acquisitions sensed by Landsat-1 through Landsat-8 (Dwyer et al., 2018).

Landsat images are constantly improving in terms of their spectral, spatial, radiometric and temporal resolution (Hansen & Loveland, 2012; Z. Zhu et al., 2016). The spatial resolution of Landsat MSS is 60 m while Landsat TM, ETM+ and OLI have spatial resolutions of 30 m. Additionally, Landsat ETM+ and OLI have a panchromatic band with spatial resolutions of 15 m which can also be used to improve the spatial resolution of other bands using pan-sharpening technique (Wulder et al., 2019). Further in 2008, the Landsat data policy changed and the Landsat archive became free and open (Woodcock et al., 2008). Free and open access has greatly benefited operational applications, scientific studies, and discoveries as informed by analyses of large numbers of Landsat images (Wulder et al., 2018; Z. Zhu et al., 2019).

2.6.1.2 Sentinel-2: Sentinel-2 is an earth observation mission developed by the European Space Agency (ESA) as part of the Copernicus Programme to perform terrestrial observations in support of services such as forest monitoring, land cover changes detection, natural disaster management, humanitarian relief operations, risk mapping and security concerns. The launch of the Sentinel-2 has dramatically changed the landscape for land observations (Wulder et al., 2018). This has a temporal resolution of 10 days with one satellite and 5 days with two satellites. The spatial resolution varies between 10m, 20m, and 60m depending on the spectral bands with a swath width of 290km (https://earth.esa.int/web/guest/missions/esa-operational-eo-missions/sentinel-2). The sentinel 2 satellite has a multi spectral Earth observation system featuring the Multispectral Instrument with 13 bands spanning from the visible and the near infrared to the shortwave infrared bands.

2.6.2 Open source satellite data: Need for spatial resolution enhancement

The precise detection of buildings is of great importance to urban planning and management, urban cadastral management, urban geo-database updating, disaster risk assessment and rescue (Huo et al. 2017). With the increasing abundance of high-resolution remote sensing images and the gradual reduction of acquisition costs, the research on extracting buildings using high-resolution images has been rapidly developed (Ding et al. 2018). High resolution remote sensing images contain a large amount of spectral, structure, and texture information and they provide more potential for accurate building detection (You et al. 2018; Song et al. 2019). However the low resolution of open satellite data restricts their utility in building detection as that of high resolution images. Thus it is important to develop methods to increase the resolution of open satellite data to make use of their full potential.

2.7 Summary

Literature shows that there is a dearth in the availability of low cost open 3D city models. With the rapid increase in the applications of 3D city models, it is increasingly important to develop low-cost 3D city models. One of the options to generate low cost 3D city models is to depend on open 2D building footprints. However, existing open data from VGI does not provide complete and reliable coverage of areas. Even though open source satellite datasets have great potential for generating 2D building footprints, their low spatial resolution may pose a challenge in generation of 3D city models. Therefore it is important to find methods to enhance the accuracy of open source satellite data to bring them to maximum use.

In this context, forthcoming core chapters focus on addressing three major issues in line with thesis objectives. Firstly, there are no low cost open source 3D footprints are globally available; Secondly, like discussed before, availability of open 2D building foot prints are not uniform worldwide which prevents generation of 3D city models using 2D open data globally; Thirdly, although open source satellite data can be used to generate 3D city models their coarse resolution is restricts its utility. Hence, this thesis will contribute in filling these research gaps by 1) exploring the availability of open data that can be used to develop a 3D city model and demonstrate developing a 3D city model for the areas where 2D footprints are available, 2) generating 2D footprint data for the data-poor regions using available open satellite data after enhancing them through sparse representation, and 3) developing 3D city models from enhanced open satellite data.

CHAPTER III

GENERATION OF 3D CITY MODELS FROM OPEN SATELLITE DATA

3.1. Introduction

Three-dimensional city models have become an important resource for planning, development, and policymaking in urban areas (Albert et al., 2017; Garouani et al., 2014; Jones et al., 2009; Liang et al., 2016; Oosterom, 2013). A 3D city model is a digital model of an urban environment with a three-dimensional geometry of urban structures, as well as related objects belonging to urban areas (Mittal, 2019). Applications using 3D city models have increased in their scope and complexity (Buyukdemircioglu et al., 2018), spanning from the analysis of electromagnetic propagation for telecommunications through environmental simulations analysing irradiation distribution (Compagnon, 2004; Robinson, 2006) and noise propagation (Kang, 2000) to virtual or augmented reality applications (Flamanc et al., 2003; Mao et al., 2009). This proliferation of applications is, in turn, driving an increasing demand for the creation and maintenance of reliable 3D city models.

A standard approach to creating city models at a large scale automatically or semi-automatically is to apply stereo vision on aerial or satellite remote sensing imagery (Garouani et al., 2014). This, however, can be an expensive and/or time/labour-consuming process, particularly if high levels of accuracy in model outputs are required (Singh et al., 2013). As a result, large-scale 3D city models are mostly available in countries with developed economies and/or those with national mapping agencies, while countries, including many that are transitioning their economies (and where this information is perhaps of most value), do not have the resources available to produce them (Albert et al., 2017). An approach underpinned by suitable open data could fill this gap in capability.

Three-dimensional city models are characterized by their level of detail (LOD) (Ohori et al., 2015). The CityGML standard defines five levels of details (LOD) from LOD0 to LOD4. The coarsest level, LOD0, represents the lowest level of geometry as a 2.5D DTM (digital terrain model) with building footprints or roof edge polygons. It is used for regional and landscape applications. LOD1, is well-known as a block model. In LOD1, the building height would be extruded with flat roofs. It is used for city and region coverage. In LOD2, buildings have differentiated roof structures and thematically differentiated boundary surfaces based on LOD1 models. It is applicable for city districts. LOD3 will add specific roof and wall structure details, such as doors and windows, to LOD2 models and it denotes architectural models. This one is widely used for landmarks. LOD4 gives interior structures, like doors, stairs, etc., within the buildings (Groeger et al., 2008, 2012; Wate & Saran, 2015). An increase in the LOD of a model enables more applications, but it also increases data demands and their processing involves higher computational costs (Biljecki et al., 2014; Ohori et al., 2015; X. Zhao et al., 2018).

Many applications of 3D city models require only low level of details—LOD1 (e.g., vulnerability models, disaster mitigation, climate change and energy models). Here, we investigate the production of spatially reliable and globally replicable 3D city models using open-licensed data in order to support that category of user. This research forms part of a wider project, ‘Sustaining Urban Habitats: An interdisciplinary approach’, which aimed to explore ways of combining environmental and economic modelling with social and cultural ethnographic work. The focus of the project was on two contrasting cities: a growth city in China (Shanghai) and a relatively stable city in Europe (Nottingham). During the implementation of the wider project, the dearth of accurate 3D models for many cities globally, including Shanghai, was observed. The project had very little budget to acquire data and thus raised the challenge of how to produce a 3D city model from open data. This study did not aim to alternate commercial 3D city models with 3D city models from open data, instead, it focused on presenting a method that produces 3D city models from open data (only) to serve those regions that cannot acquire commercial data. Given that open datasets are usually characterized by low resolution, we present a method capable of producing the desired LOD 1 city model for anywhere.

Possibilities of extracting building heights from open digital surface models (DSM) and digital elevation models (DEM) have previously been attempted (Misra et al., 2018; Wang et al., 2018). These include extraction of building heights from the Shuttle Radar Topographic Mission (SRTM), the Advanced Spaceborne Thermal Emission and Reflection Radiometer Digital Elevation Model (ASTER DEM), Advanced Land Observing Satellite (ALOS) World 3D (AW3D) DSM, and TerraSAR-X add-on for digital elevation measurements (TanDEM-X). However, using DSMs alone cannot provide exact building heights or shapes. Rather it will result in more generalized individual building heights and distorted shapes due to issues of mixed pixels (Misra et al., 2018). Using 2D data of building footprints along with high resolution DSMs can be a possible solution to extract individual building heights without distorting the building shapes. The approach is predicated on the availability of open-source 2D spatial datasets, such as OpenStreetMap (OSM), albeit with varying degrees of completeness and reliability, to provide building footprint geometries. However, the third dimension is poorly represented in these datasets; less than 2.5% of the nodes in the OSM database carry an elevation attribute (Knerr, 2013; Mehlhorn & Sanders, 2007).

The recently available satellite-derived elevation datasets provide an opportunity for data fusion by incorporating the elevation data with open-licensed 2D building data to generate 3D models. Indeed Bagheri et al., (2019) generated LOD1 height values using multisensor and multimodal DEM fusion techniques - TanDEM-X DEM and Cartosat-1 DEM data were joined with OpenStreetMap building footprints (Bagheri et al., 2019). This study confirmed that simple, prismatic building models can be reconstructed by combining OpenStreetMap building footprints with remote sensing-derived geodata. However, the assumption of a flat terrain at a constant height restricts globally applicability of this approach. Furthermore, Cartosat-1 data are not currently global in availability. Required, therefore, is a methodology that considers the terrain underlying the urban area of interest and uses datasets that are available worldwide.

In this chapter, we used open DSM data as a foundation dataset and utility in a globally replicable methodology to generate 3D city models. Recently available elevation datasets such as the AW3D DSM (with a horizontal spatial resolution of approximately 30 m) by the Japanese Aerospace Exploration Agency (JAXA) have an open license (a higher resolution (approx. 5 m) DSM is also produced, but only as a commercial product (Santillan et al., 2016). Other common elevation-rich datasets include the ASTER DEM and that from the SRTM. Although these provide mainly terrain (a digital surface model includes all the natural and built features on the earth's surface, whereas a digital terrain model is simply an elevation surface representing the bare earth referenced to a common vertical datum (https://gisgeography.com/dem-dsm-dtm-dierences/) elevation values that are freely available under permissive data licenses (Gruen, 2012). We present a methodology that uses open data of 2D building footprints, along with DSM and DTM datasets, to generate 3D buildings in two geographically and morphologically diverse cities, namely the Huangpu district in Shanghai, China, which has a relatively flat topography, and Nottingham, United Kingdom, which has a more undulating terrain. Shanghai and Nottingham are inherently different from each other, not only in terms of physiography but also in terms of level of urbanization. While Shanghai is a rapidly urbanizing city, Nottingham is stabilized and saturated. Hence, these two cities provide end members to transfer the methods globally.

A secondary objective was to consider scenarios of data availability that could improve the overall accuracy of the open source 3D building model generated (which we call a foundation model). Here, we exploited that often higher resolution elevation data are available, though not always, or never, open source, and/or of limited spatial coverage. For instance, there are a number of examples where previously proprietary LiDAR datasets are now being opened, though often these are for cities in the global North (https://gisgeography.com/top-6-free-lidar-data-sources/), or it may be the case that projects to produce 3D city models have a limited budget. Further, here we used the AW3D-30 DSM to generate building heights. AW3D-30 DSM is produced by resampling the 5 m ALOS DSM, resulting in accuracy reduction. Thus, it is not possible to use this low resolution DSM directly in the same way you would with a high resolution commercial dataset. From high resolution DSMs, roof heights or building heights could be easily measured. Whereas, in low resolution ALOS DSM, this is not possible. This study thus also explored the optimal approach to using the AW3D-30m DSM.

3.2. Materials and methods

3.2.1. Study area

The focus was on two cities of very different scale and character: Nottingham in the UK and Shanghai in China. These two cities also differ considerably with respect to data availability. The diverse topographical and urban morphologies of the two cities afforded a robust assessment of the methodology presented in this chapter to produce 3D city models openly.

The city of Nottingham (Figure 3.1) is located 206 km to the north of London, in the East Midlands region of the UK. The city has a total area of 75 km2 and accommodates a total population of 325,000 (ONS Mid-Year Population Estimates). Nottingham is situated on an area of low hills along the lower valley of the River Trent and has an undulating topography. The average elevation of Nottingham is about 61 m (http://www.floodmap.net/Elevation/ElevationMap/?gi=2641170). Although the population of Nottingham City has recently grown (by 13% between 2000 and 2010 according to the Nottingham City Economic Review, 2011), compared to Shanghai, the city is less agglomerated with greater proportions of small (i.e. buildings less than 10m) and medium sized buildings (10m to 35m), and far fewer high-rise buildings (buildings with a height of 35m or more are classified as high rise buildings). Shanghai is also almost two orders of magnitude larger than Nottingham. Four wards were selected from Nottingham that represent the spatial characteristics of the city.

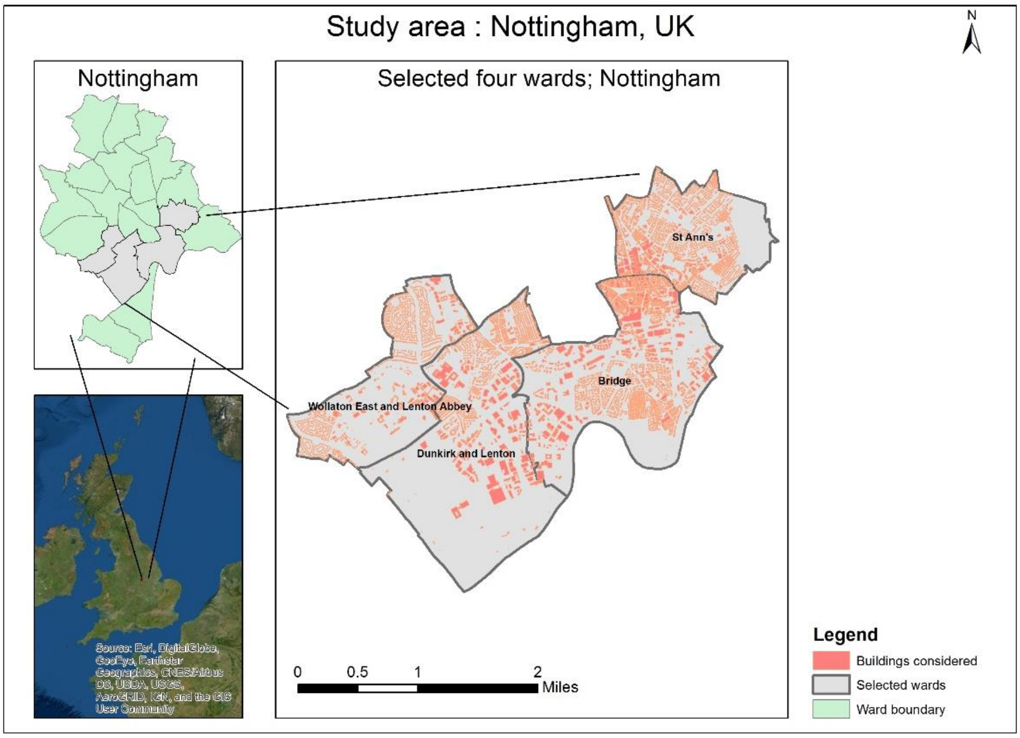

Figure 3.1 Location map of Nottingham, U.K

Shanghai (Figure 3.2), located on the east tip of the Yangtze River Delta and on the east coast of China, is one of the most urbanized areas in China. Being one of the most dynamic cities in the world, it is a difficult city to understand, plan, and manage (Morais, 2016). With a total area of 6340 km2, it is one of the fastest economically growing and most densely populated cities in East Asia. In 2014, it had a population of more than 24 million. The average elevation of the city varies between 3 to 5 m above mean sea level. At present, Shanghai has 16 districts and one county (Chongming) under its jurisdiction. In the first instance, our focus was on the Huangpu District, due to the complexity of the morphology and environs across this area. Huangpu covers an area of 20 km2 and is located in the city centre. It is comprised of a mixture of very tall buildings (more than 100 m), as well as very old and clustered buildings.

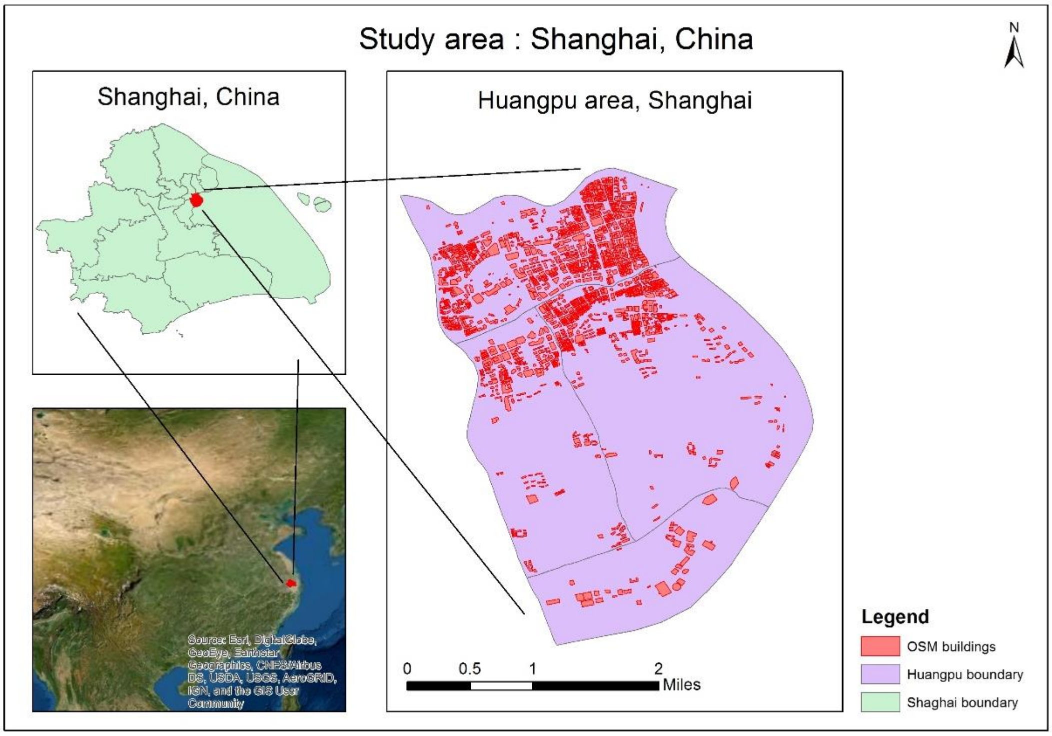

Figure 3.2 Location map of Shanghai, China

Unlike Nottingham, Shanghai is characterized by flat topography and the average elevation of the city's terrain is four meters above mean sea level (MSL). While Nottingham is less agglomerated, with greater numbers of medium and small sized buildings and far fewer high-rise buildings, Shanghai is occupied by a very dense and complex morphology with large numbers of medium and tall buildings. The availability of open data, including OSM, is very limited and non-uniform in coverage for Shanghai, particularly in comparison with Nottingham. Thus, Shanghai is an ideal case to be compared with Nottingham to gain insights on how our methodology may work across the spectrum of cities in their geographies and morphologies.

3.2.2. Data

A DSM affords the extraction a variety of features, including terrain, buildings, vegetation, and any other surface features (Albert et al., 2017). Hence, the basic principle in obtaining the building heights from the AW3D DSM data was to remove the ground elevation from the DSM. For cities that have a flat terrain, the building heights can be generated by simply subtracting a mean ground elevation from DSM values. Whereas in the case of topographically varying city terrains, digital terrain models (DTM) can be used to obtain the ground elevation. DTMs are similar to DSMs, but exclude surface features.

Thus, the datasets to be used with the OpenStreetMap data for Nottingham and Shanghai to produce globally replicable 3D city models were: (1) The open source AW3D-30 DSM, which has a spatial resolution of 30 m and (2) the open source Global Multi-resolution Terrain Elevation (GMTED2010) dataset - the minimum value layer. Although this has a resolution of 225 m, it is used since it is a globally applicable dataset. In addition to the globally available AW3D-30 DSM and GMTED2010 DTM datasets, we explored how additional datasets could enhance the quality of the 3D city models produced for both Nottingham and Shanghai under different scenarios of data availability. For the city of Nottingham, airborne LiDAR-generated DSM and DTM (2 m spatial resolution) were used and for Shanghai a commercial high-resolution DSM (AW3D Enhanced at 2 m spatial resolution) was procured and used. For validation of the 3D city models produced, the BHA MasterMap data set and the AW3D Enhanced were used for Nottingham and Shanghai, respectively. The composition and provenance of all datasets are described below and further details about their purpose is given in Table 3.1.

Table 3.1. Data types and pertinent details.

Sl. No.	Type of Data	Coverage and Accessibility	Purpose of Data Usage	Source of Data	Terms of Use/License
1	AW3D-30 DSM of 30 metres resolution	Global, free data	Foundation model height generation	JAXA	Open data license
2	LiDAR DSM & DTM, resolution of 0.25–2 m and varies by location	UK, free data	Enhanced model regression value parameter creation	Environment Agency	Open data license
3	2D building data for Huangpu, Shanghai (vector layer)	China, free data	Building footprint generation	OpenStreetMap	Open license
4	2D building data for Nottingham (vector layer)	UK, free data	Building footprint generation	OpenStreetMap	Open license
5	Administrative boundary—Shanghai (vector layer)	China, free data	Case study area selection	OpenStreetMap	Open license
6	Administrative boundary—Nottingham (vector layer)	UK, free data	Case study area selection	UK data service download	Open license
7	Nottingham building data with height (vector layer) attributes	UK, restricted for UK research only, commercial	Validation	MasterMap and BHA attribute	EDINA Digimap educational institution license
8	AW3D-Enhanced 2 metre resolution DSM for Shanghai	Commercial	Validation	Purchased from Digital Globe	Commercial license
9	GMTED2010 of 7.5-arc-second (225–250 m) for Nottingham	Global, free data	Ground elevation value generation	USGS and NGA	Open data license

3.2.2.1. OpenStreetMap (OSM)

All the required 2D building footprints were gathered from the OSM database (https://download.geofabrik.de/). Open GIS data available for Shanghai, China were downloaded from the website mapzen.com, which relies on OSM for many of its products. OSM is a collaborative project to create free editable geographic data and a prominent example of volunteered geographic information (Knerr, 2013). The OSM building footprints (with relevant attribute information) were extracted for the Huangpu district—where the coverage is relatively dense (see Figure 3.3).

OSM data are available for Nottingham from a number of sources, and include similar data layers as for Shanghai. As with Shanghai, the OSM building layer data for Nottingham is of a higher density in the city centre, with sparser coverage for the residential suburbs. Building footprints vary in their complexity and accuracy compared to the detailed mapping available from the Ordnance Survey's MasterMap dataset(https://www.ordnancesurvey.co.uk/business-ndgovernment/products/imagery-layer.html) (highest resolution digital mapping available for the UK). For some buildings, the OSM data are visually comparable to its MasterMap counterpart, although we note that in some instances, the OSM footprints have a simplified geometry and often do not include building subdivisions (e.g., between properties of terraced houses).

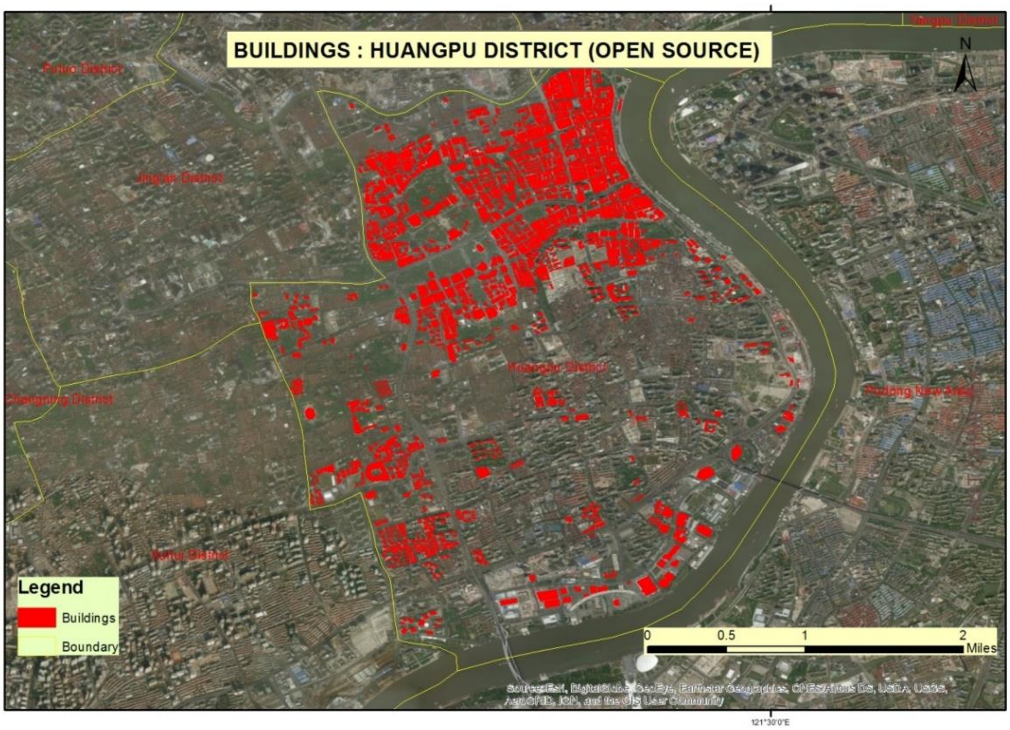

Figure 3.3. OpenStreetMap (OSM) building coverage, Huangpu District, Shanghai, China.

3.2.2.2. ALOS DSM (AW3D (At 30 m) and AW3D enhanced (At 2 m))

The DSM produced by the Japanese Aerospace Exploration Agency (JAXA) is of relatively fine resolution, at about 0.15 arcsec or approx. 5 m (Alganci et al., 2018; Tadono et al., 2014, 2016). JAXA used the archived data of the panchromatic remote-sensing instrument for stereo mapping (PRISM) on-board the ALOS to generate a DSM for the whole globe, known as "Advanced Land Observing Satellite - ALOS World 3D (AW3D)" https://www.eorc.jaxa.jp/ALOS/en/aw3d30/index.htm. The AW3D-30 global dataset, which has a 30 metre spatial resolution (1 arcsec), is a resampled version of the 5 m mesh version of the AW3D (Santillan et al., 2016). For this work, we used the latest AW3D-30 product, released in May 2017. For both Shanghai and Nottingham, 30 m ALOS DSM data are currently the most precise global scale open source elevation (Alganci et al., 2018) dataset (free to the public since 2015). The AW3D Enhanced product (at 2 m resolution) was also procured, giving a sample covering 16 sq.km of the high resolution DSM at 2 m for our study area in Shanghai.

3.2.2.3. GMTED2010

GMTED2010 is the digital elevation (DEM) model product of The United States Geological Survey (USGS) and The National Geospatial Intelligence Agency (NGA) to replace the existing model, as Global 30 ArcSecond Elevation (GTOPO30), and has been available to the public since 2010 (Athmania & Achour, 2014; Grohmann, 2016). It is available in three resolutions, i.e., with horizontal spacing of 7.5 arc-second (about 250 m), 15 arc-second (about 500 m), and 30 arc-second (about 1 km), and its main data source is a SRTM version with 01” resolution restricted to the NGA and not available to the general public (Khalid et al., 2016). This study used the minimum band of GMTED2010 with 250 m resolution due to its global coverage.

3.2.2.4. Digital terrain and surface models derived from airborne LiDAR data for the UK

The U.K Environment Agency’s LiDAR data archive contains accurate digital elevation data for over 70% of England (https://data.gov.uk/dataset/6a117171-5c59-4c7d-8e8b-8e7aefe8ee2e/lidar-composite-dtm-1m). For the city of Nottingham, LiDAR-derived DSM and DTM at 2 m resolution are openly available. For the present study, we used this dataset to extract the ground elevation value for the Nottingham study area in order to enhance the 3D city model produced.

3.2.2.5. OS Mastermap BHA

The building height attribute (BHA) dataset published in 2014 is an enhancement to the Ordnance Survey (OS) MasterMap Topography Layer. BHA data are not available for the whole country, but it covers major cities and towns of Great Britain. BHA provides a set of height attributes (ground level, base of roof, and the highest part of the roof) for topographic area features with a buildings theme within OS MasterMap Topography Layer. OS publish the data as a single CSV file containing over 20 million records (https://www.ordnancesurvey.co.uk/documents/building-height-attribute; https://www.aw3d.jp/en/products/enhanced/). For the present study, we used the BHA data for Nottingham for validation.

3.2.3. Methodology

The overall methodology adopted is illustrated in Figure 3.4. The workflow describes different steps to be taken that are dependent, first, on the terrain on which an urban area resides and, second, on whether there are any relevant additional datasets available The foundation workflow yields a 3D model output possible for all urban areas globally, with the possibility of enhancement of that 3D model should other higher resolution data be available (but these are not a necessity). Further details are below.

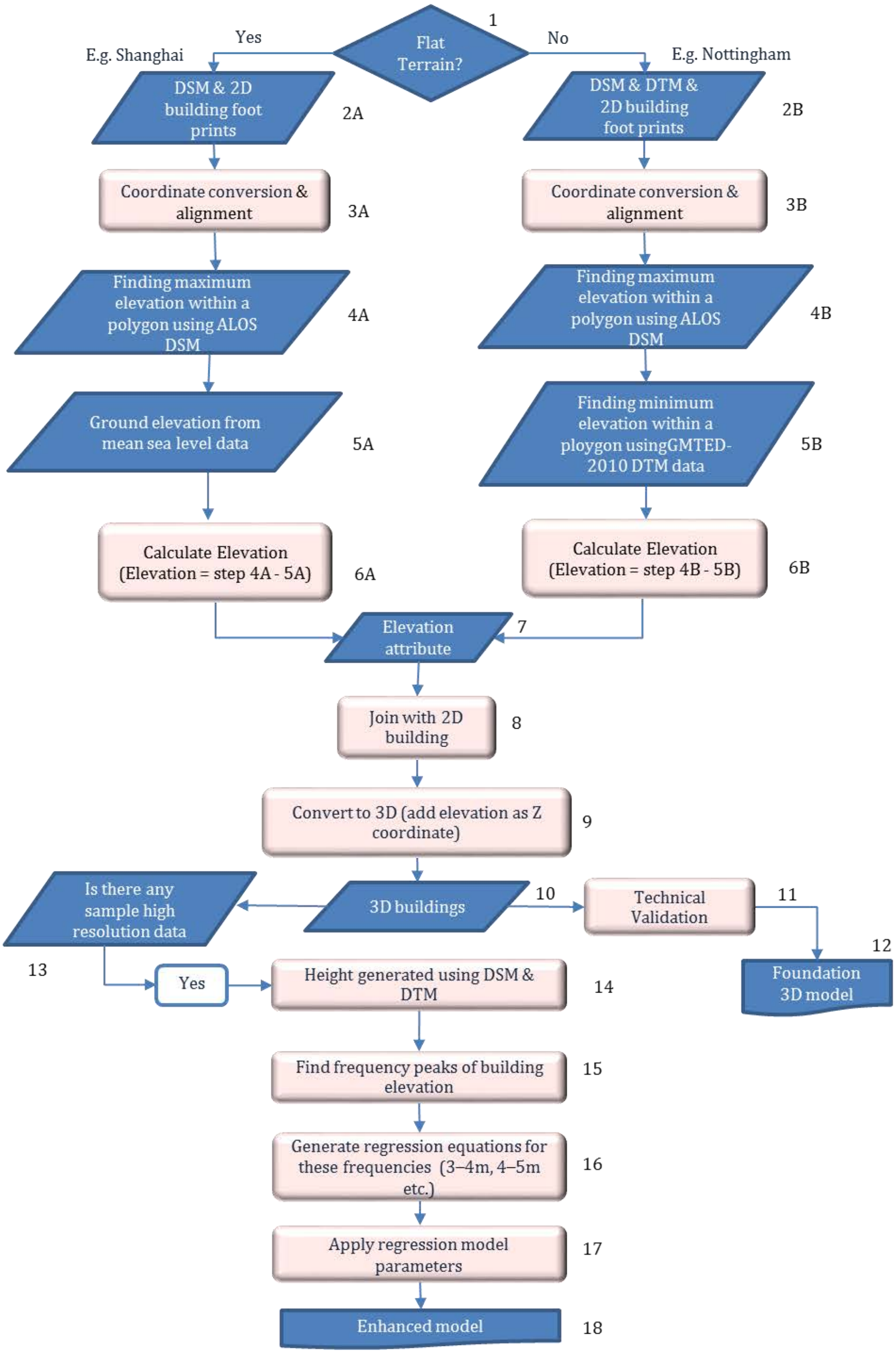

Figure 3.4. Overall methodology. Blue boxes indicates important steps and pink colour indicates intermediate steps.

3.2.3.1. Generating 3D buildings from open data (Foundation workflow)

The first stage in applying this methodology is to establish whether the urban area of interest (AOI) has a terrain that is flat or undulating (workflow chart step 1), since this determines whether additional data and processing steps are required, on a building-by-building basis, to identify the building heights. The term ‘flat’ corresponds to the urban area with relatively smooth topography and without any relief features and the topography with uneven elevation and presence of relief can be classified as ‘undulating’. However, selecting the method also should depend on the purpose and application (details on potential application is provided in the discussion chapter) of the 3D city model. If high level accuracy is required then it is advised to use a high resolution terrain model. If an error of +/-1m is negligible then choosing mean elevation is sufficient for the analysis. Detailed method is provided in below sections. After establishing the terrain type, the 2D building polygon data and the AW3D-30 data (i.e., the DSM) subsequently need to be co-registered, ensuring that there is no shift between the datasets.

The methodology is developed to extract the optimal elevation results from the low-resolution AW3D-30 DSM. As stated above the AW3D-30 open dataset has a 30 m spatial resolution (1 arcsec), which is a resampled version of the 5 m mesh version of the AW3D (Santillan et al., 2016), so already the elevation values are the average of many adjacent pixel values.

In the case of an urban AOI with a flat terrain (i.e. Shanghai in our example case), the AW3D-30 DSM is joined to the 2D shapefile (workflow chart steps 2A to 6A). The AW3D-30 DSM is in raster format and the linear interpolation method is used in to assign the elevation value from raster surface to the vertex of the polygon. This operation will assign a Z value to each vertex of the 2D building polygon. Out of these values, the maximum Z of the geometry is taken as the elevation value since this will reduce the effects of shift caused by different projection systems and to overcome the low resolution of AW3D-30 data. This is because if we calculate an average Z value it may also include ground elevations (i.e., due to height data relating to surfaces beyond the building footprint as AW3D-30 is a resampled version of many adjacent pixels), thereby reducing the overall height value; similarly, if we consider minimum Z there is a chance that this will give the ground elevation directly. It is worth noting that if the DSM was of higher resolution (e.g., 2 m resolution), we would have taken the average Z value within a polygon as the building height. After this process, the mean ground elevation of 4 m (this is the mean elevation of Shanghai) is removed from the AW3D-30 DSM data in order to obtain the building heights (workflow chart steps 7 to 10).

In the case of an undulating terrain (i.e., Nottingham in our example case), building roof heights were computed following the same steps as for Shanghai. However, to accommodate for the change in elevation of the terrain across the urban AOI an alternative workflow is necessary. In this case, to obtain the buildings' ground elevation, the GMTED2010 (i.e., a DTM) is joined with the 2D building polygon using the same interpolate shape function and the minimum Z of the geometry is calculated and assigned to the attribute table of the 2D building polygon (flow chart step 2B to 6B). Here, the minimum Z is used to reduce the effect of shift in the process. If we use an average or maximum of Z, there is a chance that it may reflect the building height values (the converse of the previous case). Once these steps are complete, the height values of the individual buildings are calculated by subtracting the maximum elevation value obtained from the AW3D-30 DSM with the minimum elevation value obtained from the GMTED2010 DTM. The output generated is the estimated heights of individual buildings (workflow chart steps 7 to 10).

3.2.3.2. Technical validation of building height (Foundation workflow)

For Nottingham, our building heights were compared with the building height values provided by the OSGB MasterMap (https://download.geofabrik.de/). The computed heights of 15,000 buildings in Nottingham were compared with the corresponding building height attributes (BHA) (https://www.ordnancesurvey.co.uk/business-andgovernment/products/imagery-layer.html) of the OSGB MasterMap for the city, using arithmetic differencing. Structured Query Languages (SQL) queries were then performed to count the instances of buildings for which height differences h were <1 m, 1 m < h ≤ 2 m, 2 m < h ≤ 5 m, and >5 m, together with the corresponding percentages. For Shanghai, a similar validation exercise was performed. However, for Shanghai, there is no openly available high resolution building height data. Therefore, to validate our results, we used the AW3D Enhanced product at 2 m spatial resolution. This product is stated to be derived from the Digital Globe WorldView satellites (https://www.aw3d.jp/en/products/enhanced/). Building heights that are derived from AW3D-30 m could then be cross-checked with the heights derived from this 2 m DSM, and the resultant height values refined (flow chart step 11 and 12). In total, 2027 buildings were used in this validation.

3.2.3.3. 3D Foundation model enhancement

The foundation workflow (Section 3.2.3.1) produces a 3D city model that is globally replicable, however, it may be the case that higher resolution elevation data are available (open) or could be procured as per limited budgetary resources. These data could enhance the accuracy of 3D buildings in the model by computing the error factor for building heights. The error factor is the deviation of height values generated in the foundation work flow to the height of the corresponding building obtained from high resolution data for each of the cities. Once computed, these values can be used to correct the building heights in other similar areas. For enhancement, a high resolution dataset needs to be available for a representative sample area of the AOI (Figure 3.5).

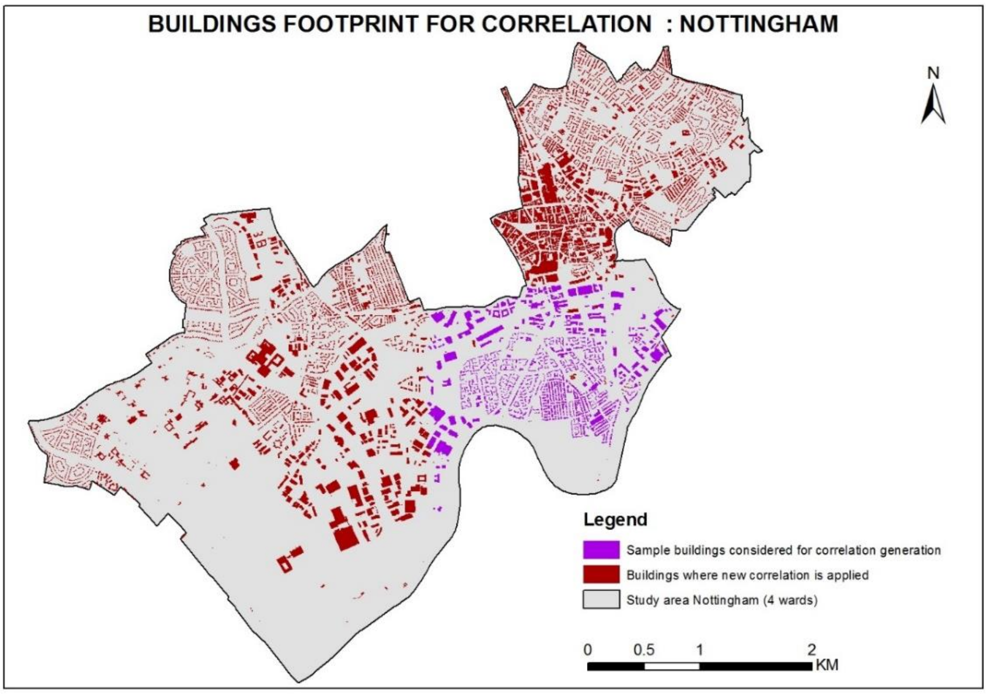

Figure 3.5. Sample buildings considered for 3D generation and correlation, Nottingham, UK.

We used consistent 1 m interval categories of maximum building height for the polygon concerned (e.g., an approximation of a ridge height for pitched roof houses). This interval selection helps in generating good correlation and is easy to apply to other similar areas. For the Nottingham case, the maximum number of building heights observed within the range of 2 m to 8 m was calculated using the AW3D-30 dataset (flowchart step 13 to 15). So, regression equations with 1 m intervals were created for this range (e.g., seven unique categories of building height: $2 \leq h \leq 3$ m, 3 m $< h \leq 4$ m, …, and 7 m $< h \leq 8$ m). These 1 m ranges were chosen because they provide improved correlation over other ranges. In order to obtain the regression equations both AW3D-30 derived heights and high resolution derived heights were exported to the excel scatter plot graphs created, from which a linear regression equation was derived (flowchart step 14). The regression equations derived from different ranges were then employed to correct building heights for all instances of that category that were found within the AW3D-30 dataset, both within and outside the high resolution sample area (flowchart step 16 to 18). The technical validation of the enhanced model was done in a similar way stated for validation of foundation model. This validation was done over exactly the same buildings using the same data that were considered for the validation of foundation model.

3.3. Results

3.3.1. Nottingham

After obtaining the foundation 3D model (Figure 3. 6 shows a sample area) for Nottingham (i.e., AW3D-30 derived building heights), we compared these building heights with MasterMap BHA to assess the accuracy of this preliminary result. This revealed that 27.7% of all buildings fall within the accuracy level of +/−1 m elevation, and 51.45% and 84.47% within +/−2 m and +/−5 m, respectively. 15.53% of buildings were above +/−5 m accuracy level.

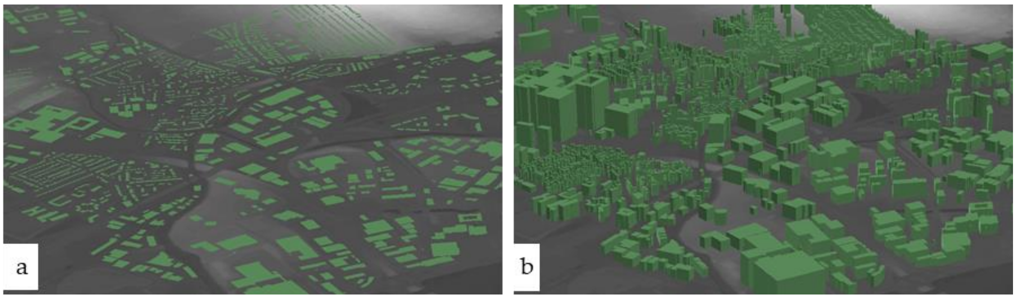

Figure 3.6. (a) 2D building footprints for Nottingham, (b) foundation 3D model building footprints generated from AW3D-30 as DSM and GMTED2010 as DTM data.

When both sets of height values we compared, it was observed that a higher level of height difference occurred in the case of taller buildings. The percentage of buildings falling under each error ranges are shown in Figure 3.7. The low- and medium-rise buildings showed relatively good correlation with the MasterMap BHA values.

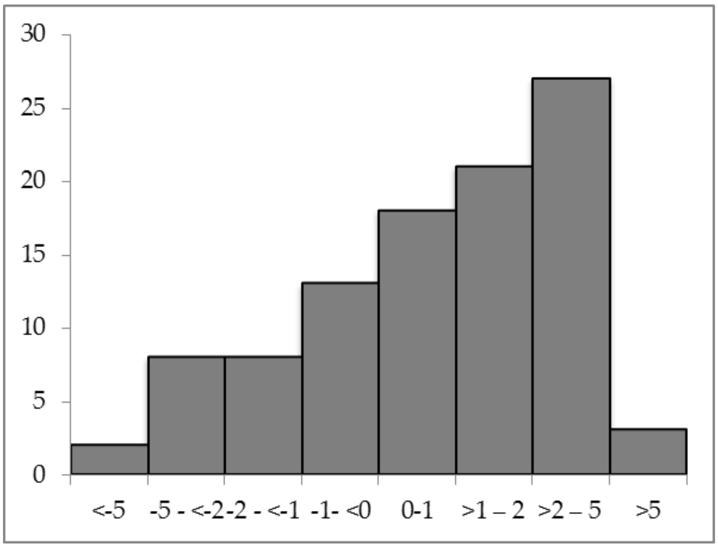

Figure 3.7. Percentage of buildings under each range for foundation 3D model in Nottingham.

In the application of the accuracy enhancement method by way of a sample of high-resolution elevation data, it was determined that the majority of building heights fall within the range of 2 m to 8 m (established using the AW3D-30 dataset). Hence, a regression equation with a 1 m interval was created for this range of 2 m to 8 m in order to enhance the accuracy of the foundation 3D model (Figure 3.8). This 1 m interval was chosen to obtain good correlation between two datasets of generated AW3D-30 height values and high resolution LiDAR data. The regression equations derived from these categories are given in Table 3.2 and these were applied to obtain an enhanced 3D city model.

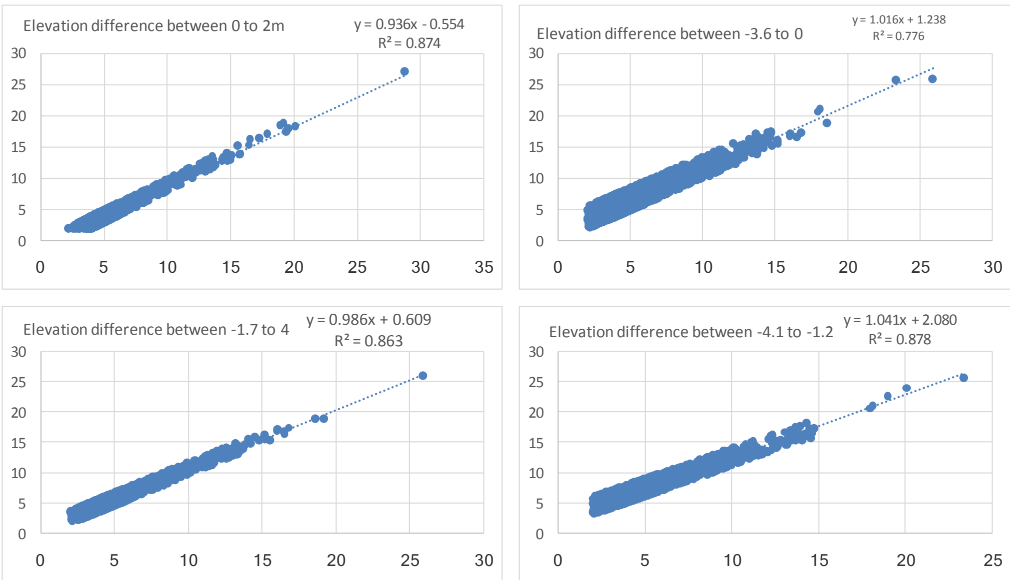

Figure 3.8. Scatter plot showing correlation between AW3D-30 DSM- and LiDAR DSM-generated heights for different ranges.

Table 3.2. Correlation values for different ranges and linear equation for accuracy enhancement (Nottingham).

Sl. No.	Height of Buildings in Meters	Height Difference Range Used for Creating Equation in Meters	Linear Equation Used for Accuracy Increase
1	2 to 3	1 to 2	y = 0.984x − 1.358
2	3 to 4	0 to 2	y = 0.936x − 0.554
3	4 to 5	No equations required as the values already have good correlation	
4	5 to 6	−1.7 to 0.4	y = 0.986x + 0.610
5	6 to 7	−3.6 to 0	y = 1.017x + 1.239
6	7 to 8	−4.1 to −1.2	y = 1.041x + 2.080

3.3.1.1. Technical validation of enhanced 3D model

Validation of the enhanced 3D model demonstrated that applying the regression equations to the foundation model had the impact of improving its accuracy across the board. The proportion of buildings in the model having an accuracy level of +/−1 m increased from 27.7% to 32.81% (Table 3.3), having an accuracy level of +/−2 m increased from 51.45% to 57.43%, an accuracy level of +/−5 m increased to 88.46% from 84.47%, and buildings having an error value above +/−5 m were reduced from 15.73% to 11.54%. It was noticed that even after enhancement, there was no significant height value correlation increase in the case of taller buildings.

Table 3.3. Validation results showing percentage of buildings within each interval before (foundation 3D model) and after accuracy enhancement (enhanced model), for Nottingham.

Sl. No.	Height Extracting Method	Percentage of Buildings Having Accuracy of			Percentage of Buildings Having an Error More than +/−5 m
		+/−1 m	+/−2 m	+/−5 m	
1	Foundation 3D model developed using AW3D 30 m DSM and GMTED 2010 DTM	27.70	51.45	84.27	15.73
2	Enhanced 3D model via a sample of high resolution LiDAR (2 m)	32.81	57.43	88.46	11.54

It is worth noting that, as stated in the methodology, we considered maximum elevation value within a polygon as the AW3D-30 DSM height. Using the height generated via the minimum and average elevation value within was not as accurate.

3.3.1.2. Replacing GMTED 2010 ground elevation data with high resolution ground elevation data

To understand how the GMTED 2010 DTM data impact on the quality of the foundation 3D model, the model was again constructed using high resolution LiDAR DTM as the ground elevation input along with the AW3D 30 m DSM. Validation using the MasterMap BHA values demonstrated that about 31.43% of total buildings achieved an accuracy within +/−1 m elevation and 60.14% were within +/−2 m (Table 3.4). Deviations for only 5.27% of all the buildings exceeded +/−5 m, but a significant proportion of the cases having this largest deviation were due to errors in the MasterMap BHA dataset or within AW3D-30 dataset (these errors were identified by cross-checking these individual sites with other datasets like Google Earth™, where open street views are available). Further results show that errors among low-rise buildings are minimal than that of high-rise buildings. For example correlation values (Table 3.3) for different height ranges of Nottingham show higher correlation among lower height ranges (2-3, 3-4, 4-5, and 5-6) than higher ranges (above 6m). It is also significant to observe that using LiDAR DTM instead of GMTED 2010 together with AW3D-30 DSM yielded only 5% more buildings within +/- 1 m accuracy level and 9% within +/- 2 m and 10% within +/- 5 m respectively (Table 3.4).

Table 3.4. Validation results showing percentage of buildings under each interval when ground elevation was extracted using high resolution LiDAR DTM data (Nottingham).

Sl. No.	Height Extracting Method	Percentage of Buildings Having Accuracy of			Percentage of Buildings Having an Error More than +/−5 m
		+/−1 m	+/−2 m	+/−5 m	
1	Foundation 3D model developed using AW3D-30m DSM and 2 m LiDAR DTM	31.43	60.14	94.73	5.27
2	Foundation 3D model developed using AW3D 30 m DSM and GMTED 2010 DTM	27.70	51.45	84.27	15.73

3.3.2. Shanghai

We considered only a sample of the 2027 OSM buildings of the Huangpu District of Shanghai to generate the 3D model, as well as to calculate a correlation coefficient. The modelled building heights from AW3D-30 DSM for Huangpu District have been compared with the commercial 2 m accuracy DSM that was procured for the study area. Unlike Nottingham, Huangpu, Shanghai has very tall buildings (Figure 3.9), hence the range of difference between the real height and generated 3D building heights were higher than for Nottingham. It was observed that about 33% of buildings fall within the error range of +/−2 m and about 30% of buildings within an error range of +/−2 m to +/−5 m (see Table 3.5). The regression equations used to enhance the accuracy of foundation model are given in Table 3.6.

Figure 3.9. Sample of foundation 3D model generated from AW3D-30 data and classified according to the elevations, Shanghai (green colour represents low-rise buildings, brown colour represents medium-rise buildings, dark brown represents high-rise buildings).

Table 3.5. Percentage of buildings under each error range for foundation 3D model in Huangpu District, Shanghai.

Sl. No.	Height Difference in Meters	Percentage of Buildings under Each Range
1	≤20	2
2	−10 to −20	7
3	−5 to −10	11
4	−2 to −5	14
5	±2	15
6	±1	18
7	2–5	16
8	5 to 10	7
9	10 to 20	3
10	>20	7

Table 3.6. Correlation values for different ranges and linear equations for accuracy enhancement (Huangpu District, Shanghai).

Sl. No.	Height Difference in Meters	Correlation Obtained/R^2 Value for Huangpu, Shanghai	Linear Equation Used for Accuracy Increase
1	5–6	0.997	$y = 1.001x - 0.071$
2	6–7	0.985	$y = 1.006x - 0.314$
3	7–8	0.989	$y = 0.978x - 2.880$
4	8–9	0.989	$y = 0.997x + 3.362$
5	11–12	0.988	$y = 0.975x - 6.329$
6	14–15	0.990	$y = 0.999x + 7.160$
7	16–17	0.961	$y = 0.953x - 12.33$
8	18–19	0.971	$y = 1.005x + 13.602$
9	>20	0.222	$y = 0.256x + 5.020$

3.3.2.1 Technical validation of enhanced 3D model

It was observed from the validation results that the overall accuracy of the foundation 3D model has improved using the accuracy enhancement method. The difference in the percentage of buildings with different accuracy level ranges before and after applying accuracy enhancement methods are given in Table 3.7. Higher rates of accuracy enhancement were observed for the lower ranges (i.e., up for +/−1 and +/−2). Where the difference in values between the actual height and the generated height increased, there was an observed decrease in accuracy enhancement level. For example, after accuracy enhancement in the range of +/−5 m, the total percentage enhanced from 62.26% to 64.54% only and there was no accuracy increase for +/−10 m accuracy range (Table 3. 7). In lower height deviations (1 or 2 m) level we obtained a good accuracy increase by correlation, but in higher deviation sections (5 or 10 m), the accuracy improvement was relatively lower or null.

Table 3. 7. Percentage of buildings under each level before (foundation 3D model) and after accuracy enhancement (enhanced model) for Huangpu District, Shanghai.

Sl. No.	**Height Extracting Method**	**Percentage of Buildings Having Accuracy of**				**Percentage of Buildings Having an Error More than +/−10 m**
		+/−1 m	**+/−2 m**	**+/−5 m**	**+/−10 m**	
1	Foundation 3D model developed using AW3D-30 DSM	17.66	32.96	62.26	79.78	20.22
2	Enhanced 3D model via a sample of high resolution commercial 2 m DSM (AW3D Enhanced)	28.3	41.69	64.54	79.78	20.22

Shanghai is characterized by high-rise buildings, hence the ranges considered for accuracy assessment were from +/−1 to more than +/−10 m. Whereas for Nottingham, the maximum range was +/−5 m, since the city is occupied by low-rise buildings. The proportion of buildings having an accuracy of +/−1 m was low (17.66%) in the case of Shanghai, which increased to 28.3% after accuracy enhancement. This contrasts with an accuracy of 27.7% for Nottingham, or 32.81% after accuracy enhancement. While 64.54% of buildings were found to be within the accuracy range of +/−5 m for Shanghai, this was much higher for Nottingham at 88.46% (after enhancement in both cases). Further, even after accuracy enhancement, 20% of all the buildings in Shanghai's Huangpu District were found to have an error of +/−10 m in their modelled height which can be attributed to the behaviour of AW3D-30DSM data which is elaborated in below section.

3.3.3 Understanding the behaviour of AW3D-30 DSM data

In order to understand the reliability of AW3D-30 DSM in generating 3D building height generation, it is important to understand how much it differs from the more accurate data (BHA data of Mastermap provided by Ordnance Survey, Figure 3.10). For this purpose a 3D city model is created by using AW3D-30 DSM (for generating building roof height elevation information) and LiDAR DTM (which gives ground elevation information). To generate it is essential to have ground elevation and building height. The LiDAR DTM with higher accuracy was selected for obtaining ground elevation, presuming that the maximum error caused may only be from AW3D-30 data alone.

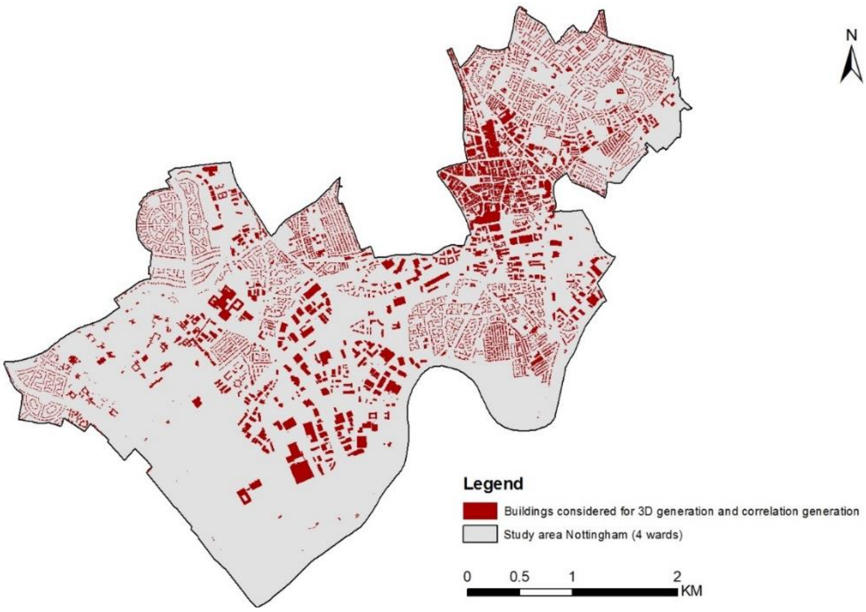

Figure 3.10 Buildings considered for 3D generation and correlation, Nottingham, UK

Thus the building height values of the generated 3D city model were compared with the corresponding building height values from BHA data of Mastermap provided by Ordinance Survey and calculated the percentage of error. The calculated percentage of buildings falling under different categories are given in the table below (Table 3.8).

Table 3.8 Percentage of buildings under each range, Nottingham

Sl. No.	Height difference in meters	Percentage of buildings under each range
1	<-5	2
2	-5 - <-2	8
3	-2 - <-1	8
4	-1- <0	13
5	0-1	18
6	>1 - 2	21
7	>2 - 5	27
8	>5	3

Linear regression model was developed in order to understand the behaviour of AW3D-30 DSM in generating 3D city models. Based on the linear regression model, not only the correlation between building heights generated using AW3D-30 DSM and BHA Mastermap is computed but also these correlation values are used for further increasing the accuracy of building heights generated from AW3D-30 DSM. To estimate the linear regression model, the two sets of values (AW3D-30 DSM and validation) were imported from the shapefile attribute tables into a spreadsheet. The results were poor when fitting this equation using all data; but improved when categorising the data according to its corresponding height deviation range – estimating unique equations for each of the eight categories [covering negative and positive values of the eight ranges]. The corresponding linear regression equations, of the form hhr = a.hlr + b, where subscripts hr and lr refer to high resolution and low resolution datasets respectively, and a,b are regression coefficients. These equations were employed to correct the heights from the low resolution 3D city model and to correspondingly update the shapefile attribute table. This analysis also helped to understand the maximum accuracy that can be gained using enhancement techniques.

For the city of Nottingham, foundation model AW3D-30 building heights were within +/- 1m of those in our high resolution (MasterMap) dataset for 31.43% of total buildings and +/-2m for 60.14% of buildings (Table 3.9). Deviations for only 5.27% of all the buildings exceeded +/-5m, but a significant proportion of the cases having this largest deviation were due to errors in the MasterMap dataset. These errors were identified by cross-checking with other datasets like google maps where open street views are available.

Table 3.9 Percentage of buildings under each level before accuracy enhancement, Nottingham

Sl. No.	Height extracting method	Percentage of buildings having accuracy of			Percentage of buildings having an error more than +/-5 meter
		+/-1 meter	+/-2 meter	+/-5 meter	
1	Building height generated from AW3D-30 DSM & LiDAR DTM (compared with BHA values)	31.43	60.14	94.73	05.27

The accuracy of the modelled building heights was improved by applying the linear regression method. The strongest correlation coefficient (R^2 = 0.986) was observed for the range of <2 to <-1m which was followed by the range >1 to 2m (R^2 value – 0.976) which suggests that there is a systematic error or a systematic pattern of variation among the height. About 29% (4373) of buildings fall within these two ranges (Table 3.10). The maximum number of buildings i.e. 27% (4081) falls within the range of >2 to 5m with a correlation value of 0.899. Maximum deviation from the trend line was observed for the range of buildings with <-5m accuracy with least correlation value (R^2 value – 0.543) (Figure 3.11, Table 3.9). However, only 310 buildings i.e. 2% of total buildings fall under this category. Using the linear model, accurate transform is more than 97% of building height values obtained from open source to the original value in the case of buildings having a height difference between 0 and 1.

Table 3.10 Correlation values for different ranges and linear equation for accuracy enhancement, Nottingham

Sl. No.	Height difference in meters	Correlation obtained/R^2 value	Linear equation used for accuracy increase
1	<-5	0.543	y = 0.9435x + 7.8151
2	-5 to <-2	0.941	y = 1.0195x + 2.9387
3	-2 to <-1	0.986	y = 0.9973x + 1.4754
4	-1 to <0	0.980	y = 1.0018x + 0.4622
5	0 to 1	0.976	y = 0.9981x - 0.5143
6	>1 to 2	0.976	y = 0.9921x - 1.4500
7	>2 to 5	0.899	y = 0.8946x - 2.2481
8	>5	0.726	y = 0.5998x - 1.7038

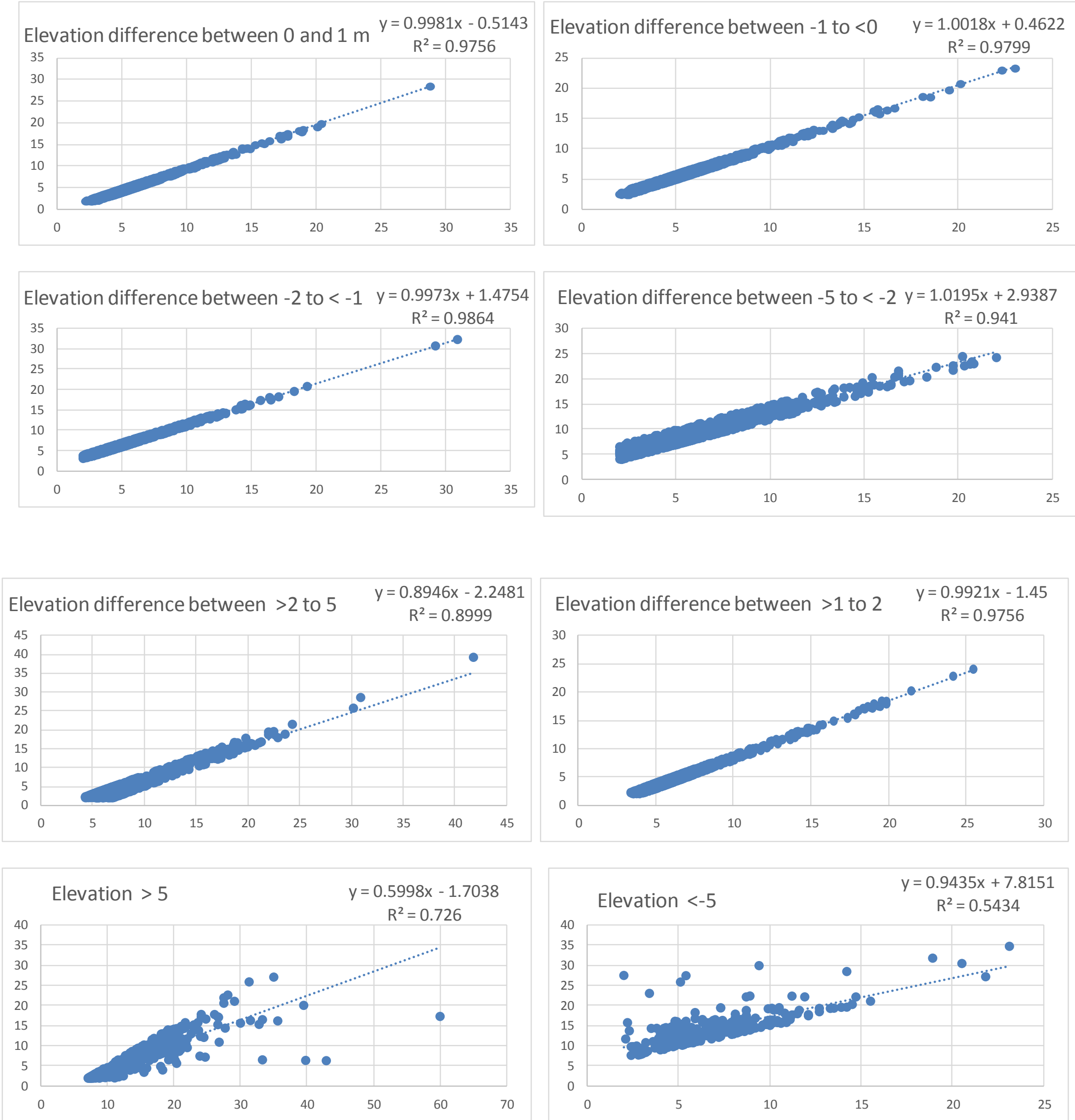

Figure 3.11 Scatter plot showing correlation between actual heights and the generated heights from open source for different ranges, Nottingham, U.K

After accuracy enhancement the proportion of buildings having accuracy level of +/-1m increased from 31.43% to 90.8% after calibration (Table 3.11). The fraction of buildings within the accuracy level of +/-2m improved to 97.73% from 60.14% and within +/-5m accuracy level increased up to 99.52% from 94.73%. Lastly, buildings having an error more than +/-5m reduced to 0.48% from 5.27%.

Table 3.11 Percentage of buildings under each level before and after accuracy enhancement for both cases, Nottingham

Sl. No.	Height extracting method	Percentage of buildings having accuracy of			Percentage of buildings having an error more than +/-5 meter
		+/-1 meter	+/-2 meter	+/-5 meter	
1	Building height generated from AW3D-30 DSM & LiDAR DTM (compared with BHA values)	31.43	60.14	94.73	05.27
2	AW3D-30 DSM data calibrated using BHA building height data base	90.8	97.73	99.52	0.48

From the analysis it is observed that given there is an accurate ground elevation model, AW3D-30 DSM is capable of producing more accurate results especially for the buildings where the deviation is less than +/-1 meter. Further errors in AW3D-30 DSM are systematic which can be reduced by correlating with other higher resolution datasets and are capable of producing high accuracy 3D city models.

3.4. Summary

This chapter demonstrated a globally replicable methodology to generate 3D buildings from open data. Generation of 3D buildings exclusively using open data was the highlight of this chapter. This method is cost-effective, making it particularly attractive to users in low- and middle-income countries, where free 3D building data is not available. Further, this largely automated method requires minimal time to generate 3D city models, and also has flexibility for improvement in accuracy should higher resolution data be available. Given the use of relatively low resolution open data, this methodology will be of particular relevance to studies that do not require high resolution 3D models, such as for global environmental change studies, global climate change and urban climate modelling, disaster vulnerability models, and energy models. Real world simulations for 3D games may be another potential area of interest.

Finally, the methodology presented in this chapter can, in the future, be employed in conjunction with alternative 2D input data, for example as quality checked OSM data become more abundant, and with more accurate height data, as upgrades to AW3D-30 are published, or other sources become available, such as those derived from LiDAR measurements.

For those urban areas where 2D footprints are not available, alternative approaches will be required to provide the 2D data to be fused with the globally available 3D data. This thesis proposes that high resolution satellite data can be used to provide 2D footprints by way of building extraction. However, the current status of open satellite data is that they are of medium spatial resolution in general. Hence, the following chapter will assess the potential of spatial resolution enhancement of one such spatial resolution dataset. Here, Sentinel-2 data bands of Green, Red and NIR having spatial resolution of 10 metres will be enhanced in its spatial resolution via sparse representation techniques to afford the extraction of 2D building footprints from the enhanced image. Here the case study city of Shanghai is used for data enhancement as the OSM 2D footprint coverage is limited in the region.

CHAPTER IV

SPATIAL RESOLUTION ENHANCEMENT OF SENTINEL – 2 (10m) SATELLITE DATA THROUGH SPARSE REPRESENTATION TECHNIQUES

4.1 Introduction

The major objective of the previous chapter (Chapter III) was to demonstrate a method to generate 3D city models from openly available 2D building footprints. Although afforded the generation of 3D city models (LOD1), this would only be applicable for areas across the world where 2D building footprints are already readily and freely available. There are still many regions for which the fine resolution 2D open building footprints are not available and or freely available. In the case of developing and least developed countries of the world especially, the availability of fine resolution 2D footprints present a major challenge, therefore generation of 3D city models can be hit and miss.

Extraction of building features from fine resolution satellite datasets with global coverage could be a solution. Since fine resolution satellite images known as Very High Resolution (VHR) contain a large amount of spectral, structure, and texture information, they provide great potential for accurate building detection (Song et al., 2019; You et al., 2018). However, to have global coverage of VHR satellite data (for example, WorldView, Pleiades) could be expensive and these data tend to be of limited temporal resolution. Alternatively, satellite imagery of coarser spatial resolution is used (for example: from Landsat, Sentinel-2), as these are openly available. One of the limitations with available open data having global coverage is their coarse resolution, and so this limitation needs to be addressed. Accordingly, the overall objective of the current chapter and the next chapter (Chapters IV and V) focuses to extract building features from coarser resolution, but openly available, satellite data to be used in 3D city modelling. The present chapter seeks to optimally enhance the satellite data (Sentinel-2), with Chapter V demonstrating how this spatially enhanced imagery can be used to produce 3D city models.

Sentinel-2 satellite data holds great potential for urban mapping due to its wide swath and frequent revisiting time (5-day revisiting time). However, the spatial resolution of 10 m is not adequate to extract building features. Therefore, this chapter explores the potential to enhance the 10 m spatial resolution of Sentinel-2 satellite data wavebands band 3 – Green, band 4 – Red and band 8 - NIR using a sample of WorldView-3 data of respective bands, to a spatial resolution of 1m based on sparse representation techniques. The respective bands of WorldView-3 multispectral data are band - 3 Green, band 5 - Red and band 7 - NIR1. If this works it should ultimately afford more accurate extraction of 2D building footprints in data void regions.

Sparse representation is defined as the dictionaries containing sparse linear combinations of image structures such as textures, corners and edges having the support of direction information (vector quantity). It is a learning-based method used in super-resolution restitution or super-resolution mapping approaches. Super-resolution refers to the task of enhancing resolution of images by combining one or more low-resolution observations of the same scene to produce high resolution images (Park et al., 2003; Kawulok et al., 2019). This chapter follows sparse representation for super-resolution analysis as used by Yang et al. (2010). The approach has yet to be used to enhance spatially the resolution of imagery in order to extract building features. Accordingly, the objective of the present chapter is to spatially enhance the Sentinel-2 image from 10m to 1m, by sparse representation techniques, so as to extract buildings features more accurately from the enhanced images. To demonstrate the resolution enhancement techniques Shanghai is taken as a testing site. In line with the broader objective, this chapter addresses mainly three questions: i) what are the optimal parameters required to enhance Sentinel-2 images, ii) what are the ideal bands to be used for the extraction of different urban features and buildings, and iii) how are the different buildings (large, small, high rise, low rise) and other urban features presented after spatial enhancement. The enhanced Sentinel-2 images are also classified to extract features of the urban landscape, from which buildings would be extracted after additional processing (and fed into the next chapter to produce 3D city models).

4.2 Study area

In the previous chapter, both Nottingham and Shanghai were the focus to generate 3D models. It was observed that, unlike Nottingham, Shanghai does not have enough spatial coverage of open 2D building footprint data to perform the 3D model generation. This situation is applicable to most of China and other Asian countries. Therefore Shanghai is taken as an ideal case to test the spatial resolution enhancement methods. Areas outside Huangpu District where WorldView-3 data were freely available was taken to generate the training set (Figure 4.1). The training sets were applied in Huangpu District to enhance the spatial resolution.

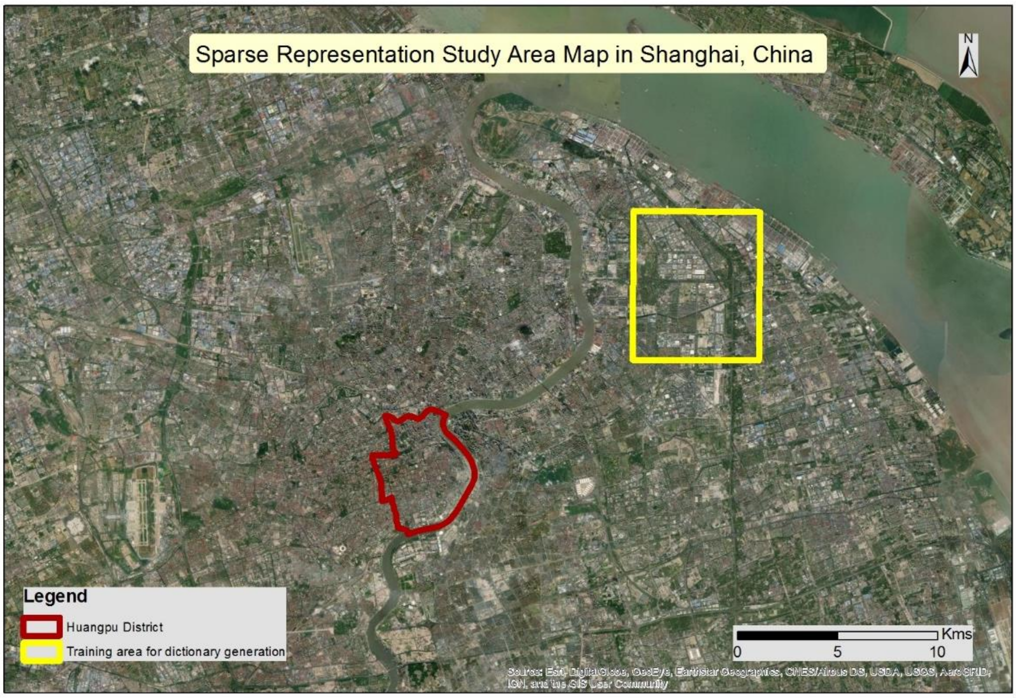

Figure 4.1 Map of study area showing Huangpu District (red polygon) and the training area (yellow box) taken for dictionary generation

4.3 Satellite EO data – openly available

For applying the sparse representation technique to achieve satellite spatial data enhancement, a sample area is required where both fine and coarse resolution satellite data are present. For the current study, Sentinel-2 data was used as the coarse resolution data input and WorldView-3 data as the fine resolution data input.

4.3.1 Sentinel-2

The Sentinel-2 series contains two satellites namely Sentinel 2A launched on 23rd June 2015 and Sentinel 2B launched on 7th March 2017 with an operational lifespan of 7.25 years. This sensor has a temporal resolution of 10 days with one satellite and 5 days with two satellites. The spatial resolution varies between 10m, 20m, and 60m based on the spectral bands (Table 4.1) with a swath width of 290km (The European Space Agency, 2014; Immitzer et al., 2016).

Table 4.1 Spectral properties of Sentinel-2, the bands considered for enhancement are highlighted as shaded values

Spectral Bands	Sentinel-2A		Sentinel-2B		
	Central wavelength (nm)	Bandwidth (nm)	Central wavelength (nm)	Band width (nm)	Spatial resolution (m)
Band 1 – Coastal aerosol	442.7	21	442.2	21	60
Band 2 – Blue	492.4	66	492.1	66	10
Band 3 – Green	559.8	36	559	36	10
Band 4 – Red	664.6	31	664.9	31	10
Band 5 – Vegetation red edge	704.1	15	703.8	16	20
Band 6 – Vegetation red edge	740.5	15	739.1	15	20
Band 7 – Vegetation red edge	782.8	20	779.7	20	20
Band 8 – NIR	832.8	106	832.9	106	10
Band 8A – Narrow NIR	864.7	21	864	22	20
Band 9 – Water vapour	945.1	20	943.2	21	60
Band 10 – SWIR – Cirrus	1373.5	31	1376.9	30	60
Band 11 – SWIR	1613.7	91	1610.4	94	20
Band 12 – SWIR	2202.4	175	2185.7	185	20

Source: Earth Observation System (https://eos.com/find-satellite/sentinel-2/)

The Sentinel-2 satellite has a multispectral EO system featuring the Multispectral Instrument with 13 bands that span from the visible and the near infrared to the shortwave infrared bands (Chastain et al., 2019). The visible and the near infrared

(NIR) bands have a spatial resolution of 10 m, the infrared bands have 20 m spatial resolution and the other bands have 60 m. The 10 m spatial resolution provides Sentinel-2 data with the potential for detailed exploration of the Earth's surface (for example, urban sprawl and agriculture) (Phiri et al., 2020). Sentinel-2 offers improved data compared to other low to medium spatial resolution satellite images (for example, Landsat), especially in temporal and spatial resolution (Novelli et al., 2016). The main advantage of Sentinel-2 is the combination of wide swath and frequent revisiting time (5-day) which makes it highly suitable for mapping and monitoring human settlements at a global level (Pesaresi et al. 2016; Vuolo et al. 2018).

The choice of image to be used from the Sentinel-2 satellite record was determined by the requirement for a negligible amount of shadowing of buildings and by the requirement for the VHR Worldview data to be close in date of capture. For the Shanghai study area, the cloud-free (less than 10% cover) satellite image captured in July 2016 was chosen for image processing and this meant that the effect of shadow on urban buildings was negligible.

4.3.2 WorldView-3 (WV-3) – openly available via a special arrangement

Selective non-continuous tiles and metadata of WV-3 satellite data is openly available for certain cities upon request soley for research purposes. Shanghai is one of the cities where WV-3 is openly available. WV-3 was successfully launched on 13th August 2014. WV-3 is the first multi-payload, super-spectral, fine resolution commercial satellite sensor operating at an altitude of 617 km (DigitalGlobe, 2016; Ye et al., 2017). WV-3 provides 31 cm panchromatic resolution, 1.24 m MS (Multispectral) resolution, 3.7 m SWIR (Short-Wave Infrared) resolution, as well as 30 m CAVIS (Clouds, Aerosols, Vapors, Ice, and Snow) with 12 bands (desert clouds, aerosol-1, aerosol-2, aerosol-3, green, water-1, water-2, water-3, NDVI-SWIR, cirrus, snow) and a ground resolution of 30 m at nadir (Barazzetti et al., 2016). CAVIS monitors the atmosphere and provides correction data to improve WorldView-3's imagery while it images earth objects through haze, soot, dust or other obscurants. Table 4.2 provides the spectral properties of WorldView-3. WV-3 has an average revisit time of < 1 day and is capable of collecting up to 680,000 km2 per day. WV-3 also collects shortwave infrared (SWIR) imagery in eight bands, offered on a commercial satellite for the first time (Barazzetti et al., 2016).

Table 4.2 Spectral properties of WorldView-3, the bands considered for the enhancement of Sentinel 2 image are highlighted as shaded values

Spectral Bands	Central wavelength (nm)	Effective band Width Δλ (µm)	Resolutio n
Panchromatic	649.4	0.2896	0.3m
Coastal	427.4	0.0405	1.2m
Blue	481.9	0.0540	
Green	547.1	0.0618	
Yellow	604.3	0.0381	
Red	660.1	0.0585	
Red Edge	722.7	0.0387	
NIR1	824.0	0.1004	
NIR2	913.6	0.0889	
SWIR1	1209.1	0.0330	
SWIR2	1571.6	0.0397	7.2m
SWIR3	1661.1	0.0373	
SWIR4	1729.5	0.0416	
SWIR5	2163.7	0.0389	
SWIR6	2202.2	0.0409	
SWIR7	2259.3	0.0476	
SWIR8	2329.2	0.0679	

Source: DigitalGlobe (2016)

4.4 Methodology of sparse representation

The overall methodology as illustrated in figure 4.2 mainly addresses two questions: 1) Is it possible to spatially enhance Sentinel-2 image using sparse representation, so that building footprints may be extracted to use in 3D city model? and 2) what are the optimal values (dictionary size, bands, sample size, patch size) required to enhance Sentinel-2 image to 1m resolution using sparse representation techniques?

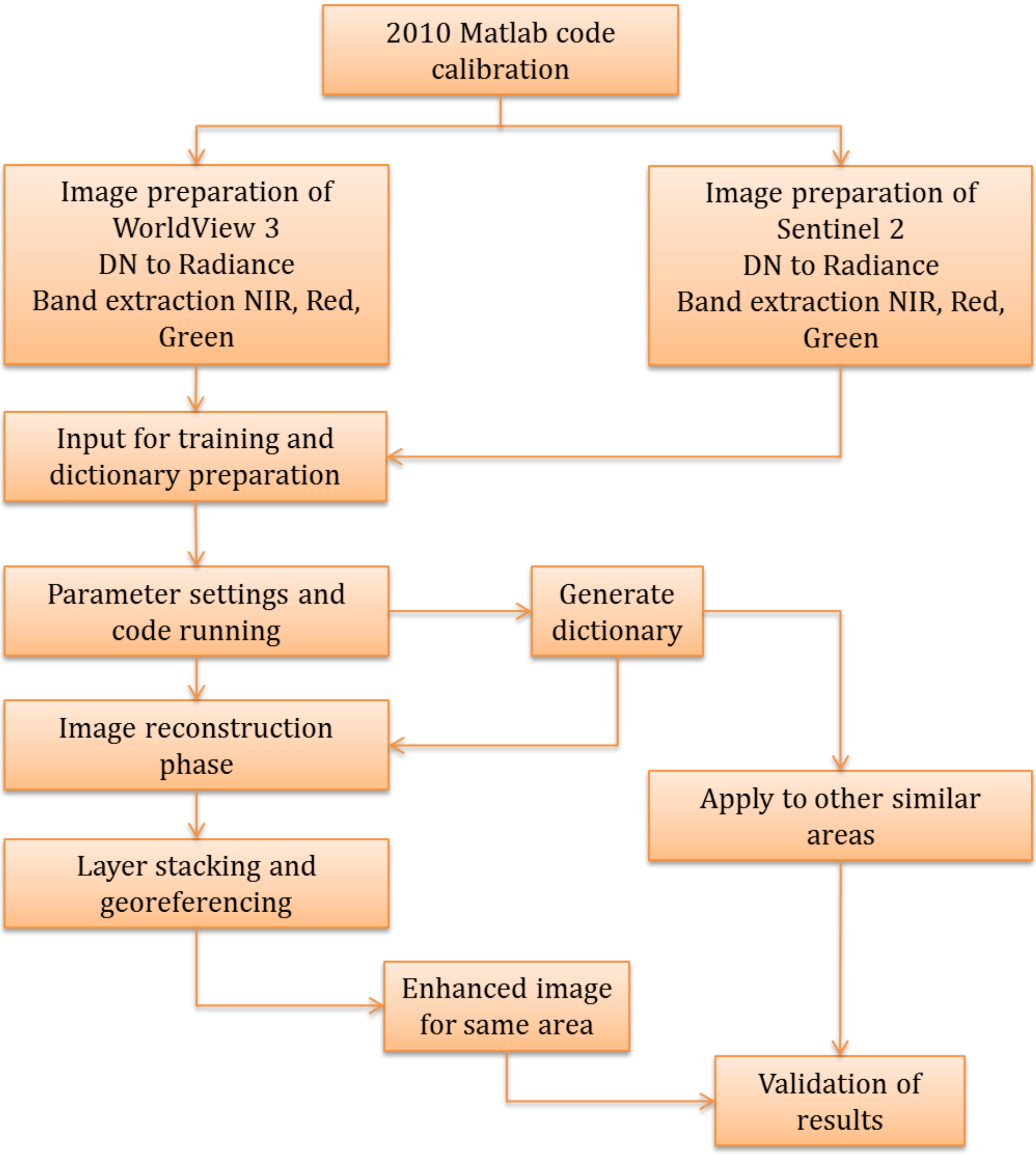

Figure 4.2 Overall methodology used for increasing the spatial resolution of Sentinel-2 (10m) satellite data based on sparse representation techniques

As stated earlier, for image spatial enhancement, sparse representation for super resolution analysis was adopted from Yang et al., (2010). The sparse representation method has two sections, one the training section where characteristics for image enhancement are acquired from a sample area, while the other is the image reconstruction phase where the enhanced image is produced using the input of the training phase. Accordingly, in general, the whole work of sparse representation can be subdivided into three sections namely the pre-processing phase, training phase and the reconstruction phase. In the pre-processing stage, the Matlab 2010 code has to be calibrated according to the Matlab 2018 version, as codes were different in earlier versions (Matlab 2010 used by (Yang et al., 2010)) than the 2018 version. Debugging and error identification would be very difficult in older versions. Following the process, satellite images were made in a specific format as the input for the training phase.

4.4.1 Pre-processing phase

4.4.1.1 Matlab calibration

Original Matlab code published in open source by Yang et al., (2010)) was taken for the study which was compatible only in older versions of Matlab code. Hence, the initial task was to run the code in Matlab 2018. After multiple debugging, the problem was fixed and the major error found was 'fmincon' error. Fmincon error occurred while running the script Demo_Dictionary_training.m. The script line 34 in the l2ls_learn_basis_dual.m was modified to options = optimset('GradObj','on', 'Hessian','on','Algorithm','trust-region-reflective'); to solve the issue. The error occurred because fmincon changed since the Matlab 2014 version. The original code was developed to enhance normal images with BMP format whereas, here the code had to be applied to individual satellite bands. The Matlab code has been modified from original RGB format input to single band input in .tif format. The output was set to get the satellite image in .tif format. Customisation of the input, output and localised paths of codes in Demo_Dictionary_training.m and Demo_SR.m were done to make the code run.

For the running of code, both fine resolution and coarse resolution satellite images of the same area have to be given as the input. The fine resolution image (WV-3) shall be stored in the training folder inside the data folder and the coarse resolution image (Sentinel-2) have to be stored in the testing folder inside the same data folder. Customising the input satellite images into a specific format is the subsequent task.

Digital number or the pixel values computation and comparison is done in sparse representation. The method aims to generate a relation between coarse resolution and fine resolution images texture and edge content (Elad, 2010). The code enhances the spatial resolution by computing the fine resolution and coarse resolution dictionaries (output of training phase) trained by the usage of fine resolution satellite data (WV-3). In order to apply these values adequately for enhancement (reconstruction phase), both coarse and fine resolution images were radiometrically corrected. As DN values are different for both Sentinel-2 and WV-3 images, it is not possible to compare both raw images; this is better done after converting both images' corresponding reflectance values. Hence DN was converted to the corresponding reflectance value.

The radiometric corrections allow a more accurate assessment of ground surface properties and facilitate comparison between images acquired at different times or for different areas (MicroImages, 2016). This study employed absolute radiometric correction for converting DN to radiance and radiance to reflection. Further it is not necessary to implement atmospheric correction as the urban area classification was the only concern (Lin et al., 2015). The equation to convert DN to the reflectance of WorldView-3 image is as follows (DigitalGlobe, 2016):

Step 1: DN to Radiance (L)

$$L = GAIN * DN * \left(\frac{abscalfactor}{effectivebandwidth}\right) + OFFSET$$

Step 2: Radiance (L) to Reflectance (ρ)

$$\rho = \frac{L}{F_0}$$

Where F_0 is the extraterrestrial solar irradiance (constant). The abscal factor, effective bandwidth and offset values are obtained from the WV-3 metadata file. The solar irradiance constant is obtained from the DigitalGlobe (2016) manual.

In the case of Sentinel-2A, pixel radiometric measurements are provided in Top-Of-Atmosphere (TOA) reflectance with all parameters, to transform them into radiances (Gascon et al., 2017; Gatti & Bertolini, 2016). The conversion formulae to apply to image DN to obtain physical values is:

Reflectance (float) = DN / (QUANTIFICATION_VALUE)

As the default quantification value for all Sentinel-2 images is 10000, Sentinel-2A image is divided by 10,000 so as to convert from DN to reflectance value. In the case of satellite data, the code looks at the spectral values of the input satellite data. Hence it is very important to identify similar spectral bands in both coarse and fine images. The wavebands NIR, Red and Green of WV-3 with a spatial resolution of 1.2m were taken for training and preparing a dictionary. The WV-3 images spatial resolution has been resampled to 1m for the smooth running of code. The corresponding NIR, Red and Green bands of Sentinel-2 with a spatial resolution of 10m have been taken as input data for spatial resolution enhancement.

Sparse representation code execution requires a single band fine resolution image (WV-3) along with the respective spectral band of coarse resolution (Sentinel-2) image as input. Accordingly, the NIR, Red and Green bands are extracted separately in .tif format and given as input. The code has to be run separately for each band enhancement.

4.4.2 Training phase

Sparse representation works mainly in two phases, out of which the training phase is the first part. In this phase, the information to enhance the coarse resolution image is created and stored in .mat format called a dictionary. Using the input fine resolution satellite data two dictionaries (coarse and fine resolution) have to be created.

To create a dictionary, optimum values for four parameters have to be found out. Further, dictionary size, sample numbers, zoom factor, and patch size have to be defined. There are no specific values to define these parameters (Yang et al., 2010), so the trial and error method has to be adopted to find optimum values.

Dictionary size can be defined in 2^n format, i.e. it can be 256, 512, 1024 and so on. Adopting a larger dictionary size could provide more accurate results (Cheng, 2015), but it also increases the computational time. The dictionary is the main part of the image reconstruction. Once a proper dictionary is generated from a sample area, then it can be applied to any similar region. By considering all these factors, the dictionary size of 2048 was chosen.

Sample number defines how many patches have to be selected. The designed dictionary will select patches randomly but the designed dictionary will select the patches having specific information. If any selected patch has repetitive information, the same will be discarded. The higher sample numbers give enrichment to the dictionary and different combinations will be stored. So a sample number of 1,00,000 were assigned.

Zoom factor (up-scale in Matlab code) lets the display zoom by a scale factor. Zoom factor is important in sparse representation during both the training and reconstruction phase, but it works the opposite in the two phases. During the training phase, the zoom factor helps to discard a relevant number of columns and rows to form a new large cell, whereas, during the reconstruction phase, it acts as a magnification factor. In the present study, during the training phase, input imagery (WV-3) was downscaled or degraded to 10m spatial resolution. i. e. 10*10 pixels of 1m were joined together to form one pixel of 10m resolution. Further during the reconstruction phase, coarse resolution (Sentinel-2) imagery was zoomed to 1m spatial resolution. Here one pixel with a spatial resolution of 10m was replaced by 10 pixels. One pixel of Sentinel-2 account for 10*10 metre.

Patch size is the other parameter to set and it determines the number of pixels or cells to be considered for forming a sample. A patch size of 10 was given as input because there is a relation between patch size and zoom factor. The minimum patch size should not be less than the zoom factor (Peleg & Elad, 2014).

Once all the parameters are set, the code was executed in a high-end workstation. A single band of fine resolution image (WV-3) was given as input in .tif format. It took approximately eight hours to generate the dictionary for one band. The optimum values were found out by the trial and error method. Two dictionaries (coarse and fine) are created for each band.

4.4.3 Reconstruction phase

This is the second phase of the sparse representation in which the coarse resolution image (Sentinel-2 of 10 metre spatial resolution) is considered. Based on the dictionaries already generated, the lost texture and edges are estimated. The zoom factor of 10 has been set as this could create an enhanced output image of one-metre pixel size from the original input of 10m Sentinel-2 image. The output locations are specified in this operation and the output will be in .tif format.

Generation of the dictionary is the key thing in sparse representation. Dictionaries generated from one region can be applied to other similar regions (areas with similar topographical features, building types and structure, roof tops etc.) to enhance the resolution of spatial features. In the present work, two reconstruction works were done with the same dictionary. First, the reconstruction phase was applied to the Sentinel-2 image for the same geographical area as the WV-3 image. Further, the reconstruction phase was applied to enhance the Sentinel-2 image of the Huangpu region. The reconstruction phase took approximately four hours to produce output for a single band. The parameters used in the training phase and the reconstruction phase are shown in the table (Table 4.3).

Resultant outputs provided individually enhanced spatial resolution for NIR, red and green spectrum. Many post-processing steps are required to prepare the satellite images ready for image classification and feature extraction. Firstly these images were stacked together to create the multispectral image. As the output of sparse representation will not have spatial referencing and projection system, the output images were georeferenced by keeping the original Sentinel-2 image as the base. Validation of the results by visual interpretation with the original Sentinel-2 image was the final task after the geo-referencing.

Table 4.3 Parameters for training and reconstruction phase

Phase	Image	Upscaling Sentinel-2 from 10 m to 1m
Training	Input Image	WorldView-3 of 1m spatial resolution
	Spectral bands	NIR, Red, Green
	Dictionary size	2048
	Number of samples	1,00,000
	Patch size	10
	Downscale factor	10
Reconstruction	Input Image	Sentinel-2 with 10 m spatial resolution
	Spectral bands	NIR, Red, Green
	Up-scale factor	10

4.5 Evaluation of output from sparse representation

This section explores how the spatial resolution of Sentinel-2 has been enhanced following sparse representation techniques with respect to its usage as an input into 3D city modelling. As explained in the methodology section, spatial resolution enhancement for Sentinel-2 images has been carried out for two areas using the dictionary generated from training. One area is where the WV-3 data is available (Figure 4.1) and the other area is the Huangpu District. Therefore, this section is organised into two sub sections: i) results for sample area (4.5.1) and ii) results for Huangpu District (4.5.2). Based on selected sample features from both areas, these sub sections mainly provide an overview of how the spatial resolution of selected features was enhanced after the usage of sparse representation techniques. The enhanced images appear reduced in colour, which is due to the histogram variation. The term variance refers to a statistical measurement of the spread between numbers in a data set. The enhanced Sentinel-2 image is for a small urban area which has more reflectance. Hence the colour shade is more towards the brighter side. While the raw Sentinel-2 image is for a larger scene and histogram include more vegetation, water and other features, so the histogram is more spread and has a little darker side or the DN representation is little different.

An assessment of the output enhanced Sentinel-2 image was done via visual assessment and comparison of the outputs (10m Sentinel-2 image vs enhanced Sentinel-2 image to 1m) and the results are elaborated in below sections. Lastly, the comparison between the 10m and 1m (enhanced) Sentinel-2 data was undertaken via comparative assessment of an unsupervised classification based method to map urban features across the scene (4.5.3).

4.5.1 Visual assessment for the area coinciding with the WorldView data

Large buildings, high rise/tall buildings, small buildings, road, water body and vegetation were the subset features identified in order to demonstrate their response to resolution enhancement from this area. Figure 4.3 to 4.8 provides subsets of these features and demonstrates how the spatial resolution of these features visually varies in WV-3, Sentinel-2 (10m) and spatially enhanced Sentinel-2 (1m) images. Each of these subsets is shown in two scales (1:10000 and 1:5000). These scales are chosen as they provide optimum visualisation as well as being easier to measure than in 4500 or 9500 scales.

4.5.1.1 Large buildings

Figure 4.3 represents a small subset of large buildings (that have a pixel size of 4*4 pixels or more in Sentinel-2 10m image). It is to be noted that the comparison should be done between Sentinel-2 (10m) and spatially enhanced Sentinel-2 (1m) images so as to understand the nature and extent of enhancement. In this case, the major difference observed between original Sentinel-2 and spatially enhanced Sentinel-2 images was on the edges of buildings. From the subset area given in Figure 3, it can be observed that the original Sentinel-2 image with 10m resolution has distorted edges with mixed pixels, whereas in the case of spatially enhanced Sentinel-2 image with 1m resolution these edges became more enhanced and sharpened.

In each of these images, the maximum length of buildings has been measured by creating transects for random buildings. This method is chosen to understand the change of length of matching buildings in different satellite images. The actual length of the building is more accurately shown in the very high resolution WV-3 satellite image and considered as true value. The measured length values of the same buildings from the other two satellite images show how much closer these values are to the true value from WV-3 satellite image. It is noted that the maximum length of buildings is greater in the Sentinel-2 (10m) image than the WV-3 images. The length of buildings for the enhanced Sentinel-2 (1m) image was found to be less than the length shown in the original Sentinel-2 (10m) but higher than the WV-3 image derived length. Further, spatially enhanced images showed minimal mixed pixels for areas closer to vegetation and edges of buildings became more distinct from the adjacent vegetation.

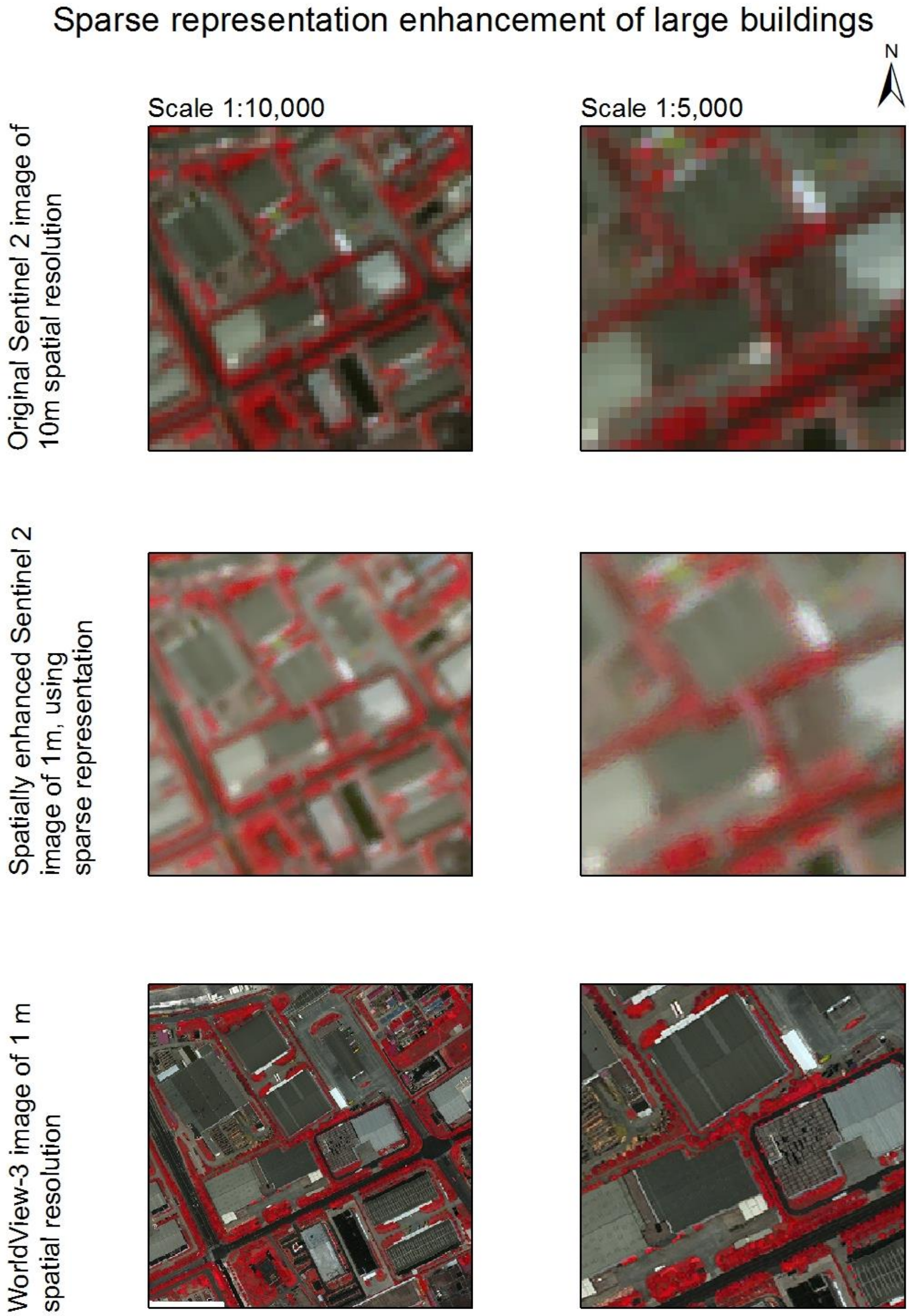

Figure 4.3 Spatial enhancement of large buildings through sparse representation

4.5.1.2 High rise buildings

Figure 4.4 represents a subset of high rise buildings in the sample area. Buildings with a height of 50m or more are classified as high rise buildings. From WV-3 it can be observed that the southern and eastern part of the image is occupied by high rise buildings. From the original Sentinel-2 image it is hard to distinguish these buildings. Especially at 1:5000 scale buildings are highly distorted and as in the case of large buildings due to mixed pixels, it is hard to define the shape and edges of buildings. In the case of high rise buildings, base areas of buildings are reduced compared to large buildings. Hence it is very difficult to identify these buildings in Sentinel-2 image with 10m resolution and they appear highly mixed up and diluted.

After the spatial enhancement, it can be observed as in Figure 4.4 that these buildings became more distinguishable. Further, the white coloured pixels are clustered together and display a very dense and accumulated appearance, unlike flat buildings.

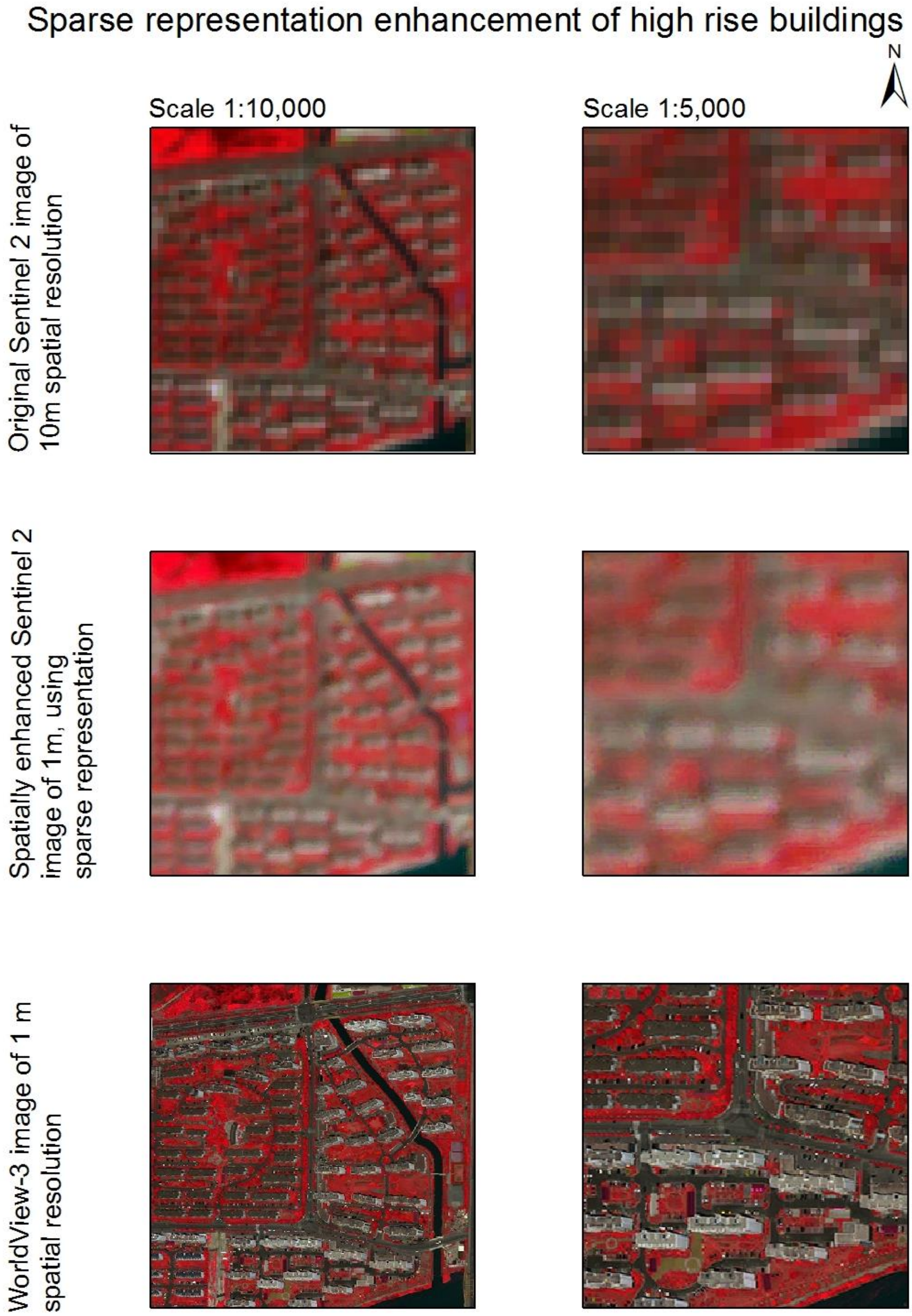

Figure 4.4 Spatial enhancement of high rise buildings through sparse representation

4.5.1.3 Small buildings

Figure 4.5 shows a subset area with a mix of small buildings i. e. buildings with a pixel size less than 2 lengths or breadth in Sentinel-2 10m image (towards the north) and medium rise buildings (southeast).

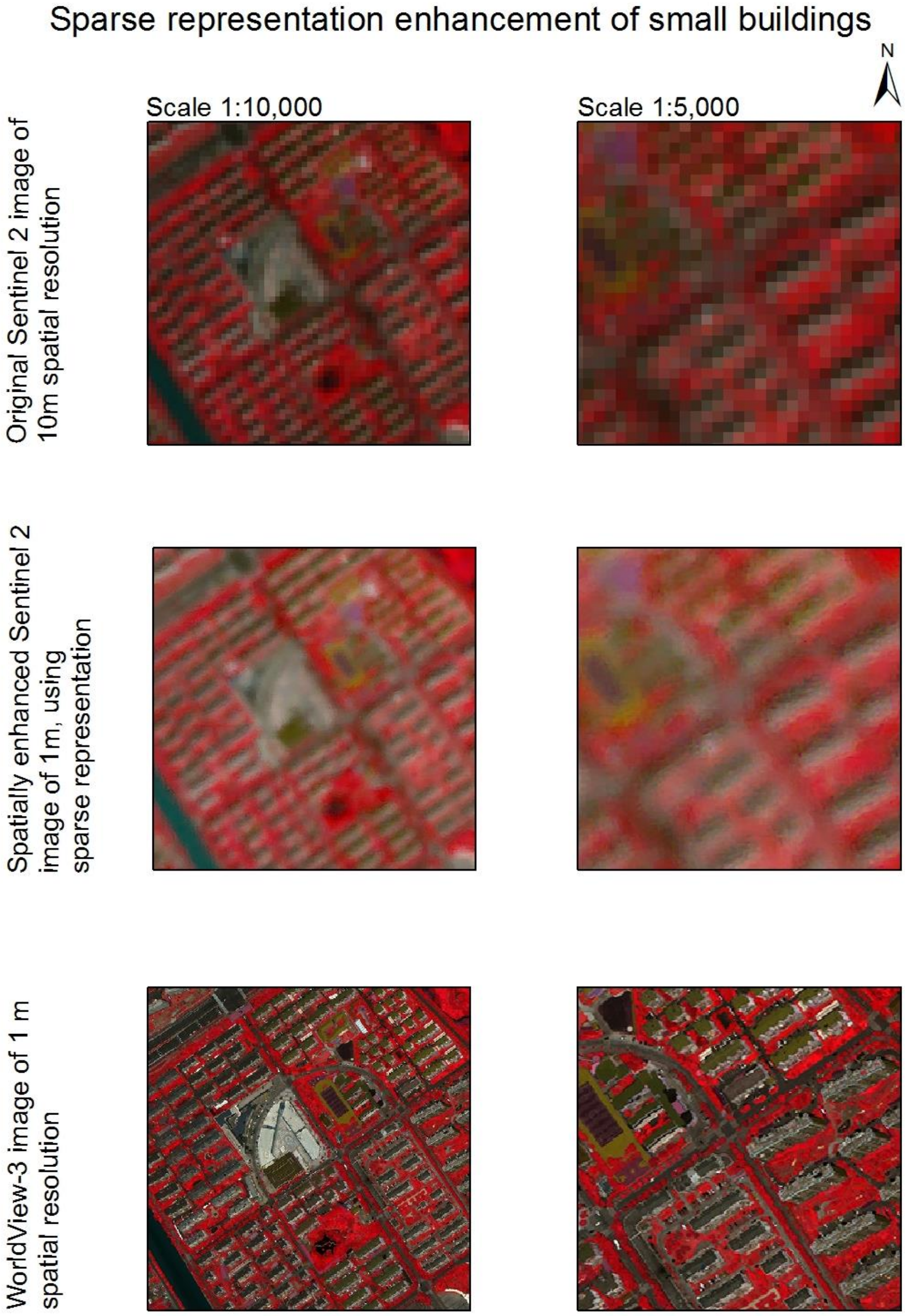

Figure 4.5 Spatial enhancement of small buildings through sparse representation

From the original Sentinel-2 image it can be observed that small buildings are visible only as small, distorted and imperceptible linear features. Medium buildings also have a distorted shape but they are denser. After performing sparse representation techniques these buildings have become more prominent, continuous and distinguishable.

To understand representation of small buildings in different images transects were created for buildings in each image and compared. WV-3 is taken as reference and length of small buildings in Sentinel-2 and enhanced Sentinel images are compared with reference to WV-3. Measurement of length of small buildings shows that these buildings are less distinguishable in Sentinel-2 images due to the issue of mixed pixels and length of buildings are longer than that of normal length. Table 4.4 shows measurement results for selected buildings and it can be observed that the deviation of length with respect to WV-3 is higher in Sentinel-2 (10m).

Table 4.4 Comparison of length of small buildings in different images

WV3	**Sentinel-2 (10m)**	**Enhanced Sentinel**	**Change in building length with respect to WV3 (in %)**	
Length in meters			Sentinel – 2 and WV3	Enhanced Sentinel and WV3
98.05	107.06	94.43	9.19	-3.70
72.72	84.77	71.27	16.57	-1.99
82.37	94.18	87.42	14.34	6.13
97.80	108.43	98.52	10.86	0.73
35.73	42.80	34.60	19.78	-3.16
120.88	120.02	113.24	-0.71	-6.32
129.27	137.96	130.49	6.72	0.94
99.07	103.13	98.99	4.10	-0.08
140.21	150.15	143.83	7.09	2.58
102.21	103.18	103.42	0.95	1.18

However it is also observed that the enhanced image tends to show lesser length in comparison to WV-3. This reduction is largely due to edge sharpening and separation between different buildings. Thus it is clear that enhanced Sentinel-2 image produces more accurate results in case of small buildings in comparison to Sentinel-2 images whereas achieving complete accuracy is not possible yet.

4.5.1.4 Road features

The response of road features to sparse representation techniques is as demonstrated in figure 4.6. In the subset area shown, big highway roads, as well as small footpaths, are visible and hence observations were made on both types. In the original Sentinel-2 image, the edges of the big highway road are diluted with adjacent vegetation. Whereas, after the spatial enhancement, highway edges became prominent and distinct from vegetation. There is a big circle in the subset where all four major roads meet. In WorldView-3, white marks along the roads at this junction point were visible, which is unclear in the original Sentinel-2 image. Figure 6 shows that after the spatial enhancement these white marks became clearer and prominent.

In the subset, image footpaths were noticed along the sides of canals. Even though these footpaths are visible in the Sentinel-2 (10m) image they are discontinuous. Spatially enhanced Sentinel-2 (1m) image shows these footpaths as a single, continuous line feature. Another important feature observed was a circular shaped footpath towards the southwestern side of the subset image. In the original Sentinel-2 image this circle is not visible but is enhanced and sharpened after the spatial enhancement.

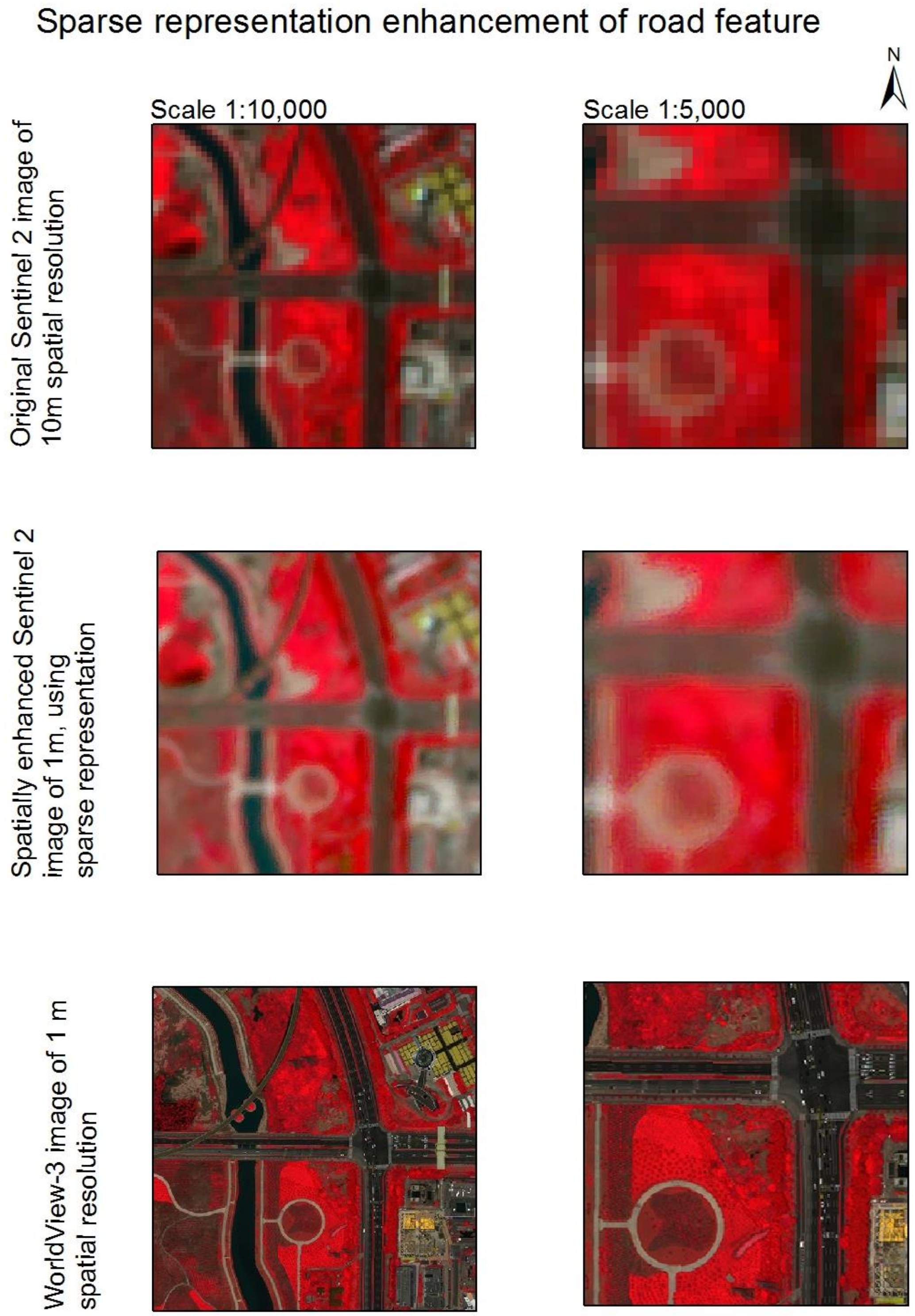

Figure 4.6 Spatial enhancement of road feature through sparse representation

4.5.1.5 Vegetation

Figure 4.7 portrays the subset for vegetation. Even though the enhancement of vegetation is not important in the current study, a clear difference before and after the spatial enhancement process was observed.

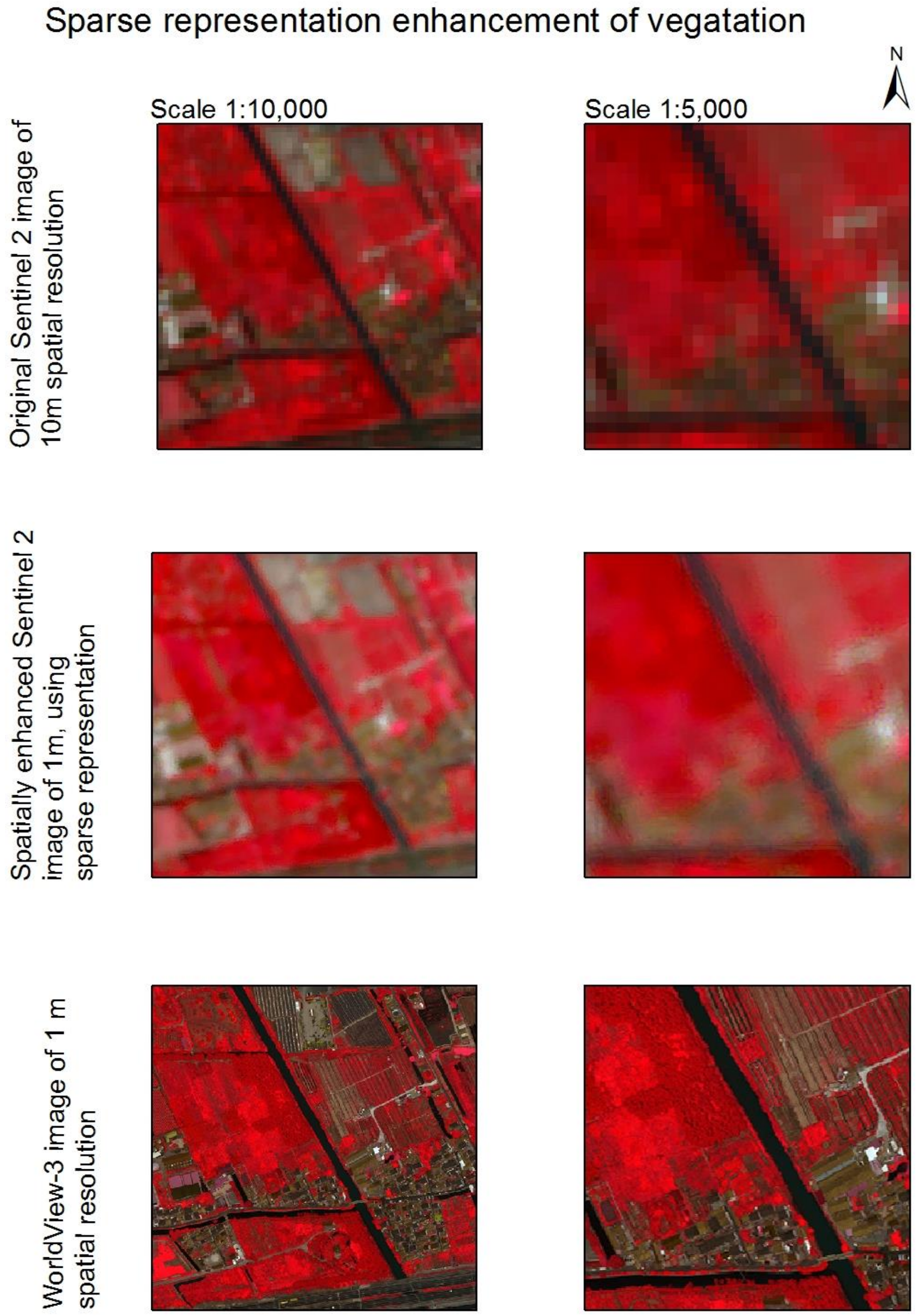

Figure 4.7 Spatial enhancement of vegetation through sparse representation

The main advantage of the spatial enhancement, in this case, is that edges of vegetation become more prominent and sharpened which easily allows to avoid mixed pixels as well as to distinguish buildings and roads from vegetation.

4.5.1.6 Waterbody

Figure 4.8 represents the subset area with a waterbody. In the original Sentinel-2 image the boundaries of vegetation and the waterbody are overlapped whereas after the spatial enhancement these boundaries became clear and sharpened. However, according to different seasons, the water level may fluctuate and the shapes of water bodies can be altered. Hence, for classifications, it is important to consider the period of images for the analysis.

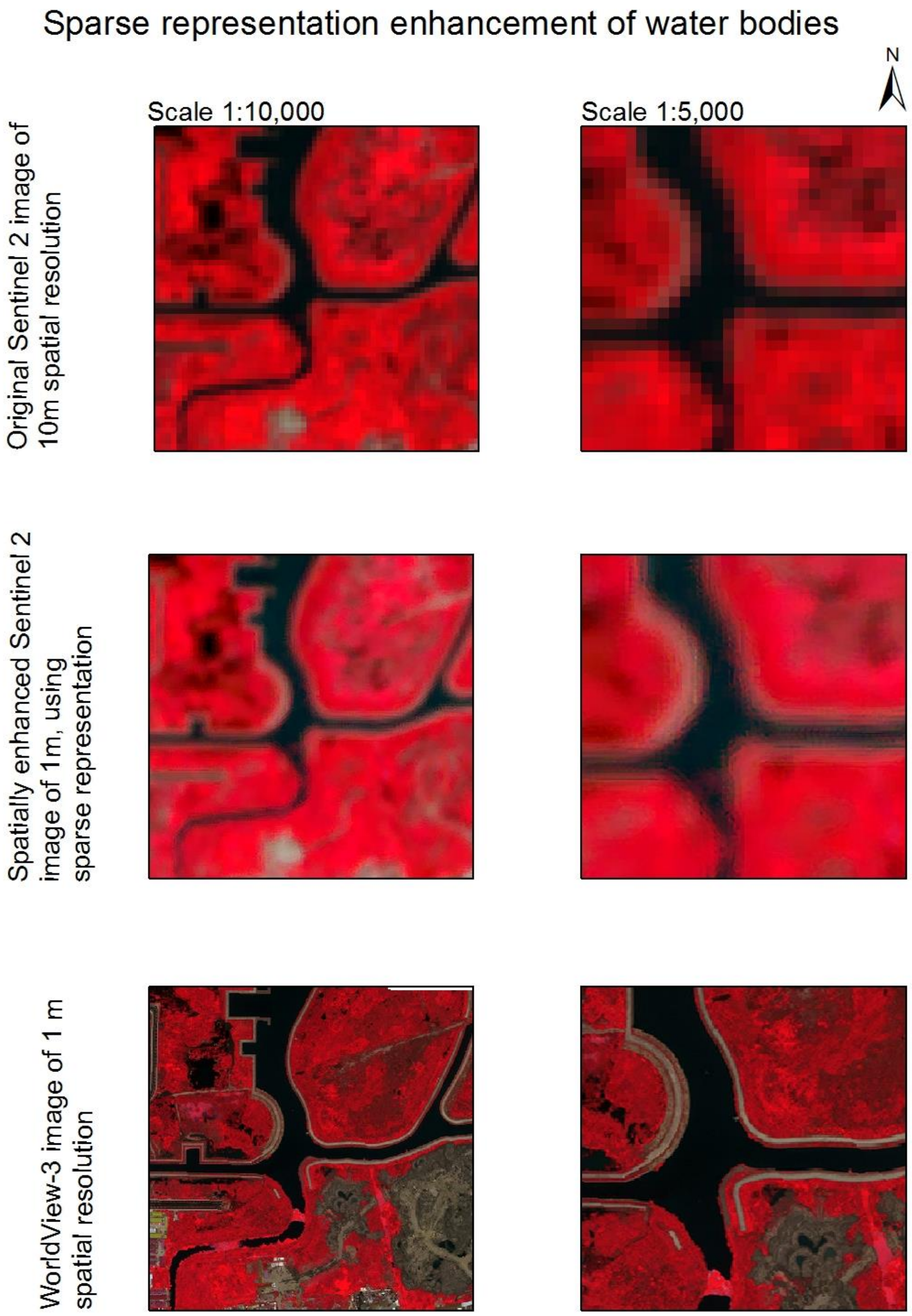

Figure 4.8 Spatial enhancement of waterbodies through sparse representation

4.5.2 Visual assessment for Huangpu District, Shanghai (beyond the Worldview area)

This section provides an overview of how the sparse representation techniques enhanced the spatial resolution in Huangpu District. It may be noted that the dictionary generated was outside the Huangpu District. Figure 4.9 shows the visual difference between the original Sentinel-2 (10m) and enhanced Sentinel-2 (1m) image with examples of three selected subsets of Huangpu District. From the subset images it is clear that, after performing the sparse representation techniques, features like buildings, roads and water bodies became more prominent, sharp and distinct. Pixels on the edges of features are grouped to the main objects or features and this avoids the issue of mixed pixels.

The subset image 4.9 (a) is occupied by very small buildings and patches of vegetation. In the original Sentinel-2 (10m) image this area looks very coarse textured and unclear. After the spatial enhancement, these features become clearer and individually identifiable. From subset images 4.9 (b) and 4.9 (c), it is clear that the shapes of individual buildings become clearer and identifiable after the sparse representation process. This is explained in more detail in the next paragraph. Likewise in the subset image 4.9 (c) the distinction between land areas and the water bodies is very clear and smooth after the spatial enhancement.

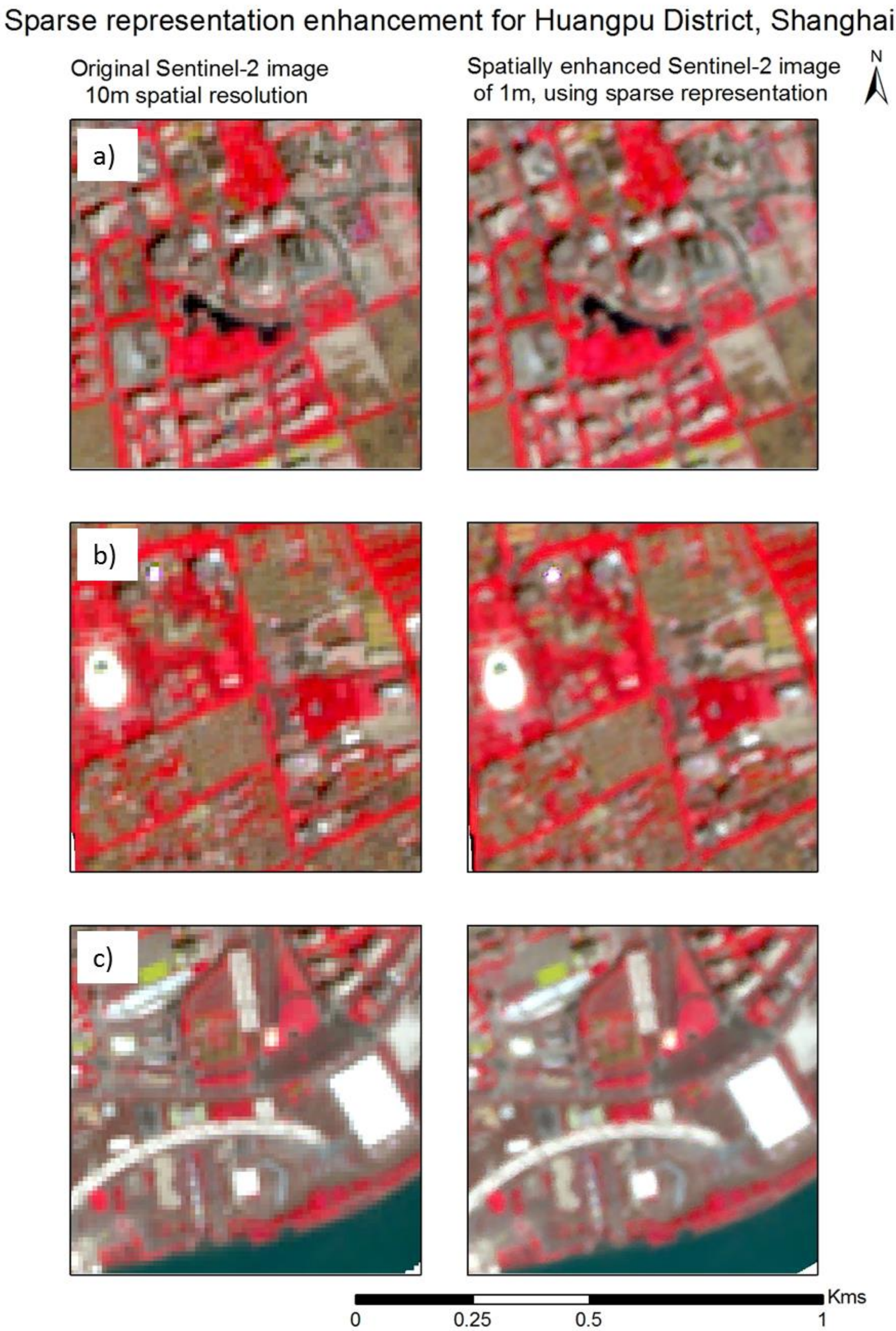

Figure 4.9 Visual difference between original Sentinel-2 (10m) and enhanced Sentinel-2 (1m) image after sparse representation with selected examples from Huangpu District

Figure 4.10 and 4.11 provides examples of different building shapes and their appearance before and after the sparse representation as well as in Google Earth Image. Figure 10 displays the subset image of an oval-shaped building. It can be observed that the shape of the building is not clear in the original Sentinel-2 (10m) image (Figure 4.10a). After spatial enhancement (Figure 4.10b) the shape of the building becomes prominent with sharp edges and matches with the shape of the building in Google Earth (Figure 4.10c).

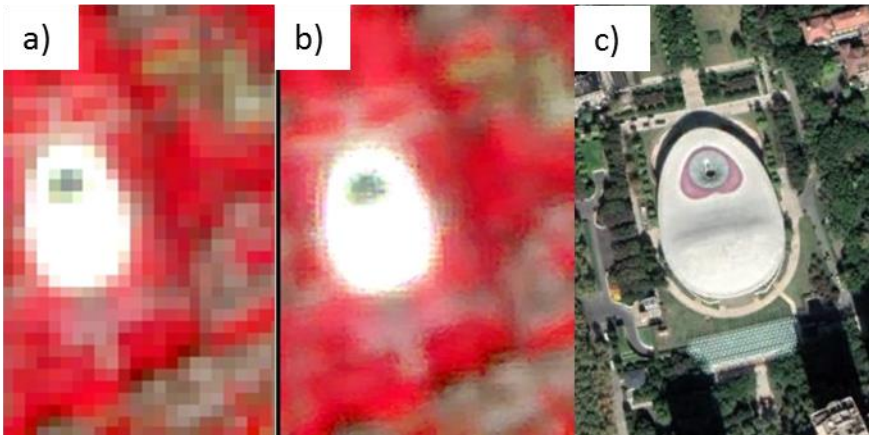

Figure 4.10 Appearance of an oval shaped building in a) Original Sentinel-2 image (10m), b) spatially enhanced Sentinel-2 image (1m), c) subset of Google Earth image (not to scale)

In figure 4.11 also similar observations were made. The subset image shows an area with a big arch-shaped building complex and a large rectangle-shaped building. As in figure 10, it was observed that the shapes and edges of these buildings became prominent and matched with that of the Google Earth image.

It may be noted that these results are obtained after using a dictionary generated outside of Huangpu District. These results shed light on the potential applications of both WV-3 and Sentinel-2 images. Generating dictionaries from WV-3 across the globe has huge potential on one hand, while on the other hand, global coverage and a frequent revisit of Sentinel-2 open up the scope of producing spatially enhanced Sentinel-2 images using dictionaries generated using WorldView-3. Further, these spatially enhanced Sentinel-2 datasets can be used in generating 2D buildings footprints for the regions where 2D building datasets are not available for free.

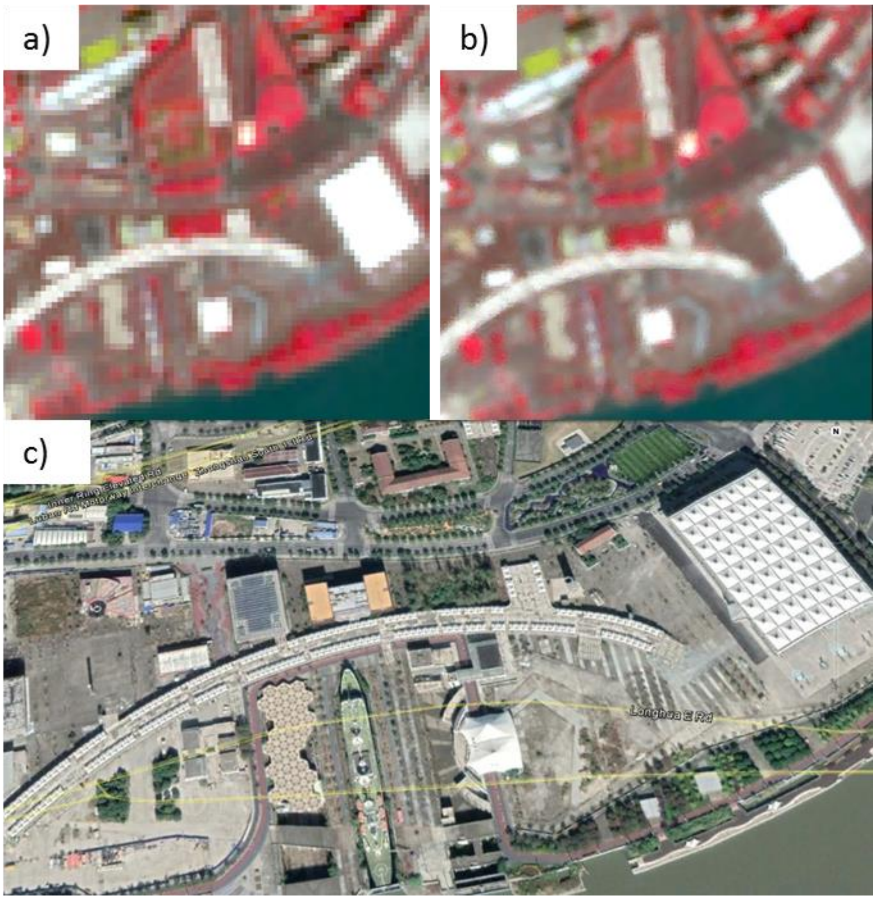

Figure 4.11 Appearance of an arch-shaped building and a rectangle-shaped building in a) Original Sentinel-2 image (10m), b) spatially enhanced Sentinel-2 image (1m), c) subset of Google Earth Image (not to scale)

4.5.3 Assessment via unsupervised classification

To extract urban features from the enhanced Sentinel-2 scene for Huangpu, an unsupervised classification was conducted and its efficacy compared with the same classification procedure being applied to the original Sentinel-2 scene. This classification process involved several steps, as outlined further. The detailed flow chart for the classification is shown in the next chapter.

4.5.3.1 Removal of vegetation from the urban scene

The Normalized Differenced Vegetation Index (NDVI) was performed to remove the healthy vegetation area from the satellite image (NDVI = ((IR - R)/(IR + R)) where IR is the pixel values from the infrared band and R is the pixel values from the red band). NDVI analyses the photosynthetic activity of vegetation and is a good indicator for the vitality of vegetation or for its growth stage. Usually, this index is largely used to analyse the spatial distribution and seasonal fluctuation of vegetation over a region. Further, the index can also be used to differentiate between vegetation and plant fewer land covers, which is helpful for image classification. Here the NDVI was used to determine, where the vegetation across the urban scene was, in order to remove these from further analyses. Once the NDVI was generated for the study area, the whole NDVI image was classified into different classes based on the spectral values and the threshold for healthy vegetation was identified by visual interpretation. These healthy vegetation areas are removed from the original satellite image using a masking function. This was done to reduce the effect of vegetation on the impervious/building layer extraction process.

4.5.3.2 Classification of an impervious layer

As previously stated, the vegetation area was removed from the satellite image and the resultant image mainly shows the impervious layer and water body of the urban area. The impervious layer consists of road, buildings and other major human made features where the water penetration is limited (Frazer 2005). The unsupervised classification was then applied to the imagery. The k-means clustering algorithm was used for the classification. The convergence threshold was set as 0.950 with the maximum iteration of 25 times. The whole image was classified into 40 different classes and the grouping of similar classes was done by comparing each class with the corresponding area on google earth. The initial classes of 40 were chosen by trial and error method. The unsupervised classes gave optimal spectral separation in the given area for Sentinel-2 image. Seven classes have been finalized by regrouping these 40 classes, which include water, road, resultant vegetation area, open area, buildings with high brightness roof, building with red/dark shade roofs and general buildings.

Even though there are other image classification methods like supervised classification and object based classification, the unsupervised classification method was chosen, as this method allowed using the high resolution Google Earth satellite image for visual interpretation. The high resolution Google Earth image was geographically linked to the classified satellite image. Each of the forty classes derived from unsupervised classification was regrouped to seven classes by looking at the high resolution satellite data via visual interpretation technique.

The grouping of classes representing water bodies was done with relative ease. The buildings which have high reflectance values or distinctive reflectance values were able to be extracted easily. The grouping of the buildings falling in a highly clustered area or with low spectral reflectance was found to be difficult to extract. In these regions, the pixel values were seen to have similarities with the pixel values of adjacent road features. These mixed pixel areas were extracted separately from the satellite image and the unsupervised classification applied again for this area to increase the overall classification accuracy.

4.5.3.3 Validation of classified images

Both Sentinel-2 image (10 m) and enhanced Sentinel-2 image (1m) were classified using the above procedure. The accuracy of each classification was validated by selecting 30 random points for each class (Richards 2012; Rwanga Olofsson et al. 2014; and Ndambuki 2017). The points were selected with the help of ArcGIS high resolution base map and by use of raw Sentinel-2 image. The water and vegetation accuracy was not considered as the water area was limited and most of the vegetation area was removed using NDVI method. So 30 points were selected for each remaining class viz road, open area, general building, bright roof building and red/grey roof buildings.

4.5.3.4 Classification outputs and comparison between original and enhanced Sentinel-2 scenes

Figure 4.12 (LHS) shows the classified output based on the original Sentinel-2 data (at 10 m spatial resolution). From the figure, it can be observed that the maximum area i. e. 42% (6.4 sq.km) falls in the open category followed by buildings with red/dark roofs (22%) and roads (16%). The area under buildings with the bright roof is less than 1% (0.14 sq.km) and of general buildings is around 6% (Table 4.5).

Classification output for the enhanced Sentinel-2 image (1m) showed a decrease in open class (Figure 4.12 RHS) compared to that obtained using the original image. In the case of the enhanced Sentinel-2 image, the area under open class is reduced to 28% (4.3 sq.km) against 42% in the Sentinel-2 (10m) image. Other classes showed real differences. For example, area under general buildings was increased from 6% to 21% and buildings with the bright roof has been increased by 5%.

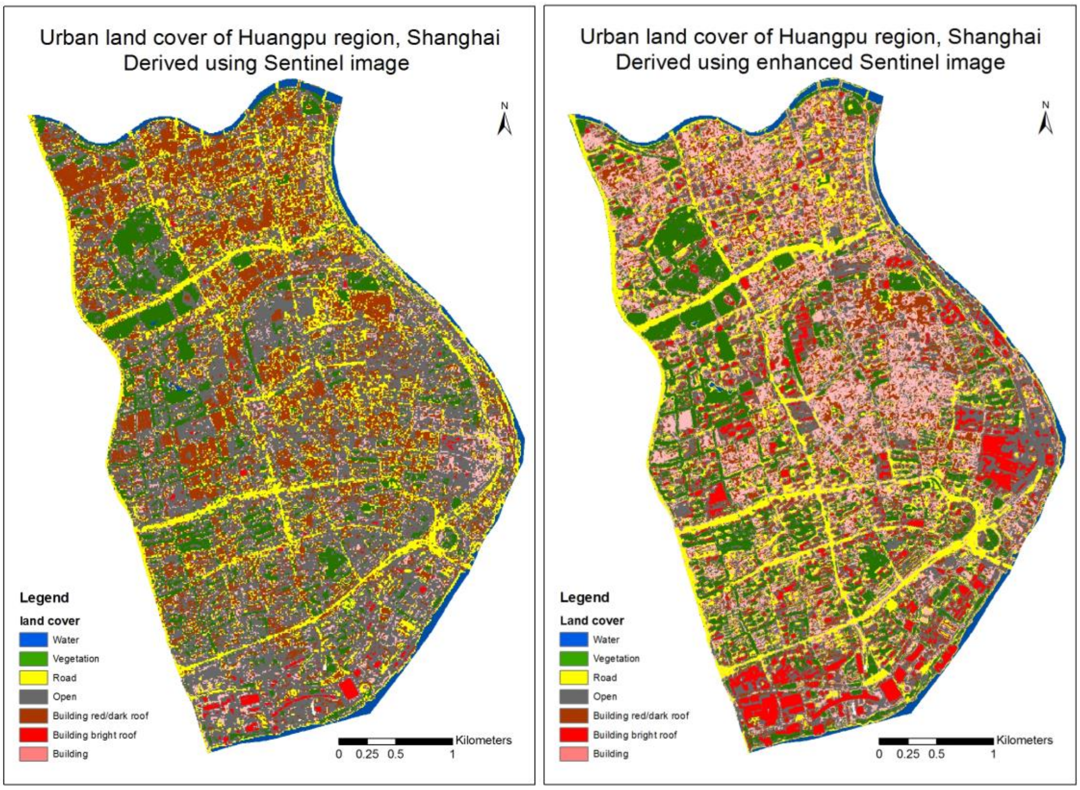

Figure 4.12 Classified map of 10 m Sentinel-2 satellite data left hand side (LHS); Classified map of enhanced 1m Sentinel-2 satellite data right hand side (RHS)

The enhanced Sentinel-2 image was found to be more able to identify bright buildings or buildings with clear patterns and uniform colour. However, in the enhanced Sentinel image area of buildings with red/dark roof declined from 22% (3.3 sq. km) to 14% (2.1 sq. km) as these buildings were largely moved to general buildings. This is due to the capability of enhanced Sentinel-2 images in distinguishing mixed pixels into corresponding classes with relative better accuracy than that of Sentinel-2 images.

Table 4.5 Areas of selected urban feature classes from Sentinel-2 (10m), enhanced Sentinel-2 (1m)

	Sentinel-2 (10m)	Enhanced Sentinel-2 (1m)
Land cover	**Area in sq.km**	
Building (general)	0.96	3.24
Building bright roof	0.14	1.00
Building red/dark roof	3.34	2.13
Open	6.44	4.34
Road	2.53	2.39
Vegetation	1.65	1.98
Water	0.31	0.30

Table 4.6 provides an overview of accuracy assessment results for Sentinel-2 images before and after spatial resolution enhancement. Results show that the accuracy of all features was improved after spatial enhancement except for the open class. While the accuracy of road features was increased from 73% in Sentinel-2 (10m) to 83% in spatially enhanced Sentinel-2 (1m), it declined for open class after spatial enhancement. The accuracy of the open class was relatively higher (83%) in the Sentinel-2 (10m) image in comparison to the enhanced sentinel-2 -1m (77%) image. Accuracy reduction in enhanced Sentinel-2 image can be attributed to relative edge sharpening and edge enhancement of features. This is because the Sentinel-2 image represents a 10*10 metre area as one pixel and it will be classified as either open or building class. Whilst in the enhanced Sentinel-2 image the same area is divided into 10 pixels and each pixel is classified into open or building class depending on their relevance. Hence it results in edge enhancement and better separation is possible in enhanced Sentinel-2 image.

Overall, the Sentinel-2 image showed very high accuracy in the case of bright buildings (97% accuracy for Sentinel-2 (10m) and 100% accuracy for enhanced Sentinel (1m) images). Likewise dark/red tile buildings also showed relatively higher accuracy in both scenarios (about 87% in Sentinel-2 (10m) and 93% in enhanced Sentinel (1m) image). Whereas, the accuracy of general buildings was relatively low (50%) in the case of Sentinel-2 (10m) image which showed considerable improvement after the spatial resolution enhancement (i. e. 80% in enhanced Sentinel-2).

Table 4.6 Accuracy assessment results (in %) of land cover classification from Sentinel-2 (10m) and enhanced Sentinel-2 (1m) images

	Road	**Open**	**Bright building**	**Dark/red tile building**	**General building**	**Overall accuracy**
Sentinel-2 Image (10m)	73	83	97	87	50	78
Enhanced sentinel-2 image	83	77	100	93	80	87

4.6 Summary

Third chapter of this thesis provided a methodology to generate 3D city models for the regions where 2D building footprints are available. Attributed to non-availability of uniform and accurate open source 2D building footprints it is important to find alternatives for generation of 2D building footprints. As discussed in the second chapter open source satellite data has huge potential for generation of 2D building footprints especially in terms of their global coverage and open license irrespective of their coarse resolution. Still to make use of their full potential it is essential to overcome their resolution issues. In this context this chapter explores probabilities in enhancing the spatial resolution of Sentinel-2 images based on sparse representation techniques.

Results show that spatial enhancement through sparse representation contributes to edge sharpening of features and thereby results in better delineation of urban features especially of buildings. After performing sparse representation techniques all buildings that were originally distorted and amorphous in Sentinel-2 (10m) have become more prominent, continuous and distinguishable. Enhanced Sentinel images are also able to delineate road features and waterbodies from buildings and vegetation more accurately. Accuracy of all categories except open class were improved after spatial enhancement and the overall accuracy of buildings has increased from 78% to 87%. Accuracy reduction in open class can be attributed to relative edge sharpening and edge enhancement of features. Thus overall enhanced Sentinel-2 found to be more capable in distinguishing buildings and other urban features from adjacent features and in enhancing their shapes.

The following chapter (Chapter V) examines the use of the enhanced Sentinel-2 imagery in combination with the DSM data (as per Chapter III) to produce 3D city models. Ultimately, the efficacy of the approaches outlined in Chapter V with respect to use in different applications requiring a 3D city model will be considered – It is the case that low level 3D city models could now be produced globally via the methods presented in this thesis.

CHAPTER V

GENERATION OF LOD0 AND LOD1 3D CITY MODELS FROM OPEN SATELLITE DATA

5.1 Introduction

Chapter III illustrated how to generate 3D city models from open data if 2D building footprint data are available. However, as discussed in previous chapters, for many areas of interest across the world, access to open source fine (enough) resolution 2D building footprints are rare, which warrants alternative means to generate 2D building footprints. One approach is to use open source satellite images for generating building footprints (Shaloni et al., 2020; Zhang et al., 2017). However, the accuracy of the resultant 2D building footprints generated from satellite data largely depends on its spatial resolution (Bittner et al., 2018; Vakalopoulou et al., 2015). Finer spatial resolution implies a higher chance of accurately identifying the buildings and other urban features (You et al., 2018). Images with coarse spatial resolution may result in absence of many features or misclassification of non-building features as buildings and vice versa (Liu et al., 2019). Further, the identification of objects that are at the edge of visibility in these images remains a challenging task (Oehmcke et al., 2019). Many open licenced satellite images are of coarse spatial resolution which restricts their utility in urban studies. For example, Sentinel-2 imagery shows features at a resolution of 10m per pixel and how distinguishable features at this spatial resolution are dependent on their size, which sometimes can reach sub-pixel size.

Chapter IV demonstrated the potential to enhance the spatial resolution of coarse resolution satellite data (Sentinel-2: 10m) with a sample of very high resolution data (WorldView-3: 1m) based on sparse representation techniques in order to extract 2D building footprints in data void regions. Results from chapter 4 show that the sparse representation is helpful in the sharpening of the boundaries of different features of Sentinel-2. However, extracting buildings from spatially enhanced images can be a challenging process as they contain a number of other objects like trees, roads, concrete pavements, shadows and the like (Chen et al., 2017). In the areas where 2D building footprints are not available, infusing satellite images with digital surface models (DSMs) can be a possible solution to differentiate buildings from non-building impervious layers and thereby generate 3D city models. Wang et al., (2018) derived 3D building structures by fusing Landsat (30m) and global elevation data based on object-based machine learning techniques. With a finer spatial resolution, the Sentinel-2 imagery could be a more suitable data source for fusion.

This chapter reports the attempt to fuse spatially enhanced Sentinel-2 data (from 10m to 1m - generated in Chapter IV) with AW3D-30 DSM data in order to generate LOD0 3D and LOD1 3D buildings and thereby facilitate 3D city modelling in data void regions. To do this, urban features (buildings, roads etc.) are classified by an unsupervised classification technique. Even though many classification techniques such as object-based classification and supervised classification exist, the use of an unsupervised classification was chosen as it allows direct comparison with Google Earth images by geographically linking the satellite data with Google Earth images.

Given the absence of openly licenced satellite data, the highly urbanised Shanghai was chosen as the study area to demonstrate this method.

The first section of this chapter attempts to generate the LOD0 3D city model, from open satellite data, while the second section provides a comparative perspective on how the LOD0 3D city model behaves in the already identified OSM building footprint area of Huangpu. Comparison has been done between the OMS derived LOD1 3D city models area (i.e., the 3D city model generated based on already existing open 2D building footprint data – as seen in Chapter III) and the LOD0 city models in the same area (i.e., the 3D city model generated from open satellite datasets where there is no availability of open 2D building footprint data). The last part of the chapter provides an overview, validation of the LOD1 3D city models and 2D building polygons generated from the spatially enhanced satellite images and the associated challenges.

5.2 Materials and methods

5.2.1 Study area and data

The area of interest for the study is the same as in chapter III, Huangpu District of Shanghai. As stated in previous chapters, Huangpu District is characterised by tall and complex building structures with no readily available open source 2D building footprint data. A 10m Sentinel-2 image (captured in July 2016), the spatially enhanced 1m Sentinel-2 image (from chapter IV) and the ALOS Digital Surface Model (30m) were used.

5.2.2 Methodology

The overall methodology adopted in this chapter is shown in the flow chart given below (Figure 5.1) and comprises two main steps.

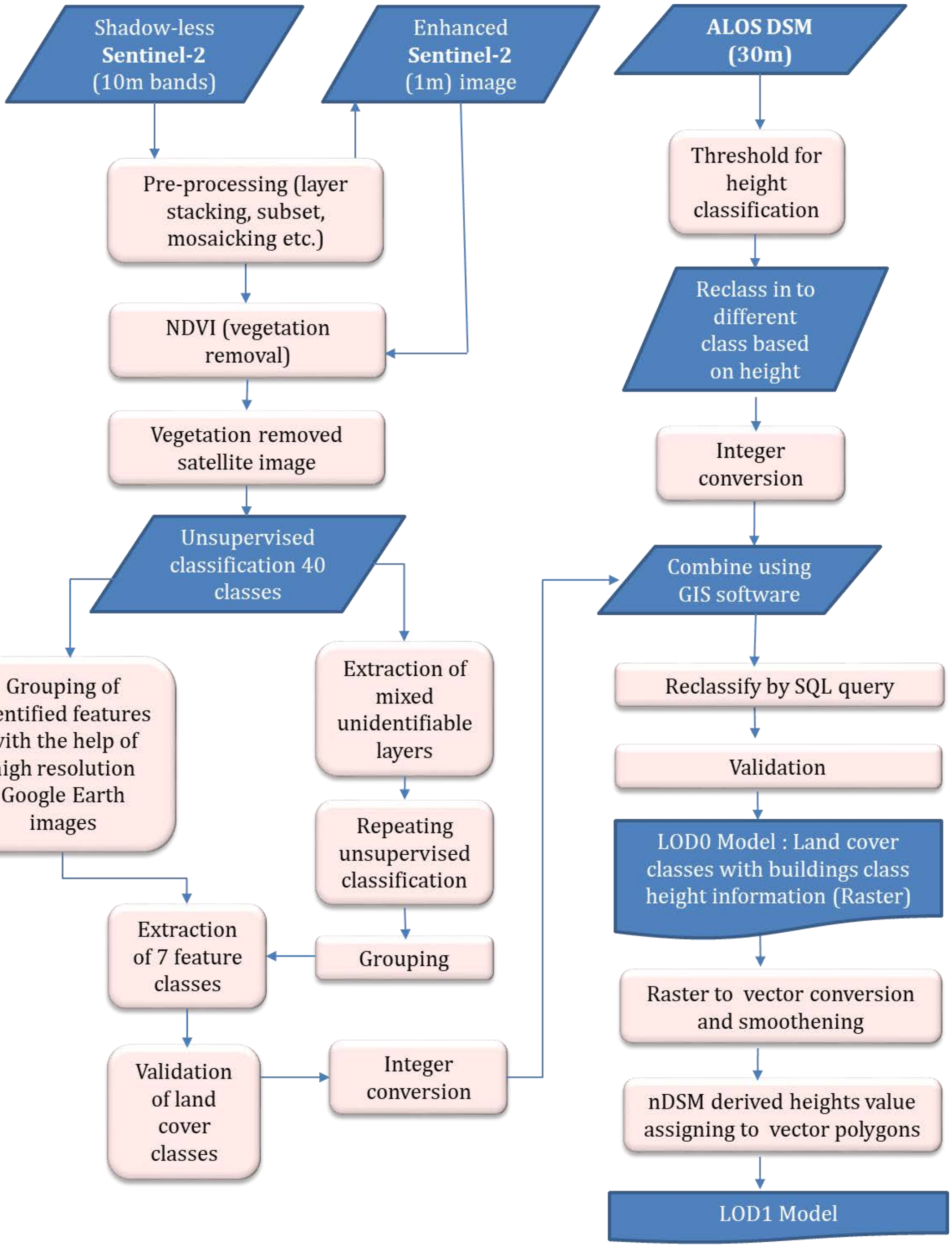

Figure 5.1 A flow chart of the steps taken to generate LOD0 and LOD1 3D city models by combining enhanced Sentinel-2 (1m) image with ALOS DSM (30m).

The enhanced 1m Sentinel-2 images generated through sparse representation are classified to extract the features with a special focus on building extraction. Further, the classified image will be joined with the height information from the ALOS DSM (30m) in the GIS environment to create more accurate building extraction in dense urban settings.

5.2.2.1 Cloud-free & shadow less Sentinel-2 (10m) data and Image pre-processing

The creation of 2D geospatial data are explained in the following steps. Earlier the Sentinel-2 satellite image which is open source and with a spatial resolution of 10 m was processed for data generation. The Sentinel-2 image has a temporal resolution of 5 days. The high temporal resolution of the Sentinel-2 image will help to choose the satellite image time period that has only a negligible amount of shadows building. For the Shanghai study area, the cloud-free and shadow-less (less than 10%) satellite image of July 2016 is taken for image processing as the effect of shadow on Urban buildings are negligible in the month (Figure 5.2 a & b).

The image pre-processing procedures such as layer stacking and sub-setting has been performed for the study area. The visible and NIR bands with a spatial resolution of 10m were taken into consideration and these bands were stacked together. The satellite image was used for image classification to measure the classification accuracy of the raw Sentinel-2 image and the spatial accuracy was increased to 1m by the sparse representation technique explained in the previous chapter. The resultant enhanced Sentinel-2 image (1m resolution) also was subsequently classified to extract the urban features.

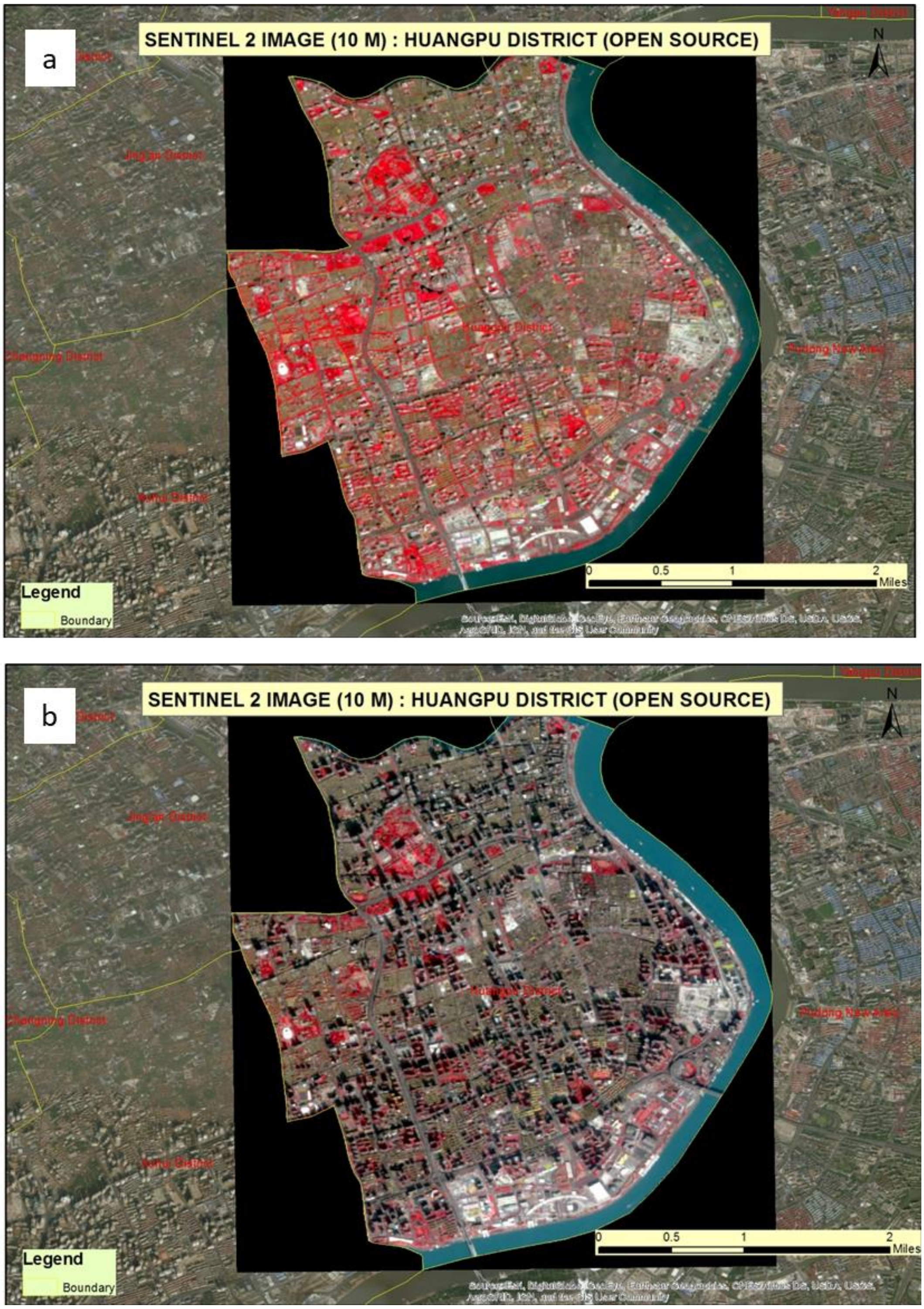

Figure 5.2 Maps showing difference between the cloud-free and shadow-less Sentinel-2 (10m) image (a) Sentinel-2 (10m) satellite with shadow and cloud cover (b) for Huangpu District, Shanghai

5.2.2.2 Utilising the digital surface model (DSM)

As urban area building extraction is challenging, the above classified image has been fused with the elevation information from the AW3D-30 DSM to increase the accuracy. The DSM has been classified into seven different classes as per the height information in the DSM. The classes were selected by the knowledge of the general terrain and building information of the area. The seven classes selected were <0, 0 to 6, 6 to 10, 10 to 15, 15 to 25, 25 to 50 and >50 metres. The logic is that as Shanghai has a mean elevation of four metres, the classified buildings that fall into the 0 to 6 metre range have a high probability of being a paved area or parking area. Any area above 25 metres will be tall buildings and the area falling above 50 metres will have very high rise buildings.

Road, open area and building mixed classification problems can be improved by looking at the intermediate elevation values and thereby the accuracy of the classified image can be increased. The land cover classified raster image was joined with the classified elevation raster information by the 'combine' operation in ArcGIS. With the assignment of integer values for each class, the 'combine' operation fuses multiple rasters so that a unique output value is assigned to each unique combination of input. As there are seven classes for both land cover and ALOS DSM (30m) image, integer values from one to seven are assigned for respective classes. Subsequently, the fused operation is performed so that the attribute information of elevation classes will be added to the land cover classification attribute.

5.2.2.3 Reclassification

Both land cover and associated height information were added in the attribute table and the land cover class was modified as per the height information. The vegetation class with an elevation above 25 metres was reclassified to the building class while the building class with an elevation below mean sea level was reclassified to road class. The ArcGIS base map was also used to fix the respective class. The open area with an elevation above 25 metres was reclassified to the building class. Altogether all the 49 (7 land cover and 7 elevation class combination) class combinations were checked by this logic and interchange of land cover classes was done.

5.2.2.4 Validation and building extraction of LOD0 3D city models

Validation of the fuse operation land cover was done by the same method adopted for satellite image derived classified data. All the building classes were extracted separately out of the resultant land cover classes and were classified as per the height information in the attribute. The resultant output in the raster format was LoD0 3D city model spatial data. Each pixel stores the height value of the area.

5.2.2.5 Raster to vector conversion for footprint generation - LOD1 3D city models

The raster output was converted to respective vector polygons to extract the building footprints. The polygons associated with height ranges of 6 to 10, 10 to 15, 15 to 25, 25 to 50 and >50 metres were extracted separately. Each of these polygons acts as a building footprint for LOD1 3D city model generation and the associated height range as the height of the building. The validation of the footprint was done by comparing it against the manually digitized building footprint of the area.

5.3 Results

5.3.1 Results of land cover classification from fused Sentinel-2 (1m) image with ALOS DSM (30m) and their accuracy for Huangpu District, Shanghai

The main objective of the chapter was attained by combining the spatially enhanced Sentinel-2 (1m) satellite image with AW3D-30 DSM so as to distinguish between different urban features and buildings as well as to extract the building footprints and further to generate LOD1 3D city model from the fused image. Same as in Chapter IV, fused enhanced Sentinel-2 (1m) image and AW3D-30 DSM was classified and grouped into seven classes (road, vegetation, water, buildings with red/dark roof, buildings with bright roof, buildings in general, and open) based on unsupervised classification. Based on the clarity of distinguishable classes, the buildings were mainly classified into two additional groups with red/dark roof and with bright roof and all other buildings were categorised as general buildings. The additional two classes of bright and red/dark roof buildings were classified just to show the potential ability of the Sentinel-2 satellite data in distinguishing these two spectrally different buildings. The non-building urban features that are not exactly distinguishable were categorised as open. Figure 5.3 shows the results of the classification of enhanced Sentinel-2 image (1m) fused with AW3D-30 DSM.

The resultant image after classification (Figure 5.3 and Table 5.1) shows that, in comparison to Sentinel-2 (10m) and enhanced Sentinel-2 (1m) image, the latter fused with AW3D-30 DSM distinguishes buildings from open class in a better way. The objective of the chapter is to segregate the buildings class more accurately within the dense urban area, so an increase in the percentage of accurate buildings class accounts for better results.

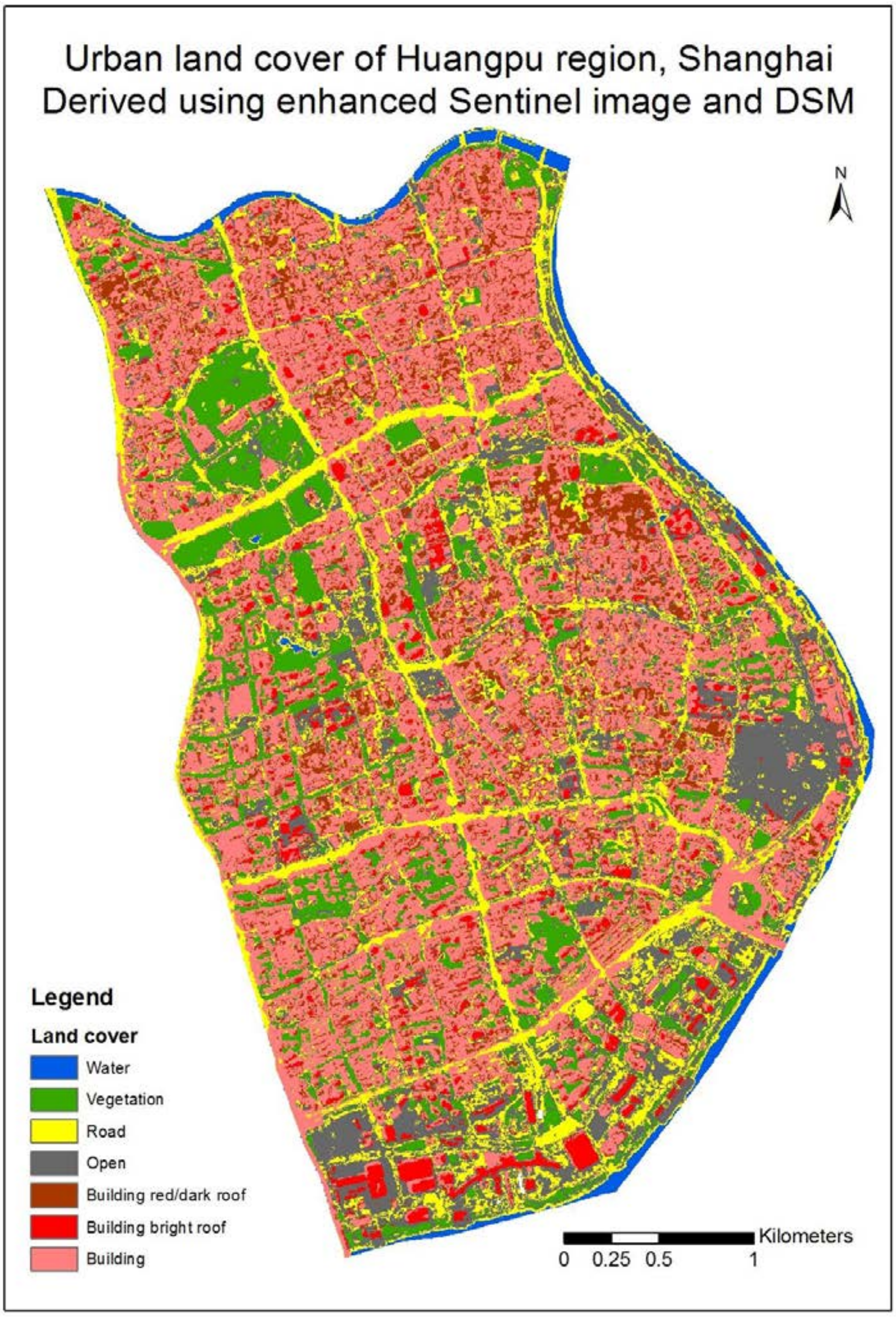

Figure 5.3 Classified map of enhanced 1m Sentinel-2 fused with ALOS DSM (30m)

Table 5.1 Calculated areas of selected urban feature classes with Sentinel-2 (10m), enhanced 1m Sentinel-2 and enhanced 1m Sentinel-2 image fused with ALOS DSM (30m)

	Sentinel-2 (10m)	**Enhanced 1m Sentinel-2**	**Enhanced 1m Sentinel-2 & ALOS DSM fused**
LULC	Area in sq.km		
Building (general)	0.96	3.24	5.99
Building bright roof	0.14	1.00	0.56
Building red/dark roof	3.34	2.13	1.68
Open	6.44	4.34	2.68
Road	2.53	2.39	2.43
Vegetation	1.65	1.98	1.76
Water	0.31	0.30	0.29

For example, while areas classified under buildings were about 4.44 sq.km (28%) based on Sentinel-2 (10m), it was increased to 6.38 sq. km (41%) in enhanced Sentinel-2 (1m) and further increased to 8.23 sq.km (53%) in enhanced Sentinel-2 image (1m) fused with AW3D-30 DSM. However, within the building category, those with the bright roof are better identified in enhanced Sentinel-2 image (1m) while general buildings were found to be more distinguishable from those with red/grey tile in enhanced Sentinel-2 image (1m) fused with AW3D-30 DSM.

It was also observed that the area under open class reduced to 2.68 sq.km (17%) in enhanced Sentinel-2 (1m) image fused with AW3D-30 DSM from 6.44 sq. km (42%) in Sentinel-2 (10m) and 4.34 sq.km (28%) in enhanced Sentinel-2 (1m) image (Figure 5.4). On the other hand, roads show only slight variation among three images with increased area in the enhanced Sentinel-2 (1m) image that can be attributed to the edge enhancement in the enhanced image.

After the classification of urban features, the accuracy of classified urban features was assessed based on selecting 30 random points from each class with a total of 150 points from the whole image. Vegetation and water classes are excluded from accuracy assessment as vegetation was removed earlier by NDVI and water was easier to exclude from other classes. Figure 5.4 shows the accuracy results for different classes. The overall accuracy results show that the accuracy of building classification has significantly improved to 97% after combining the enhanced Sentinel-2 (1m) image with AW3D-30 DSM in comparison to 78% in Sentinel-2 (10m) and 87% in enhanced Sentinel-2 (1m) image. Detailed interpretation of results shows that the accuracy of all urban features is higher in fused enhanced Sentinel-2 (1m) images with AW3D-30 DSM.

Both roads and open classes showed an accuracy of 97% in enhanced Sentinel-2 (1m) fused with ALOS DSM (30m), while it was 73% in Sentinel-2 (10m) and 83% in spatially enhanced Sentinel-2 (1m) for roads , whereas 83% and 77% respectively for Sentinel-2 (10m) image and Sentinel-2 -1m (77%) image for open classes. It is significant to note that bright buildings and dark/red tile buildings both yielded maximum (100%) accuracy after combining ALOS DSM (30m) with enhanced Sentinel-2 (1m) image. However, it was also noted that the overall Sentinel-2 image is good for the detection of bright buildings irrespective of image enhancement as it yielded higher accuracies in all three scenarios. i. e. 97% in Sentinel-2 (10m) and 100% accuracy both after enhancement as well as after the fuse process.

The maximum accuracy increase among urban features was observed for general buildings after the fuse process. While the accuracy of general buildings was only

50% in the case of Sentinel-2 (10m) image, it has improved significantly up to 80% after the image enhancement (1m Sentinel-2) and 93% after combining the enhanced Sentinel-2 (1m) with ALOS DSM (30m). Thus all the urban features show higher accuracy after the fuse process.

Figure 5.4 Accuracy results of urban land cover classification

5.3.2 Building classification and generation of LOD0 3D city model from enhanced Sentinel-2 (1m) fused with ALOS DSM (30m)

The building features were successfully extracted separately after removing water, vegetation, road, and open classes from the land cover classified image to obtain LoD0 3D city model. Buildings were classified into 5 different classes based on building heights as >50 m, 25 to 50m, 15 to 25m, 10 to 15m and 6 to 10m , while areas under different height ranges were calculated based on the pixel values (Figure

5.5). Results of the building classification show that 13% of the total building areas are under high rise building class. i. e. buildings with an elevation above 50 meters and another 18.4% of building areas are of medium rise buildings with an elevation between 25 and 50 metres.

Cumulatively, it was identified by this method that 31% of buildings of this region falls under the category of height range with an elevation more than 25 metres, while about 26.54% of area falls within the range of 15 to 25, and 23%, further 18.92% falls under the ranges of 10 to 15 metre and below 10 metres respectively. It is to be noted that all these values correspond to building areas under different height ranges as this classified image is in raster format and does not provide individual building heights.

The number of pixels of the buildings gives the area of buildings and the multiplication with corresponding height values of the pixels provides the volume. Accordingly, this method could give building volume information of the corresponding area. For example, the user can easily identify the volume of buildings with 10 metres of height by a simple SQL query and multiplying the height value (10 m in this case) to the count of pixels. Thus the raster area of buildings with height information pixels will constitute a LOD0 level 3D or 2.5 D city model. So understanding the classification accuracy is of high importance to assess the accuracy of building area and building volume.

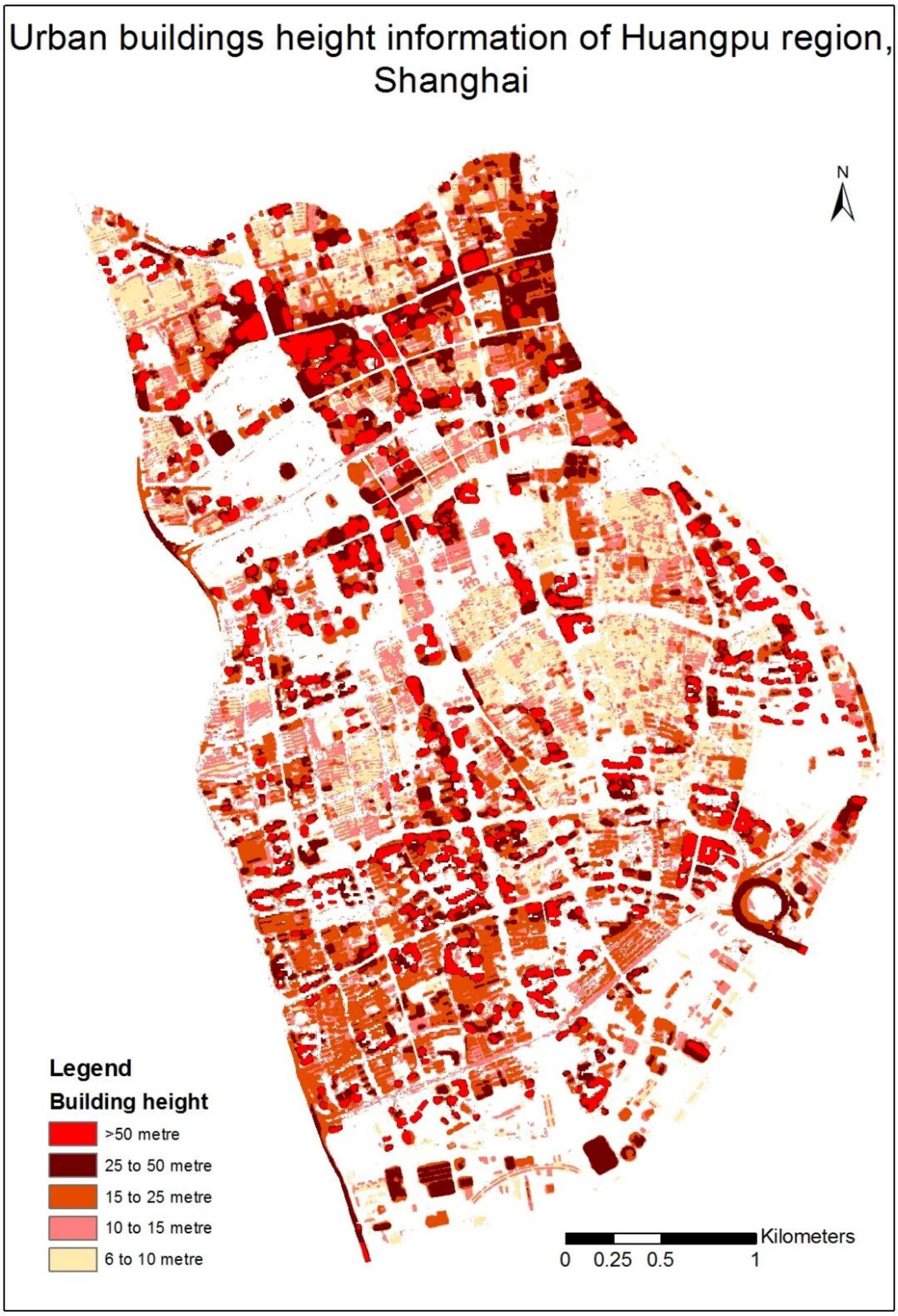

Figure 5.5 Map of extracted buildings in raster format (LOD0 3D city model information) from DSM fused with enhanced 1m Sentinel-2 image

5.4 Validation of classification with OSM building footprint area

As stated in chapter I, some areas in the Huangpu region had OSM building footprints. In the current chapter, an approach to extract building area for the whole region has been developed and data is generated. So a comparison of classification accuracy in the region of OSM building footprint is attempted as the OSM building footprints represent the area with actual buildings.

To do this, the land cover mapping derived by the spatially enhanced Sentinel-2 (1m) fused with ALOS DSM (30m) data under the exact locations of the 2D building footprint (obtained from OSM) area were extracted and is as shown in Figure 5.6. The derived land cover classification contains mostly classes of buildings and few open areas, road, vegetation and even water. The area of these different land covers was calculated by the pixel information and it is the case that 88.8% of the land cover class in these areas was marked as buildings which underline the efficiency of this method to extract buildings in highly dense cities. It may be noted that we are comparing with the building footprint polygons obtained from open source. 4.4% of these areas were classified as roads in the satellite image derived land cover map, while further 4.14% was classified in open class and 2.5% fall under the vegetation class. Only 0.008% of the area falls under water class which is a very negligible amount and shows good classification accuracy with the identified building area. Table 5.2 shows the associated statistics.

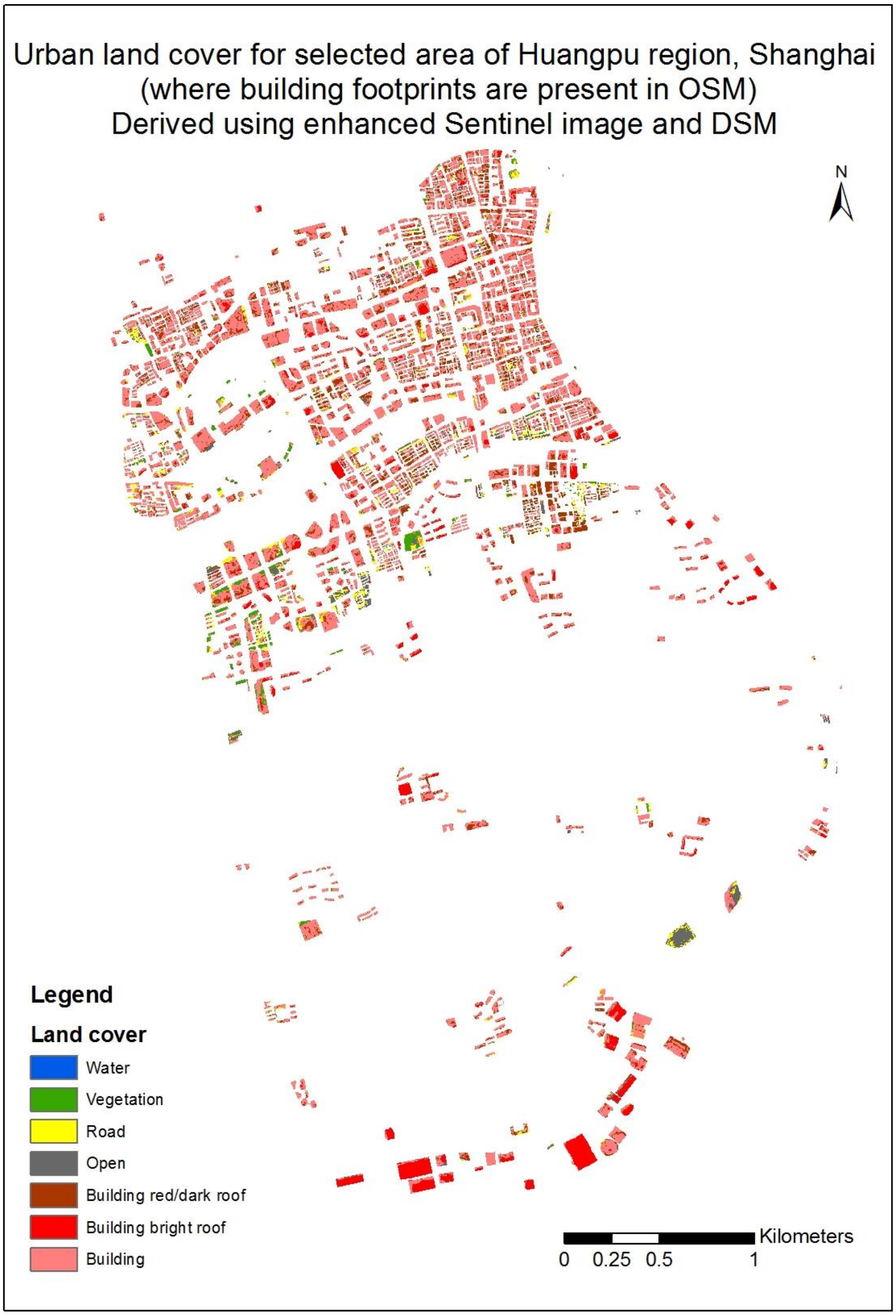

Figure 5.6 Raster land cover data corresponding to the OSM building footprints for Huangpu, Shanghai

Table 5.2 Area of different land cover classes calculated based on the pixels for raster land cover data corresponding to the OSM building footprints for Huangpu, Shanghai

Sl. No.	Land cover class	Percentage
1	Building	88.8
2	Open	4.14
3	Road	4.4
4	Vegetation	2.5
5	Water	0.008

Further analysis of the vegetation class revealed that the two building polygons were wrongly classified as buildings in the open data. Similarly, an open area was classified wrongly as a building in the open data. This was confirmed by looking at the corresponding satellite base map in the GIS environment. Accordingly, comparing the building footprint data with a satellite-derived land cover map could also help in identifying some of the digitisation errors in open data. As more than 88.8% pixel areas were correctly classified as buildings in satellite-derived land cover data, it is purported here that this method can be used to enhance the existing open data of 2D building footprints, or where data are completely sparse the use of an enhanced Sentinel-2 image can be used to provide the 2D building footprints.

As expected, the Huangpu region of Shanghai comprises tall buildings (Figure 5.7). More than 20% of the pixels have a height value of more than 50 metres and another 28.87% of buildings have a height value between 25 to 50 metres. The low rise buildings which have a height value of less than 15 metres comprises 23%. The height level classification statistics are given in Table 5.3.

Figure 5.7 Building volume information for the areas where OSM 2D building footprints are available for Huangpu, Shanghai

Table 5.3 Percentage of buildings under different height ranges calculated from DSM infused enhanced Sentinel-2 (1m) image.

Sl. No.	Building height	Percentage of buildings
1	>50 metre	20.1
2	10 to 15 metre	28.87
3	15 to 25 metre	27.48
4	25 to 50 metre	15.09
5	6 to 10 metre	7.99

One of the advantages of satellite-derived buildings is that they also indicate the type of buildings such as bright buildings, red or dark roof buildings etc. The buildings which show very distinctive brightness values were easy to classify as a separate class, whereas for the building footprint data in open source, this information was not available. The overall analysis shows that there was a good correlation between building information within the building footprint available area. But the satellite-derived footprints still do not sufficiently give the exact shape of the building; hence it is recommended to use building footprint wherever available to generate the 3D city model. In the absence of the same, the method mentioned in this chapter can be used to generate the 3D city model of the range of LOD0. This method mainly provides the building volume rather than the building height. Whereas the method mentioned in chapter III shall provide building heights and can generate the 3D city model of the range of LOD1. The different potential application areas of these 3D city models data are described further.

5.5 LOD1 3D city model from open satellite data and extraction of 2D building footprints

For the generation of LOD1 3D city model, vector polygon is needed as building footprints along with respective height information. As the generated LOD0 3D city model area derived from the combination of Sentinel-2 (1m) and ALOS DSM (30m) are in raster format, a raster to vector conversion is needed to generate building footprints.

But the raster to vector conversion has some limitations. If the building is a flat roof and an isolated one, then it could generate a good separate building polygon. Whereas, if the roof is undulated, then multiple raster values will be there in a single building polygon and when single height values are taken (for example, 10m) it won't provide exact building shape (as the building may have a raster value with example 11m or 12m). Hence, it is important to take all these height ranges to get more meaningful values (that's why different height ranges were taken in this chapter). However, without knowing the height of the buildings of an area, it is not possible to set exact groups. Also in the dense urban areas, mixed pixels will be higher, which further prevents generation of the exact building shape.

Nevertheless, in a raster (LOD0), it is easier to identify the number of pixels with different elevations (for example, 10m, 12m etc.) in an area/region because of which the calculation of building volume will be more accurate. Thus the enhanced Sentinel-2 (1m) shows higher accuracy in building volume rather than individual building polygons.

With this limitation, the LOD1 3D city model for whole Huangpu was generated from the enhanced Sentinel-2 (1m) fused AW3D-30 DSM data by giving height range (6 to 10m, 10 to 15m, 15 to 25m, 25 to 50m and above 50m), and thereby extracting the corresponding vector polygons. However, it is poorer in accuracy in comparison with manually digitized polygons for the reasons mentioned above. Still, this LOD1 3D city model will give the user an indication of locations of high-rise buildings and low-rise buildings etc., which shall be handy for many applications. Figure 5.8 shows the LoD1 3D city model generated from spatially enhanced Sentinel-2 satellite data fused with AW3D-30 DSM.

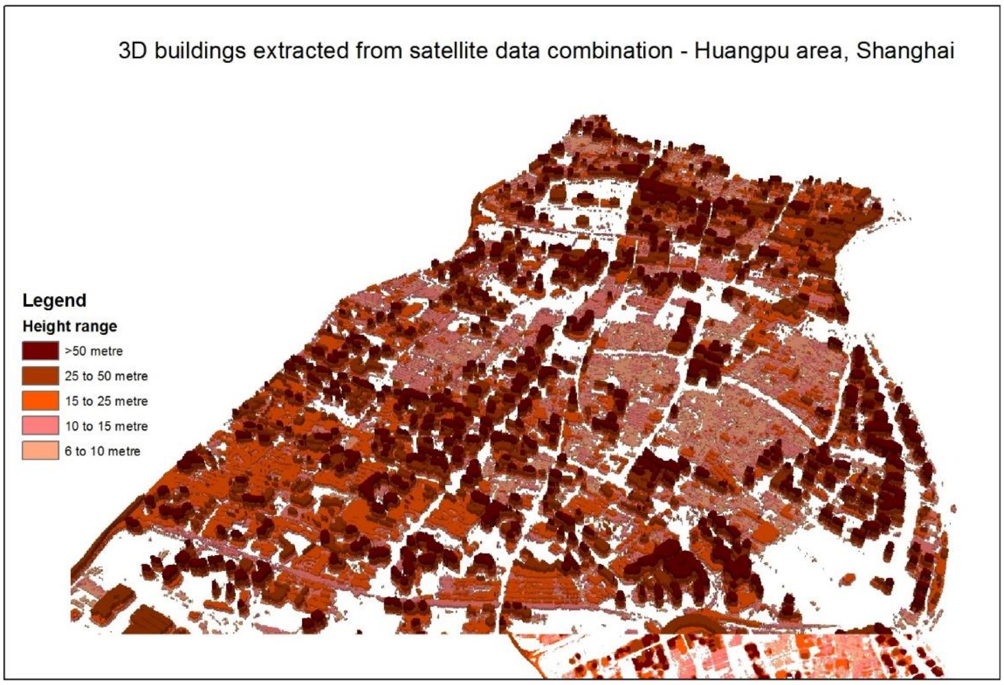

Figure 5.8 LOD1 3D city model generated from enhanced Sentinel-2 data fused with DSM

5.5.1 Validation of 2D footprints generated for LOD1 3D city model

The validation of these vector polygons which act as building footprints was conducted by comparing them with the manually digitized vector building polygons of the area. Buildings obtained from satellite data were extracted, grouped into five different height ranges (6 – 10m, 10-15m, 15-25m, 25-50m, and >50m) and overlaid on corresponding manually digitized 2D building footprints for comparison (Figure 5.9a). Results show that, larger and taller buildings (>50m) (Figure 5.9b) provides more accurate shapes than small (<15m) or narrow and elongated buildings (Figures 5.10a & 5.10d) which is the opposite of the results from chapter III where 2D building footprints were used for 3D city model generation. In that method, more accuracy was observed for smaller buildings and accuracy tended to reduce for taller buildings.

From the visual interpretation of results shown in the images for different height ranges, it is evident that adequate identification of the exact shapes of the buildings is not possible for all cases. For areas with small and congested buildings, this method tends to group all buildings together and results in a larger single polygon. The buildings with good height (for example, 25 to 50m or above 50m) and with good ground area tend to segregate more evidently. Large buildings with a flat roof tend to segregate accurately in the raster to vector conversion.

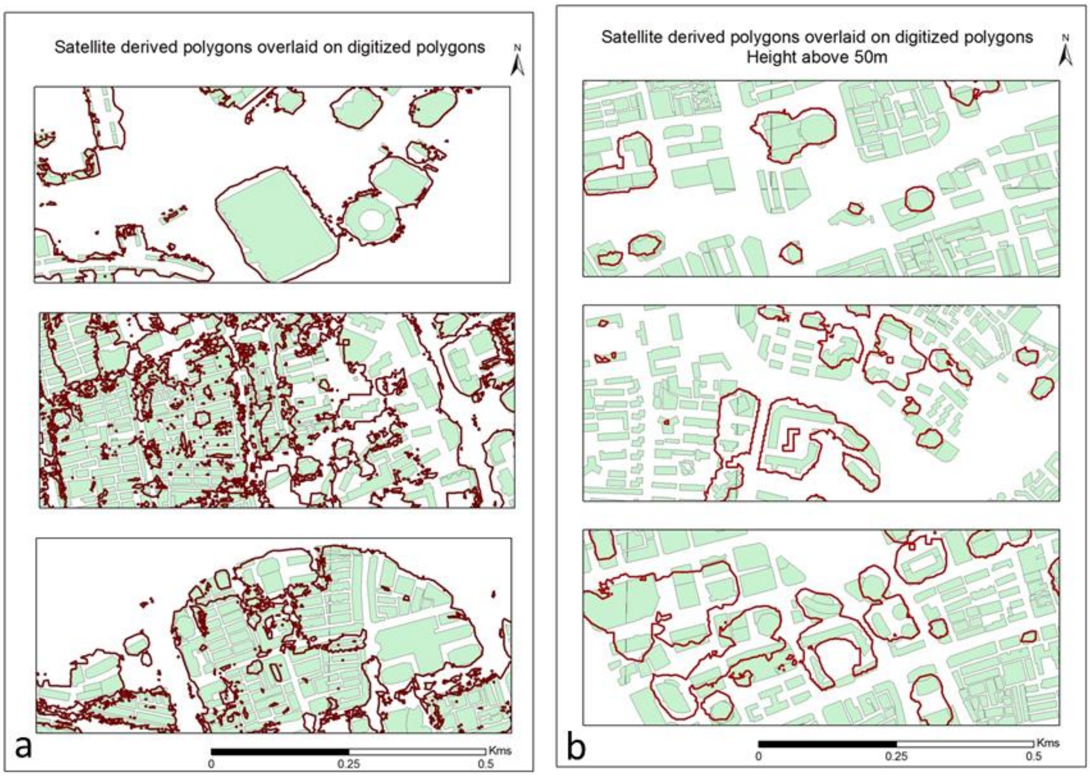

Figure 5.9 Satellite derived 2D footprints overlaid on digitized 2D building footprints of Huangpu District a) Shows all buildings, b) polygons for buildings greater than 50m

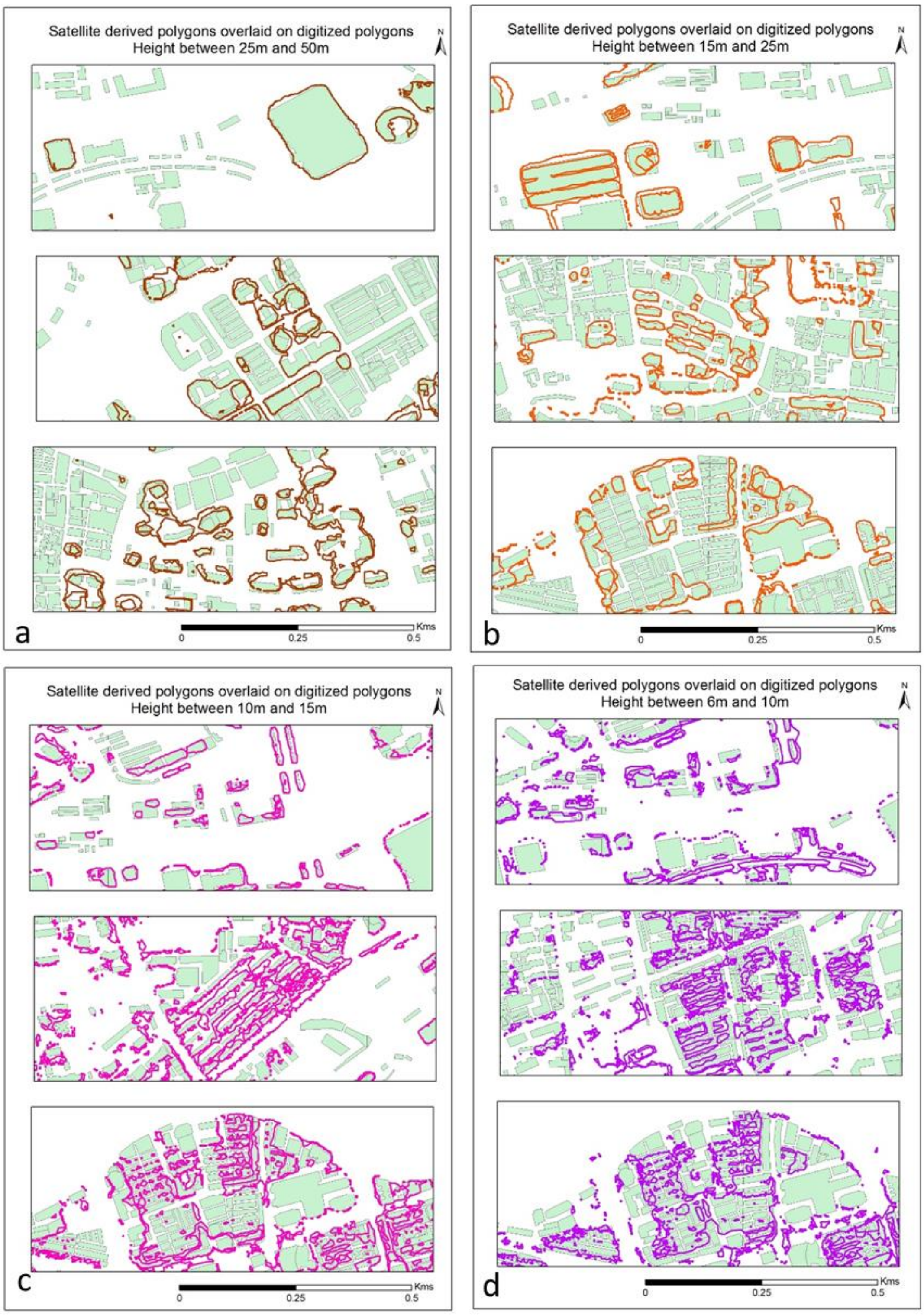

Figure 5.10 Satellite derived 2D footprints overlaid on digitized 2D building footprints of Huangpu a) polygons for buildings 25-50m, b) polygons for buildings 15-25m, c) polygons for buildings 10-15m, d)polygons for buildings 6-10m

Even with all the limitations shown above, this LOD1 3D city model will give an indication of where the small and tall buildings are. Hence this model has many application potentials and some of the potential areas are explained in the discussion chapter.

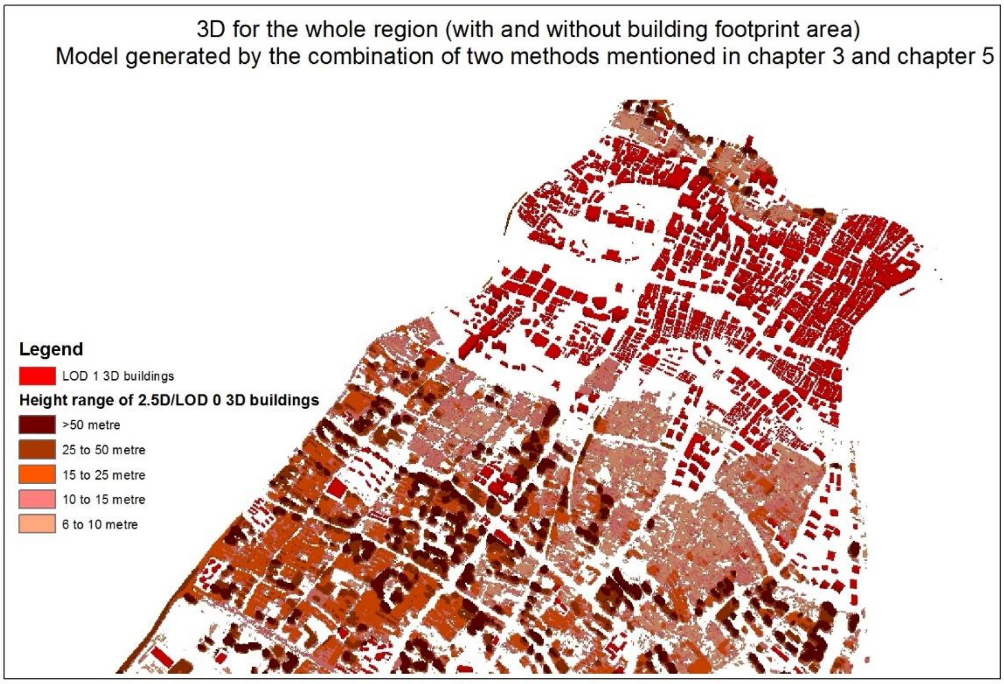

Figure 5.11 Final map combining LOD1 3D city model generated from 2D building footprints (wherever available) and from enhanced Sentinel-2 data fused with DSM (for the areas where 2D building footprints are unavailable)

The map (Figure 5.11) shows the final 3D city model, where methods from chapter III are used wherever OSM building footprints were available and the rest of the area uses a 3D city model generated by the method of this chapter.

5.7 Summary

The overall objective of the thesis was to develop methods to generate cost effective and globally replicable 3D city models from open data using geospatial techniques. During the study, it was observed that there is a huge discrepancy in the availability of the 2D building open data both in terms of accessibility as well as in terms of quality. Hence, it was of the need to develop two different methods for generating 3D city models. One method was for the areas where 2D open building footprints are available and another was for the areas without any open 2D building footprint datasets. With this background, chapter III of the thesis demonstrated a method to generate 3D city models for the areas where 2D building footprints were available, following examples of the Nottingham city, UK and the city of Shanghai in China.

The fourth and fifth chapters of the thesis depict the methods required to generate 3D LOD0 and the 3D LOD1 city models from the open satellite data for the areas where there is no availability of open source 2D building footprints. As discussed in previous chapters, open satellite datasets are mostly characterised by coarser resolution, which restricts their utility in building demarcation. In order to overcome this constraint, chapter IV of the thesis showed a method to increase the spatial resolution of Sentinel-2 satellite data from 10m resolution to 1m and used the resultant spatially enhanced 1m Sentinel-2 image in the present chapter (chapter V) to generate building volumes.

Accordingly, chapter V illustrated the fusion of the ALOS DSM (30m) to the spatially enhanced (1m) Sentinel-2 satellite data and extraction of buildings from this fused data. The chapter also demonstrated the accuracy of various urban land cover classes after combining DSM with enhanced satellite data and briefly compared them with the accuracy of urban features before and after spatial resolution enhancement. It was observed from the analysis that both sparse representation techniques and combining of DSM with enhanced 1m Sentinel-2 data improves urban land cover classification accuracy and thereby enables improved extraction of building volumes from open data. The overall accuracy of urban land cover classification found to be around 78% in Sentinel-2 (10m) image which has improved to 87% in enhanced 1m Sentinel-2 image after sparse representation and further to 97% after combining the enhanced 1m Sentinel-2 image with ALOS DSM. Thus, the chapter also substantiates the advantage of using sparse representation techniques and the fuse process in building extraction from open data.

It is important to note that, by this method, it is only possible to extract the LOD0 3D/2.5D city model more accurately than the LOD1 3D city model as well as the building footprints with limited accuracy. Hence, the last section of this chapter provides short comparative insights between 3D city models developed by the two methods: i.e. LoD1 3D city model developed by using open 2D building footprints and LoD0 3D city model generated by combining spatially enhanced 1m Sentinel-2 image with ALOS DSM. One of the major difference between these two models is that in Chapter III (i.e. LOD1 3D city model generated using 2D building footprints), LOD1 3D city model is generated after infusing the building heights to the 2D building footprints, whereas in satellite based 3D city model, 2D building footprints are extracted only after infusing the elevation data to the satellite image.

One of the disadvantages of the satellite derived 3D city model is that it does not accurately depict the exact shape of the building, but largely provides building volume. However, a satellite derived 3D city model was found to be beneficial in identifying different types of buildings (such as bright buildings, red/dark roof buildings) which otherwise cannot be derived in the other method that uses 2D footprint. Further, this can also provide first-hand information on building areas, distribution and density of buildings etc. which is important in applications such as disaster mitigation and flood evacuation. However, as the satellite derived 3D city model does not provide accurate building shapes, it is recommended to use 2D building footprints wherever it is available.

Finally, as this chapter produced LOD1 3D city model buildings for the areas which did not have building footprints, a complete 3D city model for the Huangpu region was developed by combining the results of both chapter III and chapter V (refer to Figure 5.11). The following chapter (VI) provides discussions of the thesis.

CHAPTER VI

DISCUSSIONS

6.1 Summary

The central premise of this thesis is the requirement to generate 3D city models using globally available open-source data with an intent to do so via globally reproducible methodologies. Specific objectives of the study included to, i) develop workflows that afford the generation of LOD1 3D city models from open source data, ii) explore approaches to open data generation that could be used within the workflows developed, and iii) evaluate the execution and suitability of the different city data models (i.e., levels of detail) produced from open source data for use in urban studies.

The level of detail (LOD) of a 3D city model is one of its most important characteristics. It denotes the adherence of the model to its real world counterpart, and it has implications on its usability (Biljecki et al., 2014). The CityGML standard defines five Levels of Details (LOD) varying from LOD0 to LOD4 to describe 3D objects building with respect to their geometry, topology, semantics and appearance (Groeger et al., 2008). As the LOD level of the model increases, it will have more detailed architectural information of the structures. Accordingly, different LODs can be used for different purposes (Buyukdemircioglu et al., 2018). The coarsest level LOD0 represents the lowest level of geometry as a 2.5D DTM with building footprints or roof edge polygons, while LOD1, is well known as the blocks model. In LOD1 the building height would be extruded with flat roofs and is widely used for city and region coverage. Compared to LOD1 models, LOD2 buildings differentiate roof structures as well as boundary surfaces. LOD3 have more architectural details including specific roof structures and wall structure details such as doors and windows and LoD4 has the highest level of detail and all interior details are represented with textures including rooms and furniture (Buyukdemircioglu et al., 2018; Groeger et al., 2008). It is also to be noted that, the data demand increases for each LOD class, and this demand needs consideration with the intended application for the models to be generated.

Achieving the objectives of the thesis requires remote sensing and geospatial technology within urban studies to go beyond the 2-dimensional perspectives (for instance in urban landuse change analysis, analysis of urban sprawl dynamics (Ahmad & Goparaju, 2016), urban facility management (Boyle & Michell, 2017), and sustainable transport planning (Pojani & Stead, 2015)), to the 3rd dimension - 3D modelling of urban systems (i.e., to address climate change challenges (Danahy et al., 2016; Masson et al., 2014) or to estimate energy demand as well as to improve energy efficiency (Kaden & Kolbe, 2014)).

Studies have shown that the potential of geospatial technologies together with improved allied visual and 3D modelling technologies holds far greater promise for sustainable urban management than earlier waves of technology (LeGates et al., 2009). However, to fully exploit this potential in urban studies, it must be possible to replicate the methods to generate 3D city models the world over (Jovanović et al., 2020). The current status is that the creation of 3D city models typically relies upon time consuming editing, expensive proprietary datasets or both. Several research already demonstrated that 3D city model can be derived from different data resources, such as LiDAR point clouds (Kada & Mckinley, 2009), airborne images (Haala et al., 2015), satellite images

(Krauß et al., 2009), UAV (unmanned air vehicle) images or combination of DSM (digital surface model) data with cadastral maps (Buyukdemircioglu et al., 2018). The approach however can be an expensive and time/labour consuming process, particularly if high levels of accuracy in model outputs are required (Ohori et al., 2015). Large scale 3D city models are mostly available in countries with developed economies and/or those with national mapping agencies. Whereas countries, including many that are transitioning their economies (and where this information is perhaps of most value), could not afford the resources to produce high accuracy 3D models. In such situations, the use of low cost or open source online free satellite datasets (open data) as a source of input data for 3D generation can be a feasible solution.

The three research chapters (Chapter III, IV and V) of the thesis demonstrate approaches to generate 3D city models that are globally accessible. In Chapter III 3D models are generated for two contrasting cities, Nottingham in the UK and Shanghai in China, and further the features as well as limitations of the resultant approaches were discussed. A major limitation to the approach outlined is that the 3D models require open source 2D building footprints, yet this may not be readily available over the globe. Accordingly, the subsequent research chapters (Chapters IV and V) presented methods to generate 2D building data and LOD1 3D city models from open source satellite data (which tend to be of a lower resolution than the VHR commercial data).

6.2 3D city model generation from open 2D building footprint data

The first analytical chapter (Chapter III) of this thesis presented a relatively simple method of generating a 3D city model from open data that can be applied globally. The results presented in this chapter show that AW3D-30 DSM data provides more accurate results in the case of low and medium rise buildings and that errors can be improved through a calibrated enhancement process. Using OSM in combination with the medium resolution AW3D-30 DSM a set of building footprints with height information were created and their quality ascertained.

For Nottingham, by this method, about 27.7% of buildings with +/-1m accuracy, 51.45% with +/-2m accuracy and 84.27% with +/-5m were generated. In Shanghai, the accuracy was much lower than that of Nottingham i.e. percentage of buildings within the accuracy levels of +/-1m, +/-2m, and +/-5m were 17.66, 32.96 and 62.26 respectively. The accuracy reduction in Shanghai is attributed to the increased number of tall buildings compared to the city of Nottingham. It is significant to observe that the AW3D-30 DSM provides more accurate results for low and medium rise buildings, but exhibits relatively large errors in height for very tall buildings. This result echoes the findings of Alganci et al., (2018) but contradicts that of Misra et al., (2018). Accuracy assessments of different DSMs by Alganci et al., (2018) revealed that the AW3D-30 DSM performed worse for high rise buildings compared to SPOT DSM and PHR DSM; and further that AW3D-30 DSM has a high accuracy level in residential areas.

This is due to the characteristics of AW3D-30 DSM global dataset that this dataset has has been originally resampled from 5 m mesh version of the AW3D to 30 metre spatial resolution (1 arcsec) (Santillan et al., 2016). This thesis used the latest AW3D-30 product, released in May 2017 as AW3D-30 DSM data is currently the most precise global scale open source elevation (Alganci et al., 2018) dataset (free to the public since 2015). To generate the same, many actions like sea mask correction, void filling by applying filters etc have been performed (Takaku et al., 2020). During this accuracy reduction 5m to 30m DSM, the spike area or sudden variation might have smoothened. The tall buildings might act as sudden spikes and the same shall be smoothened during the accuracy reduction procedure. This accuracy reduction problem is mentioned in the paper (Girindran et al., 2020).

In contrast to this, Misra et al., (2018) reported that AW3D-30 is most suitable for observing buildings taller than 9 m in height. However, this was in comparison with ASTER and SRTM based building heights, which are less suitable for extracting building height variation Misra et al., (2018). This chapter considered all buildings with height above 2 meters and results showed higher accuracy. Hence, the presented method even without any accuracy enhancement could provide better accuracy in cities with low and medium rise buildings compared to cities with high rise buildings.

The chapter also evaluated enhancements of height accuracy through statistical analysis of a small sample area of high resolution data (thus limiting expense, where these data are not freely available). The application of this accuracy enhancement method (by way of a sample of high resolution elevation data) resulted in improved reliability of 3D models from open data (Nottingham study demonstrated enhancements in the percentages of buildings from 27.7% to 32.81% for an accuracy level of +/-1m, and from 51.45% to 57.43% for an accuracy level of +/-2m). However, this method is limited to the containment of only systematic errors; random errors are not accounted for.

Further, to understand the reliability of AW3D-30 DSM in generating 3D building height generation, a 3D city model was also created by using AW3D-30 DSM and high resolution LiDAR DTM. Results of uncorrected AW3D-30 building heights (compared with Mastermap) within an accuracy level +/- 1m was 31.43% of total buildings and +/-2m accounted for 60.14% of buildings. Deviations for only 5.27% of all the buildings exceeded +/-5m. After applying the accuracy enhancement method the proportion of buildings having accuracy levels of +/-1m increased to 90.8%, +/-2m to 97.73% and +/-5m to 99.52% respectively. Further, buildings having an error more than +/-5m reduced to 0.48% from 5.27%. Thus it is clear from the analysis that there is a huge potential to improve the accuracy of 3D city models generated based on AW3D-30 DSM provided that the errors within the AW3D-30 DSM is identified and there is an accurate ground elevation model.

There are only a few studies that have attempted to extract building heights from open DSMs. For example, Nghiem et al., (2001) attempted to extract building heights from SRTM DSM data for large scale area mapping; Wang et al., (2018) derived 3D city structures by fusing Landsat and global elevation data; Misra et al., (2018) attempted a comparison of building heights extracted from open DSMs including AW3D, TanDEM-X, ASTER, and SRTM over Yangon City. After using SRTM DSM in Los Angeles (Gamba et al., 2000) and in Baltimore City (Quartulli & Datcu, 2003), it has been concluded that the SRTM could be used for detecting tall buildings. Since then, other global DSMs, including AW3D30, TanDEM-X (TerraSAR-X Add-On for Digital Elevation Measurements), and ASTER Global DEM (GDEM), have also been shared publicly.

Usage of OSM in combination with AW3D-30 DSM data has substantial potential for future scientific research due to the former's ever-growing size, and the latter's global coverage (Alganci et al., 2018; Bagheri et al., 2019; Tadono et al., 2016; Takaku & Tadono, 2009). Studies report a considerable increase in OSM building data in recent years. For example, from 2012 to 2017 alone there has been a 20 times increase in OSM building data in China (Tian et al., 2019). Effective derivation of elevation values for OSM data will likely extend its utility (Knerr, 2013). However, the absence of a global completeness assessment may hamper the use of OSM for urban planning and development, unless it is resolved (Barrington-Leigh & Millard-Ball, 2017). Quality is one of the major concerns in using OSM data as mostly non-professionals provide the OSM data and therefore both the coverage as well as the quality of the data becomes debatable (Haklay, 2008; Nasiri et al., 2018; Senaratne et al., 2017). Despite the disadvantage, OSM can be a good source of 2D building data, especially in the context of non-availability of free 2D building data, as in China, where authorized building data are not freely available (Tian et al., 2019). Studies also reveal that the rate at which OSM is receiving contributions from users has been constantly increasing and continues to grow; complemented by collaborative mapping efforts amongst the OSM community to check and improve the quality of contributions (Arsanjani et al., 2015).

AW3D-30 DSM also has considerable future potential, particularly for low and middle income countries, given its global coverage and open license. The JAXA released its first version AW3D-30 DSM with a horizontal resolution of approx. 30 meter mesh, free of charge in May 2015. This dataset was generated from the DSM dataset (5 meter mesh version) of the precise global digital 3D map ALOS World 3D" (AW3D), which is the world’s first and the most precise 3D map covering all global land scales with a 5 meter mesh (https://www.eorc.jaxa.jp/ALOS/en/aw3d30/index.htm). Although the AW3D-30 DSM had a 30 m grid spacing, it could be deduced that this was due to the acquisition of strong signals from the original 5 m DSM, which was produced from the 2.5 m images (Alganci et al., 2018). In March 2017, version 1.1 was released filling the void height values with existing DEMs in cloud and snow pixels between 60 degree North and 60 degree South. In April 2018 AW3D was upgraded to version 2. Continuous enhancements of AW3D-30 DSM are expected, improving its future utility.

The approach presented in chapter III of this thesis can be applied by any user that has 2D building footprint data and AW3D data and terrain information (i.e., from GMTED2010). AW3D-30 is the most suitable open DSM for building height generation in comparison with ASTER, SRTM and TanDEM-X However, while using AW3D-30 DSM there is a challenge of dealing with mixed pixels, due to instances when buildings in the AW3D-5 digital building heights with a ground footprint of approximately 30 m or less were split into adjacent 30 m resolution pixels, each with a lower height than the original (Misra et al., 2018). Thus one of the important advantages of using OSM together with AW3D-30 DSM is that it helps to avoid the issues of mixed pixels and provides more accurate individual building heights and shapes. To the researcher’s knowledge, this is the first attempt at combining OSM data with AW3D data to generate 3D models. This research builds on previous studies that fuse OSM with satellite derived elevation data over flat terrain (Bagheri et al., 2019) however the study in chapter III of the thesis provides a method to generate 3D models for both flat and undulated terrain using open data, which makes it feasible to replicate globally with any kind of terrain.

As this thesis intended to develop LOD1 models, it did not consider topological errors. If the 2D topological relationships between the footprints are not taken into account, the resulting 3D city models will not necessarily be topologically consistent (i.e., primitives shared by 3D buildings will be duplicated and/or intersected and overlapped building parts etc.) (Giovanella et al., 2019; Ledoux & Meijers, 2011; Z. Zhao et al., 2013). Models with topological inaccuracies often cannot be accepted by downstream analytical applications that demand 2-manifold exterior shells (Giovanella et al., 2019; Ledoux & Meijers, 2011). However, the objective of the thesis was to develop LOD1 3D city models, which do not require higher levels of accuracy. Hence all incomplete and irregular buildings are removed after creating the 3D city model. As the data used is 2D polygons from OSM, any topological errors in this dataset will be reflected in results as well. Hence it is recommended consideration of topology should higher accuracy in resultant models be required (i.e., LOD 2 +).

6.2.1 Challenges in using OSM to generate global models

Chapter III of this thesis presented an approach to generate 3D city models from open data considering OSM as a source for 2D building footprints wherever available. However, the completeness of OSM varies significantly. In particular, OSM has good coverage in urban areas when considering particular completeness factors (Neis et al., 2012). However, the example of Shanghai from this research shows that the completeness of OSM in urban areas is not far-reaching, unlike that of Nottingham. Studies from European cities show that in these regions, OSM provides quantitatively larger amounts of geodata and a better representation of the real world in the dataset (Barrington-Leigh & Millard-Ball, 2017; Graser et al., 2015; Neis & Zielstra, 2014). Some studies even show that road network OSM data for European countries is comparable to or better than official or proprietary data sources (Graser et al., 2015; Neis et al., 2012). This was achieved by importing commercial or governmental road network datasets that comply with the OSM license (for example, Netherlands and Austria) as well as by importing cadastral building information to the OSM database (for example, Spain and France).

However, when it comes to other parts of the world, such as China, Tehran and Brazil, completeness of OSM is not as good as Europe (Camboim et al., 2015; Forghani & Delavar, 2014). Barrington-Leigh & Millard-Ball, (2017)Barrington Leigh & Millard Bal 2017, estimated that globally about 77 countries among 185 have more than 95% of completeness of OSM road map whereas, countries like Kiribati, Afghanistan, Egypt and China are all have less than one third completeness. Their studies also revealed that not just developed countries have the maximum completeness but also areas with dense population and low income countries that faced humanitarian disasters. For example, Nepal and Haiti had intense mapping efforts following humanitarian disasters (Mooney & Corcoran, 2013). The recent 'Mapathon VGI project' introduced by the Government of Kerala, India (https://mapmykerala.in/about) after the disastrous floods in 2018 and 2019 also contributes as an example to the above mentioned argument.

Though studies reveal that OSM data is increasing all over the world, the equal availability and quality of OSM data could not be ensured globally due to several factors such as the lack of uniformity in attributes, diversity in spatial coverages (Barrington-Leigh & Millard-Ball, 2017), biases of contributors (Neis et al., 2012) and unequal distribution of digital infrastructure (Zook & Breen, 2017). The scenario highlights the necessity to generate building data from other reliable sources like open source satellite images.

6.2.2 Need for high resolution digital terrain models

This research in chapter III also demonstrated ways to increase the accuracy of the generated 3D city models using a sample of high resolution DSM and DTM data. Further, it demonstrates that the usage of high resolution DTM for ground elevation extraction can result in higher accuracy of building height values. This research recommends using high resolution Digital Terrain Model (DTM) wherever possible and in the absence of the same, GMTED 2010 data shall be used as ground elevation for undulating terrain and the mean elevation value as ground elevation for flat terrains like Shanghai. The study also highlights the need for the geospatial community to generate a global open access high resolution DTM. The need for generating global high resolution DEM in open access was also highlighted by Schumann & Bates, (2018). There are also initiatives like 'Open Topography' which facilitates community access to high resolution topographic data (https://opentopography.org/). These high resolution data (meter to sub metre scale) are derived from LiDAR and other technologies. These high accuracy terrain data further sheds light on to the extensive potential of generating highly accurate 3D city models using open data.

6.2.3 Advantages of generating 3D city models from open 2D building footprints

Thus, one of the great advantages of our methodology is that 3D city models can be generated from any 2D building data in combination with any DSM and not just OSM and AW3D-30 DSM data. In case of the availability of any 2D building data, the user could generate the building elevation in combination with DSM data. Currently, only AW3D provides free DSM data. Even though ASTER DEM and SRTM provide elevation data, such datasets are not used to generate 3D city elevation, as they are not surface models. However, in future higher resolution DSMs shall probably evolve like in the case of LiDAR DSM and ICESat-2 data. LiDAR DSM data are already available for about 70% of England from the UK Environmental Agency (https://data.gov.uk/). Whereas, ICESat-2 (ICE, CLOUD, and Land Elevation Satellite) is an ambitious mission of NASA that provides a global distribution of geodetic measurements, of both the terrain surface and relative canopy heights; besides it also surveys the urban areas (Neuenschwander et al., 2018). Further, Global Ecosystem Dynamics Investigation (GEDI) LIDAR from NASA with its dense track sampling and precise geolocation form the basis of an important dataset of ground control points, to validate and calibrate global and regional DEMs as well as a reference for surface elevation change (https://gedi.umd.edu/). Thus, it is hypothesised that when more accurate DSMs become available, it will enable the user to produce more accurate 3D city models with better shape descriptions of buildings, especially roof modelling, and thereby generating higher LODs using the defined methodology. Knowing the nature of the terrain in the modelling area is a factor in our method. For cases with flat terrain (for example, Shanghai), the mean ground elevation is deducted from the DSM data to obtain the building height; whereas in cases of undulated terrain (for example, Nottingham), terrain elevation can be obtained from multiple sources, such as contour topographic data or from satellite based sources like GMTED2010 and LiDAR DTM.

The method also allows users to generate data in a cost effective manner. Though high resolution 3D datasets are very expensive, in fact, many applications do not require very precise datasets. Often, a model with LOD1 data is enough. Studies shows that LOD1 models provide a relatively high information content and usability compared to their geometric detail (Henn et al., 2012; Hofierka & Zlocha, 2012). LOD1 model is the simplest volumetric 3D city model and fundamentally considered coarse and inferior to an LOD2. However, it may be more valuable than an LOD2 model for certain scenarios, especially when a finer footprint is more useful than the acquired roof shape (Biljecki et al., 2016). Examples of such cases include: climate change and urban climate modelling, property registration, energy modelling (Sousa et al., 2018), energy demand estimation (Bahu et al., 2013; Strzalka et al., 2012), shadowing simulations (M. Alam et al., 2012; Z. Li et al., 2015), navigation, estimation of noise pollution (Stoter et al., 2014), design of urban green spaces, crisis management, vulnerability assessments for disaster mitigation and management, simulating floods (Varduhn et al., 2015), for analysing wind comfort (Amorim et al., 2012), global change assessments (Biljecki et al., 2015; Pesaresi et al., 2016), and visualisation (Gesquière & Manin, 2014). Computation of the net internal area of a building is another application area of LoD1 data, useful for energy estimations, real estate valuation, and population counts (Boeters et al., 2015; Kaden & Kolbe, 2014; Lwin & Murayama, 2009; Novelli et al., 2016).

As the method presented in this thesis relies on open datasets, it could be of great use for developing and low income nations to generate 3D city models in a cost negated manner as well as with minimal effort and time. The approach has advantages over the usual tedious, time consuming procedures towards the generation of 3D city models and also bypasses the lengthy process of data procurement. Many applications like hazard and risk management require faster results and the data generation technique of the thesis can be very handy in such circumstances. The method presented in this thesis helps to develop 3D city information of LOD1 in case 2D building footprints are available, and accordingly could be adopted globally, where building height information of multiple cities is required. For example, this method has been used by

Shi et al., (2020) to find the building volume of buildings over multiple cities in Europe and the USA and the same were compared against the night time light data.

6.2.4 Challenges in using AW3D-30m data and possible solutions

One of the major disadvantages observed related to using AW3D-30m data was the accuracy limitation with high rise buildings (more than 100m). It was unable to obtain the accurate information of building heights for this region. In addition, even when a high resolution satellite data (AW3D-Enhanced 2 metre resolution DSM) used for validation and accuracy enhancement it yielded only a correlation of 20%. Hence it is important to find additional data sources for calibration of high rise buildings in data void regions. In this context building height data from websites like Skyscraper (which publishes the tall building information data from Council on Tall Buildings and Urban Habitat) can be used to compare the height values of these buildings. Further, as the accuracy level reduces with the increased percentage of tall buildings, it would be advantageous to know about the characteristics of a particular city before applying this methodology.

Further, though this thesis used AW3D-30 DSM data which was published in 2017 this dataset utilizes the 2011 satellite data as base data. Hence, there could be an accuracy difference for the buildings that are constructed after 2011. While using this method, it is also recommended to cross check the results of building elevation having low height values for larger 2D footprints, as tall buildings may have a large low height podium. This can be done by visual interpretation from Google Earth satellite images. Original AW3D-30 DSM has some data void regions and these values are filled with the values from adjacent pixels (https://www.aw3d.jp/en/products/enhanced/). So some accuracy difference could have originated due to this procedure. Large digitization errors or shifts in the 2D building footprints can result in the misrepresentation of height information.

6.3 Spatial resolution enhancement of Sentinel-2 image through sparse representation

The chapter IV of this thesis focused on the enhancement of the spatial resolution of the Sentinel-2 image using sparse representation techniques. The precise detection of buildings is of great importance to urban planning and management and urban cadastral management (Huo et al., 2018). As discussed in previous sections, open 2D footprints are incomplete or unavailable in many regions of the world. Hence, it is important to find other means to generate 2D buildings in order to develop 3D city models. High resolution satellite images provide great potential for accurate building detection since they contain a large amount of spectral, structure, and texture information (Song et al., 2019; You et al., 2018). Chapter IV explored the potential to enhance the 10 m spatial resolution of Sentinel-2 (10m) satellite data using a sample very high resolution WorldView-3 (1m) based on sparse representation techniques. So far, there are no studies on enhancing the spatial resolution of the Sentinel-2 image. Spatial enhancement of the Sentinel-2 aimed to extract 2D building footprints in data void regions by the image classification technique.

This chapter adopted sparse representation techniques for super-resolution analysis. Several studies have already discussed how super-resolution analysis can help in overcoming the limitations of low spatial resolution associated with relatively low cost or even free image data sources (Yang et al., 2010). An increase in spatial resolution can result in better identification of urban features.

This sparse representation has a much wider application capability. The main advantage of this method is that the dictionary generated from a sample fine resolution image can be applied to enhance not only the features in the same geographical location, but can be applied to any other geographical locations with similar characteristics. We have effectively demonstrated this capability by enhancing the Huangpu district Sentinel-2 image using the dictionary generated from other areas. Considering the global coverage of the Sentinel-2 image, the generation of a worldwide library of sparse representation dictionaries itself can be taken for further study. This would enable it to enhance the spatial resolution of open source Sentinel-2 data.

The chapter concentrated on the method to increase the spatial resolution of NIR, Red and Green bands having the spatial resolution of 10m of Sentinel-2. This chapter focussed on these bands as the major objective of the study is to extract urban features. The key requirement of the sparse representation is that the spectral bands of satellite imagery used both in the training phase and reconstruction phase should be similar. So the other coarser spectral bands (20m and 60m) of Sentinel-2 can also be enhanced, if relevant sample fine resolution bands can be obtained.

In the results section, it is clear that the sparse representation is particularly helpful in the sharpening of boundaries of different features of Sentinel-2. These enhancements are helpful in extracting dense urban features such as buildings and roads, where spatial resolution plays a very important role. This method also shows significant improvement in edge delineation of water bodies from land. So waterbody extraction could be more accurate using this method. However, this method is yet to prove its capability in distinguishing between different vegetation. So it is recommended to remove the vegetation layer before attempting image classification by running a normalised vegetation index (NDVI) operation. Studies already highlighted the advantage of involving NDVI for the potential increase in accuracy of classification (Hamedianfar & Shafri, 2015).

6.3.1 Influence of spatial resolution on sparse representation

In sparse representation analyses, one coarse and one fine resolution image are used jointly to train both the low resolution and high resolution dictionary (Cheng, 2015). In this thesis, mainly six classes (large buildings, high rise/tall buildings, small buildings, road, water body, and vegetation) were identified to demonstrate their response to resolution enhancement. After applying sparse representation to Sentinel-2 (10m) images, resultant images with 1m spatial resolution showed a considerable increase in their spatial resolution, which resulted in an overall accuracy of urban land cover classification of around 87%. This is a large increase from the 78% accuracy obtained based on the Sentinel-2 (10m) image. This increase was further improved by combining AW3D-30 DSM with the spatially enhanced Sentinel-2 (1m) image, resulting in an overall accuracy of 97%. Thus this chapter pointed to the real potential of using sparse representation techniques to produce data from which the 2D building extraction could be undertaken.

The spatial enhancement observed included edge enhancement or boundary enhancement of urban features. Results of the research showed sharpening of edges for all six classes, and consequently all urban features became easily distinguishable from enhanced Sentinel-2 (1m) image. After performing the sparse representation techniques, features like buildings, roads and water bodies became more prominent, sharp and distinct. Pixels on the edges of features are grouped to the main objects or features and avoid the issues of mixed pixels.

The process of sharpening edges and boundaries is referred to as the removal of the boundary effect. In low resolution images, boundaries of features are usually characterized by mixed pixels and are less distinguishable. Because of the boundary effect, individual features that are often smaller than individual pixels may fall within mixed pixels (Y. Sun et al., 2017). An early study from Latty et al., (1985) suggested that the boundary effect reduces by increasing the spatial resolution among the smaller size features and also reduces misclassification of features. According to Elad, (2010), sparse representation techniques are more robust to the noise of the training image and the technique can perform both denoising and spatial enhancement tasks simultaneously. The findings of Yang et al., (2010) also states that sparse representation techniques generate both realistic textures and sharp edges from the single input image.

This research also demonstrated that edges of linear features like roads and water bodies became more prominent and continuous after resolution enhancement due to the removal of mixed pixels. Therefore, this approach can be particularly applied to extract road networks, to demarcate roads and buildings. The capability to delineate water bodies from land has also been established and hence, waterbody extraction could be more accurate by using this method.

6.3.2 Influence of spectral resolution on sparse representation

Spectral bands are designated to detect electromagnetic radiation within a particular spectrum. Hence, in general, it is expected that having more spectral information could result in the identification of a wider range of land cover types and thereby higher mapping accuracy for urban areas, particularly in discriminating different land use types. The research of chapter IV aimed to increase the spatial resolution of the Sentinel-2 (10m) data. Thus, NIR, Red and Green bands of Sentinel-2 image were enhanced in the spatial resolution. Similarly, bands NIR, Red and Green of WorldView (WV)-3 having a spatial resolution of 1.2m were used for training and preparing the required dictionary. These bands were particularly selected as the objective of this research is to extract urban features. It was important to use bands with the same wavelengths from both images in order to avoid mis-classification as well as for better results. As the spectral resolution of VHR increases (for example, as promised by Planet), the chance of mirroring the spectral resolution of these with the coarser (but open) satellite data and thus improving the spectral properties of the spatially enhanced data.

6.3.3 Influence of sparse representation on Sentinel-2's recognition of urban features

As mentioned in the previous section, a total of six urban features were selected to verify the changes before and after enhancement. Our results show that the area of small buildings that appear blurred/unclear in Sentinel-2 (10m) images became sharper and individually identifiable after undergoing sparse representation. Likewise, the distinction between land areas and the waterbody became more prominent and smooth after the spatial resolution enhancement. Further, results also showed that the shapes and appearance of different buildings become more accurate after sparse representation analysis. Example Figures (4.10a, 4.10b & 4.10c) shows how building shapes differ before and after sparse representation techniques in comparison to Google Earth images. It may be noted that these results are obtained after using a dictionary generated outside of the Huangpu District. These results shed light on the potential applications of both sparse representation techniques as well as WorldView-3 and Sentinel-2 images.

Results from this study showed that waterbody extraction shall be more accurate using this method. However, this method is yet to prove its capability in spatial enhancement between different vegetation types. Sparse representation techniques can be more effective in an environment with a diverse texture like a dense urban environment rather than the agricultural application which represents limited types of crops. Hence, it is recommended to remove the vegetation layer before attempting image classification by running a normalised vegetation index (NDVI) operation.

6.3.4 Training phase and dictionary generation

In this research, the WorldView-3 image has been taken as input for dictionary generation. The spatial resolution of the enhanced image is directly proportional to the resolution of the training image. i.e., when the training image is of higher resolution, then the enhanced image will show more features when compared to the enhanced image using a low resolution training image. Results from this study show that using WorldView-3 for dictionary generation was suitable. Hence, generating dictionaries from WorldView-3 across the globe has huge potential on one hand and on the other hand, global coverage and frequent revisit of Sentinel-2 open up the scope of producing spatially enhanced Sentinel-2 images using dictionaries generated by WorldView-3. Albeit with the caveat that WorldView-3 data are not open source. However, a sampling approach that would reduce costs could be adopted to ensure global application.

Further, the dictionary generated from a sample high resolution image of a small area can be applied to enhance not only the features in the same geographical location but also can be applied to any other geographical locations with similar characteristics. This study has effectively demonstrated this capability by enhancing the Huangpu district Sentinel-2 image using the dictionary generated from other areas. Considering the global coverage of the Sentinel-2 image, the generation of a worldwide library of sparse representation dictionaries itself can be taken for further study. This would enable it to enhance the spatial resolution of open source Sentinel-2 data. Further, these spatially enhanced Sentinel-2 datasets can be used in generating 2D buildings footprints for the regions where 2D building datasets are not available for free.

6.3.5 Zoom factor

The zoom factor is an important parameter that influences the sparse representing accuracy. The display could be zoomed by a scale factor and is important in sparse representation at both the training and reconstruction phase, though it works opposite in two phases. In the training phase, the zoom factor helps to discard a relevant number of columns and rows to form a new large cell, whereas, in the reconstruction phase, it acts as a magnification factor. In the present study, during the training phase, input imagery (WV-3) was downscaled or degraded to 10m spatial resolution. i.e. 10 pixels of 1m were joined together to form one pixel of 10m resolution. Further during the reconstruction phase, the coarse resolution (Sentinel-2) imagery was zoomed to 1m spatial resolution. Here one pixel with a spatial resolution of 10m was replaced by 10 pixels. In previous studies, the zoom factor used was 3 (Yang et al., 2010) and it has been concluded that the accuracy of the sparse representation method is more likely to degrade rapidly using a greater zoom factor.

6.4 Extraction of building footprints from enhanced satellite images

The third core research chapter (Chapter V) attempts to classify spatially enhanced Sentinel-2 (1m) images and to fuse DSM with classified (enhanced) images so as to extract buildings. To understand the difference between various scenarios, three types of images were classified: Sentinel-2 (10m) image, Enhanced Sentinel-2 (1m) image and enhanced Sentinel-2 (1m) fused with AW3D-30 DSM. This chapter also demonstrated the difference in the accuracy of various urban land cover classes before and after spatial resolution enhancement, as well as, after combining DSM with enhanced satellite data. It was observed from the analysis that both sparse representation techniques and combining of DSM with enhanced Sentinel-2 data improves urban land cover classification and thereby enables improved extraction of building footprints from open data.

6.4.1 Urban classification using Sentinel-2 (10m), enhanced Sentinel-2 (1m) and enhanced Sentinel-2 (1m) fused with DSM

It was found that, in comparison to Sentinel-2 (10m) and enhanced Sentinel-2 (1m) images, AW3D-30 DSM DSM fused enhanced Sentinel-2 image distinguishes buildings from open class in a better way. For example, while areas classified under buildings were about 28% based on Sentinel-2 (10m), it further increased to 41% in enhanced Sentinel-2 (1m) and to 8.23 sq.km 53% in DSM fused enhanced Sentinel-2 image. However, buildings with bright roofs are better identified in the enhanced Sentinel-2 imagery while general buildings found to be more distinguishable from buildings with red/grey tile in DSM fused enhanced Sentinel-2 imagery.

It is further observed that area under open class reduced to 2.68 sq.km (17%) in the fused map from 6.44 sq. km (42%) in Sentinel-2 (10m) and 4.34 sq.km (28%) in enhanced Sentinel-2 images. However, it was also observed that roads show only slight variation among the three images. Roads are shown higher in enhanced Sentinel-2 images which can be attributed to the edge enhancement in enhanced images.

The buildings were extracted after removing water, vegetation, road, and open classes from classified images. The buildings were classified into five height classes (6-10, 10-15, 15-25, 25-50, >50) based on building heights. Areas with less than 6m height have been excluded, as in general these areas are less likely to be buildings. Building classification eased the capture of a medium and large building (area-wise), as well as all buildings with more than 6m heights. However, considering the area, small buildings with less than 10 sq.m could not be well captured in classified images. Further, it was also observed that some of the flyovers were classified as high rise buildings. Especially, in a country like China flyovers are very common and unless cross-checked with other sources like Google Earth and validated, it may result in mis-classification of results. Hence, it is very important to have a good understanding of the study area before applying this method.

6.4.2 Accuracy assessment of classification outputs using Sentinel-2 (10m), enhanced Sentinel-2 (1m) and enhanced Sentinel-2 (1m) fused with DSM

Accuracy assessment of each three classified images was carried out based on the confusion matrix and the point-based checking was conducted to compute the accuracy. 30 random points were selected from each of the five classes and overall 150 points each from three images were verified. Our results showed that the accuracy of all features except bright buildings exhibits a considerable difference in each of the three scenarios. All classes showed comparatively low accuracy rates in Sentinel-2 (10m) image, which further increased in enhanced Sentinel-2 (1m) as well as in enhanced Sentinel-2 (1m) fused with AW3D-30 DSM.

While the accuracy of road features was 73% in Sentinel-2 (10m) it increased to 83% in spatially enhanced Sentinel-2 (1m) and further combining DSM with enhanced Sentinel-2 image yielded 97% accuracy rate. As discussed before, sparse representation techniques help to enhance road features considerably. Further, combining DSM with enhanced Sentinel-2 image, augments to differentiate road features from other impervious layers.

The accuracy of the open class was found to be relatively higher (83%) for the Sentinel-2 (10m) image in comparison with the enhanced Sentinel-2 -1m (77%) image. However, DSM fused enhanced images showed higher accuracy (97%) than both scenarios. Urban features that are not distinguishable were categorized as an open class. Also due to shadows or low spectral resolution, small buildings sometimes become unidentifiable and tend to fall within open class. Accuracy reduction in enhanced Sentinel-2 image can be again attributed to relative edge sharpening and edge enhancement features. According to Labib & Harris, (2018) Sentinel-2 tended to misclassify several built up and vegetation classes like water, in case the shadow was dominant. Hence, after sparse representation, mixed pixels especially in the presence of shadows can be largely grouped to associated pixels and thereby pixels from open classes tend to fall within other urban classes.

It was also observed that the Sentinel-2 image was able to capture bright buildings as well as buildings with dark/red tiles very effectively. The accuracy of bright buildings is very high in all scenarios. While Sentinel-2 (10m) provided 97% accuracy for bright buildings, the accuracy of Dark/red tile buildings in Sentinel-2 (10m) image was about 87%, and in enhanced Sentinel-2 (1m) image, accuracy was about 93%. Accuracy of both bright buildings and buildings with dark/red tiles showed 100% after combining the DSM with enhanced Sentinel-2 image. Hence, this method can be effectively used to capture in areas with homogenous building roofs.

General buildings, i.e. buildings that do not have specific shapes or heterogeneous structures or buildings that do not have homogenous roof colours etc showed relatively lower accuracy before enhancement. Accuracy was about 50% in the case of the Sentinel-2 image, whereas general buildings exhibited relatively very lower (50%) for the Sentinel-2 (10m) image. However, accuracy has shown a considerable increase up to 80% in enhanced Sentinel-2 (1m) images and further to 93% after the fuse process. Hence, it can be assumed that this method can be very effectively used for building detection and classification in those areas with non-homogenous buildings in terms of shapes, structure and roof colour.

6.4.3 The normalized differenced vegetation index (NDVI) and urban classification

NDVI analyses the photosynthetic activity of vegetation and is a good indicator for the vitality of vegetation or for the growth status. Usually, this index is used to analyze the spatial distribution and seasonal fluctuation of vegetation over a region. However, this can also be used to differentiate between vegetation and plant fewer land covers, which is helpful to remove vegetation and supports accurate urban classification. According to Bhang & Lee, (2013), urban studies have several difficulties in segregating land covers as well as defining their properties with remote sensing images, as mixtures of land covers are very complex and spectrally ambiguous, typically with multispectral images.

In this chapter through NDVI, areas under vegetation cover were demarcated and removed from Sentinel-2 images. Results highlight that NDVI can be effectively used in vegetation removal during urban classification. Several studies also used the same method. A study conducted by Braun & Herold, (2004) explores and compares two methods, based on the vegetation fraction from linear spectral unmixing and the NDVI to map the degree of imperviousness in the urban agglomeration of Cologne/Bonn in Western Germany. Bhang & Lee, (2013) attempted to retrieve and investigate pure land cover characteristics of urban areas in terms of NDVI and surface brightness temperature and found that urban covers, especially building rooftops, had a few factors controlling NDVI values. Bhandari et al., (2012) attempted feature extraction based on NDVI for Jabalpur City in India and their results showed that the NDVI is highly useful in detecting the surface features of the visible area which are extremely beneficial for municipal planning and management.

6.4.4 Unsupervised classification for building extraction

In this thesis, unsupervised classification is used to classify urban features and to generate 3D city models. Images were classified into 40 different classes and further were grouped into seven classes. The seven classes include water, road, resultant vegetation area, open area, buildings with high brightness roofs, buildings with red/dark shade roofs, and general buildings.

Among the several classification methods, pixel based classification is generally grouped as supervised or unsupervised classification. The major difference between supervised and unsupervised classification is that training of the images is involved in supervised classification while no training is done for unsupervised classification (Li et al., 2017). Data training is the process of selecting a sample of pixels from the image and using it to establish thresholds to delineate specific land covers on the ground. A representative set of pixel values for each class is the key to the implementation of a supervised classification (Foody, 2008). The accuracy of the methods highly depends on familiarity with geographical conditions as well as with the samples taken for training.

Whereas, in unsupervised classification techniques prior field knowledge is not necessary and clustering mechanisms are used to group satellite image pixels into unlabeled classes/clusters. Training datasets are not required in unsupervised classification procedure and only specification of the number of classes is required by the user. In this research, initially, 40 classes were generated and later those classes were again clustered and grouped into seven classes. The K-means clustering algorithm was used for classification. Even though, several clustering algorithms exist that can be used to group the pixels present in the image based on spectral values (Phiri & Morgenroth, 2017), the most popular classifiers that use this algorithm are K-means and iterative self-organizing data analysis (ISODATA).

Both supervised and unsupervised classification techniques are used in building extraction from satellite images. For example, Ghaffarian & Ghaffarian (2014) presented a novel approach to detect the buildings by automating the training area collecting stage for supervised classification. The performance of the proposed approach was evaluated for both pixel based and object based classification. Evaluation of the results of the proposed study showed that based on the approach precision performances of overall buildings detected were about 88.4% and 85.3% in pixel based and object based classification respectively. Belgiu & Dra, (2014) compared supervised and unsupervised multiresolution segmentation approaches for extracting buildings from very high resolution QuickBird and WorldView-2 images with the inference that, though the two approaches produced different image objects, both yielded more or less similar classification results, with overall accuracies ranging from 82% to 86%. Further, they also concluded that as supervised segmentation requires prohibitive amounts of effort and time, unsupervised methods offer an important alternative that could improve the applicability of object based image analysis.

As mentioned before this research was carried out based on unsupervised classification. The main advantage of the method is its non-requirement of prior knowledge about land cover types before classification and the interpreter is responsible for assigning a class to each cluster of pixels. Hence, this technique is quicker, cheaper, and simpler than supervised methods (Goetz et al., 2003). Further, the result of the unsupervised approach could reveal some hidden characteristics of data, while the pixels in the same class may not necessarily illustrate identical features. Accordingly, the result of the unsupervised technique does not necessarily correspond to the classes that users are interested in. Another advantage of unsupervised classification is that this method allows using the high resolution Google Earth hosted satellite imagery for visual interpretation (in line with the desire to use open data, although image updates do vary geographically). The high resolution Google Earth image was geographically linked to the classified satellite image and each of the forty classes derived from unsupervised classification was regrouped to respective seven classes by looking at the high resolution satellite data via visual interpretation technique. Hence, for studies that link with Google Earth or similar kinds of images, it is recommended to use unsupervised classification techniques.

During the grouping process, classes representing water bodies were found to be much easier than other classes. Further, buildings with high reflectance values (i.e bright buildings or buildings with red tile roofs etc.) were relatively easier to extract. However, the grouping of buildings in highly clustered areas, buildings with low spectral reflectance values (for example roofs with multiple colours of tiles or with heterogeneous structures), smaller buildings with a mix of vegetation etc. were relatively difficult. In these regions, the pixel values have similarities with the pixel values of adjacent road features. These mixed pixel areas were extracted separately from the satellite image and the unsupervised classification has been applied again for this area to increase the overall classification accuracy. Shadows of bigger buildings pose an issue and to solve this requires analysis of multi temporal images captured during different times of the day.

6.5 Generating LOD1 3D city model from remote sensing satellite data

Chapter V of the thesis presented methods to generate LOD0 and LOD1 3D city models from satellite remote sensing data with varying accuracies by taking the example of Huangpu District, Shanghai. Few studies have already attempted to generate 3D city models from remote sensing satellite data, however they are mostly limited to urban structure characterisation and building height and volume extraction (Gamba et al., 2000; Goetz et al., 2003; Wang et al., 2018). The method used to generate LOD0 city model consisted of fusing enhanced Sentinel-2 (1m) with AW3D- 30 DSM and land cover classification. Accuracy assessment of building classification shows that this method yielded high accuracy in extracting buildings, i. e. 100% for both bright and dark/red building category and 93% for general buildings. Similarly, the fusion method fused with object based machine learning was adopted by Wang et al., 2018 to extract building heights by fusing Landsat image with Global Elevation Models (GEM) including AW3D30, SRTM and ASTER GDEM. However, their study showed relatively higher error in urban centre areas as a result of insufficient spatial resolution to resolve complex height variations which can be reduced to some extent by using enhanced Sentinel-2 (1m) images. Further, the fusion of the method adopted by Wang et al., 2018 with the enhanced Sentinel-2 (1m) as developed in this thesis may provide better results in building extraction.

Further, the LOD0 3D city model generated in this chapter largely provided building volume information for the entire area and found more suitable for categorising the buildings of an area according to their height, as it could not provide the exact shape and height of individual buildings. Thus, this method is highly suitable for applications that require information on building volume as well as distribution of buildings according to elevation ranges (for example disaster vulnerability assessment (Geiß et al., 2015) mapping of human settlements (Pesaresi et al., 2016), socio economic studies (Wang et al., 2018) etc.)).

The second section of the chapter provided the method to generate LOD1 3D city models from fused enhanced Sentinel-2 (1m) and AW3D-30 DSM images. One prerequisite to build LOD1 3D city models is generation of 2D footprints, in this case from the open satellite data. Hence, 2D footprints were generated by converting raster building data (pixels) to corresponding vector polygons. However, it involved some challenges as this method cannot extract exact individual building footprints in cases where the buildings are undulated or clustered. It was observed that when the roof is undulated, it results in presence of multiple pixel values with different height attributes within the same building polygon area and consecutively it results in the classification of the same building as many or vice versa. Thus one of the main disadvantages of this method is that, without knowing the height of the buildings, exact groups for building classification cannot be set. This is one of the major challenges of generating 2D footprints from open satellite data. In this chapter, the LOD1 buildings are generated by setting arbitrary height ranges of buildings within the city. Due to this limitation, the 2D building vector polygons generated are not of accurate shape but give the indication of the spread of buildings in the city. This method shall give the LOD1 3D city model but with limited accuracy. However, this LOD1 can provide the user with an indication of locations of high rise buildings and low rise buildings etc., which shall be handy for many applications (discussed in section 6.7).

6.6 Major limitations of the methods presented in this thesis

The thesis demonstrated two different methods to generate 3D city models from open data. The limitations of both methods are discussed in the next sections.

6.6.1 Major challenges associated with generation of 3D City Models from open 2D building footprints

Few challenges exist related to the generation of 3D city models from 2D open building footprint data based on the method demonstrated in the chapter III and are herewith elaborated further.

6.6.1.1 Lack of accuracy in the input data

The method used in Chapter III uses open 2D building data as an input (for example OSM) and as discussed in the chapter itself, the accuracy of these open datasets cannot be assured. All the errors including topological and data inconsistencies in the 2D building footprint data will be reflected in the resultant 3D city models (Girindran et al., 2020). Hence, the accuracy of the 3D city models largely depends on the accuracy of the input 2D open building footprint data. Likewise, another input data used includes AW3D-30 DSM. Data void regions of AW3D-30 DSM is filled with the height values of existing DEMs in cloud and snow pixels between 60◦ north and 60◦ south. Accordingly, the building height values in corresponding areas may not be accurate and the method may incur such errors.

6.6.1.2 Generalization of building heights

Another limitation of the method is that it cannot provide height differences within the same polygon. As building heights in 2D building data are generalized and represented as single polygons, micro level height variations within the buildings cannot be well represented. Hence, this method is most effective for macro level simulations.

6.6.2 Major challenges associated with the extraction of urban buildings from satellite images

Chapter V of the thesis demonstrated how to extract building volumes from spatially enhanced Sentinel-2 images. Even though this method proved to be capable of extracting buildings in data-void regions still there are underlying issues such as the shape of buildings, differentiation among buildings with other impervious layers, temporal image requirements in the context of urban growth and shadows of big buildings, as explained further.

6.6.2.1 Shape of buildings

In satellite images, features are represented as different pixels no matter what the shape of that particular feature is. In high resolution satellite images, these shapes are visible and easy to demarcate, whereas in low resolution images these shapes may not be accurate. Sentinel-2 has a spatial resolution of 10m and hence all features less than 10m will be represented only as a pixel. Further, small features may mostly be represented as mixed pixels. After spatial resolution enhancement, edges get sharpened reducing the mixed pixels. However, in this process, most of the small size features may lose their shape or even their existence. Hence, this method is not that useful for building shape extraction, especially in the case of small buildings.

6.6.2.2 Differentiation between buildings and other impervious layers

Higher spatial resolution implies, higher the chance of accurately identifying of buildings and other urban features. Images with low spatial resolution may either result in absence of many features or misclassification of non-building features as well as other impervious layers as buildings and vice versa. Impervious surfaces are usually defined as the entirety of impermeable surfaces such as roads, buildings, parking lots, and other urban infrastructures, where water cannot infiltrate through the ground (Sun et al., 2019). Challenges for mixed pixels may create confusion to delineate buildings from impervious surfaces in the large area mapping (Sun et al., 2019).

Results from this study showed that there are instances where flyovers are mis-classified as large buildings. Thus negating chances of mis-classification of buildings with other impervious layers such as roads or parking lots can be done to some extent by combining DSM. Whereas, in the case of flyovers or elevated roads simply combining DSM may not solve the issue. In this case, c and cross verification with OSM or Google Earth may help to solve the problem. Barrington-Leigh & Millard-Ball, (2017), estimated that globally about 77 countries among 185 have more than 95% of completeness of OSM road map. Hence, usage of OSM to delineate roads can be a possible solution.

6.6.2.3 Rapid urban growth and the importance of temporal image requirements

Urban areas are growing rapidly and in order to generate 3D city models more accurately, it is important to use the latest sets of satellite images. In this research AW3D-30 DSM is used to generate building elevation. Each DSM is captured during different times using different acquisition methods. For example, AW3D and TanDEM-X were acquired around the early 2010s, while ASTER and SRTM were acquired in the early 2000s (Misra et al., 2018). This affects what can be ‘seen’ in these DSMs which is important in the case of buildings. Hence, it is also important to use datasets that have continuous revisiting periods. In this study, AW3D-30 DSM was used to generate building heights. Continuous enhancements of AW3D-30 DSM are expected, which will improve its future utility. Hence, AW3D-30 DSM has considerable future potential in sustainable urban development due to its global coverage and open license.

Using the newer satellite data as the input image to fuse with DSM also can increase the accuracy of output. Sentinel-2 and WorldView-3 images are used as input images for this study. Both of these datasets have frequent revisit times which enables continuous updating of urban features. Sentinel-2 has a temporal resolution of 10 days with one satellite and 5 days with two satellites. The spatial resolution varies between 10m, 20m, and 60m depending on the spectral bands with a swath width of 290km. The main advantage of Sentinel-2 is the combination of wide swath and frequent revisiting time which makes it highly suitable for the mapping and monitoring of human settlements at a global level (Pesaresi et al., 2016). As the “Landsat-like” component of Copernicus, Sentinel-2 shares many of the technical characteristics of the existing Landsat system (Wulder et al., 2019).

The WorldView-3 satellite launched in 2014 has an average revisit time of < 1 day and is capable of collecting up to 680,000 km2 per day, further enhancing the DigitalGlobe collection capacity for more rapid and reliable collection. Hence Sentinel-2, WorldView-3, and AW3D-30 DSM have greater potential for urban management studies as well as for building generation.

6.6.2.4 Shadows of big buildings

High spatial resolution images produce detailed land cover and land use information, but the spectral similarity of different objects and shadows of tall buildings or large trees limit the impervious surface extraction (Guo et al., 2010). In this research, cloud free and shadowless images were procured. However, shadows of tall buildings still remain an issue in building extraction while using open data. These shadows create a higher number of mixed pixels and reduce the spectral reflection of small buildings. Hence, it has resulted in a larger area under open class. However, after combining DSM with enhanced Sentinel-2 image, the area under open class has been reduced to 2.68 sq.km against 4.34 sq.km from Sentinel-2 (10m). The major reason for this reduction can be attributed to the improved classification of mixed pixels into other classes including small buildings after combining DSM.

6.7 Potential applications of LOD1 and LOD0 3D city models

The methods discussed in this thesis mainly dealt with the generation of LOD1 and LOD0 3D city models. As briefly discussed in chapter III, many applications require only low LOD 3D city models, especially when a finer footprint is more useful than the acquired roof shape and this method will support such kinds of applications. Examples of such cases include climate change and urban climate modelling, property registration, energy modelling, navigation, design of urban green spaces, crisis management, vulnerability assessments for disaster mitigation and management, global change assessments and visualization.

Further, not all applications require high LOD but rather are task specific and data volume dependent. For example, noise emission simulation is computationally expensive and the inclusion of the exact slope of roofs has little influence on the results, thus a LOD1 model is more appropriate in such an instance. In Westphalia, Germany, based on CityGML LOD1 Data, the mapping of environmental noise pollution has been done for the whole state of North Rhine that contains approximately 8.6 million buildings. Recently several studies show that LOD1 or LOD0 3D city model data has great potential to carry out global level studies. Selected studies that have used 3D city models are briefly elaborated in the following sections with implications on where the methods for the 3D city model generation described in this thesis could be used.

6.7.1 Estimation of building volume and night time light (NTL)

A study by Shi et al., (2020) used LOD1 building volume data to assess the relationship between night time light data and the area extent of urbanized land. The study hypothesized that the strength of the relationship with NTL (Night Time Light) can be increased by consideration of the volume rather than simply the area of urbanized land. In order to determine the relationships between NTL, the area and volume of urbanized land, the towns and cities of the UK, the USA and countries of the European Union were considered. Further, the study also suggests the need to provide more attention to the building volumes. As the height data becomes easier to acquire and increasingly available, this may allow studies using NTL to relate more closely to key variables of urbanized areas and their populations.

It is to be noted that, Shi et al., (2020) followed the method developed in chapter III of this thesis as the study fused building footprint data together with building height data, to estimate building volumes and thereby also reaffirms the potential of the present method for global level studies.

6.7.2 Estimation of building volume for macro simulations including housing stock energy models decarbonisation strategies

LOD1 building models have huge potential in urban heat estimation and decarbonisation strategies. Building stock models have already been successfully used for modelling urban building energy at different spatial scales in different studies (Evans et al., 2009; Rosser et al., 2019). Further, studies like Sousa et al., (2018) demonstrated the use of building volume estimation to support the formulation of housing stock decarbonisation strategies. The Sousa study paid particular attention to the systematic identification of housing models and their corresponding attributes to represent the stock. Further, it emphasised the relevance of a volumetric representation of archetypes, or the semantically attributed 3D representations of the archetypes comprising the housing stock, in achieving the housing stock decarbonisation. Similarly in another study, Wurm et al., (2021) used deep learning based LOD1 building stock modelling with aerial images for urban heat demand modelling. Wurm et al., (2021) further highlighted the advantage of open data urban building energy modelling which substantiates the relevance of the current method.

Modern buildings built in our cities have high levels of energy consumption because of the requirements for air conditioning as well as lighting and in such scenarios, it is necessary to critically assess the utilization of resources for these activities. The 3D volume of buildings will be much needed for accurate energy modelling. For this application LOD1 3D city model developed using the method mentioned in chapter III would be handy or LOD0 3D city model generated for a city from satellite data shall be useful for macro modelling.

6.7.3 Estimating building geometry and shadow cast

Estimating shadows cast by buildings is an important utility of LOD1 3D modelling to assess the effect of a planned building onto its neighbourhood or to estimate the solar potential of buildings (Alam et al., 2013). Further, it can also be used to estimate how much a building is exposed to the sun, so as to assess the suitability for installation of solar panels on roofs (Strzalka et al., 2012).

Geometric information about buildings such as the tilt, orientation and area of the roof etc can be acquired from 3D models which also enhance its utility for the solar empirical models (Biljecki et al. 2015b). Further, 3D city models have a potential application in the estimation of the internal size of a building including net area, floor space etc. which is of importance for energy usage estimation of buildings (Boeters et al., 2015). In this case, the LOD1 building model mentioned in chapter III can be used, whereas the LOD0/LOD1 3D city model derived from satellite data will not be handy, as the exact shape of buildings cannot be developed through the methodology of Chapter V with the usage of current open satellite data.

6.7.4 Climate change studies

The application of 3D modelling in climate change studies has gained significant attention in recent years. There are several applications (especially for mitigation and adaptation strategies) that require only LOD1 or LOD0 3D visualization. For example, Danahy et al., (2016) investigated the use of 3D city models as a visualization reference against which analytical models were visualized to identify micro scale mitigation scenarios of urban heat island effects in the Toronto region. In another study, Masson et al., (2014) reported the usage of 3D city models in systemic modelling approaches to explore the ways of climate change adaptation. Further, several studies have already explored the utility of LOD1 3D city models in microclimate analyses including prediction of ground surface temperatures and to understand the urban thermal environment, estimate of the wind flow and evaluate pedestrian wind comfort around buildings (Amorim et al., 2012; Janssen et al., 2013; Ujang et al., 2015; Upadhyay & Sharma, 2014). The LOD1 3D city model generated by both methodologies as well as the LOD0 3D city model mentioned in chapter V of this thesis will be highly useful in such studies.

6.7.5 Disaster mitigation and management

One of the advantages of the proposed 3D generation from open source is the relative speed at which the 3D information can be generated. The faster generation will be handy at the time of disaster management as the 3D information of buildings will help in modelling the movement of cyclones in a particular city. Similarly, the 3D information will be highly advantageous for the earthquake mitigation activities. One potential application of low LOD 3D city modelling is the estimation of the number of inhabitants in a disaster affected area (such as marking of flood affected population or estimating the number of people affected by earthquakes or explosions etc.). Since the size of a building and its type provide a cue on the number of residents, usage of 3D geoinformation to estimate the population has been a key topic for research. Already, studies have explored the applicability of using building data in mapping dwelling units and estimating the number of people living in the buildings (Kunze & Hecht, 2015).

The outcome of this case can be used in multiple application domains. For instance, to optimise the coverage of mobile radio signal coverage (i.e., to optimise the network to cover more people) (Tutschku, 1997), as emergency response for aid delivery and evacuation (for example, by estimating the population affected by flooding (Akbar et al., 2013; Schneiderbauer & Ehrlich, 2005). For disaster mitigation and management, LOD1 buildings generated by chapter III methodology can be used wherever possible and in the absence of the same, LOD1 3D city models can be derived from open satellite data. The ability to fastly generate the 3D city model using the mentioned methodologies shall be convenient at disaster response time too.

6.7.6 Environmental management and planning

To cope up with rapid urbanisation and higher population growth, the city exerts immense pressure on the environment, which demands sustainable solutions for better environmental management practices. Environmentally sustainable planning of urban centres is difficult and potentially ineffective in the absence of reasonably adequate spatial information.

3D city models developed in this study will be particularly helpful in river management as well as in flood management and mitigation activities. Cities usually face problems from recurrent floods for several years. Intense short duration rains result in flash floods disrupting city life considerably. Changes in land use associated with urban development also result in flooding. Developmental projects taken up in the urban space over the years have created certain serious issues including flooding. A thorough understanding of the rivers and river basins in all their pluralities and intricacies is an essential pre-requisite for ensuring effective river conservation, river revival and management and in turn ensuring the wellbeing of the people and livelihoods. The rivers and their shores are precariously balanced, interacting ecosystems, easily upset by man, and there is increasing evidence to reiterate that man made activities have drastically modified the health of riverine ecosystems in a negative manner; many rivers no longer support socially valued native species or sustain dynamism that provides important goods and services. The pressure of urbanisation usually forces the construction of buildings even in flood plains. The 3D city information will help river planners to understand the volume of buildings in the floodplain and the information can be vital in case of evacuation at the time of the flood.

Increasing impervious surface area (ISA) due to urban development is one of the most important components of human induced land use and land cover change. ISA increment impacts storm water discharge in terms of influencing the runoff and associated erosion. Drainage capacity in the urban area is primarily made up of a local storm water drainage system composed of storm drain pipes, inlets, manholes, channels, roadside drains and culverts. This system is intended to converge storm flows efficiently to the community's primary drainage system, such as the main river channel or the nearest large body of water. Estimation of built up areas in a drainage basin with the degree of actual imperviousness is a must for estimating surface runoff and peak flow in an urban watershed. The information on the volume of buildings generated using 3D models will be very apt in this scenario.

The frequent flood logging area can be mapped and the building volume falling in these areas can be estimated for town planners. Uncontrolled growth of the urban population in developing countries in recent years has made changes in land use and other activities. An increase in concrete structures and pavements consuming bare soils without proper drainage systems may cause water logging/flooding. Apart from this, lack of maintenance of existing drainage systems and blockage of natural watercourses lead to water log problems during rain. Storm water drainage and sewerage system of cities, especially in developing nations, will be in a complex situation. Many cities have witnessed widespread water logging and disruption of traffic in recent days. Critical water logging is observed during intense rainfall, which results in the breakdown of vehicles, failure of signal systems, power disruptions and uprooting of trees. Non-maintenance of drainage lines together with unmanaged waste dumping cause blockages and is a serious issue in many developing cities. The smooth flow of water is hindered in the rainy season and further results in water logging/flooding over roads. The 3D city model will help planners to properly understand the building density and thereby access the population pressure exerted in these frequently waterlogged areas.

Similarly, the LOD0 and LOD1 3D city models will be useful for planners in conducting Environment Impact Assessment (EIA) for new building construction in an area, as the volume information gives a more accurate estimate of pressure exerted by the already constructed buildings in an area. EIA is a prior exercise to be carried out in any large project or major activity to be undertaken, so as to negate any harm to the environment on a short term or long term basis. Any developmental endeavor requires the analysis of the need of such a project, the monetary costs as well as benefits involved and further most importantly requires consideration and detailed assessment of the effect of a proposed development on the environment.

An EIA aims to ensure that potential impacts are identified and addressed at an early stage in the project's planning and design. The output of the assessment is to be communicated to all the relevant stakeholders that make informed decisions about the proposed projects, the project developers, investors as well as regulators, planners and politicians. Upon reading the report of an environmental impact assessment, project planners and engineers can shape the project so that the objectives and benefits can be achieved in a sustained manner without causing adverse impacts. Geographical Information System (GIS), which is a tool for collecting, storing, retrieving at will, transforming and displaying spatial data for a particular set of purposes, is widely used for verifying EIA reports. The 3D city information along with the other GIS variables will greatly equip the planners to make decisions related to permitting new building constructions in the existing area.

The 3D city information also helps in understanding the urban heat island issues related to climate change. Climate change is perhaps the most challenging environmental crisis confronting humanity today. Anthropocentric activities have substantially altered and fragmented our landscape and such disturbances can change the global atmospheric concentration of carbon dioxide, the principal heat trapping gas, further affect local, regional, and global climate by changing the energy balance on Earth's surface. Overwhelming scientific evidence suggests that emissions of several greenhouse gases such as carbon dioxide, methane, and nitrous oxides in particular, are contributing to climatic change. The global trend toward increased urbanisation indicates that climate change impacts in most countries will mainly affect urban populations. Climate change and urban growth are therefore inextricably linked, and general issues of sustainability require an urban focus. In addition, rising temperatures and enhanced 'heat island' effects may alter the energy consumption spatial and temporal patterns of cities. Remote sensing and GIS is a sophisticated technology already in widespread use by planners, engineers, and scientists to display and analyze all forms of location referenced data related to climate change and its impacts. RS and GIS techniques make it easier to handle a large volume of spatial data and temporal data. The 3D data will help to advance in urban climate change studies especially related to urban heat island.

Drainage characteristics of urban areas can be studied effectively using geospatial tools. It is important to understand the construct of likely flood events in a given situation to take preventive actions to mitigate likely damages. Domain knowledge on hydrology combined with spatial data assimilation and analyses using Remote Sensing and GIS would equip to precisely define the locations that are likely to get affected by flash floods during storm events. Changes in the urban area and storm intensity produce higher flows that exceed the capacity of small culverts under roads designed for the un-urbanized situation. Although adequate when designed, their carrying capacity may turn out to be inadequate and thereby overflow onto the roads creating new water paths and flood built up areas. In developing cities mostly inadequate maintenance of the drainage channels, debris and solid waste disposed into such drainage systems may accentuate the situation. Authorities shall be able to understand the root cause of these by integrating the volume of buildings in an area along with these existing parameters.

LOD1 3D city model generated using both methodologies shall be useful in the mentioned situations.

6.7.7 Land information system and tax collection

The application of geospatial technology in urban land management is widely accepted. But the 3D city information can revolutionize the building tax collection for the city. As the 3D information gives the volume of buildings, the tax checker can use this information to estimate the ratio of tax collected in a particular area proportional to the volume. The cost effective 3D model development will be particularly useful for cities in developing countries as the commercial 3D generation is still relatively costly. The LOD1 3D city model mentioned in chapter III shall be useful for this application.

6.7.8 Solid waste management

The amount and type of waste being generated largely varies within the areas of the city, which warrants proper management. Solid waste management in an effective manner is one of the key challenges cities across the globe are facing, as population and consumption growth results in an increasing quantity of waste. Solid waste if not handled properly potentially threatens and degrades environmental resources (air pollution through noxious smell, surface and ground water pollution through seepage of deposited and decomposed waste). Geospatial data along with 3D city information will help to understand the spatial distribution of the waste generation, its quantity and type. The 3D city volume information will help authorities to conduct route optimisation for solid waste collection. Similarly, the adequate allocation of waste bin collection can be done to the building density in a region. LOD1 3D city model generated using both methodologies shall be handy in this type of analysis.

6.7.9 Tourism geo portal creation

Information technologies and tourism, especially in cities are the two most dynamic motivators of the emerging global economy. Both tourism and IT increasingly provide strategic opportunities and powerful tools for economic growth, redistribution of wealth and development of equity around the globe. Usually, city tourism houses several attractions like captivating monuments, fascinating museums, architectural wonders, vivacious performing art scene, fabulous eating places, bustling markets, majestic forts etc. that lure the tourists. Attracting tourists is one of the prime focuses of every city and usually, tourists will be eager to gather reliable information for travel planning. The 3D display of important buildings along with an interactive spatial web portal exclusively for tourism information that has all the relevant spatial information regarding tourism to attract tourists to a particular city. The LOD1 3D city model mentioned in chapter III shall be an effective contributor for developing such solutions.

6.8 Sustainable development goals and 3D city models

As discussed in the introduction chapter, cities play a significant role in achieving sustainable development. Reflecting the essential role of cities in our transition to sustainable global development, the 11th Sustainable Development Goal, aims to "make cities and human settlements inclusive, safe, resilient and sustainable". Furthermore, several other SDGs are also linked to city development. The UN Habitat assumes that SDG 11 is directly related to at least eleven other SDGs and that one third of all 234 UN indicators can be assessed at the urban level (Un-Habitat, n.d.). The targeted implementation of SDGs in cities has the potential to support the integration of sustainability into urban planning (Kharrazi et al., 2016). Klopp & Petretta, (2017) argue that an ongoing challenge for the SDGs is the poor availability of urban data and highlights that the availability of open datasets at the city level can contribute to innovations and value added city services (Meschede & Siebenlist, 2019). Literature shows that 3D city models aid in sustainable city planning, as well as management and there is a dearth of low cost open 3D city data globally. This thesis demonstrates methods to generate low cost open 3D city models and thereby contributes towards narrowing the gap.

Further, the generation of low cost 3D city models can contribute to achieving multiple goals of SDGs that includes i) improving accessible and sustainable transport systems (SDG 11.2) where the LOD1 3D city models can aid in the simulation of the transport network, ii) enhancing integrated as well as sustainable human settlement planning and management in all countries (SDG 11.3), iii) minimising the number of deaths and the number of people affected and substantially decrease the direct economic losses relative to global gross domestic product caused by disasters, including water related disasters, with a focus on protecting the poor and people in vulnerable situations (SDG 11.5). and iv) increase the mitigation and adaptation capacities of cities to climate change, resilience to disasters, and develop and implement, in line with the Sendai Framework for Disaster Risk Reduction 2015 - 2030, holistic disaster risk management at all levels through proper planning (SDG 11.B).

This chapter windsup with the discussion over the potential applications of the generated 3D city models. The following chapter (VII) provides future outlook and salient findings of the thesis.

CHAPTER VII

FUTURE OUTLOOK AND CONCLUSIONS

7.1 Outlook and scope of future research

All data capture of relevance to this thesis continues to develop (for example, OSM data (which is now moving to 3D), optical satellite imagery, DSM and DTM data) and this has implications for improving the efficacy of the methods presented in this thesis. The new data set can be incorporated for 3D city model generation by analysing and slightly modifying the existing methodologies accordingly. For example, a new high resolution DSM can be used for height generation of the buildings, but the height value capture technique to be applied will depend on characteristics of the available DSM. There will more than likely be a need for recalibration of the methods presented in this thesis to use these new data sources, but the concept remains applicable. In short, more accurate DSM and DTM will help to generate more accurate 3D city models.

In the future, there will likely be higher resolution DSMs. LiDAR DSM and ICESat-2 data are examples. Many countries are already providing accurate LiDAR DSM data. For example, LiDAR DSM data are already available for about 70% of England from the UK Environmental Agency. ICESat-2 (ICE, CLOUD, and Land Elevation Satellite) is an ambitious mission from NASA, which will provide global distribution of geodetic measurements of both the terrain surface and relative canopy heights and it will also survey urban areas (Neuenschwander et al., 2018). Further, Global Ecosystem Dynamics Investigation (GEDI) LIDAR from NASA , with its dense track sampling and precise geolocation, forms the basis of an important dataset of ground control points to validate and calibrate global and regional DEMs and serves as a reference for surface elevation change (https://gedi.umd.edu/mission/mission-overview/; Dubayah et al., 2020; Healey et al., 2020).

The methodologies presented in this thesis afford the development of 3D models with LOD1 for any urban setting globally. High resolution 3D datasets with up to LOD2 are, of course, possible with the use of high resolution DSM and DTM but are very expensive to produce currently as many are not open source. But as more and more data like LiDAR DSM etc. are available as open data, a higher level of LOD building generation shall be possible. Especially to extract the roof top height shall be possible with the arrival of higher DSM and DTM data. Thus, it is hoped that when more accurate DSMs become available, it will enable the user to produce more accurate 3D models with better shape descriptions of buildings, especially roof modelling, thereby generating higher LODs using the defined methodology.

Further, part of this study used open software (GDAL, QGIS). In the future, it is possible to develop open source software and tools to generate 3D city models and to automate the entire procedure which will considerably increase the application as well as usage of LOD1 3D city models. Likewise, producing a global repository of open source enhanced Sentinel-2 images (for example, open data repositories of ready-to-use global street network models from OSM (Boeing, 2021)) could be achieved in the future to further the current research.

The increase in the coverage and accuracy of OSM will also help in generating more accurate 3D city models. Studies have reported that there has been a considerable increase in OSM building data in recent years. For example, from 2012 to 2017 alone there has been a 20 times increase in OSM building data in China (Tian et al., 2019). Effective derivation of elevation values for OSM data will likely extend its utility (Knerr, 2013). However, the absence of a global completeness assessment may hamper the use of OSM for urban planning and development, unless it is resolved (Barrington-Leigh & Millard-Ball, 2017). One of the major concerns in using OSM data is quality. Even though the quality is more difficult to ascertain these data (Veregin, 1999), most OSM data are provided by non-professionals and hence both the coverage and the quality of the data can be questionable (Senaratne et al. 2017; Nasiri et al. 2018).

Despite this disadvantage, OSM is a source of 2D building data, especially where free 2D building data are unavailable, as in China, where authorized building data are not freely available (Tian et al., 2019). Studies have also revealed that the rate at which OSM is receiving contributions from users has been constantly increasing and is continuing to grow; complemented by collaborative mapping efforts amongst the OSM community to check and improve the quality of contributions (Arsanjani et al., 2015). The Humanitarian OpenStreetMap Team (HOT) which applies the principles of open source and open data sharing for humanitarian response and community led development are also positive developments in this field. Further, ArcGIS Living Atlas of the World provides foundation elevation layers and tools to support analysis and visualization across the ArcGIS system. These layers get updated quarterly with high resolution elevation data from open sources and the community maps program which will in turn provide a good source of open data whilst it also shows that the relevance of open data is getting widely accepted (ArcGIS Living Atlas, 2021).

If another satellite data type is being used for 2D footprint generation (for instance, Landsat data would be attractive for historical analyses of cities' 3D landscapes), the parameters for enhancing that particular satellite data have to be analysed and generated for applying sparse representation techniques. This thesis has established the optimal parameters for enhancing Sentinel-2 satellite data of certain bands having a spatial resolution of 10m. As new higher resolution open data satellites come in, that data can be used for 2D footprint generation, but the parameters for applying sparse representation has to be found out. So in general, with these adjustments, any new satellite data can be incorporated in the developed methodology for 3D city model generation. The Planet data of 5m spatial resolution is promising and similar satellite data can be incorporated in future. Usually, these data are not open, but recently an initiative has opened these data for the tropics (Planet, 2020) and thus opens up opportunity.

3D city modelling has significantly advanced in the last decades and digital twin finds widespread favour recently as digital infrastructure becomes ever more embedded in our industries, cities and communities (Batty, 2018). Digital twin is the virtual representation of the real world including physical objects or processes and about its relationship and behaviour (ArcGIS Blog, 2021). Digital twin uses real time world data to create simulations that can predict how a product or process will perform in the real world and to solve real world problems (Yan et al., 2019). There is an increasing demand in the geospatial industry over the emergence of digital twin. Three different phases involved in geospatial digital twin concept are the data collection and visualisation, analytics and deployment (Park & Yang, 2020). The historic data as well as present data forms part of the analysis and both can be generated based on current methods. The 3D city model generated in this thesis using open data can act as the base of this digital twin process especially in the data poor regions.

Further, the latest advancements in big data analysis through deep learning techniques have led to a paradigm shift in terms of accuracy for image analysis including city-scale building extraction (Le et al., 2015; Zhu et al., 2016; Wurm et al., 2019). Especially the methods using convolutional neural networks for the semantic segmentation of individual buildings in very high resolution imagery have proven their better performance compared to traditional image classification methods (Lin et al., 2016; Huang et al., 2019). In combination with height data from DSMs, deep learning may be used in successfully generating building stocks (Wurm et al., 2021). Considering the cutting-edge developments in deep learning-based image analysis there is undoubtedly a large scope for producing more accurate 3D city models from open data.

7.2 Conclusions

This thesis investigated and provided globally replicable methodologies to generate 3D city models from open data. Generation of 3D city models from open data is the highlight of the research. The thesis broadly covered two different cases that typically arise in cities of developing/underdeveloped countries, for developing LOD1 3D city models. The first case is for areas having 2D building footprints available in open data such as OSM, while the second case is for areas that do not have 2D building footprint in open-source. Two different methods are developed for generating 3D city models in both cases.

For the areas already having 2D building footprint, the 3D city model is generated from AW3D-30 DSM and GMTED 2010 data. For the area that doesn't have 2D building footprint, enhanced Sentinel-2 satellite data were used to develop the building footprints. The enhancement of Sentinel-2 data is done with the help of a sample high resolution satellite data. The thesis henceforth also demonstrates the way to increase the spatial resolution of Sentinel-2 satellite data.

The 3D city model developed using 2D building footprint from open source showed more structural accuracy as compared to the 3D city model developed using 2D building footprint generated via open satellite data. In both cases, a 3D city model of LOD1 level is generated, but the model generated using open satellite data has limited accuracy upon comparison with the other. Hence it is recommended that open source 2D building footprints be used for generating 3D city models wherever possible and only in the absence of the same, the other option shall be considered. The 3D city model derived using open satellite data is best suited for providing building volume information in a City and the 3D city model developed using open data 2D building footprint is best suited to give individual building heights.

The whole method is cost effective, making it particularly attractive to users in low and middle income countries, where free 3D city data are not available. Further, this largely automated method requires minimal time to generate 3D city models and also has flexibility for improvement in accuracy if higher resolution data be available. Given the use of relatively low resolution open data, this methodology will be of particular relevance to studies that do not require high resolution 3D city models, such as for global environmental change studies, global climate change and urban climate modelling, real world simulations for 3D games, energy models and disaster vulnerability models.

Finally, the methodologies presented in this thesis can, in the future, be employed in conjunction with alternative 2D input data. Examples for such instances are quality checked OSM data as these become more abundant with more accurate height data, upgrades to AW3D-30 or availability of other sources, such as those derived from LiDAR measurements. Similarly, advancement in the availability of high resolution satellite open data shall help to develop a more accurate 3D city model using the methodology mentioned in the thesis.

It is concluded that the methodologies presented go some way to meeting the 3D data gap that currently exists for many cities especially in the developing and underdeveloped world. The successful use of these methods will depend on the application for which they are employed, which in turn should point to what improvements in data models are required. This thesis represents a step in the journey towards digital twins of all cities – privileged with data or not.

References

Ahadnejad Reveshty, M. (2011). The Assessment and Predicting of Land Use Changes to Urban Area Using Multi-Temporal Satellite Imagery and GIS: A Case Study on Zanjan, IRAN (1984-2011). *J. Geographic Information System*, *3*, 298–305. https://doi.org/10.4236/jgis.2011.34026

Ahmad, F., & Goparaju, L. (2016). Analysis of Urban Sprawl Dynamics Using Geospatial Technology in Ranchi City, Jharkhand, India. *Journal of Environmental Geography*, *9*(1–2), 7–13. https://doi.org/10.1515/jengeo-2016-0002

Ahmadi, F., & Toghyani, S. (2011). *The Role of Urban Planning in Achieving Sustainable Urban Development*.

Ahmed, S. (2018). Assessment of urban heat islands and impact of climate change on socioeconomic over Suez Governorate using remote sensing and GIS techniques. *The Egyptian Journal of Remote Sensing and Space Science*, *21*(1), 15–25. https://doi.org/https://doi.org/10.1016/j.ejrs.2017.08.001

Ahvenniemi, H., Huovila, A., Pinto-seppä, I., & Airaksinen, M. (2017). What are the differences between sustainable and smart cities ? *JCIT*, *60*, 234–245. https://doi.org/10.1016/j.cities.2016.09.009

Akanbi, A. K., Kumar, S., Fidelis, U., Akanbi, A. K., Kumar, S., & Fidelis, U. (2013). Application of remote sensing , GIS and GPS for efficient urban management plan – A case study of part of Hyderabad city: HAL Id : hal-01254902. *NovusInternational Journal OfEngineering&Technology*, 14. https://hal.archives-ouvertes.fr/hal-01254902

Akbar, M., Aliabadi, S., Patel, R., & Watts, M. (2013). A fully automated and integrated multi-scale forecasting scheme for emergency preparedness. *Environmental Modelling & Software*, *39*, 24–38. https://doi.org/https://doi.org/10.1016/j.envsoft.2011.12.006

Alam, M., Begum, I., Buysse, J., & Van Huylenbroeck, G. (2012). Energy consumption, carbon emissions and economic growth nexus in Bangladesh: Cointegration and dynamic causality analysis. *Energy Policy*, *45*. https://doi.org/10.1016/j.enpol.2012.02.022

Alam, N., Coors, V., & Zlatanova, S. (2013). *Detecting shadow for direct radiation using CityGML models for photovoltaic potentiality analysis* (pp. 191–210). https://doi.org/10.1201/b14914-23

Albert, A., Kaur, J., & Gonzalez, M. C. (2017). Using convolutional networks and satellite imagery to identify patterns in urban environments at a large scale. *Proceedings of the ACM SIGKDD International Conference on Knowledge*

Discovery and Data Mining, Part F1296, 1357–1366. https://doi.org/10.1145/3097983.3098070

Al-Bilbisi, H. (2019). Spatial monitoring of urban expansion using satellite remote sensing images: A case study of Amman City, Jordan. *Sustainability (Switzerland)*, *11*(8). https://doi.org/10.3390/su11082260

Alexander, C., Smith-Voysey, S., Jarvis, C., & Tansey, K. (2009). Integrating building footprints and LiDAR elevation data to classify roof structures and visualise buildings. *Computers Environment and Urban Systems*, *33*, 285–292. https://doi.org/10.1016/j.compenvurbsys.2009.01.009

Alexander, S. (2012) What is a Transition Town? Available at: https://www.permaculturenews.org/2012/07/21/what-is-a-transition-town/, Accessed on 30 September 2021

Alganci, U., Besol, B., & Sertel, E. (2018). Accuracy Assessment of Different Digital Surface Models. *ISPRS International Journal of Geo-Information*, *7*(3), 114. https://doi.org/10.3390/ijgi7030114

ALOS Global Digital Surface Model ALOSWorld 3D-30 m (AW3D30). Available online: https://www.eorc.jaxa.jp/ALOS/en/aw3d30/index.htm (accessed on 19 January 2019).

Amorim, J., Valente, J., C., P., Miranda, A. I., & Borrego, C. (2012). *Detailed modelling of the wind comfort in a city avenue at the pedestrian level* (pp. 03008p.1-03008p.6). https://doi.org/10.1051/3u3d/201203008

Arc GIS Living Atlas, Available at: https://www.esri.com/arcgis-blog/products/arcgis-living-atlas/imagery/high-resolution-data-updates-to-living-atlas-world-elevation-layers-and-tools-march-2021/?adumkts=social&utm_source=social&aduc=social&adum=external&aduca=social_technical&adusf=linkedin&adut=1344dcf9-4d37-4e43-9957-71adc61e82c3, Accessed on 29 March 2021.

ArcGIS: A Foundation for Digital Twins, Available at: https://www.esri.com/arcgis-blog/products/arcgis/aec/gis-foundation-for-digital-twins/, Accessed on 29 March 2021

Arsanjani, J. J., Mooney, P., Helbich, M., & Zipf, A. (2015). An Exploration of Future Patterns of the Contributions to OpenStreetMap and Development of a Contribution Index. *Transactions in GIS*, *19*(6), 896–914. https://doi.org/10.1111/tgis.12139

Athmania, D., & Achour, H. (2014). External Validation of the ASTER GDEM2, GMTED2010 and CGIAR-CSI- SRTM v4.1 Free Access Digital Elevation Models (DEMs) in Tunisia and Algeria. In *Remote Sensing* (Vol. 6, Issue 5). https://doi.org/10.3390/rs6054600

AW3D Products, the Highest Precision DEM in 0.5m Resolution. Available online: https://www.aw3d.jp/en/products/enhanced/ (accessed on 19 January 2019).

Bagheri, H., Schmitt, M., & Zhu, X. (2019). Fusion of Multi-Sensor-Derived Heights and OSM-Derived Building Footprints for Urban 3D Reconstruction. In *ISPRS International Journal of Geo-Information* (Vol. 8, Issue 4). https://doi.org/10.3390/ijgi8040193

Bahu, J.-M., Koch, A., Kremers, E., & Murshed, S. M. (2013). Towards a 3D spatial urban energy modelling approach. *ISPRS Annals of Photogrammetry, Remote Sensing and Spatial Information Sciences*, *II-2/W1*, 33–41. https://doi.org/10.5194/isprsannals-II-2-W1-33-2013

Baig, S., Rahman, A., & Rahman, A. (2012). Generalization and Visualization of 3D Building Models in CityGML. In *Lecture Notes in Geoinformation and Cartography* (pp. 63–77). https://doi.org/10.1007/978-3-642-29793-9_4

Baker, J. L. (2013). Climate change, disaster risk, and the urban poor: cities building resilience for a changing world. In *Choice Reviews Online* (Vol. 50, Issue 05). https://doi.org/10.5860/choice.50-2769

Ballatore, A., Bertolotto, M., & Wilson, D. (2013). Geographic Knowledge Extraction and Semantic Similarity in OpenStreetMap. *Knowledge and Information Systems*, *37*. https://doi.org/10.1007/s10115-012-0571-0

Barazzetti, L., Roncoroni, F., Brumana, R., & Previtali, M. (2016). Georeferencing accuracy analysis of a single worldview-3 image collected over milan. *International Archives of the Photogrammetry, Remote Sensing and Spatial Information Sciences - ISPRS Archives*, *2016-Janua*(July), 429–434. https://doi.org/10.5194/isprsarchives-XLI-B1-429-2016

Barrington-Leigh, C., & Millard-Ball, A. (2017). The world's user-generated road map is more than 80% complete. *PLOS ONE*, *12*(8), e0180698. https://doi.org/10.1371/journal.pone.0180698

Barron, C., Neis, P., & Zipf, A. (2014). A Comprehensive Framework for Intrinsic OpenStreetMap Quality Analysis. *Transactions in GIS*, *18*. https://doi.org/10.1111/tgis.12073

Batty, M, Axhausen, K. W., Giannotti, F., Pozdnoukhov, A., Bazzani, A., Wachowicz, M., Ouzounis, G., & Portugali, Y. (2012). Smart cities of the future. *European Physical Journal: Special Topics*, *214*(1), 481–518. https://doi.org/10.1140/epjst/e2012-01703-3

Batty, Michael. (2018). Digital twins. *Environment and Planning B: Urban Analytics and City Science*, *45*(5), 817–820. https://doi.org/10.1177/2399808318796416

Belgiu, M., & Dra, L. (2014). *ISPRS Journal of Photogrammetry and Remote Sensing Comparing supervised and unsupervised multiresolution segmentation* *approaches for extracting buildings from very high resolution imagery ˇ gut*. *96*, 67–75. https://doi.org/10.1016/j.isprsjprs.2014.07.002

Bertaud, M. A. (1989). *The Use of Satellite Images for Urban Planning: A Case Study from Karachi, Pakistan - Report INU 42*.

Beumier, C., & Idrissa, M. (2016). Digital terrain models derived from digital surface model uniform regions in urban areas. *International Journal of Remote Sensing*, *37*, 1–17. https://doi.org/10.1080/01431161.2016.1182666

Bhandari, A., Kumar, A., & Singh, G. K. (2012). Feature Extraction using Normalized Difference Vegetation Index (NDVI): A Case Study of Jabalpur City. *Procedia Technology*, *6*, 612–621. https://doi.org/10.1016/j.protcy.2012.10.074

Bhang, K., & Lee, J. (2013). Normalized Difference Vegetation Index (NDVI) characteristics for urban land covers: A case study in an industrial area of Gumi, Korea. *AGU Fall Meeting Abstracts*, *2013*, IN24B-02.

Bibri, S. E. (2019). On the sustainability of smart and smarter cities in the era of big data: an interdisciplinary and transdisciplinary literature review. *Journal of Big Data*, *6*(1), 25. https://doi.org/10.1186/s40537-019-0182-7

Biljecki, F., Ledoux, H., & Stoter, J. (2016). An improved LOD specification for 3D building models. *Computers, Environment and Urban Systems*, *59*, 25–37. https://doi.org/https://doi.org/10.1016/j.compenvurbsys.2016.04.005

Biljecki, F., Ledoux, H., Stoter, J., & Zhao, J. (2014). Formalisation of the level of detail in 3D city modelling. *Computers, Environment and Urban Systems*, *48*, 1–15. https://doi.org/10.1016/j.compenvurbsys.2014.05.004

Biljecki, F., Stoter, J., Ledoux, H., Zlatanova, S., & Çöltekin, A. (2015). Applications of 3D city models: State of the art review. *ISPRS International Journal of Geo-Information*, *4*(4), 2842–2889. https://doi.org/10.3390/ijgi4042842

Bittner, K., Adam, F., Cui, S., & Marco, K. (2018). Building Footprint Extraction from VHR Remote Sensing Images Combined with Normalized DSMs using Fused Fully Convolutional Networks. *IEEE Journal of Selected Topics in Applied Earth Observations and Remote Sensing*, *11*(8). https://doi.org/doi: 10.1109/JSTARS.2018.2849363.

Boeters, R., Ohori, K., Biljecki, F., & Zlatanova, S. (2015). Automatically enhancing CityGML LOD2 models with a corresponding indoor geometry. *International Journal of Geographical Information Science*, *29*, 2248–2268. https://doi.org/10.1080/13658816.2015.1072201

Boyle, L., & Michell, K. (2017). Urban facilities management: A systemic process for achieving urban sustainability. *International Journal of Sustainable Development and Planning*, *12*, 446–456. https://doi.org/10.2495/SDP-V12-N3-446-456

Braun, M., & Herold, M. (2004). Mapping imperviousness using NDVI and linear spectral unmixing of ASTER data in the Cologne-Bonn region (Germany). *Proc SPIE*, *5239*, 274–284. https://doi.org/10.1117/12.510978

Brédif, M., Tournaire, O., Vallet, B., & Champion, N. (2013). Extracting polygonal building footprints from digital surface models: A fully-automatic global optimization framework. *ISPRS Journal of Photogrammetry and Remote Sensing*, *77*, 57–65. https://doi.org/10.1016/j.isprsjprs.2012.11.007

Budhathoki, N. R., & Haythornthwaite, C. (2012). Motivation for Open Collaboration: Crowd and Community Models and the Case of OpenStreetMap. *American Behavioral Scientist*, *57*(5), 548–575. https://doi.org/10.1177/0002764212469364

Buyukdemircioglu, M., Kocaman, S., & Isikdag, U. (2018). Semi-automatic 3D city model generation from large-format aerial images. *ISPRS International Journal of Geo-Information*, *7*(9). https://doi.org/10.3390/ijgi7090339

Camboim, S. P., Meza Bravo, J. V., & Sluter, C. R. (2015). An investigation into the completeness of, and the updates to, OpenStreetMap data in a heterogeneous area in Brazil. *ISPRS International Journal of Geo-Information*, *4*(3), 1366–1388. https://doi.org/10.3390/ijgi4031366

Carter, J. G., Cavan, G., Connelly, A., Guy, S., Handley, J., & Kazmierczak, A. (2015). Climate change and the city: Building capacity for urban adaptation. *Progress in Planning*, *95*, 1–66. https://doi.org/https://doi.org/10.1016/j.progress.2013.08.001

Chang, D. L., Sabatini-Marques, J., da Costa, E. M., Selig, P. M., & Yigitcanlar, T. (2018). Knowledge-based, smart and sustainable cities: A provocation for a conceptual framework. *Journal of Open Innovation: Technology, Market, and Complexity*, *4*(1). https://doi.org/10.1186/s40852-018-0087-2

Chastain, R., Housman, I., Goldstein, J., Finco, M., & Tenneson, K. (2019). Empirical cross sensor comparison of Sentinel-2A and 2B MSI, Landsat-8 OLI, and Landsat-7 ETM+ top of atmosphere spectral characteristics over the conterminous United States. *Remote Sensing of Environment*, *221*, 274–285. https://doi.org/https://doi.org/10.1016/j.rse.2018.11.012

Chauvin, J., Glaeser, E., Ma, Y., & Tobio, K. (2016). What is Different About Urbanization in Rich and Poor Countries? Cities in Brazil, China, India and the United States. *Journal of Urban Economics*, *98*. https://doi.org/10.1016/j.jue.2016.05.003

Chen, C., Gong, W., Hu, Y., Chen, Y., & Ding, Y. (2017). Learning Oriented Region-based Convolutional Neural Networks for Building Detection in Satellite Remote Sensing Images. *ISPRS - International Archives of the Photogrammetry, Remote Sensing and Spatial Information Sciences*, *42W1*, 461–464.

https://doi.org/10.5194/isprs-archives-XLII-1-W1-461-2017

Chen, R. (2011). The development of 3D city model and its applications in urban planning. *Proceedings - 2011 19th International Conference on Geoinformatics, Geoinformatics 2011*, 1–5. https://doi.org/10.1109/GeoInformatics.2011.5981007

Cheng, H. (2015). *Sparse Representation, Modeling and Learning in Visual Recognition Theory, Algorithms and Applications*. Springer.

Chrysoulakis, N., Feigenwinter, C., Triantakonstantis, D., Penyevskiy, I., Tal, A., Parlow, E., Fleishman, G., Duzgun, S., Esch, T., & Marconcini, M. (2014). A Conceptual List of Indicators for Urban Planning and Management Based on Earth Observation. *ISPRS International Journal of Geo-Information*, *3*, 980–1002. https://doi.org/10.3390/ijgi3030980

Cohen, M. (2017). A Systematic Review of Urban Sustainability Assessment Literature. In *Sustainability* (Vol. 9, Issue 11). https://doi.org/10.3390/su9112048

Compagnon, R. (2004). Solar and daylight availability in the urban fabric. *Energy and Buildings*, *36*, 321–328. https://doi.org/10.1016/j.enbuild.2004.01.009

Creutzig, F., Baiocchi, G., Bierkandt, R., Pichler, P.-P., & Seto, K. C. (2015). Global typology of urban energy use and potentials for an urbanization mitigation wedge. *Proceedings of the National Academy of Sciences*, *112*(20), 6283 LP – 6288. https://doi.org/10.1073/pnas.1315545112

Czyńska, K., & Rubinowicz, P. (2014). APPLICATION OF 3D VIRTUAL CITY MODELS IN URBAN ANALYSES OF TALL BUILDINGS – TODAY PRACTICE AND FUTURE CHALLENGES. *ARCHITECTURAE et ARTIBUS*, *19*, 9–13.

Dalla Longa, F., Strikkers, T., Kober, T., & van der Zwaan, B. (2018). Advancing Energy Access Modelling with Geographic Information System Data. *Environmental Modeling & Assessment*, *23*(6), 627–637. https://doi.org/10.1007/s10666-018-9627-1

Danahy, J., Mitchell, J., Wright, R., Hoinkes, R., & Feick, R. (2016). Multi-Scale 3D Geovisualization of Urban Heat Island Data for Planning Dialogue in Toronto. In *Natural Resources Management: Concepts, Methodologies, Tools, and Applications* (pp. 570–591). https://doi.org/10.4018/978-1-5225-0803-8.ch026

Darabi, H., Haghighi, A. T., Mohamadi, M. A., Rashidpour, M., Ziegler, A. D., Hekmatzadeh, A. A., & Kløve, B. (2019). Urban flood risk mapping using data-driven geospatial techniques for a flood-prone case area in Iran. *Hydrology Research*, *51*(1), 127–142. https://doi.org/10.2166/nh.2019.090

de Jong, M., Joss, S., Schraven, D., Zhan, C., & Weijnen, M. (2015). Sustainable–

smart–resilient–low carbon–eco–knowledge cities; making sense of a multitude of concepts promoting sustainable urbanization. *Journal of Cleaner Production*, *109*, 25–38. https://doi.org/https://doi.org/10.1016/j.jclepro.2015.02.004

DEM, DSM & DTM Differences—A Look at Elevation Models in GIS. Available online: https://gisgeography.com/dem-dsm-dtm-dierences/ (accessed on 19 January 2019).

Diamantini, C., & Zanon, B. (2000). Planning the urban sustainable development The case of the plan for the province of Trento, Italy. *Environmental Impact Assessment Review*, *20*, 299–310. https://doi.org/10.1016/S0195-9255(00)00042-1

DigitalGlobe. (2016). *Radiometric Use of WorldView-3 Imagery*. https://dg-cms-uploads-production.s3.amazonaws.com/uploads/document/file/207/Radiometric_Use_of_WorldView-3_v2.pdf

Döllner, J., Kolbe, T., Liecke, F., Sgouros, T., & Teichmann, K. (2006). The virtual 3D city model of Berlin - Managing, integrating, and communicating complex urban information. *Proceedings of the 25th Urban Data Management Symposium UDMS*.

Dubayah, R., Blair, J. B., Goetz, S., Fatoyinbo, L., Hansen, M., Healey, S., Hofton, M., Hurtt, G., Kellner, J., Luthcke, S., Armston, J., Tang, H., Duncanson, L., Hancock, S., Jantz, P., Marselis, S., Patterson, P. L., Qi, W., & Silva, C. (2020). The Global Ecosystem Dynamics Investigation: High-resolution laser ranging of the Earth's forests and topography. *Science of Remote Sensing*, *1*, 100002. https://doi.org/https://doi.org/10.1016/j.srs.2020.100002

Dwyer, J. L., Roy, D. P., Sauer, B., Jenkerson, C. B., Zhang, H. K., & Lymburner, L. (2018). Analysis Ready Data: Enabling Analysis of the Landsat Archive. In *Remote Sensing* (Vol. 10, Issue 9). https://doi.org/10.3390/rs10091363

Elad, M. (2010). *Sparse and Redundant Representations From Theory to Applications in Signal and Image Processing*. Springer.

Elevation of Nottingham, UK Elevation Map, Topo, Contour. Available online: http://www.floodmap.net/Elevation/ElevationMap/?gi=2641170 (accessed on 5 January 2019).

Elfadaly, A., & Lasaponara, R. (2019). On the use of satellite imagery and GIS tools to detect and characterize the urbanization around heritage sites: The case studies of the Catacombs of Mustafa Kamel in Alexandria, Egypt and the Aragonese Castle in Baia, Italy. *Sustainability (Switzerland)*, *11*(7). https://doi.org/10.3390/SU11072110

Elwood, S., Goodchild, M., & Sui, D. (2012). Researching Volunteered Geographic Information: Spatial Data, Geographic Research, and New Social Practice.

Annals of the Association of American Geographers, *102*, 571–590. https://doi.org/10.1080/00045608.2011.595657

Eshghi, M., & Alesheikh, A. A. (2015). Assessment of completeness and positional accuracy of linear features in Volunteered Geographic Information (VGI). *International Archives of the Photogrammetry, Remote Sensing and Spatial Information Sciences - ISPRS Archives*, *40*(1W5), 169–174. https://doi.org/10.5194/isprsarchives-XL-1-W5-169-2015

Evans, A., Strezov, V., & Evans, T. (2009). Assessment of sustainability indicators for renewable energy technologies [J]. *Renewable and Sustainable Energy Reviews*, *13*, 1082–1088. https://doi.org/10.1016/j.rser.2008.03.008

Fan, H., Yang, A., & Zipf, A. (2016). *Intrinsic OSM data quality assessment The intrinsic quality assessment of building footprints data on OpenStreetMap in Baden- Württemberg* (pp. 253–260).

Feltynowski, M. (2017). Urban spatial policy and its impact on open areas – Płock case study. *Bulletin of Geography. Socio-Economic Series*, *36*, 87–94. https://doi.org/10.1515/bog-2017-0016

Flamanc, D., Maillet, G., & Jibrini, H. (2003). *3D CITY MODELS : AN OPERATIONAL APPROACH USING AERIAL IMAGES AND CADASTRAL MAPS*. *XXXIV*, 53–58.

Fonji, S., & Taff, G. (2014). Using satellite data to monitor land-use land-cover change in North-eastern Latvia. *SpringerPlus*, *3*, 61. https://doi.org/10.1186/2193-1801-3-61

Fonte, C. C., Antoniou, V., Bastin, L., Estima, J., Arsanjani, J. J., L, B. J., See, L., & Vatseva Rumiana. (2017). Assessing VGI Data Quality. *Mapping and the Citizen Sensor*, *September*, 137–163. https://doi.org/10.5334/bbf.g

Foody, G. M, & Boyd, D. (2013). Using Volunteered Data in Land Cover Map Validation: Mapping West African Forests. *Selected Topics in Applied Earth Observations and Remote Sensing, IEEE Journal Of*, *6*, 1305–1312. https://doi.org/10.1109/JSTARS.2013.2250257

Foody, G. M., (2008). *Harshness in image classification accuracy assessment*. *1161*(May). https://doi.org/10.1080/01431160701442120

Foody, G. M., See, L., Fritz, S., Van der Velde, M., Perger, C., Schill, C., & Boyd, D. S. (2013). Assessing the Accuracy of Volunteered Geographic Information arising from Multiple Contributors to an Internet Based Collaborative Project. *Transactions in GIS*, *17*(6), 847–860. https://doi.org/https://doi.org/10.1111/tgis.12033

Forghani, M., & Delavar, M. (2014). A Quality Study of the OpenStreetMap Dataset for Tehran. *ISPRS International Journal of Geo-Information*, *3*, 750–763.

https://doi.org/10.3390/ijgi3020750

Fuenfschilling, L., Frantzeskaki, N., & Coenen, L. (2019). Urban experimentation & sustainability transitions. *European Planning Studies*, *27*(2), 219–228. https://doi.org/10.1080/09654313.2018.1532977

Gamba, P., Houshmand, B., & Saccani, M. (2000). Detection and extraction of buildings from Interferometric SAR data. *Geoscience and Remote Sensing, IEEE Transactions On*, *38*, 611–617. https://doi.org/10.1109/36.823956

Garouani, A. E., Alobeid, A., & Garouani, S. E. (2014). Digital surface model based on aerial image stereo pairs for 3D building. *International Journal of Sustainable Built Environment*, *3*(1), 119–126. https://doi.org/10.1016/j.ijsbe.2014.06.004

Gascon, F., Bouzinac, C., Thépaut, O., Jung, M., Francesconi, B., Louis, J., Lonjou, V., Lafrance, B., Massera, S., Gaudel-Vacaresse, A., Languille, F., Alhammoud, B., Viallefont, F., Pflug, B., Bieniarz, J., Clerc, S., Pessiot, L., Trémas, T., Cadau, E., … Fernandez, V. (2017). Copernicus Sentinel-2A calibration and products validation status. *Remote Sensing*, *9*(6). https://doi.org/10.3390/rs9060584

Gatti, A., & Bertolini, A. (2016). *Sentinel-2 Products Specification Document (PSD) - S2-PDGS-TAS-DI-PSD. Sentin.-2 Prod. Specif. Doc. PSD 489*.

GEDI Ecosystem Lidar. Available online: https://gedi.umd.edu/applications/topography-and-surfacedeformation/ (accessed on 15 March 2019).

Geiß, C., Wurm, M., Breunig, M., Felbier, A., & Taubenböck, H. (2015). Normalization of TanDEM-X DSM Data in Urban Environments With Morphological Filters. *Geoscience and Remote Sensing, IEEE Transactions On*, *53*, 4348–4362. https://doi.org/10.1109/TGRS.2015.2396195

Gesquière, G., & Manin, A. (2014). 3D visualization of urban data based on CityGML with WebGL. *International Journal of 3-D Information Modeling*, *1*, 1–15. https://doi.org/10.4018/ij3dim.2012070101

Giovanella, A., Bradley, P. E., & Wursthorn, S. (2019). Evaluation of topological consistency in CityGML. *ISPRS International Journal of Geo-Information*, *8*(6). https://doi.org/10.3390/ijgi8060278

Girindran, R., Boyd, D. S., Rosser, J., Vijayan, D., Long, G., & Robinson, D. (2020). On the Reliable Generation of 3D City Models from Open Data. *Urban Science*, *4*(4), 47. https://doi.org/10.3390/urbansci4040047

Goetz, M., & Zipf, A. (2012). Towards Defining a Framework for the Automatic Derivation of 3D CityGML Models from Volunteered Geographic Information. *International Journal of 3-D Information Modeling*, *1*. https://doi.org/10.4018/ij3dim.2012040101

Goetz, S. J., Wright, R. K., Smith, A. J., Zinecker, E., & Schaub, E. (2003). *IKONOS imagery for resource management : Tree cover , impervious surfaces , and riparian buffer analyses in the mid-Atlantic region*. *88*, 195–208. https://doi.org/10.1016/j.rse.2003.07.010

Goodchild, M. F. (2007). Citizens as sensors: the world of volunteered geography. *GeoJournal*, *69*(4), 211–221. https://doi.org/10.1007/s10708-007-9111-y

Goward, S. N., Masek, J. G., Williams, D. L., Irons, J. R., & Thompson, R. J. (2001). *The Landsat 7 mission Terrestrial research and applications for the 21st century*. *78*, 3–12.

Graser, A., Straub, M., & Dragaschnig, M. (2015). *Is OSM Good Enough for Vehicle Routing? A Study Comparing Street Networks in Vienna*. https://doi.org/10.1007/978-3-319-11879-6_1

Groeger, G., Kolbe, T. ., Czerwinski, A., & Nagel, C. (2012). *OGC City Geography Markup Language (CityGML) Encoding Standard v2.0. OGC Doc*. Open Geospatial Consortium: Wayland, MA, USA.

Groeger, G., Kolbe, T. H., Czerwinski, A., & Nagel, C. (2008). *OpenGIS City Geography Markup Language (CityGML) Encoding Standard, v1.0.0, OGC Doc. No. 08-007r1*. Open Geospatial Consortium Inc .Wayland, MA, USA.

Grohmann, C. (2016). COMPARATIVE ANALYSIS OF GLOBAL DIGITAL ELEVATION MODELS AND ULTRA-PROMINENT MOUNTAIN PEAKS. *ISPRS Annals of Photogrammetry, Remote Sensing and Spatial Information Sciences*, *III–4*, 17–23. https://doi.org/10.5194/isprs-annals-III-4-17-2016

Gruen, A. (2012). Development and Status of Image Matching in Photogrammetry. *Photogrammetric Record*, *26*(137), 36–57.

Guo, J., Liang, L., & Gong, P. (2010). Removing shadows from Google Earth images. *International Journal of Remote Sensing*, *31*, 1379–1389. https://doi.org/10.1080/01431160903475316

Haack, B. N. (1982). Landsat: A tool for development. *World Development*, *10*(10), 899–909. https://doi.org/https://doi.org/10.1016/0305-750X(82)90064-X

Haala, N., & Anders, K.-H. (2001). *Fusion of 2D-GIS and Image Data for 3D Building Reconstruction*. *31*.

Haala, N., Rothermel, M., & Cavegn, S. (2015). Extracting 3D Urban Models from Oblique Aerial Images. In *2015 Joint Urban Remote Sensing Event, JURSE 2015*. https://doi.org/10.1109/JURSE.2015.7120479

Haklay, M. (2008). How good is Volunteered Geographical Information ? A comparative study of OpenStreetMap and Ordnance Survey datasets Abstract. *Environ. Plan. B Plan. Des*. https://doi.org/10.1111/j.1548-1433.2011.01334.x

Hamedianfar, A., & Shafri, H. (2015). Detailed intra-urban mapping through transferable OBIA rule sets using WorldView-2 very-high-resolution satellite images. *International Journal of Remote Sensing*, *36*, 3380–3396. https://doi.org/10.1080/01431161.2015.1060645

Hansen, M. C., & Loveland, T. R. (2012). Remote Sensing of Environment A review of large area monitoring of land cover change using Landsat data. *Remote Sensing of Environment*, *122*, 66–74. https://doi.org/10.1016/j.rse.2011.08.024

Hawchar, L., Naughton, O., Nolan, P., Stewart, M. G., & Ryan, P. C. (2020). A GIS-based framework for high-level climate change risk assessment of critical infrastructure. *Climate Risk Management*, *29*, 100235. https://doi.org/https://doi.org/10.1016/j.crm.2020.100235

Haworth, B. T., Bruce, E., Whittaker, J., & Read, R. (2018). The Good, the Bad, and the Uncertain: Contributions of Volunteered Geographic Information to Community Disaster Resilience. *Frontiers in Earth Science*, *6*, 183. https://doi.org/10.3389/feart.2018.00183

Healey, S. P., Yang, Z., Gorelick, N., & Ilyushchenko, S. (2020). Highly Local Model Calibration with a New GEDI LiDAR Asset on Google Earth Engine Reduces Landsat Forest Height Signal Saturation. In *Remote Sensing* (Vol. 12, Issue 17). https://doi.org/10.3390/rs12172840

Henn, A., Römer, C., Gröger, G., & Plümer, L. (2012). Automatic classification of building types in 3D city models. *GeoInformatica*, *16*(2), 281–306. https://doi.org/10.1007/s10707-011-0131-x

Hofierka, J., & Zlocha, M. (2012). A New 3-D Solar Radiation Model for 3-D City Models. *Transactions in GIS*, *16*. https://doi.org/10.1111/j.1467-9671.2012.01337.x

Hofmann, A., & Wan, G. (2013). Determinants of urbanization. *ADB Economics Working Paper Series*, *355*(355), 1–31. https://doi.org/10.2139/ssrn.2295736

Hu, T., Yang, J., Li, X., & Gong, P. (2016). Mapping urban land use by using landsat images and open social data. *Remote Sensing*, *8*(2). https://doi.org/10.3390/rs8020151

Huang, J., Zhang, X., Xin, Q., Sun, Y., & Zhang, P. (2019) Automatic Building Extraction from High-Resolution Aerial Images and LiDAR Data Using Gated Residual Refinement Network. *ISPRS J. Photogramm. Remote Sens.*151, 91–105.

Huang, L., Wu, J., & Yan, L. (2015). Defining and measuring urban sustainability: a review of indicators. *Landscape Ecology*, *30*(7), 1175–1193. https://doi.org/10.1007/s10980-015-0208-2

Huo, L.-Z., Silva, C. A., Klauberg, C., Mohan, M., Zhao, L.-J., Tang, P., & Hudak, A.

T. (2018). Supervised spatial classification of multispectral LiDAR data in urban areas. *PLOS ONE, 13*(10), e0206185. https://doi.org/10.1371/journal.pone.0206185

Immitzer, M., Vuolo, F., & Atzberger, C. (2016). First experience with Sentinel-2 data for crop and tree species classifications in central Europe. *Remote Sensing, 8*(3). https://doi.org/10.3390/rs8030166

Jacobson, A., Dhanota, J., Godfrey, J., Jacobson, H., Rossman, Z., Stanish, A., Walker, H., & Riggio, J. (2015). A novel approach to mapping land conversion using Google Earth with an application to East Africa. *Environmental Modelling & Software, 72*, 1–9. https://doi.org/https://doi.org/10.1016/j.envsoft.2015.06.011

Janečka, K. (2019). Transformation of 3D geospatial data into CityGML – a case of Prague. *Reports on Geodesy and Geoinformatics, 107*(1), 41–48. https://doi.org/10.2478/rgg-2019-0005

Janssen, W. D., Blocken, B., & van Hooff, T. (2013). Pedestrian wind comfort around buildings: Comparison of wind comfort criteria based on whole-flow field data for a complex case study. *Building and Environment*, *59*, 547–562. https://doi.org/https://doi.org/10.1016/j.buildenv.2012.10.012

Jensen, R. J. (2005). *Introductory Digital Image Processing* (Third). Upper Saddle River, New Jersey: Prentice Hall,.

Jing, C., Shortridge, A., Lin, S., & Wu, J. (2014). Comparison and validation of SRTM and ASTER GDEM for a subtropical landscape in Southeastern China. *International Journal of Digital Earth*, *7*(12), 969–992. https://doi.org/10.1080/17538947.2013.807307

Jones, R. R., McCaffrey, K. J. W., Clegg, P., Wilson, R. W., Holliman, N. S., Holdsworth, R. E., Imber, J., & Waggott, S. (2009). Integration of regional to outcrop digital data: 3D visualisation of multi-scale geological models. *Computers & Geosciences, 35*, 4–18.

Jovanović, D., Milovanov, S., Ruskovski, I., Govedarica, M., Sladić, D., Radulović, A., & Pajić, V. (2020). Building virtual 3D city model for smart cities applications: A case study on campus area of the university of novi sad. *ISPRS International Journal of Geo-Information*, *9*(8). https://doi.org/10.3390/ijgi9080476

Kada, M., & Mckinley, L. (2009). 3D building reconstruction from LiDAR based on a cell decomposition approach. *International Archives of the Photogrammetry, Remote Sensing and Spatial Information Sciences, 38*.

Kaden, R., & Kolbe, T. (2014). Simulation-Based Total Energy Demand Estimation of Buildings using Semantic 3D City Models. *International Journal of 3-D Information Modeling, 3*, 35–53. https://doi.org/10.4018/ij3dim.2014040103

Kammen, D. M., & Sunter, D. A. (2016). City-integrated renewable energy for urban sustainability. *Science*, *352*(6288), 922–928. https://doi.org/10.1126/science.aad9302

Kang, J. (2000). Sound propagation in street canyons: Comparison between diffusely and geometrically reflecting boundaries. *Journal of the Acoustical Society of America*, *107*(3), 1394–1404.

Kar, R., Obi Reddy, G. P., Kumar, N., & Singh, S. K. (2018). Monitoring spatio-temporal dynamics of urban and peri-urban landscape using remote sensing and GIS – A case study from Central India. *The Egyptian Journal of Remote Sensing and Space Science*, *21*(3), 401–411. https://doi.org/https://doi.org/10.1016/j.ejrs.2017.12.006

Kawulok, M., Benecki, P., Piechaczek, S., Hrynczenko, K., Kostrzewa, D., & Nalepa, J. (2019). Deep Learning for Multiple-Image Super-Resolution. *IEEE Geoscience and Remote Sensing Letters.* PP. 1-5. 10.1109/LGRS.2019.2940483.

Keivani, R. (2010). A review of the main challenges to urban sustainability. *International Journal of Urban Sustainable Development*, *1*(1–2), 5–16. https://doi.org/10.1080/19463131003704213

Khalid, N. ~F., Din, A. ~H. ~M., Omar, K. ~M., Khanan, M. ~F. ~A., Omar, A. ~H., Hamid, A. ~I. ~A., & Pa'suya, M. ~F. (2016). Open-Source Digital Elevation Model (DEMs) Evaluation with GPS and LiDAR Data. *ISPRS - International Archives of the Photogrammetry, Remote Sensing and Spatial Information Sciences*, *62W1*, 299–306. https://doi.org/10.5194/isprs-archives-XLII-4-W1-299-2016

Kharrazi, A., Qin, H., & Zhang, Y. (2016). Urban Big Data and Sustainable Development Goals: Challenges and Opportunities. In *Sustainability* (Vol. 8, Issue 12). https://doi.org/10.3390/su8121293

Klopp, J., & Petretta, D. (2017). The urban sustainable development goal: Indicators, complexity and the politics of measuring cities. *Cities*, *63*, 92–97. https://doi.org/10.1016/j.cities.2016.12.019

Knerr, T. (2013). *Merging Elevation Raster Data and OpenStreetMap Vectors for 3D Rendering*. *May*, 67. http://tobias-knerr.de/publications/thesis/Master Thesis Knerr.pdf

Koch, F., Kabisch, S., & Krellenberg, K. (2017). A Transformative Turn towards Sustainability in the Context of Urban-Related Studies? A Systematic Review from 1957 to 2016. *Sustainability*, *10*, 58. https://doi.org/10.3390/su10010058

Kolbe, T. H. (2009). Representing and exchanging 3D city models with CityGML. In J. Zlatanova, S., Lee (Ed.), *3D Geo-Information Sciences* (pp. 15–31). Springer Berlin Heidelberg.

Krauß, T., Schneider, M., & Reinartz, P. (2009). Orthorectification and DSM generation with ALOS-Prism data in urban areas. *International Geoscience and Remote Sensing Symposium (IGARSS)*, *5*, 2–5. https://doi.org/10.1109/IGARSS.2009.5417739

Kuddus, M. A., Tynan, E., & McBryde, E. (2020). Urbanization: a problem for the rich and the poor? *Public Health Reviews*, *41*(1), 1. https://doi.org/10.1186/s40985-019-0116-0

Kunze, C., & Hecht, R. (2015). Semantic enrichment of building data with volunteered geographic information to improve mappings of dwelling units and population. *Computers, Environment and Urban Systems*, *53*. https://doi.org/10.1016/j.compenvurbsys.2015.04.002

Labetski, A. ., Ledoux, H. ., & Stoter, J. (2017). Generalising 3D Buildings from LoD2 to LoD1. In Proceedings of the GISRUK. *25th GIS Research UK Conference*, 18–21.

Labib, S. M., & Harris, A. (2018). The potentials of Sentinel-2 and LandSat-8 data in green infrastructure extraction, using object based image analysis (OBIA) method. *European Journal of Remote Sensing*, *51*(1), 231–240. https://doi.org/10.1080/22797254.2017.1419441

Latty, R. S., Nelson, R., Markham, B., Williams, D., & Toll, D. (1985). Performance comparisons between information extraction techniques using variable spatial resolution data. *Photogrammetric Engineering and Remote Sensing*, *51*.

LeCun, Y., Bengio, Y., & Hinton, G. (2015) Deep Learning. *Nature*, 521, 436–444.

Ledoux, H. (2018). val3dity: validation of 3D GIS primitives according to the international standards. *Open Geospatial Data, Software and Standards*, *3*. https://doi.org/10.1186/s40965-018-0043-x

Ledoux, H., & Meijers, M. (2011). Topologically consistent 3D city models obtained by extrusion. *International Journal of Geographical Information Science*, *25*, 557–574. https://doi.org/10.1080/13658811003623277

LeGates, R., Tate, N., & Kingston, R. (2009). Spatial thinking and scientific urban planning. *Environment and Planning B: Planning and Design*, *36*, 763–768. https://doi.org/10.1068/b3605com

Li, M., Zang, S., Zhang, B., Li, S., & Wu, C. (2017). *A Review of Remote Sensing Image Classification Techniques : the Role of Spatio*-contextual Information *A Review of Remote Sensing Image Classification Techniques : the Role of Spatio-contextual Information*. *7254*. https://doi.org/10.5721/EuJRS20144723

Li, X., Gong, P., & Liang, L. (2015). A 30-year (1984–2013) record of annual urban dynamics of Beijing City derived from Landsat data. *Remote Sensing of Environment*, *166*, 78–90.

https://doi.org/https://doi.org/10.1016/j.rse.2015.06.007

Li, Z., Zhang, Z., & Davey, K. (2015). Estimating Geographical PV Potential Using LiDAR Data for Buildings in Downtown San Francisco. *Transactions in GIS, 19*. https://doi.org/10.1111/tgis.12140

Liang, J., Gong, J., Liu, J., Zou, Y., Zhang, J., Sun, J., & Chen, S. (2016). Generating orthorectified multi-perspective 2.5D Maps to FacilitateWeb GIS-Based visualization and exploitation of massive 3D city models. *ISPRS International Journal of Geo-Information*, *5*(11), 1–18. https://doi.org/10.3390/ijgi5110212

Lin, C., Wu, C.C., Tsogt, K., Ouyang, Y.C., & Chang, C.I. (2015) Effects of atmospheric correction and pansharpening on LULC classification accuracy using WorldView-2 imagery. *Inf. Process. Agric*. 2, 25–36.

Lin, G., Milan, A., Shen, C., & Reid, I. (2016) RefineNet: Multi-Path Refinement Networks for High-Resolution Semantic Segmentation. arXiv, arXiv:1611.06612.

Liu, W., Yang, M., Xie, M., Guo, Z., Li, E., Zhang, L., Pei, T., & Wang, D. (2019). Accurate Building Extraction from Fused DSM and UAV Images Using a Chain Fully Convolutional Neural Network. In *Remote Sensing* (Vol. 11, Issue 24). https://doi.org/10.3390/rs11242912

Lwin, K., & Murayama, Y. (2009). A GIS Approach to Estimation of Building Population for Micro-spatial Analysis. *Transactions in GIS*, *13*(4), 401–414. https://doi.org/https://doi.org/10.1111/j.1467-9671.2009.01171.x

Mahabir, R., Stefanidis, A., Croitoru, A., Crooks, A. T., & Agouris, P. (2017). Authoritative and volunteered geographical information in a developing country: A comparative case study of road datasets in Nairobi, Kenya. *ISPRS International Journal of Geo-Information*, *6*(1). https://doi.org/10.3390/ijgi6010024

Maktav, D., Erbek, F. S., & Jürgens, C. (2006). Remote sensing of urban areas. *International Journal of Remote Sensing*, *26*(4), 655–659. https://doi.org/10.1080/01431160512331316469

Malarvizhi, K., Kumar, S. V., & Porchelvan, P. (2016). Use of High Resolution Google Earth Satellite Imagery in Landuse Map Preparation for Urban Related Applications. *Procedia Technology*, *24*, 1835–1842. https://doi.org/10.1016/j.protcy.2016.05.231

Manley, E., & Dennett, A. (2019). New Forms of Data for Understanding Urban Activity in Developing Countries. *Applied Spatial Analysis and Policy*, *12*(1), 45–70. https://doi.org/10.1007/s12061-018-9264-8

Manonmani, R., Prabaharan, S., Vidhya, R., & Ramalingam, M. (2012). Application of GIS in urban utility mapping using image processing techniques. *Geo-Spatial*

Information Science, *15*(4), 271–275. https://doi.org/10.1080/10095020.2012.714660

Mao, B., Ban, Y., Harrie, L., & Lund, S.-. (2009). a Framework for Generalization of 3D City Models Based on Citygml and X3D. *WG II/2, II/3, II/4 Workshop on Quality, Scale and Analysis Aspects of City Models*, *XXXVIII*, 9. http://www.isprs.org/proceedings/XXXVIII/2-W11/Mao_Ban_Harrie.pdf

Masek, J., Vermote, E., Saleous, N., Wolfe, R., Hall, F., Huemmrich, K., Gao, F., Kutler, J., & Lim, T.-K. (2006). A Landsat Surface Reflectance Data Set for North America, 1990–2000. *Geoscience and Remote Sensing Letters, IEEE*, *3*, 68–72. https://doi.org/10.1109/LGRS.2005.857030

Masson, V., Marchadier, C., Adolphe, L., Aguejdad, R., Avner, P., Bonhomme, M., Bretagne, G., Briottet, X., Bueno, B., de Munck, C., Doukari, O., Hallegatte, S., Hidalgo, J., Houet, T., Le Bras, J., Lemonsu, A., Long, N., Moine, M.-P., Morel, T., … Zibouche, K. (2014). Adapting cities to climate change: A systemic modelling approach. *Urban Climate*, *10*, 407–429. https://doi.org/https://doi.org/10.1016/j.uclim.2014.03.004

Mcgranahan, G., & Satterthwaite, D. (2014). Urbanisation concepts and trends. *International Institute for Environment and Development*, *June*, 1–27.

McPhearson, T., Pickett, S. T. A., Grimm, N. B., Niemelä, J., Alberti, M., Elmqvist, T., Weber, C., Haase, D., Breuste, J., & Qureshi, S. (2016). Advancing Urban Ecology toward a Science of Cities. *BioScience*, *66*(3), 198–212. https://doi.org/10.1093/biosci/biw002

Mehlhorn, K., & Sanders, P. (2007). *Algorithms and Data Structures The Basic Toolbox*. Springer Berlin Heidelberg.

Meilland, M., Comport, A. I., Rives, P., Meilland, M., Comport, A. I., Rives, P., & Rives, P. (2015). Dense omnidirectional RGB-D mapping of large scale outdoor environments for real-time localisation and autonomous navigation To cite this version : HAL Id : hal-01010429 Dense omnidirectional RGB-D mapping of large scale outdoor environments for real-time. *Journal of Field Robotics*, *32*(4), .474-503. https://doi.org/10.1002/rob.21531

Meschede, C., & Siebenlist, T. (2019). *Open Urban Data and the Sustainable Development Goals*. https://doi.org/10.1145/3325112.3325269

Michelin, J. C., Tierny, J., Tupin, F., Mallet, C., & Paparoditis, N. (2013). Quality evaluation of 3D city building models with automatic error diagnosis. *International Archives of the Photogrammetry, Remote Sensing and Spatial Information Sciences - ISPRS Archives*, *40*(7W2), 161–166. https://doi.org/10.5194/isprsarchives-XL-7-W2-161-2013

MicroImages. (2016). *TNTgis - Advanced Software for Geospatial Analysis*. www.microimages.com

Misra, P., Avtar, R., & Takeuchi, W. (2018). Comparison of Digital Building Height Models Extracted from AW3D, TanDEM-X, ASTER, and SRTM Digital Surface Models over Yangon City. In *Remote Sensing* (Vol. 10, Issue 12). https://doi.org/10.3390/rs10122008

Mittal, A. (2019). *Applications of 3D City Modelling*. https://skymapglobal.com/applications-of-%0A3d-city-modelling/

Mooney, P., & Corcoran, P. (2013). Analysis of Interaction and Co-editing Patterns amongst OpenStreetMap Contributors. *Transactions in GIS*, *18*. https://doi.org/10.1111/tgis.12051

Morais, P. (2016). Centring space: the possibility of planning in urban community (shequ) construction in Shanghai. *In Carola Hein (Ed.) International Planning History Society Proceedings, 17th IPHS Conference, History-Urbanism-Resilience, TU Delft*, 151. https://doi.org/http://dx.doi.org/10.7480/iphs.2016.7.1343

Mori, K., & Yamashita, T. (2015). Methodological framework of sustainability assessment in City Sustainability Index (CSI): A concept of constraint and maximisation indicators. *Habitat International*, *45*, 10–14. https://doi.org/https://doi.org/10.1016/j.habitatint.2014.06.013

Mori, K., Fujii, T., Yamashita, T., Mimura, Y., Uchiyama, Y., & Hayashi, K. (2015). Visualization of a City Sustainability Index (CSI): Towards transdisciplinary approaches involving multiple stakeholders. *Sustainability (Switzerland)*, *7*(9), 12402–12424. https://doi.org/10.3390/su70912402

Murshed, S. M., Picard, S., & Koch, A. (2018). Modelling, validation and quantification of climate and other sensitivities of building energy model on 3D city models †. *ISPRS International Journal of Geo-Information*, *7*(11), 1–22. https://doi.org/10.3390/ijgi7110447

Nasiri, A., Ali Abbaspour, R., Chehreghan, A., & Jokar Arsanjani, J. (2018). Improving the Quality of Citizen Contributed Geodata through Their Historical Contributions: The Case of the Road Network in OpenStreetMap. In *ISPRS International Journal of Geo-Information* (Vol. 7, Issue 7). https://doi.org/10.3390/ijgi7070253

Nebiker, S., Bleisch, S., & Christen, M. (2010). Rich point clouds in virtual globes - A new paradigm in city modeling? *Computers Environment and Urban Systems*, *34*, 508–517. https://doi.org/10.1016/j.compenvurbsys.2010.05.002

Nebiker, S., Cavegn, S., & Loesch, B. (2015). Cloud-Based Geospatial 3D Image Spaces—A Powerful Urban Model for the Smart City. In *ISPRS International Journal of Geo-Information* (Vol. 4, Issue 4). https://doi.org/10.3390/ijgi4042267

Neis, P., & Zielstra, D. (2014). Recent Developments and Future Trends in

Volunteered Geographic Information Research: The Case of OpenStreetMap. *Future Internet*, *6*(1), 76–106. https://doi.org/10.3390/fi6010076

Neis, P., Zielstra, D., & Zipf, A. (2012). The Street Network Evolution of Crowdsourced Maps: OpenStreetMap in Germany 2007–2011. *Future Internet*, *4*(1), 1–21. https://doi.org/10.3390/fi4010001

Neuenschwander, A., Popescu, S., Nelson, R., Harding, D., Pitts, K., Robbins, J., Pederson, D., Sheridan, R., & Neuenschwander, A. (2018). Ice, cloud, and land elevation satellite (ICESat-2) algorithm theoretical basis document (ATBD) for land—Vegetation along-track products (ATL08). *In National Aeronautics and Space Administration. Goddard Space Flight Centre, NASA, Washington D.C., June*.

Nghiem, S. ., Balk, D. ., Small, C. ., Deichmann, U. ., Wannebo, A. ., Blom, R. ., Sutton, P. ., Yetman, G. ., Chen, R. ., & Rodriguez, E. (2001). *Global infrastructure: The potential of SRTM data to break new ground. White Paper; NASA-JPL and CIESIN*.

Nour, A. M. (2011). The Potential of GIS Tools in Strategic Urban Planning Process; as an Approach for Sustainable Development in Egypt. *Journal of Sustainable Development*, *4*(1), 284–298. https://doi.org/10.5539/jsd.v4n1p284

Novelli, A., Aguilar, M. A., Nemmaoui, A., Aguilar, F. J., & Tarantino, E. (2016). Performance evaluation of object based greenhouse detection from Sentinel-2 MSI and Landsat 8 OLI data: A case study from Almería (Spain). *International Journal of Applied Earth Observation and Geoinformation*, *52*, 403–411. https://doi.org/https://doi.org/10.1016/j.jag.2016.07.011

Oehmcke, S., Thrysøe, C., Borgstad, A., Antonio, M., Salles, V., & Gieseke, F. (2019). Detecting Hardly Visible Roads in Low-Resolution Satellite Time Series Data. *IEEE International Conference on Big Data*.

Ogryzek, M., Adamska-Kmieć, D., & Klimach, A. (2020). Sustainable transport: An efficient transportation network-case study. *Sustainability (Switzerland)*, *12*(19), 1–14. https://doi.org/10.3390/su12198274

Ohori, K. A., Ledoux, H., Biljecki, F., & Stoter, J. (2015). Modeling a 3D City Model and Its Levels of Detail as a True 4D Model. In *ISPRS International Journal of Geo-Information* (Vol. 4, Issue 3). https://doi.org/10.3390/ijgi4031055

Olofsson, P., Foody, G. M., Herold, M., Stehman, S. V., Woodcock, C. E., & Wulder, M. A. (2014). Good practices for estimating area and assessing accuracy of land change. *Remote Sensing of Environment*, *148*, 42–57. https://doi.org/10.1016/j.rse.2014.02.015

ONS Mid-year Population Estimates. Available online: https://www.ons.gov.uk/peoplepopulationandcommunity/populationandmigratio n/populationestimates/datasets/populationestimatesforukenglandandwalesscotlandandnorthernireland (accessed on 5 January 2019).

Oosterom, P. Van. (2013). Computers , Environment and Urban Systems Research and development in 3D cadastres. *COMPUTERS, ENVIRONMENT AND URBAN SYSTEMS*, 1–6. https://doi.org/10.1016/j.compenvurbsys.2013.01.002

OpenStreetMap Data Extracts. Available online: https://download.geofabrik.de/ (accessed on 26 June 2019).

OpenTopography: High-Resolution Topography Data and Tools. Available online: https://opentopography.org/about (accessed on 26 June 2019).

Ordnance Survey. OS MasterMap Topography Layer—Building Height Attribute v1.1. Available online: https://www.ordnancesurvey.co.uk/documents/building-height-attribute-getting-started-guide.pdf (accessed on 26 June 2019).

OS MasterMap Imagery Layer. Available online: https://www.ordnancesurvey.co.uk/business-andgovernment/products/imagery-layer.html (accessed on 26 June 2019).

Over, M., Schilling, A., Neubauer, S., & Zipf, A. (2010). Generating web-based 3D City Models from OpenStreetMap: The current situation in Germany. *Computers, Environment and Urban Systems*, *34*(6), 496–507. https://doi.org/https://doi.org/10.1016/j.compenvurbsys.2010.05.001

Park, J., & Yang, B. (2020). *GIS-Enabled Digital Twin System for Sustainable Evaluation of Carbon Emissions : A Case Study of Jeonju City , South Korea*.

Park, S. C., Park, M. K., & Kang, M. G. (2003) Super-resolution image reconstruction: a technical overview, *IEEE Signal Processing Magazine*, vol. 20, no. 3, pp. 21–36

Peleg, T., & Elad, M. (2014). A statistical prediction model based on sparse representations for single image super-resolution. *IEEE Transactions on Image Processing : A Publication of the IEEE Signal Processing Society*, *23*(6), 2569–2582. https://doi.org/10.1109/TIP.2014.2305844

Pesaresi, M., Corbane, C., Julea, A., Florczyk, A. J., Syrris, V., & Soille, P. (2016). Assessment of the added-value of sentinel-2 for detecting built-up areas. *Remote Sensing*, *8*(4). https://doi.org/10.3390/rs8040299

Phiri, D., & Morgenroth, J. (2017). Developments in Landsat land cover classification methods: A review. *Remote Sensing*, *9*(9). https://doi.org/10.3390/rs9090967

Phiri, D., Simwanda, M., Salekin, S., Nyirenda, V. R., Murayama, Y., & Ranagalage, M. (2020). Sentinel-2 Data for Land Cover/Use Mapping: A Review. In *Remote Sensing* (Vol. 12, Issue 14). https://doi.org/10.3390/rs12142291

Planet. (2020). *Planet, KSAT and Airbus Awarded First-Ever Global Contract to*

Combat Deforestation. https://www.planet.com/pulse/planet-ksat-and-airbus-awarded-first-ever-global-contract-to-combat-deforestation/

Pojani, D., & Stead, D. (2015). *Sustainable Urban Transport in the Developing World: Beyond Megacities*. *2*, 7784–7805. https://doi.org/10.3390/su7067784

Quartulli, M. ., & Datcu, M. (2003). Information fusion for scene understanding from interferometric SAR data in urban environments. *IEEE Transactions on Geosci. Remote Sensing*, *41*, 1976–1985.

Rahman, M. A. U. (2016). Urban sustainability through strategic planning: A case of metropolitan planning in Khulna city, Bangladesh. *Journal of Urban Management*, *5*(1), 16–22. https://doi.org/https://doi.org/10.1016/j.jum.2016.06.001

Rai, P., & Kumra, K. V. (2011). Role of Geoinformatics in Urban Planning. *Journal of Scientific Research*, *55*, 11–24.

Rajpriya, N. R., Vyas, A., & Sharma, S. A. (2014). Generation of 3D Model for Urban area using Ikonos and Cartosat-1 Satellite Imageries with RS and GIS Techniques. *The International Archives of the Photogrammetry, Remote Sensing and Spatial Information Sciences*, *XL–8*, 899–906. https://doi.org/10.5194/isprsarchives-XL-8-899-2014

Rasoolimanesh, S. M., Roldán, J., Jaafar, M., & Ramayah, T. (2016). Factors Influencing Residents' Perceptions toward Tourism Development; Differences across Rural and Urban World Heritage Sites. *Journal of Travel Research*, *56*. https://doi.org/10.1177/0047287516662354

Rautenbach, V., Bevis, Y., Coetzee, S., & Combrinck, C. (2015). Evaluating procedural modelling for 3D models of informal settlements in urban design activities. *South African Journal of Science*, *Volume 111*. https://doi.org/10.17159/sajs.2015/20150100

Richards, J. A. (2012). *Remote Sensing. Digital Image Analysis. An Introduction*. Springer.

Ritchie, H., & Roser, M. (2018). Urbanization. *Our World in Data*. https://ourworldindata.org/urbanization

Robinson, D. (2006). Urban morphology and indicators of radiation availability. *International Journal of Solar Energy*, *80*(12), 1643–1648.

Rosser, J., Long, G., Zakhary, S., Boyd, D., Mao, Y., & Robinson, D. (2019). Modelling Urban Housing Stocks for Building Energy Simulation using CityGML EnergyADE. *ISPRS International Journal of Geo-Information*, *8*, 163. https://doi.org/10.3390/ijgi8040163

Roy, A. (2009). The 21st-Century Metropolis: New Geographies of Theory. *Regional Studies*, *43*(6), 819–830. https://doi.org/10.1080/00343400701809665

Ruhé, M., Thamm, H.-P., Fornauf, L., & Lorbacher, M. R. (2013). GIS Based Urban Design for Sustainable Transport and Sustainable Growth for Two-Wheeler Related Mega Cities like HANOI. In B. Murgante, S. Misra, M. Carlini, C. M. Torre, H.-Q. Nguyen, D. Taniar, B. O. Apduhan, & O. Gervasi (Eds.), *Computational Science and Its Applications -- ICCSA 2013* (pp. 452–465). Springer Berlin Heidelberg.

Rumpler, M., Irschara, A., Wendel, A., & Bischof, H. (2012). Rapid 3D City Model Approximation from Publicly Available Geographic Data Sources and Georeferenced Aerial Images. *17th Computer Vision Winter Workshop Matej Kristan, Rok Mandeljc, Luka Cehovin (Eds.), Lod 2*.

Rwanga, S. S., & Ndambuki, J. M. (2017). Accuracy Assessment of Land Use/Land Cover Classification Using Remote Sensing and GIS. *International Journal of Geosciences, 08*(04), 611–622. https://doi.org/10.4236/ijg.2017.84033

Santillan, J. R., Makinano-Santillan, M., & Makinano, R. M. (2016). *VERTICAL ACCURACY ASSESSMENT OF ALOS WORLD 3D – 30M DIGITAL ELEVATION MODEL OVER NORTHEASTERN MINDANAO , PHILIPPINES Jojene R . Santillan , Meriam Makinano-Santillan , Ronald M . Makinano CSU Phil-LiDAR 1 Project , College of Engineering and Information T*. 5374–5377.

Schneider, S., Hollmuller, P., Le Strat, P., Khoury, J., Patel, M., & Lachal, B. (2017). Spatial–Temporal Analysis of the Heat and Electricity Demand of the Swiss Building Stock. *Frontiers in Built Environment, 3*, 53. https://doi.org/10.3389/fbuil.2017.00053

Schneiderbauer, S., & Ehrlich, D. (2005). *Risk Assessments – People's Vulnerability to Natural Hazards* (pp. 81–82).

Schumann, G. J.-P., & Bates, P. D. (2018). The Need for a High-Accuracy, Open-Access Global DEM. *Frontiers in Earth Science, 6*, 225. https://doi.org/10.3389/feart.2018.00225

See, L., Comber, A., Salk, C., Fritz, S., van der Velde, M., Perger, C., Schill, C., McCallum, I., Kraxner, F., & Obersteiner, M. (2013). Comparing the Quality of Crowdsourced Data Contributed by Expert and Non-Experts. *PLOS ONE, 8*(7), e69958. https://doi.org/10.1371/journal.pone.0069958

See, L., Mooney, P., Foody, G., Bastin, L., Comber, A., Estima, J., Fritz, S., Kerle, N., Jiang, B., Laakso, M., Liu, H. Y., Milèinski, G., Nikšieč, M., Painho, M., Podör, A., Olteanu-Raimond, A. M. R., & Rutzinger, M. (2016). Crowdsourcing, citizen science or volunteered geographic information? The current state of crowdsourced geographic information. *ISPRS International Journal of Geo-Information, 5*(5). https://doi.org/10.3390/ijgi5050055

Sefercik, U. G., Karakis, S., Bayik, C., Alkan, M., & Yastikli, N. (2014). Contribution of normalized DSM to automatic building extraction from HR mono optical satellite imagery. *European Journal of Remote Sensing*, *47*(1), 575–591. https://doi.org/10.5721/EuJRS20144732

Senaratne, H., Mobasheri, A., Ali, A. L., Capineri, C., & Haklay, M. (Muki). (2017). A review of volunteered geographic information quality assessment methods. *International Journal of Geographical Information Science*, *31*(1), 139–167. https://doi.org/10.1080/13658816.2016.1189556

Senaratne, H., Mobasheri, A., Ali, A., Cristina, C., & Haklay, M. (2016). A review of volunteered geographic information quality assessment methods. *International Journal of Geographical Information Science*, *31*. https://doi.org/10.1080/13658816.2016.1189556

Seto, K. C., Golden, J. S., Alberti, M., & Turner, B. L. (2017). Sustainability in an urbanizing planet. *Proceedings of the National Academy of Sciences of the United States of America*, *114*(34), 8935–8938. https://doi.org/10.1073/pnas.1606037114

Seto, K., Golden, J. S., Alberti, M., & Turner, B. L. (2017). Sustainability in an urbanizing planet. *Proceedings of the National Academy of Sciences of the United States of America*, *114*(34), 8935–8938. https://doi.org/10.1073/pnas.1606037114

Seto, K., Parnell, S., & Elmqvist, T. (2013). A Global Outlook on Urbanization. *Urbanization, Biodiversity and Ecosystem Services: Challenges and Opportunities*, 1–12. https://doi.org/10.1007/978-94-007-7088-1_1

Shaloni, Dixit, M., Agarwal, S., & Gupta, P. (2020). Building Extraction from Remote Sensing Images: A Survey. *2020 2nd International Conference on Advances in Computing, Communication Control and Networking (ICACCCN)*, 966–971. https://doi.org/10.1109/ICACCCN51052.2020.9362894

Shi, L., Foody, G. M., Boyd, D. S., Girindran, R., Wang, L., Du, Y., & Ling, F. (2020). Night-time lights are more strongly related to urban building volume than to urban area. *Remote Sensing Letters*, *11*(1), 29–36. https://doi.org/10.1080/2150704X.2019.1682709

Singh, S. P., Jain, K., & Mandla, V. R. (2013). Virtual 3D city modeling: Techniques and Applications. *International Archives of the Photogrammetry, Remote Sensing and Spatial Information Sciences - ISPRS Archives*, *XL-2/W2*(November), 73–91. https://doi.org/10.5194/isprsarchives-XL-2-W2-73-2013

Soma, K., Dijkshoorn-Dekker, M. W. C., & Polman, N. B. P. (2018). Stakeholder contributions through transitions towards urban sustainability. *Sustainable Cities and Society*, *37*, 438–450. https://doi.org/https://doi.org/10.1016/j.scs.2017.10.003

Song, S., Liu, J., Pu, H., Liu, Y., & Luo, J. (2019). The comparison of fusion methods for HSRRSI considering the effectiveness of land cover (Features) object recognition based on deep learning. *Remote Sensing*, *11*(12). https://doi.org/10.3390/rs11121435

Sousa, G., Jones, B., Mirzaei, P., & Robinson, D. (2018). An open-source simulation platform to support the formulation of housing stock decarbonisation strategies. *Energy and Buildings*, *172*, 459–477. https://doi.org/10.1016/j.enbuild.2018.05.015

Stilla, U., & Jurkiewicz, K. (1999). *Reconstruction of Building Models from Maps and Laser Altimeter Data* (pp. 34–46). https://doi.org/10.1007/3-540-46621-5_3

Stock, K., & Guesgen, H. (2016). *Chapter 10 - Geospatial Reasoning With Open Data* (R. Layton & P. A. B. T.-A. O. S. I. Watters (eds.); pp. 171–204). Syngress. https://doi.org/https://doi.org/10.1016/B978-0-12-802916-9.00010-5

Stoter, J., & Zlatanova, S. (2009). 3D GIS, where are we standing? *ISPRS Joint Workshop on "Spatial, Temporal and Multi-Dimensional Data Modelling and Analysis", Québec, October, 2003*.

Stoter, J., Vosselman, G., Dahmen, C., Oude Elberink, S., & Ledoux, H. (2014). CityGML Implementation Specifications for a Countrywide 3D Data Set: The Case of The Netherlands. *Photogrammetric Engineering & Remote Sensing*, *80*, 1069–1077. https://doi.org/10.14358/PERS.80.11.1069

Strzalka, A., Alam, N., Duminil, E., Coors, V., & Eicker, U. (2012). Large scale integration of photovoltaics in cities. *Applied Energy*, *93*. https://doi.org/10.1016/j.apenergy.2011.12.033

Sun, Yaqin, Tian, S., & Di, B. (2017). Extracting mineral alteration information using WorldView-3 data. *Geoscience Frontiers*, *8*(5), 1051–1062. https://doi.org/10.1016/j.gsf.2016.10.008

Sun, Yeran, & Du, Y. (2017). Big data and sustainable cities: applications of new and emerging forms of geospatial data in urban studies. *Open Geospatial Data, Software and Standards*, *2*(1), 24. https://doi.org/10.1186/s40965-017-0037-0

Sun, Z., Zhao, X., Wu, M., & Wang, C. (2019). Extracting Urban Impervious Surface from WorldView-2 and Airborne LiDAR Data Using 3D Convolutional Neural Networks. *Journal of the Indian Society of Remote Sensing*, *47*(3), 401–412. https://doi.org/10.1007/s12524-018-0917-5

Sztubecka, M., Skiba, M., Mrówczynska, M., & Bazan-Krzywoszanska, A. (2020). An innovative decision support system to improve the energy efficiency of buildings in urban areas. *Remote Sensing*, *12*(2). https://doi.org/10.3390/rs12020259

Tachikawa, T., Kaku, M., Iwasaki, A., Gesch, D., Oimoen, M., Zhang, Z., Danielson, J., Krieger, T., Curtis, B., & Haase, J. (2011). ASTER Global Digital Elevation

Model Version 2 – Summary of validation results. In *Report to the ASTER GDEM Version 2 Validation Team*.

Tadono, T., Ishida, H., Oda, F., Naito, S., Minakawa, K., & Iwamoto, H. (2014). Precise Global DEM Generation by ALOS PRISM. *ISPRS Annals of Photogrammetry, Remote Sensing and Spatial Information Sciences*, *II–4*(May), 71–76. https://doi.org/10.5194/isprsannals-ii-4-71-2014

Tadono, T., Nagai, H., Ishida, H., Oda, F., Naito, S., Minakawa, K., & Iwamoto, H. (2016). Generation of the 30 M-MESH global digital surface model by alos prism. *International Archives of the Photogrammetry, Remote Sensing and Spatial Information Sciences - ISPRS Archives*, *41*(July), 157–162. https://doi.org/10.5194/isprsarchives-XLI-B4-157-2016

Takaku, J., & Tadono, T. (2009). High resolution DSM generation from ALOS PRISM — Status updates on over three year operations. *2009 IEEE International Geoscience and Remote Sensing Symposium*, *3*, III-769-III–772. https://doi.org/10.1109/IGARSS.2009.5417878

Tan, Q., & Wang, J. (2007). HYPERSPECTRAL VERSUS MULTISPECTRAL SATELLITE DATA FOR URBAN LAND COVER AND LAND USE MAPPING — BEIJING , AN EVOLVING CITY. *ASPRS 2007 Annual Conference*.

Tao, W. (2013). Interdisciplinary urban GIS for smart cities: advancements and opportunities. *Geo-Spatial Information Science*, *16*(1), 25–34. https://doi.org/10.1080/10095020.2013.774108

Tara O'Shea, Planet, KSAT and Airbus Awarded First-Ever Global Contract to Combat Deforestation. Available at: https://www.planet.com/pulse/planet-ksat-and-airbus-awarded-first-ever-global-contract-to-combat-deforestation/, Accessed on 28 March 2021

The European Space Agency. (2014). *The Sentinel missions*. http://www.esa.int/Applications/Observing_the_Earth/Copernicus/Overview4, Accessed on 15th February 2019

Tian, J., Schneider, T., Straub, C., Kugler, F., & Reinartz, P. (2017). Exploring digital surface models from nine different sensors for forest monitoring and change detection. *Remote Sensing*, *9*(3). https://doi.org/10.3390/rs9030287

Tian, Y., Zhou, Q., Fu, X., Tian, Y., Zhou, Q., & Fu, X. (2019). An Analysis of the Evolution, Completeness and Spatial Patterns of OpenStreetMap Building Data in China. *ISPRS International Journal of Geo-Information*, *8*(1), 35. https://doi.org/10.3390/ijgi8010035

Tomljenovic, I., Tiede, D., & Blaschke, T. (2016). A building extraction approach for Airborne Laser Scanner data utilizing the Object Based Image Analysis paradigm. *International Journal of Applied Earth Observation and*

Geoinformation, *52*, 137–148. https://doi.org/https://doi.org/10.1016/j.jag.2016.06.007

Top 6 Free LiDAR Data Sources. Available online: https://gisgeography.com/top-6-free-lidar-data-sources/ (accessed on 19 January 2019).

Toschi, I., Nocerino, E., Remondino, F., Revolti, A., Soria, G., & Piffer, S. (2017). Geospatial data processing for 3D City Model generation, management and visualization. *ISPRS - International Archives of the Photogrammetry, Remote Sensing and Spatial Information Sciences*, *XLII-1/W1*, 527–534. https://doi.org/10.5194/isprs-archives-XLII-1-W1-527-2017

Transition Cities, Available at: https://www.climate-kic.org/projects/transition-cities/, Accessed on 30 September 2021

Tutschku, K. (1997). Demand-based Radio Network Planning of Cellular Communication Systems. *University of Würzburg - Research Report*.

Ujang, U., Anton, F., Ariffin, A., Mioc, D., & Azri, S. (2015). An Amalgamation of 3D City Models in Urban Air Quality Modeling for Improving Visual Impact Analysis. In *WIT Transactions on Ecology and the Environment* (Vol. 198). https://doi.org/10.2495/AIR150051

UN Department of Economic and Social Affairs. (n.d.). *The 17 Goals*. Retrieved May 28, 2019, from https://sdgs.un.org/goals

UN-HABITAT. (2009). *Planning Sustainable Cities — Global Report on Human Settlements 2009*.

Un-Habitat. (n.d.). Planning Sustainable Cities. *Planning Sustainable Cities*. https://doi.org/10.4324/9781315541389

United Nations (2015) Transforming our world: The 2030 Agenda for sustainable development. https://undocs.org/A/RES/70/1, Accessed on 23 July 2021

United Nations. (2019). World population prospects 2019: Highlights (ST/ESA/SER.A/423). In *Department of Economic and Social Affairs. World Population Prospects 2019.* (Issue 141). http://www.ncbi.nlm.nih.gov/pubmed/12283219

Upadhyay, S., & Sharma, M. (2014). A review on configurations, control and sizing methodologies of hybrid energy systems. *Renewable and Sustainable Energy Reviews*, *38*, 47–63. https://doi.org/10.1016/j.rser.2014.05.057

Using OS MasterMap®Building Height Attribute (BHA) Alpha Release. Available online: https://digimap.edina.ac.uk/webhelp/digimapgis/bha/bha.htm (accessed on 26 June 2019).

Vakalopoulou, M., Karantzalos, K., Komodakis, N., Vakalopoulou, M., Karantzalos, K., Komodakis, N., & Building, N. P. (2015). Building detection in very high resolution multispectral data with deep learning features To cite this version : HAL Id : hal-01264084. *IEEE International Geoscience and Remote Sensing Symposium (IGARSS)*, 1873–1876. https://doi.org/0.1109/IGARSS.2015.7326158

Valencia, S. C., Simon, D., Croese, S., Nordqvist, J., Oloko, M., Sharma, T., Taylor Buck, N., & Versace, I. (2019). Adapting the Sustainable Development Goals and the New Urban Agenda to the city level: Initial reflections from a comparative research project. *International Journal of Urban Sustainable Development*, *11*(1), 4–23. https://doi.org/10.1080/19463138.2019.1573172

Vandecasteele, A., & Devillers, R. (2013). Improving Volunteered Geographic Data Quality Using Semantic Similarity Measurements. *ISPRS - International Archives of the Photogrammetry, Remote Sensing and Spatial Information Sciences*, *XL-2/W1*(June), 143–148. https://doi.org/10.5194/isprsarchives-xl-2-w1-143-2013

Vanden Bergh, B. G., Lee, M., Quilliam, E. T., & Hove, T. (2011). The multidimensional nature and brand impact of user-generated ad parodies in social media. *International Journal of Advertising*, *30*(1), 103–131. https://doi.org/10.2501/IJA-30-1-103-131

Varduhn, V., Mundani, R.-P., & Rank, E. (2015). *Multi-resolution Models: Recent Progress in Coupling 3D Geometry to Environmental Numerical Simulation* (pp. 55–69). https://doi.org/10.1007/978-3-319-12181-9_4

Verrucci, E., Perez-Fuentes, G., Rossetto, T., Bisby, L., Haklay, M., Rush, D., Rickles, P., Fagg, G., & Joffe, H. (2016). Digital engagement methods for earthquake and fire preparedness: a review. *Natural Hazards*, *83*. https://doi.org/10.1007/s11069-016-2378-x

Vuolo, F., Neuwirth, M., Immitzer, M., Atzberger, C., & Ng, W.-T. (2018). How much does multi-temporal Sentinel-2 data improve crop type classification? *International Journal of Applied Earth Observation and Geoinformation*, *72*, 122–130. https://doi.org/https://doi.org/10.1016/j.jag.2018.06.007

Wagner, D., Alam, N., Wewetzer, M., Pries, M., & Coors, V. (2015). Methods for geometric data validation of 3D city models. *International Archives of the Photogrammetry, Remote Sensing and Spatial Information Sciences - ISPRS Archives*, *40*(1W5), 729–735. https://doi.org/10.5194/isprsarchives-XL-1-W5-729-2015

Wagner, Detlev, Alam, N., & Coors, V. (2013). Geometric validation of 3D city models based on standarized quality criteria. In *Urban and Regional Data Management, UDMS Annual 2013 - Proceedings of the Urban Data Management Society Symposium 2013* (pp. 197–210). https://doi.org/10.1201/b14914-24

Wang, P., Huang, C., & Tilton, J. C. (2018). Mapping Three-dimensional Urban Structure by Fusing Landsat and Global Elevation Data. *ArXiv:1807.04368 [Physics.Soc-Ph]*, 1–26.

Wate, P., & Saran, S. (2015). Implementation of CityGML energy application domain extension (ADE) for integration of urban solar potential indicators using object-oriented modelling approach. *Geocarto International*, *30*(10), 1144–1162. https://doi.org/10.1080/10106049.2015.1034192

Wiginton, L., Nguyen, H., & Pearce, J. (2010). Quantifying rooftop solar photovoltaic potential for regional renewable energy policy. *Computers Environment and Urban Systems*, *34*, 345–357. https://doi.org/10.1016/j.compenvurbsys.2010.01.001

Woodcock, C., Allen, R., Anderson, M., Belward, A., Bindschadler, R., Cohen, W., Gao, F., Goward, S., Helder, D., Helmer, E., Nemani, R., Oreopoulos, L., Schott, J., Thenkabail, P., Vermote, E., Vogelmann, J., Wulder, M., & Wynne, R. (2008). Free Access to Landsat Imagery. *Science (New York, N.Y.)*, *320*, 1011. https://doi.org/10.1126/science.320.5879.1011a

Wu, J. (2010). Urban sustainability: An inevitable goal of landscape research. *Landscape Ecology*, *25*(1), 1–4. https://doi.org/10.1007/s10980-009-9444-7

Wulder, M. A., Coops, N. C., Roy, D. P., White, J. C., & Hermosilla, T. (2018). Land cover 2.0. *International Journal of Remote Sensing*, *39*(12), 4254–4284. https://doi.org/10.1080/01431161.2018.1452075

Wulder, M. A., Loveland, T. R., Roy, D. P., Crawford, C. J., Masek, J. G., Woodcock, C. E., Allen, R. G., Anderson, M. C., Belward, A. S., Cohen, W. B., Dwyer, J., Erb, A., Gao, F., Griffiths, P., Helder, D., Hermosilla, T., Hipple, J. D., Hostert, P., Hughes, M. J., … Zhu, Z. (2019). Current status of Landsat program, science, and applications. *Remote Sensing of Environment*, *225*, 127–147. https://doi.org/https://doi.org/10.1016/j.rse.2019.02.015

Wurm, M., Droin, A., Stark, T., Geiß, C., & Sulzer, W. (2021). Deep Learning-Based Generation of Building Stock Data from Remote Sensing for Urban Heat Demand Modeling. *International Journal o f Geo-Information*, *10*(23).

Wurm, M., Droin, A., Stark, T., Geiß, C., Sulzer, W., & Taubenböck, H. (2021) Deep Learning-Based Generation of Building Stock Data from Remote Sensing for Urban Heat Demand Modeling. *ISPRS International Journal of Geo-Information.* 10(1):23. https://doi.org/10.3390/ijgi10010023

Wurm, M., Stark, T., Zhu, X.X., Weigand, M., & Taubenböck, H. (2019) Semantic Segmentation of Slums in Satellite Images Using Transfer Learning on Fully Convolutional Neural Networks. *ISPRS J. Photogramm. Remote Sens.* 150, 59–69.

Yamazaki, D., Ikeshima, D., Tawatari, R., Yamaguchi, T., O’Loughlin, F., Neal, J., Sampson, C., Kanae, S., & Bates, P. (2017). A high-accuracy map of global terrain elevations: Accurate Global Terrain Elevation map. *Geophysical Research Letters*, *44*. https://doi.org/10.1002/2017GL072874

Yan, J., Zlatanova, S., Aleksandrov, M., Diakite, A. A., Pettit, C., Building, R. C., & Twins, D. (2019). *INTEGRATION OF 3D OBJECTS AND TERRAIN FOR 3D MODELLING SUPPORTING THE DIGITAL TWIN*. *IV*(September), 24–27.

Yang, J., Wright, J., & Yu, L. (2010). Image Super-Resolution Via Sparse Representation. *Image Processing, IEEE Transactions On*, *19*, 2861–2873. https://doi.org/10.1109/TIP.2010.2050625

Yao, Z., Nagel, C., Kunde, F., Hudra, G., Willkomm, P., Donaubauer, A., Adolphi, T., & Kolbe, T. H. (2018). 3DCityDB - a 3D geodatabase solution for the management, analysis, and visualization of semantic 3D city models based on CityGML. *Open Geospatial Data, Software and Standards*, *3*(1), 5. https://doi.org/10.1186/s40965-018-0046-7

Ye, B., Tian, S., Ge, J., & Sun, Y. (2017). Assessment of WorldView-3 Data for Lithological Mapping. *Remote Sensing*, 1–19. https://doi.org/10.3390/rs9111132

Yigitcanlar, T., & Teriman, S. (2015). Rethinking sustainable urban development: towards an integrated planning and development process. *International Journal of Environmental Science and Technology*, *12*(1), 341–352. https://doi.org/10.1007/s13762-013-0491-x

You, Y., Wang, S., Ma, Y., Chen, G., Wang, B., Shen, M., & Liu, W. (2018). Building detection from VHR remote sensing imagery based on the morphological building index. *Remote Sensing*, *10*(8), 1–22. https://doi.org/10.3390/rs10081287

Yu, B., Liu, H., Wu, J., Hu, Y., & Zhang, L. (2010). Automated derivation of urban building density information using airborne LiDAR data and object-based method. *Landscape and Urban Planning*, *98*(3–4), 210–219. https://doi.org/10.1016/j.landurbplan.2010.08.004

Zhang, A., Liu, X., Gros, A., & Tiecke, T. (2017). Building Detection from Satellite Images on a Global Scale. *ArXiv:1707.08952*.

Zhao, X., Pu, J., Wang, X., Chen, J., Yang, L. E., & Gu, Z. (2018). Land-use spatio-temporal change and its driving factors in an artificial forest area in Southwest China. *Sustainability (Switzerland)*, *10*(11), 1–19. https://doi.org/10.3390/su10114066

Zhao, Z., Ledoux, H., & Stoter, J. (2013). AUTOMATIC REPAIR OF CITYGML LOD2 BUILDINGS USING SHRINK-WRAPPING. *ISPRS Annals of the Photogrammetry, Remote Sensing and Spatial Information Sciences*, *II-2/W1*, 309–317. https://doi.org/10.5194/isprsannals-II-2-W1-309-2013

Zheng, S., & Zheng, J. (2014). *Assessing the Completeness and Positional Accuracy of OpenStreetMap in China* (pp. 171–189). https://doi.org/10.1007/978-3-319-08180-9_14

Zheng, Y., Weng, Q., & Zheng, Y. (2017). A hybrid approach for three-dimensional building reconstruction in indianapolis from LiDAR data. *Remote Sensing*, *9*(4), 1–24. https://doi.org/10.3390/rs9040310

Zhu, Q., Hu, M., Zhang, Y., & Du, Z. (2009). Research and practice in three-dimensional city modeling. *Geo-Spatial Information Science*, *12*(1), 18–24. https://doi.org/10.1007/s11806-009-0195-z

Zhu, X.X., Tuia, D., Mou, L., Xia, G.S., Zhang, L., Xu, F., & Fraundorfer, F. (2017) Deep Learning in Remote Sensing: A Comprehensive Review and List of Resources. *IEEE Geosci. Remote Sens. Mag.* 5, 8–36.

Zhu, Z., Fu, Y., Woodcock, C. E., Olofsson, P., Vogelmann, J. E., Holden, C., Wang, M., Dai, S., & Yu, Y. (2016). Remote Sensing of Environment Including land cover change in analysis of greenness trends using all available Landsat 5 , 7 , and 8 images : A case study from Guangzhou , China (2000 – 2014). *Remote Sensing of Environment*, *185*, 243–257. https://doi.org/10.1016/j.rse.2016.03.036

Zhu, Z., Wulder, M. A., Roy, D. P., Woodcock, C. E., Hansen, M. C., Radeloff, V. C., Healey, S. P., Schaaf, C., Hostert, P., Strobl, P., Pekel, J.-F., Lymburner, L., Pahlevan, N., & Scambos, T. A. (2019). Benefits of the free and open Landsat data policy. *Remote Sensing of Environment*, *224*, 382–385. https://doi.org/https://doi.org/10.1016/j.rse.2019.02.016

Zhuo, X., Fraundorfer, F., Kurz, F., & Reinartz, P. (2018). Optimization of OpenStreetMap building footprints based on semantic information of oblique UAV images. *Remote Sensing*, *10*(4). https://doi.org/10.3390/rs10040624

Zielstra, D., Hochmair, H., & Neis, P. (2013). Assessing the Effect of Data Imports on the Completeness of OpenStreetMap – A United States Case Study. *Transactions in GIS*, *17*. https://doi.org/10.1111/tgis.12037

Zook, M. A., & Graham, M. (2007). The creative reconstruction of the Internet: Google and the privatization of cyberspace and DigiPlace. *Geoforum*, *38*(6), 1322–1343. https://doi.org/https://doi.org/10.1016/j.geoforum.2007.05.004

Zook, M., & Breen, J. (2017). *Volunteered Geographic Information BT - Encyclopedia of GIS* (S. Shekhar, H. Xiong, & X. Zhou (eds.); pp. 2434–2438). Springer International Publishing. https://doi.org/10.1007/978-3-319-17885-1_1656